รายงานวิจัยฉบับสมบูรณ์

โครงการ

การศึกษาอันตรกิริยาของโลหะกับตัวรองรับในวัฏภาคของเหลวและแก๊สสำหรับตัวเร่งปฏิกิริยาแบบวิวิธพันธุ์

Study of metal-support interaction in liquid and gas phases for heterogeneous catalysis

โดย

รองศาสตราจารย์ ดร. บรรเจิด จงสมจิตร

ภาควิชาวิศวกรรมเคมี คณะวิศวกรรมศาสตร์
จุฬาลงกรณ์มหาวิทยาลัย

25 มิถุนายน 2553

สัญญาเลขที่ RMU5080028

รายงานวิจัยฉบับสมบูรณ์

โครงการ

การศึกษาอันตรกิริยาของโลหะกับตัวรองรับในวัฏภาคของเหลวและแก๊สสำหรับตัวเร่งปฏิกิริยาแบบวิวิธพันธุ์

Study of metal-support interaction in liquid and gas phases for heterogeneous catalysis

โดย

รองศาสตราจารย์ ดร. บรรเจิด จงสมจิตร

ภาควิชาวิศวกรรมเคมี คณะวิศวกรรมศาสตร์
จุฬาลงกรณ์มหาวิทยาลัย

สนับสนุนโดยทบวงมหาวิทยาลัย และสำนักงานกองทุนสนับสนุนการวิจัย
(ความเห็นในรายงานนี้เป็นของผู้วิจัย ทบวงฯ และสกว. ไม่จำเป็นต้องเห็นด้วยเสมอไป)

บทคัดย่อ

โดยทั่วไปตัวเร่งปฏิกิริยาในระบบวิวิธพันธุ์ (Heterogeneous catalyst) จะประกอบได้ด้วยสองส่วนหลัก ๆ คือ ส่วนที่ว่องไว (Active site) และตัวรองรับ (Support) โดยส่วนใหญ่ส่วนที่ว่องไวจะเป็นโลหะแทรนซิชันซึ่งมีเลขออกซิเดชันได้หลายค่าทำให้สามารถเร่งปฏิกิริยาได้หลากหลาย ปกติส่วนที่ว่องไวจะถูกทำให้เกิดการกระจายตัวที่ดีโดยการเคลือบฝัง (Deposition) ลงบนตัวรองรับซึ่งเป็นสารที่มีรูพรุนและพื้นที่ผิวสูงก่อให้เกิดการกระจายตัวที่ดีของโลหะทำให้เกิดปฏิกิริยาได้ดี เนื่องจากปฏิกิริยาเคมีส่วนใหญ่จะเกิดขึ้นที่ผิวของตัวเร่งปฏิกิริยา อย่างไรก็ตามพบว่านอกจากชนิดของโลหะและตัวรองรับที่ใช้แล้ว สิ่งหนึ่งที่เป็นปัจจัยสำคัญในการกำหนดความว่องไว (Activity) ของตัวเร่งปฏิกิริยา คือ อันตรกิริยา (Interaction) ระหว่างโลหะกับตัวรองรับ ซึ่งมีงานวิจัยน้อยมากที่ศึกษาปัจจัยดังกล่าวนี้ ดังนั้นโครงการวิจัยนี้จึงได้เสนอแนวทางในการศึกษาอันตรกิริยาระหว่างโลหะกับตัวรองรับ

งานวิจัยนี้ทำโดยการเตรียมตัวเร่งปฏิกิริยาบนตัวรองรับที่สนใจ โดยแยกเป็นการศึกษาอันตรกิริยาในวัฏภาคของเหลวและแก๊ส โดยในส่วนของวัฏภาคของเหลวจะศึกษาตัวเร่งปฏิกิริยาเมทัลโลซีนบนตัวรองรับต่าง ๆ ได้แก่ ซิลิกา ไทเทเนีย MCM-41 และออกไซด์ผสม และนำตัวเร่งปฏิกิริยาเมทัลโลซีนบนตัวรองรับไปใช้ในการพอลิเมอร์ไรเซชันของเอทิลีนเพื่อสังเคราะห์พอลิเอทิลีนต่อไป นอกจากนี้ยังมีการศึกษาตัวเร่งปฏิกิริยากรดสำหรับปฏิกิริยาเอสเทอริฟิเคชันของกรดและแอลกอฮอล์ในวัฏภาคของเหลวอีกด้วย ในส่วนของวัฏภาคแก๊สจะศึกษาตัวเร่งปฏิกิริยาโคบอลต์บนตัวรองรับต่าง ๆ ได้แก่ เซอร์โคเนีย และอะลูมินา และนำตัวเร่งปฏิกิริยาโคบอลต์บนตัวรองรับไปใช้ในปฏิกิริยาไฮโดรจิเนชันของคาร์บอนมอนอกไซด์เพื่อผลิตเชื้อเพลิงสังเคราะห์ต่อไป จากการศึกษาอันตรกิริยาทั้งในวัฏภาคของเหลวและแก๊สพบว่าถ้าอันตรกิริยาระหว่างโลหะกับตัวรองรับมากเกินไปจะส่งผลให้ความว่องไวของตัวเร่งปฏิกิริยาลดลงอย่างชัดเจน จึงมีความจำเป็นที่จะต้องปรับสภาพของตัวรองรับ (Support modification) ก่อนนำโลหะไปเคลือบฝังเพื่อลดอันตรกิริยาดังกล่าว นอกจากนี้ยังพบว่ามีหลายปัจจัยที่ส่งผลต่ออันตรกิริยา เช่น ขนาดผลึกของโลหะและตัวรองรับ เทคนิคในการเคลือบฝังและวิธีการเตรียมตัวเร่งปฏิกิริยา ชนิดของโลหะและตัวรองรับที่ใช้ และผลของการใช้สารปรับปรุงตัวรองรับ ผลงานวิจัยดังกล่าวทำให้สามารถผลิตผลงานวิจัยในระดับนานาชาติจำนวน 12 เรื่อง ผลิตมหาบัณฑิตจำนวน 9 คน และดุษฎีบัณฑิตจำนวน 1 คน

คำสำคัญ อันตรกิริยา ตัวเร่งปฏิกิริยาแบบวิวิธพันธุ์ ความว่องไว วัฏภาคแก๊ส วัฏภาคของเหลว

Abstract

In general, a heterogeneous catalyst consists of two main components: the active site and the support. The active site is usually a transition metal having various oxidation states. Thus, it can catalyze different chemical reactions. Mostly, the active sites are deposited on the support having large surface area to facilitate the dispersion of the active sites. It is well known that the high dispersion of active sites can result in high activity of catalysts due to most of reactions occurs at surface. However, besides the types of metal and support, it is found that one of the most crucial parameters that would affect the catalytic activity is interactions between metal and support. It has been only a few reports on the effect of interaction. Therefore, this study focuses on such an interaction between the metal and support.

In this study, the selected heterogeneous catalysts were prepared and employed in different liquid and gas phases. In fact, in the liquid phase, the supported metallocene catalysts having silica, titania, MCM-41, and mixed oxides as support for ethylene polymerization were investigated. In addition, the heterogeneous acid catalysts were also studied for esterification in liquid phase as well. For the gas phase reaction, the zirconia- and alumina-supported cobalt catalysts for CO hydrogenation to produce the synthetic fuels were investigated. Based on this study, it reveals that the too strong interaction for both liquid and gas phases can definitely result in low catalytic activity. Therefore, in some case, the modification of support is required prior to deposition of the active sites in order to decrease the interaction. It was also found that different interaction can be attributed to factors, such as the crystallite size of metal and support, deposition method, preparation of catalyst, types of metal and support, and the support modification. Based on this research, we can produce twelve international research articles, nine master degree students and one doctoral degree student.

Keywords: Interaction; Heterogeneous catalyst; Activity; Gas phase; Liquid phase

สารบัญ

หน้า

หน้าสรุปโครงการ (Executive Summary)
ทุนเพิ่มขีดความสามารถด้านการวิจัยของอาจารย์รุ่นกลางในสถาบันอุดมศึกษา

1. **ชื่อโครงการ (ภาษาไทย)** การศึกษาอันตรกิริยาของโลหะกับตัวรองรับในวัฏภาคของเหลวและแก๊ส สำหรับการเร่งปฏิกิริยาแบบวิวิธพันธ์

   (ภาษาอังกฤษ) Study of metal-support interaction in liquid and gas phases for heterogeneous catalysis

2. **ชื่อหัวหน้าโครงการ หน่วยงานที่สังกัด ที่อยู่ หมายเลขโทรศัพท์ โทรสาร และ e-mail**

ดร. บรรเจิด จงสมจิตร
ภาควิชาวิศวกรรมเคมี คณะวิศวกรรมศาสตร์
จุฬาลงกรณ์มหาวิทยาลัย
กรุงเทพฯ 10330
โทรศัพท์ 02-2186869 โทรสาร 02-2186877
e-mail: bunjerd.j@chula.ac.th

3. **สาขาที่ทำการวิจัย** วิศวกรรมตัวเร่งปฏิกิริยา

Keywords: Catalyst; support; interaction; catalyst characterization

4. **ระยะเวลาดำเนินการ** 3 ปี

5. **ได้เสนอโครงการนี้ หรือโครงการที่มีส่วนเหมือนกับเรื่องนี้บางส่วน เพื่อขอทุนต่อแหล่งอื่นที่ใดบ้าง**

   √ ไม่ได้เสนอต่อแหล่งทุนอื่น

   O เสนอต่อ
   ชื่อโครงการ
   กำหนดทราบผล

6. **ปัญหาที่ทำการวิจัย และความสำคัญของปัญหา**

ในปัจจุบันแม้ว่าจะมีการศึกษาวิจัยเกี่ยวกับตัวเร่งปฏิกิริยากันอย่างกว้างขวางทั้งในและต่างประเทศ โดยเฉพาะอย่างยิ่งการเร่งปฏิกิริยาแบบวิวิธพันธ์ (Heterogeneous catalysis) อย่างไรก็ตามพบว่าการศึกษาที่ผ่านมาจะมุ่งเน้นถึงการพัฒนาตัวเร่งปฏิกิริยาที่เหมาะสมโดยเปลี่ยนชนิดของตัวเร่งปฏิกิริยา

และตัวรองรับ หรืออาจจะเป็นการปรับปรุงสภาวะในการทำปฏิกิริยา (Reaction condition) และกระบวนการผลิตให้เหมาะสมเป็นส่วนใหญ่เพื่อให้สามารถใช้ตัวเร่งปฏิกิริยาเหล่านั้นได้อย่างมีประสิทธิภาพ แต่ทั้งนี้การพัฒนาตัวเร่งปฏิกิริยาที่ง่ายที่สุดอาจไม่ใช่แต่เพียงแค่การคิดค้นตัวเร่งปฏิกิริยาใหม่ ๆ ที่แตกต่างจากเดิมอย่างสิ้นเชิงเท่านั้น แต่การปรับปรุง (Modification) ตัวเร่งปฏิกิริยาที่มีอยู่เดิมให้มีประสิทธิภาพดียิ่งขึ้นกลับเป็นสิ่งที่น่าจะศึกษามากกว่าเมื่อพิจารณาถึงเวลาและงบประมาณที่ใช้ในการวิจัยซึ่งมีอยู่จำกัด

เป็นที่ทราบกันเป็นอย่างดีว่าตัวเร่งปฏิกิริยาในระบบวิวิธพันธ์จะประกอบไปด้วยตัวเร่งปฏิกิริยาที่อยู่บนตัวรองรับชนิดต่าง ๆ การเลือกใช้ตัวเร่งปฏิกิริยานั้นจะต้องมีความเฉพาะเจาะจง (Specific) เพื่อให้เกิดความว่องไว (Activity) และค่าการเลือกเกิดของผลิตภัณฑ์ที่ต้องการ (Product selectivity) ที่เหมาะสม นั่นหมายความว่าตัวเร่งปฏิกิริยาต้องมีความเฉพาะเจาะจงสำหรับการเกิดปฏิกิริยานั้น ๆ นอกจากชนิดของโลหะและตัวรองรับที่นำมาใช้เป็นตัวเร่งปฏิกิริยาแล้ว สิ่งสำคัญอย่างหนึ่งที่จะต้องนำมาประกอบการพิจารณาคือ อันตรกิริยา (Interaction) ระหว่างโลหะที่ใช้เป็นตัวเร่งปฏิกิริยากับตัวรองรับ โดยที่อันตรกิริยาดังกล่าวจะมีผลอย่างมากต่อสมบัติการเป็นตัวเร่งของตัวเร่งปฏิกิริยานั้น ๆ ทั้งนี้กล่าวได้ว่าปัจจัยที่มีผลต่ออันตรกิริยา ได้แก่ ชนิดของโลหะและตัวรองรับที่นำมาใช้ ขนาดของตัวรองรับ (ระดับนาโนหรือไมโครเมตร) สภาวะในการกระตุ้นตัวเร่งปฏิกิริยา (Activation of catalyst) วัฏภาคของปฏิกิริยาและชนิดของปฏิกิริยา ดังนั้นการพัฒนาความรู้ความเข้าใจในเรื่องดังกล่าวจะทำให้สามารถออกแบบการใช้ตัวเร่งปฏิกิริยาที่เหมาะสมได้ ซึ่งในปัจจุบันพบว่าการพัฒนาความรู้ทางด้านนี้ยังมีน้อยมากทำให้ขาดข้อมูลที่จะนำมาใช้เป็นแนวทางในการพัฒนาตัวเร่งปฏิกิริยาที่มีอยู่เดิมให้มีประสิทธิภาพมากยิ่งขึ้น ดังนั้นข้อเสนอของโครงการวิจัยนี้จะนำไปสู่การพัฒนาองค์ความรู้ใหม่ที่เป็นประโยชน์ต่อการออกแบบตัวเร่งปฏิกิริยาแบบวิวิธพันธ์ที่เหมาะสมโดยมุ่งเน้นการศึกษาของอันตรกิริยาที่เกิดขึ้นระหว่างตัวเร่งปฏิกิริยากับตัวรองรับในสภาวะต่าง ๆ โดยแสดงได้ตามแผนภูมิใน**รูปที่ 1**

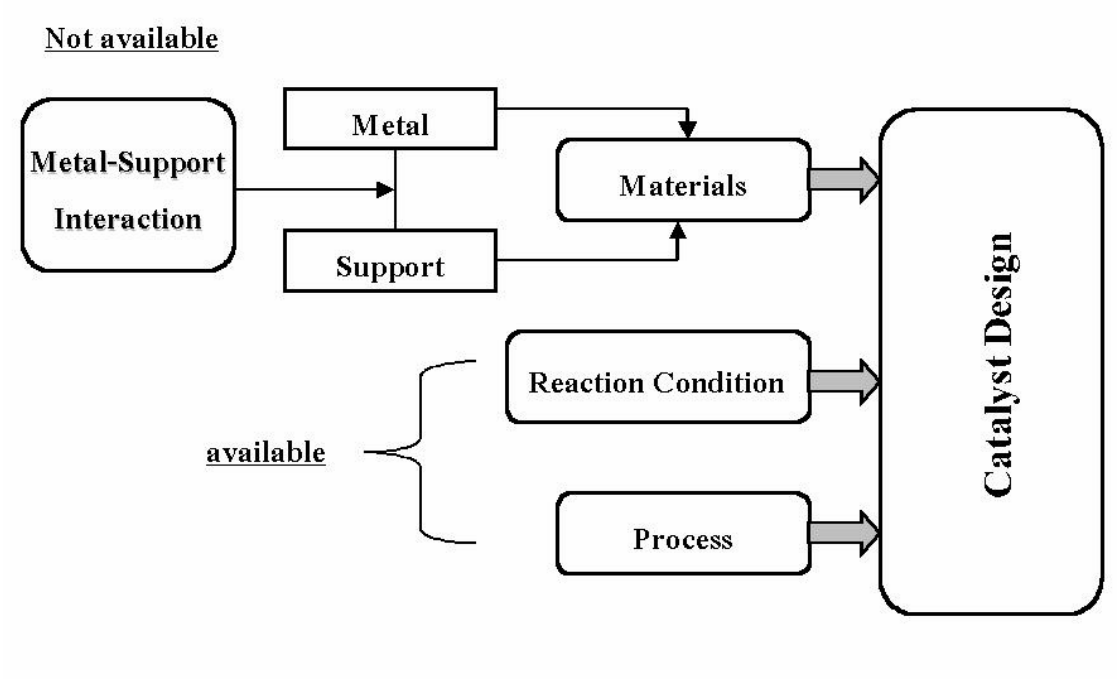

รูปที่ 1 แสดงความสำคัญของการศึกษาอันตรกิริยาระหว่างโลหะกับตัวรองรับ

7. วัตถุประสงค์

เพื่อศึกษาผลของอันตรกิริยาระหว่างโลหะกับตัวรองรับที่มีต่อสมบัติการเป็นตัวเร่งของตัวเร่งปฏิกิริยาในวัฏภาคของเหลวและแก๊ส โดยมีปัจจัยที่ศึกษาได้แก่ ชนิดของโลหะ ชนิดของตัวรองรับ ขนาดของตัวรองรับ ชนิดของปฏิกิริยาที่ใช้ เป็นต้น

8. ระเบียบวิธีวิจัย

1) รวบรวมข้อมูลของเอกสารที่เกี่ยวข้อง (Literature review)
2) สังเคราะห์ หรือ ปรับปรุง ตัวรองรับที่ใช้ ได้แก่ ซิลิกา อะลูมินา ไทเนีย เป็นต้น
3) เตรียมตัวเร่งปฏิกิริยาโดยทำการยึดเกาะโลหะลงบนตัวรองรับที่ได้จากข้อ 2
4) ทดสอบคุณลักษณะของตัวเร่งปฏิกิริยาที่เตรียมได้
5) ตรวจวัดความว่องไวและค่าการเลือกเกิดของตัวเร่งปฏิกิริยาในปฏิกิริยา
6) วิเคราะห์ข้อมูล จัดทำรายงาน เขียนบทความวิจัยต่างประเทศ

9. จำนวนโครงการที่ผู้วิจัยกำลังดำเนินการอยู่ โดยขอให้ระบุระยะเวลาเริ่มต้นและสิ้นสุดของแต่ละโครงการแหล่งทุน และงบประมาณสนับสนุนที่ได้รับ เวลาที่ใช้ทำโครงการวิจัยในแต่ละโครงการเป็นกี่ชั่วโมงต่อสัปดาห์ ทั้งในฐานะหัวหน้าโครงการ ผู้ร่วมโครงการของแต่ละโครงการที่กำลังดำเนินการอยู่ โปรดระบุรายละเอียดแต่ละโครงการที่ดำเนินการอยู่ดังต่อไปนี้

โครงการ	การศึกษาคุณลักษณะและสมบัติการเป็นตัวเร่งปฏิกิริยาเมทัลโลซีนบนตัวรองรับจากการโคพอลิเมอร์ไรเซชันของเอทิลีนกับแอลฟาโอเลฟิน
แหล่งทุน	สกว. (MRG-48)
ระยะเวลา	เริ่มต้น 1 มิถุนายน 2548 ถึง 31 พฤษภาคม 2550
งบประมาณ	480,000 บาท
สถานะภาพ	หัวหน้าโครงการ
เวลาในการทำงาน	20 ชั่วโมงต่อสัปดาห์

10. ความเชื่อมโยงกับต่างประเทศ (หากมี)

ขณะนี้ผู้เสนอขอรับทุนได้ทำงานวิจัยในศูนย์เชี่ยวชาญเฉพาะทางด้านคาตาไลซิสและวิศวกรรมปฏิกิริยาที่ใช้ตัวเร่งปฏิกิริยา โดยในส่วนของห้องปฏิบัติการได้มีการติดต่อเชื่อมโยงกับนักวิจัยที่มีความเชี่ยวชาญเฉพาะด้านตัวเร่งปฏิกิริยาอย่างในแต่ละประเทศ โดยมีการส่งนิสิตปริญญาเอกซึ่งได้รับทุนกาญจนาภิเษกและนักวิจัยในศูนย์ไปอบรมและทำงานวิจัยกับนักวิจัยต่างประเทศเหล่านั้นอย่างต่อเนื่อง ได้แก่ Professor Takeshi Shiono ณ Department of Applied Chemistry, Hiroshima University ประเทศญี่ปุ่น Professor James G. Goodwin, Jr. ณ Department of Chemical and Biomolecular Engineering, Clemson University ประเทศสหรัฐอเมริกา ความร่วมมือดังกล่าวนี้เองทำให้ศูนย์เชี่ยวชาญเฉพาะทางฯสามารถผลิตผลงานวิจัยที่มีคุณภาพได้อย่างต่อเนื่องทั้งในปัจจุบันและอนาคต

เนื้อหางานวิจัย

<u>สรุปผลผลิตวิจัยรวมของโครงการ</u>

โครงการวิจัยนี้เป็นการศึกษาถึงผลของอันตรกิริยาระหว่างโลหะกับตัวรองรับในวัฏภาคของเหลวและแก๊สสำหรับตัวเร่งปฏิกิริยาแบบวิวิธพันธุ์ ทั้งนี้ตัวเร่งปฏิกิริยาแบบวิวิธพันธุ์จะประกอบไปด้วยโลหะซึ่งเป็นจุดที่ว่องไวต่อการเกิดปฏิกิริยากับตัวรองรับซึ่งเป็นสารอนินทรีย์ โดยในส่วนของวัฏภาคของเหลวนั้นผู้วิจัยจะเลือกศึกษาอันตรกิริยาระหว่างตัวเร่งปฏิกิริยาร่วมของเมทัลโลซีนกับตัวเร่งซึ่งเป็นสารอนินทรีย์ โดยตัวเร่งปฏิกิริยาดังกล่าวนี้จะใช้ในการเร่งปฏิกิริยาพอลิเมอร์ไรเซชันของเอทิลีนกับหนึ่งโอเลฟินซึ่งเป็นการเตรียมพอลิเอทิลีนความหนาแน่นต่ำเชิงเส้น การทดลองโดยทั่วไปจะทำการเคลือบฝังตัวเร่งปฏิกิริยาร่วมลงบนตัวรองรับที่แตกต่างกัน แล้วนำไปทำปฏิกิริยากับเมทัลโลซีนเพื่อใช้ในการพอลิเมอร์ไรเซชันของเอทิลีนกับหนึ่งโอเลฟิน โดยตัวเร่งปฏิกิริยาเมทัลโลซีนที่ใช้ ได้แก่ [t-BuNSiMe$_2$Flu]TiMe$_2$ [1], สารประกอบเชิงซ้อนของไทเทเนียมที่มีหมู่ฟีนอกซีเอมีนเป็นองค์ประกอบ [2] และ *rac*-Et(bis)IndZrCl$_2$ [3-9] โดยมีเมทิลอะลูมินอกเซนเป็นตัวเร่งปฏิกิริยาร่วม ส่วนของตัวรองรับอนินทรีย์ที่ใช้ ได้แก่ ไทเทเนีย ซิลิกา ออกไซด์ผสมระหว่างซิลิกากับไทเทเนีย [1,2] MCM-41 [3] และ MCM-41 ที่ผ่านการปรับปรุงด้วยโบรอน [4] เซอร์โคเนีย [5] ซิลิการที่ผ่านการปรับปรุงด้วยเซอร์โคเนีย [5,6] ซิลิกาที่มีขนาดรูพรุนต่าง ๆ กัน [7] นอกจากนี้แล้วยังมีได้ทำการศึกษาถึงผลของตัวกลางของเหลวที่มีต่ออันตรกิริยาดังกล่าวอีกด้วย [1,2] นอกจากนี้ผลงานวิจัยเพิ่มเติมทำให้ทราบว่าขนาดอนุภาคของตัวรองรับไทเทเนียที่อยู่ในระดับนาโนเมตรและองค์ประกอบของเฟสก็ยังส่งผลถึงอันตรกิริยาดังกล่าวอีกด้วย [8] นอกจากระบบของเมทัลโลซีนแล้วผู้วิจัยยังได้ศึกษาผลของอันตรกิริยาที่มีต่อระบบตัวเร่งปฏิกิริยาซีเกลอ-นัตตาที่ใช้ตัวรองรับซิลิกาอีกด้วย [9] ผลงานวิจัยที่กล่าวมาทั้งหมดทำให้ทราบว่าอันตรกิริยาที่แตกต่างกันจะส่งผลต่อค่าความว่องไวของตัวเร่งปฏิกิริยาโดยรวมของตัวเร่งปฏิกิริยา โดยมีปัจจัยที่ส่งผลแตกต่างกันไป เช่น ชนิดของระบบการเร่งปฏิกิริยา ชนิดของตัวเร่งปฏิกิริยาร่วม ชนิดของตัวรองรับ ขนาดอนุภาคของตัวรองรับ เป็นต้น ผลของงานวิจัยดังกล่าวทำให้สามารถผลิตบทความวิจัยที่ได้รับการตีพิมพ์ในวารสารระดับนานาชาติ จำนวน 9 เรื่อง

ในส่วนของการศึกษาอันตรกิริยาของโลหะกับตัวรองรับในวัฏภาคแก๊ส ผู้วิจัยได้เลือกศึกษาตัวเร่งปฏิกิริยาโคบอลต์บนตัวรองรับอะลูมินาซึ่งเตรียมโดยวิธีโซลโวเทอร์มอล [10] และตัวเร่งปฏิกิริยาโคบอลต์บนตัวรองรับเซอร์โคเนียที่ถูกปรับปรุงด้วยโบรอน [11] ซึ่งพบว่าวิธีการเตรียมตัวเร่งปฏิกิริยาและการปรับปรุงสภาพของตัวรองรับจะส่งผลถึงอันตรกิริยาของโลหะโคบอลต์บนตัวรองรับและส่งผลต่อมาต่อความว่องไวของตัวเร่งปฏิกิริยาในการเร่งปฏิกิริยาไฮโดรจิเนชันของคาร์บอนมอนอกไซด์และค่าการเลือกเกิดของไฮโดรคาร์บอนอีกด้วย นอกจากนี้ในส่วนของวัฏภาคแก๊สผู้วิจัยยังได้ศึกษาผลต่อการปรับสภาพของตัวเร่งปฏิกิริยากรดสำหรับปฏิกิริยาเอสเทอริฟิเคชันโดยพบว่าน้ำที่ถูกที่แทนบนผิวกรดก็ส่งผลกระทบต่ออันตรกิริยาเช่นกัน [12] ผลของงานวิจัยดังกล่าวทำให้สามารถผลิตบทความวิจัยที่ได้รับการตีพิมพ์ในวารสารระดับนานาชาติ จำนวน 3 เรื่อง

เอกสารอ้างอิง

[1] "Characteristics and catalytic properties of [t-BuNSiMe$_2$Flu]TiMe$_2$/dMMAO catalyst dispersed on various supports towards ethylene/1-octene copolymerization", Applied Catalysis A: General, 327 (2007), 270-277, [Chanintorn Ketloy, Bunjerd Jongsomjit*, and Piyasan Praserthdam]. Impact factor (ISI-2008) = 3.190.

[2] "Effect of supports and solvents on ethylene polymerization with titanium complex consisting of phenoxy-imine ligands/dMMAO catalytic system", Journal of Molecular Catalysis A: Chemical, 294, 2008, 1-7, [Sonthaya Srijumnong, Bunjerd Jongsomjit*, Pattiya Suttipitakwong and Piyasan Praserthdam]. Impact factor (ISI-2008) = 2.814.

[3] "Impact of bimodal pore MCM-41-supported zirconocene/dMMAO catalyst on copolymerization of ethylene/1-octene", Catalysis Communications, 9, 2008, 789-795,[Sirinlak Bunchongturakarn, Bunjerd Jongsomjit*, and Piyasan Praserthdam]. Impact factor (ISI-2008) = 2.791.

[4] "Effect of boron-modified MCM-41-supported dMMAO/zirconocene catalyst on copolymerization of ethylene/1-octene for LLDPE synthesis", Iranian Polymer Journal, 16 (8), 2007, 549-559, [Supaluk Jiamwijitkul, Bunjerd Jongsomjit, and Piyasan Praserthdam]. Impact factor (ISI-2008) = 1.027.

[5] "A comparative study of SiO_2-ZrO_2-supported zirconocene/MAO catalysts on ethylene/1-olefin copolymerization", Catalysis Communications, 9, 2008, 1426-1431, [Tipawan Pothirat, Bunjerd Jongsomjit*, and Piyasan Praserthdam]. Impact factor (ISI-2008) = 2.791.

[6] "Effect of Zr-modified SiO_2-supported metallocene/MAO catalyst on copolymerization of ethylene/1-octene", Catalysis Letters, 121, 2008, 266-273, [Tipawan Pothirat, Bunjerd Jongsomjit*, and Piyasan Praserthdam]. Impact factor (ISI-2008) = 1.867.

[7] "Copolymerization of ethylene/1-octene via different pore sized silica-based supported zirconocene/dMMAO catalysts", Catalysis Communications, 10, 2008, 118-122, [Pongsathorn Wongwaiwattanakul, Bunjerd Jongsomjit*]. Impact factor (ISI-2008) =2.791.

[8] "A comparative study on synthesis of LLDPE/TiO_2 nanocomposites using different TiO_2 by in situ polymerization with zirconocene/dMMAO catalyst", Materials Chemistry and Physics, 112, 2008, 954-961. [Wathanyoo Owpradit and Bunjerd Jongsomjit*]. Impact factor (ISI-2008) = 1.799.

[9] "Catalytic behaviors of SiO_2-supported various aluminoxanes as coactivator in $MgCl_2$/DEP/$TiCl_4$-TEA catalysts for propylene polymerization", Catalysis Communications, 10, 2009, 1319-1323, [Kitti Tangjituabun, Bunjerd Jongsomjit*, Piyasan Praserthdam]. Impact factor (ISI-2008) = 2.791.

[10] "Synthesis of cobalt on cobalt-aluminate via solvothermal method and its catalytic properties for carbon monoxide hydrogenation", Catalysis Communications, 10, 2008, 232-236, [Sirirat Rojanapipatkul, Bunjerd Jongsomjit*]. Impact factor (ISI-2008) =2.971.

[11] "A study on characteristics and catalytic properties of Co/ZrO_2-B catalysts towards methanation", Catalysis Letters, 128, 2009, 119-126, [Nithinart Chitpong, Piyasan Praserthdam, Bunjerd Jongsomjit*]. Impact factor (ISI-2008) = 1.867.

[12] "Observation on different turnover number in two-phase acid catalyzed esterification of dilute acetic and 1-heptanol", Catalysis Letters, 130, 2009, 583-587, [Supareak Praserthdam, Bunjerd Jongsomjit*]. Impact factor (ISI-2008) = 1.867.

ภาคผนวก A

Reprint บทความวิจัย

จำนวน 12 เรื่อง

Research output paper for RMU-5080028- Bunjerd Jongsomjit

No	Title	Year	Role	Journal	IF (2009)	Acknowledgement (in paper)
1	"Characteristics and catalytic properties of [t-BuNSiMe$_2$Flu]TiMe$_2$/dMMAO catalyst dispersed on various supports towards ethylene/1-octene copolymerization", Applied Catalysis A: General, 327 (2007), 270-277, [Chanintorn Ketloy, **Bunjerd Jongsomjit**[*], and Piyasan Praserthdam].	2007	Corresponding author	Applied Catalysis A: General	3.564	TRF-RMU-50
2	"Effect of supports and solvents on ethylene polymerization with titanium complex consisting of phenoxy-imine ligands/dMMAO catalytic system", Journal of Molecular Catalysis A: Chemical, 294, 2008, 1-7, [Sonthaya Srijumnong, **Bunjerd Jongsomjit**[*], Pattiya Suttipitakwong and Piyasan Praserthdam].	2008	Corresponding author	Journal of Molecular Catalysis A: Chemical	3.135	TRF-RMU-50
3	"Impact of bimodal pore MCM-41-supported zirconocene/dMMAO catalyst on copolymerization of ethylene/1-octene", Catalysis Communications, 9, 2008, 789-795,[Sirinlak Bunchongturakarn, **Bunjerd Jongsomjit**[*], and Piyasan Praserthdam]. Impact factor	2008	Corresponding author	Catalysis Communications	3.000	TRF-RMU-50
4	"A comparative study of SiO_2-ZrO_2-supported zirconocene/MAO catalysts on ethylene/1-olefin copolymerization", Catalysis Communications, 9, 2008, 1426-1431, [Tipawan Pothirat, **Bunjerd Jongsomjit**[*], and Piyasan Praserthdam].	2008	Corresponding author	Catalysis Communications	3.000	TRF-RMU-50

Research output paper for RMU-5080028- Bunjerd Jongsomjit

No	Title	Year	Role	Journal	IF (2009)	Acknowledgement (in paper)
5	"Copolymerization of ethylene/1-octene via different pore sized silica-based supported zirconocene/dMMAO catalysts, Catalysis Communications, 10, 2008, 118-122, [Pongsathorn Wongwaiwattanakul, **Bunjerd Jongsomjit**[*]].	2008	Corresponding author	Catalysis Communications	3.000	TRF-RMU-50
6	"Synthesis of cobalt on cobalt-aluminate via solvothermal method and its catalytic properties for carbon monoxide hydrogenation", Catalysis Communications, 10, 2008, 232-236, [Sirirat Rojanapipatkul, **Bunjerd Jongsomjit**[*]].	2008	Corresponding author	Catalysis Communications	3.000	TRF-RMU-50
7	"Effect of Zr-modified SiO_2-supported metallocene/MAO catalyst on copolymerization of ethylene/1-octene", Catalysis Letters, 121, 2008, 266-273, [Tipawan Pothirat, **Bunjerd Jongsomjit***, and Piyasan Praserthdam].	2008	Corresponding author	Catalysis Letters	2.021	TRF-RMU-50
8	"A study on characteristics and catalytic properties of Co/ZrO_2-B catalysts towards methanation", Catalysis Letters, 128, 209, 119-126, [Nithinart Chitpong, Piyasan Praserthdam, **Bunjerd Jongsomjit**[*]].	2009	Corresponding author	Catalysis Letters	2.021	TRF-RMU-50

Research output paper for RMU-5080028- Bunjerd Jongsomjit

No	Title	Year	Role	Journal	IF (2009)	Acknowledgement (in paper)
9	"A comparative study on synthesis of LLDPE/TiO_2 nanocomposites using different TiO_2 by in situ polymerization with zirconocene/dMMAO catalyst", Materials Chemistry and Physics, 112, 2008, 954-961, [Wathanyoo Owpradit and **Bunjerd Jongsomjit**[*]].	2008	Corresponding author	Materials Chemistry & Physics	2.015	TRF-RMU-50
10	"Effect of boron-modified MCM-41-supported dMMAO/zirconocene catalyst on copolymerization of ethylene/1-octene for LLDPE synthesis", Iranian Polymer Journal, 16 (8), 2007, 549-559, [Supaluk Jiamwijitkul, **Bunjerd Jongsomjit**[*], and Piyasan Praserthdam].	2007	Corresponding author	Iranian Polymer Journal	0.932	TRF-RMU-50
11	"Catalytic behaviors of SiO_2-supported various aluminoxanes as coactivator in $MgCl_2$/DEP/$TiCl_4$-TEA catalysts for propylene polymerization", Catalysis Communications, 10, 2009, 1319-1323 [Kitti Tangjituabun, **Bunjerd Jongsomjit**[*], Piyasan Praserthdam].	2009	Corresponding author	Catalysis Communications	3.000	TRF-RMU50
12	"Observation on different turnover number in two-phase acid catalyzed esterification of dilute acetic and 1-heptanol", Catalysis Letters, 130, 2009, 583-587, [Supareak Praserthdam, **Bunjerd Jongsomjit**[*]].	2009	Corresponding author	Catalysis Letters	2.021	TRF-RMU50

Total IF (ISI, 2009) = 30.709

Available online at www.sciencedirect.com
ScienceDirect
Applied Catalysis A: General 327 (2007) 270–277
APPLIED CATALYSIS A: GENERAL
www.elsevier.com/locate/apcata

Characteristics and catalytic properties of [*t*-BuNSiMe$_2$Flu]TiMe$_2$/dMMAO catalyst dispersed on various supports towards ethylene/1-octene copolymerization

Chanintorn Ketloy, Bunjerd Jongsomjit *, Piyasan Praserthdam

Center of Excellence on Catalysis and Catalytic Reaction Engineering, Department of Chemical Engineering, Faculty of Engineering, Chulalongkorn University, Bangkok 10330 Thailand

Received 10 December 2006; received in revised form 14 May 2007; accepted 18 May 2007
Available online 25 May 2007

Abstract

In the present study, the characteristics and catalytic properties of [*t*-BuNSiMe$_2$Flu]TiMe$_2$/dMMAO catalyst dispersed on various supports towards ethylene/1-octene copolymerization were investigated. First, the dMMAO was impregnated onto various supports, such as SiO_2, SiO_2–TiO_2, and TiO_2. Then, copolymerization of ethylene/1-octene was conducted with and without the presence of supports in different solvent mediums. The SiO_2–TiO_2 support exhibited the highest activity among all the supports. The high activity observed for the SiO_2–TiO_2 support can be attributed to fewer interactions between the support and dMMAO, as confirmed by XPS and TGA results. The different solvents can alter the nature of the catalyst in two ways: (i) changing the interactions between the support and cocatalyst and/or (ii) changing the form of active species i.e., active ion-pair and solvent-separated ion-pair, as seen in the homogeneous system. However, there was no effect with regards to activity of the solvent mediums employed for the homogeneous system. It is worth noting that the Ti-complex made possible high incorporation of 1-octene having the triblock (OOO) and diblock (EOO) copolymers. The properties of copolymers by means of GPC, DSC, and ^{13}C NMR were further discussed in more detail.

Keywords: Metallocene catalyst; Copolymerization; Ti complex; Silica; Titania; Supports

1. Introduction

Linear low-density polyethylene (LLDPE) is one of the most important commercial products. Recent industrial efforts have been directed towards finding novel and efficient polymerization catalysts for the synthesis of the desired copolymer. Metallocene catalysts are particularly useful for the production of LLDPE through the copolymerization of ethylene and α-olefins such as 1-butene, 1-hexene, and 1-octene [1]. The single-site characteristic of metallocene makes it possible to improve polymer properties; control the degree of α-olefin insertion upon the stereochemistry and provide higher activity than the values obtained by conventional Ziegler–Natta catalyst. They can also result in a narrow molecular weight distribution (MWD) and a uniform distribution of short-chain branches in the polymer chain as well [2]. It should be noted that different distributions and compositions in the polymer backbone would result in various properties for polymers [3–5]. Therefore, by knowing the nature of catalysts, the researchers can alter the properties of polymers.

Several studies comparing different group 4 metallocene structures in ethylene/α-olefin copolymerization have been reported [6–9]. Nevertheless, the homogeneous catalyst systems based on metallocene require high aluminum-to-transition metal molar ratios and extensive polymer washing, so as to remove residual aluminum. In addition, they are not suitable for industrial applications such as gas-phase and slurry polymerization processes. To overcome these disadvantages, researchers have supported metallocene compounds mainly on inorganic carriers such as SiO_2, Al_2O_3, TiO_2, and zeolites [10–12]. These carriers have been extensively studied as supported cocatalysts for years. The heterogeneous metallocene system is necessary to produce polymer particles of desired morphology to avoid reactor fouling with finely dispersed swelling of polymers [5].

* Corresponding author. Tel.: +66 2 218 6869; fax: +66 2 218 6769.
E-mail address: bunjerd.j@chula.ac.th (B. Jongsomjit).

0926-860X/$ – see front matter
doi:10.1016/j.apcata.2007.05.025

It is known that the catalytic behaviors depend on polymerization conditions, catalytic compositions, metal dispersion, and types of supports used. In the case of solution and slurry polymerization, the kind of solvent is also one of factors which can influence the polymerization behaviors [13]. Indeed, literature data regarding α-olefin homopolymerization report that the polarity of the solvent remarkably affects the catalytic activities [14] and, in some cases, also the microstructure of polymer [15–18].

In previous studies, a unique catalyst type called ''constrained geometry catalyst (CGC)'' using half-sandwich titanocenes has been found. Such catalysts can give high activity and can incorporate a large amount of α-olefin into a copolymer [19,20]. Research revealed that [*t*-BuNSiMe$_2$Flu]-TiMe$_2$ complex could be employed to polymerize propylene, norbornene and ethylene [21–25]. Several papers reported that [*t*-BuNSiMe$_2$Flu]TiMe$_2$ catalyst was suitable for the propylene polymerization in various polymerization conditions due to the effects of activators and solvents used. They found that the kind of activators and the polarity of solvents played important roles on the catalytic activities and microstructure of polymer as well [17,18,26,27]. Only few papers, however, have discussed the copolymerization of ethylene with α-olefins [28,29] and only one reported the supporting system [30].

The present work has focused on the effect of supports in different solvent mediums in ethylene/1-octene (EO) copolymerization using three supports: SiO_2, TiO_2, and SiO_2–TiO_2. Some solvent mediums such as toluene and chlorobenzene (CB) having different dielectric constant values (ε) were studied. The supports and catalyst precursors were prepared, characterized and tested for the catalyst activity. The properties of the copolymers obtained were further investigated by means of GPC, DSC, and ^{13}C NMR analysis.

2. Experimental

2.1. Materials

All operations were manipulated under an argon atmosphere using glove box and/or standard Schlenk techniques. The [*t*-BuNSiMe$_2$Flu]TiMe$_2$ (Ti-complex) was synthesized according to the procedure described by Hagihara et al. [29]. Ethylene (polymerization grade) was obtained from the National Petrochemical Co. Ltd., Thailand. 1-Octene (98%, 0.715 g mL^{-1}) was purchased from Aldrich Chemical Company and further purified by distilling over CaH_2 for 6 h. Modified methyl aluminoxane, MMAO (1.86 M in toluene) was donated by Tosoh Akzo, Japan. Silica gel (Cariact P-10) came from Fuji Silysia Chemical Ltd., Japan. Titanium (IV) oxide (pure anatase) was obtained from Aldrich Chemical Company. Toluene was donated by the Exxon Chemical, Thailand Co. Ltd. It was dried over dehydrated $CaCl_2$ and distilled over sodium/benzophenone.

2.2. Preparation of SiO_2–TiO_2 mixed oxide support

Each SiO_2–TiO_2 mixed oxide support [surface area of SiO_2 = 281 m^2 g^{-1} and TiO_2 = 70 m^2 g^{-1}] was prepared according to the method described by Conway et al. [31]. In particular, 1 g of SiO_2–TiO_2 (4:1 by weight) [32] mixed oxide support was physically mixed by dispersing in toluene (ca. 20 mL). The mixture was stirred for 30 min, filtered, and then dried under vacuum.

2.3. Removal of trialkylaluminiums from MMAO

Removal of trialkylaluminiums from MMAO was carried out according to the reported procedure [33]. The toluene solution of MMAO was dried under vacuum for 6 h at room temperature to evaporate the solvent, $AlMe_3$, and Al(*i*Bu)$_3$. Then, we continued to dissolve the material with 100 mL of heptane; finally, the solution was evaporated under vacuum to remove the remaining $AlMe_3$ and Al(*i*Bu)$_3$. This procedure was repeated four times and the white powder of dried MMAO (dMMAO) was obtained.

2.4. Preparation of supported dMMAO

Silica-supported dMMAO (dMMAO/SiO_2) was prepared according to the literature [33]. SiO_2 was calcined at 573 K for 6 h. A toluene solution (100 mL) of dMMAO (15 g) was added into the SiO_2 slurry in toluene (20 g, 250 mL), and the mixture was stirred for 30 min at room temperature. After the toluene was evaporated under vacuum, then material was washed with hexane (150 mL × 7) and finally dried under vacuum for 5 h to give SiO_2/dMMAO. Similarly, silica–titania mixed oxide-supported dMMAO (dMMAO/SiO_2–TiO_2) and titania-supported dMMAO (dMMAO/TiO_2) were prepared according to the method as described above.

2.5. Polymerization procedure

Ethylene/1-octene copolymerization reaction was carried out in a 100 mL semibatch stainless steel autoclave reactor equipped with a magnetic stirrer. At first, the desired amounts of the supported dMMAO and the toluene (CB) [needed to make the total volume of 30 mL] were introduced into the reactor. The titanium complex in toluene (10 μmol mL^{-1}) was put into the reactor to make the $[Al]_{dMMAO}/[Ti]_{cat}$ = 400. Then, the reactor was immersed in liquid nitrogen. 1-Octene [5 mL (0.031 mol)] was added into the frozen reactor. The reactor was heated up to the polymerization temperature at 343 K. The polymerization was started by feeding ethylene into the reactor. The ethylene pressure and reactor temperature were kept constant during the polymerization (pressure in reactor = 50 psi). After 5 min, the reaction was terminated by adding acidic methanol and the material was stirred for 30 min. After filtration, the copolymer obtained was washed with methanol and dried at room temperature.

2.6. Supports and supported dMMAO characterization

2.6.1. Scanning electron microscopy (SEM) and energy dispersive X-ray (EDX) spectroscopy

SEM and EDX were respectively used to determine the sample morphologies and elemental distribution throughout the sample

granules. The SEM of JEOL mode JSM-6400 was applied. EDX was performed using a Link Isis series 300 program.

2.6.2. X-ray diffraction (XRD)

XRD was performed to determine the bulk crystalline phases of samples. It was conducted using a SIEMENS D-5000 X-ray diffractometer with CuK_α ($\lambda = 1.54439$ Å). The spectra were scanned at a rate of 2.4° min^{-1} in the range $2\theta = 20–80°$.

2.6.3. Raman spectroscopy

The Raman spectra of the samples were collected by projecting a continuous wave YAG laser of neodymium (Nd) red (810 nm) through the samples at room temperature. A scanning range of 100–1000 cm^{-1} with a resolution of 2 cm^{-1} was applied.

2.6.4. X-ray photoelectron spectroscopy (XPS)

XPS was used to determine the binding energy (BE) and the amount of Al on sample surfaces. It was carried out using the Shimazu AMICUS with VISION 2-control software. Spectra were recorded at room temperature in high-resolution mode (0.1 eV step, 23.5 eV pass energy) for Al 2p core-level region. The samples were mounted on pieces of adhesive carbon tape as pellets. The energy reference for Ag metal (368.0 eV for $3d_{5/2}$) was used for this study.

2.6.5. Thermogravimetric analysis (TGA)

TGA was performed using a TA Instruments SDT Q 600 analyzer. The samples of 10–20 mg and a temperature ramping from 298 to 873 K at 2 K min^{-1} were used in the operation. The carrier gas was N_2 UHP.

2.7. Polymer characterization

2.7.1. Gel permeation chromatography (GPC)

The molecular weight and molecular weight distribution of polymer was determined using GPC (PL-GPC-220). Samples were prepared having approximate concentrations of 1–2 mg mL^{-1} in trichlorobenzene (mobile phase) by using the sample preparation unit (PL-SP 260) with filtration system at a temperature of 423 K. The dissolved and filtered samples were transferred into the GPC instrument at 423 K. The calibration was conducted using the universal calibration curve based on narrow polystyrene standards.

2.7.2. Differential scanning calorimetry (DSC)

Thermal analysis measurements were performed using a Perkin-Elmer DSC P7 calorimeter. The DSC measurements reported here were recorded during the second heating/cooling cycle with the rate of 20 K min^{-1}. This procedure ensured that the previous thermal history was erased and provided comparable conditions for all samples. Approximately 10 mg of sample was used for each DSC measurement.

2.7.3. ^{13}C NMR spectroscopy

^{13}C NMR spectroscopy was used to determine the α-olefin incorporation and copolymer microstructure. Chemical shifts were referenced internally to the $CDCl_3$ and calculated according to the method described by Randall [34]. Each sample solution was prepared by dissolving 50 mg of copolymer in 1,2,4-trichlorobenzene and $CDCl_3$. ^{13}C NMR spectra were taken at 333 K using a BRUKER AVANCE II 400 operating at 100 MHz with an acquisition time of 1.5 s and a delay time of 4 s.

3. Results and discussion

3.1. Catalytic activities

Here, various supports such as silica, titania, and mixed silica–titania (4:1 by weight) were used for supporting the [*t*-BuNSiMe$_2$Flu]TiMe$_2$ (the Ti-complex)/dMMAO catalyst. Prior to impregnation of the supports with dMMAO, they were characterized by means of XRD and Raman spectroscopy. XRD patterns of the supports before impregnation to dMMAO are shown in Fig. 1. It was observed that silica exhibited a broad XRD peak, as seen typically for the conventional amorphous silica. Similar to silica, the XRD patterns for titania indicated only the characteristics peaks of anatase titania at 25° (major), 37°, 48°, 55°, 56°, 62°, 71°, and 75°. XRD patterns of the mixed silica–titania revealed that the combinations of silica and titania were present, as mentioned above. Raman spectra of supports are shown in Fig. 2. It was found that the titania support exhibited the Raman bands at 639, 516, and 397 cm^{-1} for titania in its anatase form as seen from our previous work [35,36] whereas silica was Raman-insensitive over the scanning range applied. After impregnation with dMMAO, the $[Al]_{dMMAO}$ content was measured using EDX. The typical measurement curve for the quantitative analysis using EDX is shown in Fig. 3. The amounts of $[Al]_{dMMAO}$ in various supports are also listed. It can be seen that the amounts of $[Al]_{dMMAO}$ in various supports varied due to the adsorption ability of each support. Results revealed that titania exhibited the highest amount of $[Al]_{dMMAO}$ being present, probably due to its strong interaction. On the other hand, an increasing amount of $[Al]_{dMMAO}$ can be observed with the presence of titania, as can

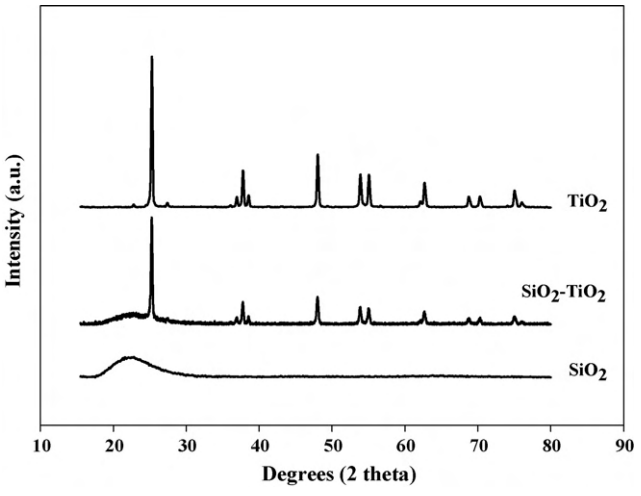

Fig. 1. XRD patterns of various supports prior to impregnation with dMMAO.

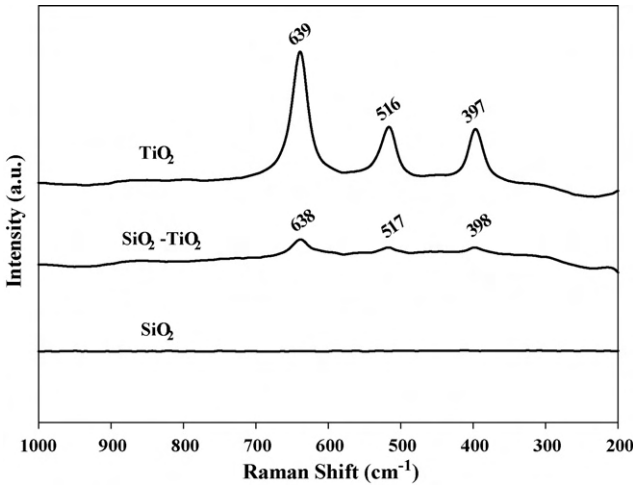

Fig. 2. Raman spectra of various supports prior to impregnation with dMMAO.

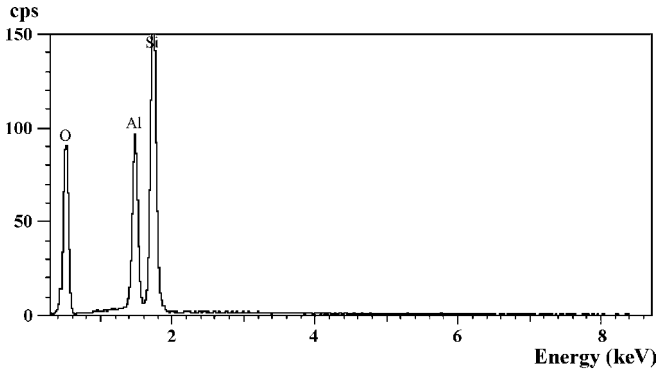

Cocatalyst	$[Al]_{dMMAO}$ (%mass)
dMMAO/SiO_2	12.56
dMMAO/SiO_2-TiO_2	14.69
dMMAO/TiO_2	18.56

Fig. 3. A typical spectrum of the supported dMMAO from EDX analysis used to measure the average [Al]dMMAO concentration on various supports.

also be seen in the mixed silica–titania compared with that in the sole silica. Besides the content of $[Al]_{dMMAO}$ in supports, one should consider the distribution of $[Al]_{dMMAO}$ in the supports. The elemental distribution was also performed using EDX mapping on the external surface. The $[Al]_{dMMAO}$ distribution in the various supports is shown in Fig. 4. As seen, all samples exhibited good distributions of Al without any changes in the support morphology.

For comparative studies, the catalytic activities towards the copolymerization of ethylene/1-octene upon various supports were measured. The polymerization activities of the homogeneous system and various supports employed in toluene are shown in Table 1. The polymerization activities were in the order of homogeneous system $>SiO_2$–$TiO_2 > SiO_2 > TiO_2$. As known, the supported system exhibited lower activity than the homogeneous one due to the supporting effect. Among the supported systems, the SiO_2–TiO_2 rendered the highest activity. In fact, the presence of TiO_2 in SiO_2 can result in decreased interaction between the cocatalyst and SiO_2 supports. It was reported that TiO_2 may acted as a spacer group to anchor MAO to the SiO_2 support, resulting in less steric hindrance and less interaction on the support surface, as seen for the zirconocene/MAO system as well [32]. Hence, a similar effect was consistently observed for the titanocene/dMMAO system. It should be mentioned that the lowest polymerization activity obtained for the TiO_2 support was due to the strong support interaction [37]. In order to give a better understanding on species present on supports, we conducted XPS studies of the dMMAO on various supports. In fact, the binding energy of Al

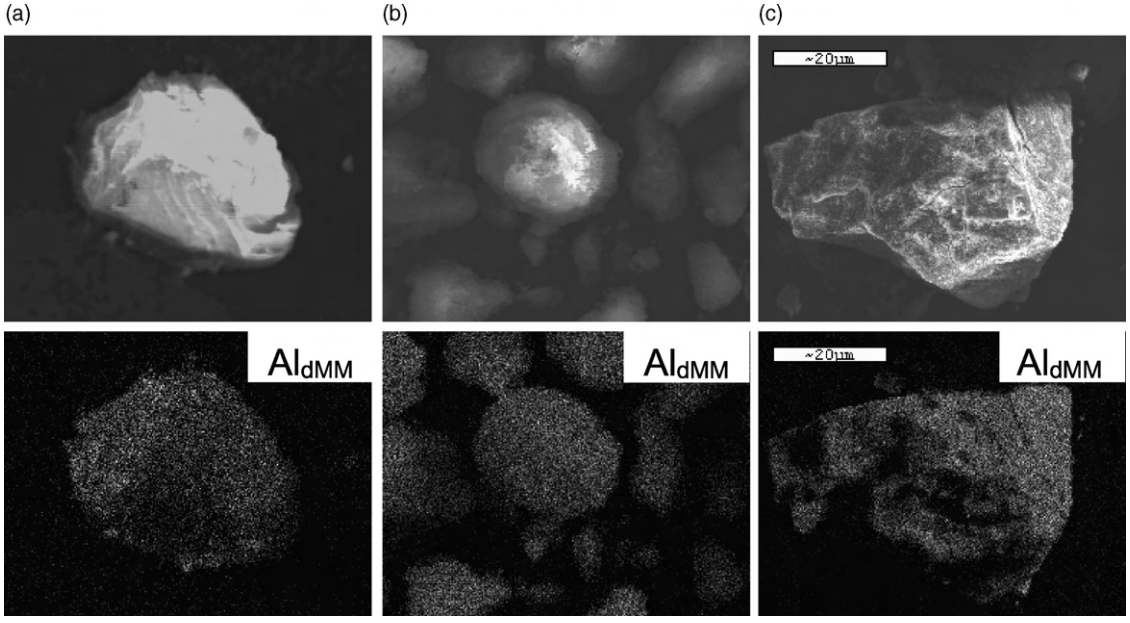

Fig. 4. SEM/EDX mapping for Al distributions on (a) SiO_2, (b) SiO_2–TiO_2, and (c) TiO_2 supports.

Table 1
Polymerization[a] activity

System	Solvent	Yield (g)	Activity (kg of polymer mol^{-1} Ti h)
Homogeneous	Toluene	3.25	3897
SiO_2 support		2.49	2984
SiO_2–TiO_2 support		2.61	3131
TiO_2 support		2.33	2795
Homogeneous	CB	3.23	3871
SiO_2 support		1.68[b]	10095
SiO_2–TiO_2 support		2.69[c]	12127
TiO_2 support		2.53	3032

[a] Polymerization condition: Ti = 10 μmol, Al/Ti = 400, temperature = 343 K, time = 5 min, 50 psi of ethylene pressure was applied.
[b] Polymerization time = 1 min.
[c] Polymerization time = 1.5 min.

2p core-level of $[Al]_{dMMAO}$ was measured. A typical XPS profile of Al 2p on various supports is shown in Fig. 5, indicating the BE of 74.6–74.8 eV. These values were also in accordance with the MMAO present on the silica support, as reported by Hagimoto et al. [33]. Such results suggested that no significant change in the oxidation state of $[Al]_{dMMAO}$ occurred upon the various supports employed. As a matter of fact, the differences in polymerization activities observed on various supports were not caused by any changes of the surface species. The surface concentrations of Al 2p measured by XPS are also shown in Table 2. On the other hand, changes in activity upon various supports were mainly attributed to both the amounts of $[Al]_{dMMAO}$ present and its interaction with the support. Among the various supports employed, the surface concentrations of Al 2p were in the order of $TiO_2 > SiO_2$–$TiO_2 > SiO_2$ as seen from the bulk results using EDX. It was obvious that the TiO_2 support contained the highest amount of surface Al 2p due to strong interactions resulting in less leaching of dMMAO during the preparation. The presence of TiO_2 in the mixed SiO_2–TiO_2 also enhanced the interaction of dMMAO due to the synergistic effect arising from TiO_2. Based on the surface concentrations of Al 2p, one might argue that with TiO_2 support the polymerization activity should be the highest since it apparently had the highest concentration of Al 2p. However, based on our results, the polymerization activity using the TiO_2

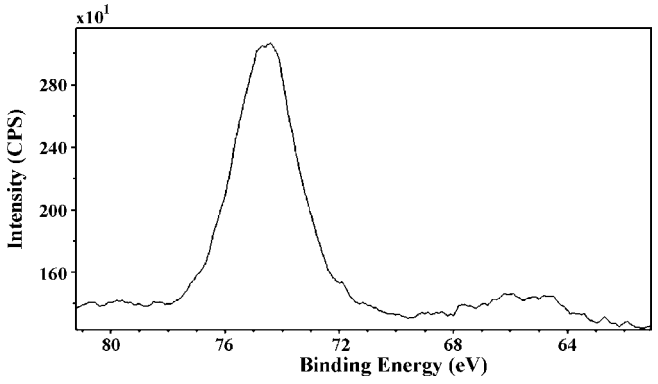

Fig. 5. A typical XPS spectrum of Al 2p core-level of dMMAO and dMMAO on various supports.

Table 2
XPS data of Al 2p core-level of cocatalysts

Cocatalyst	BE (eV) for Al^{3+}	Amount of Al^{3+} at surface (%mass)
dMMAO	74.7	28.5
dMMAO/SiO_2	74.6	25.0
dMMAO/SiO_2–TiO_2	74.8	25.6
dMMAO/TiO_2	74.7	27.1

was the lowest. This indicated that, besides the surface concentration of $[Al]_{dMMAO}$, the interactions between the $[Al]_{dMMAO}$ and support were quite important. In fact, the strong interaction of species with TiO_2 or other supports employed in this study was referred to the interaction between the support and the cocatalyst (dMMAO). Based on this study, dMMAO was dispersed by impregnation onto the support prior to polymerization. The degree of interaction between the support and dMMAO can be determined by the TGA measurement. In order to give a better understanding, we propose the interaction of support and dMMAO based on the review paper by Severn et al. [38]. They explained that the connection of the support and cocatalyst occurred via the $O_{support}$–$Al_{cocatalyst}$ linkage. In particular, the TGA can only provide useful information on the degree of interaction for the dMMAO bound to the support in terms of weight loss and removal temperature. The stronger interaction can result in it being more difficult for the dMMAO bound to the support to react with the Ti-complex during activation processes, leading to lower catalytic activity for polymerization. As mentioned, the TiO_2 support is known to have a strong interaction with species present on it. The TGA measurement was performed in order to prove the interaction between the $[Al]_{dMMAO}$ and various supports. The TGA profiles of $[Al]_{dMMAO}$ on various supports are shown in Fig. 6, indicating similar profiles for various supports. We observed that the weight losses of $[Al]_{dMMAO}$ present on various supports were in the order of SiO_2 (22%) > SiO_2–TiO_2 (21%) > TiO_2 (19%). The species having strong interaction with the support were removed at ca. 538, 542, and 588 K for SiO_2, SiO_2–TiO_2,

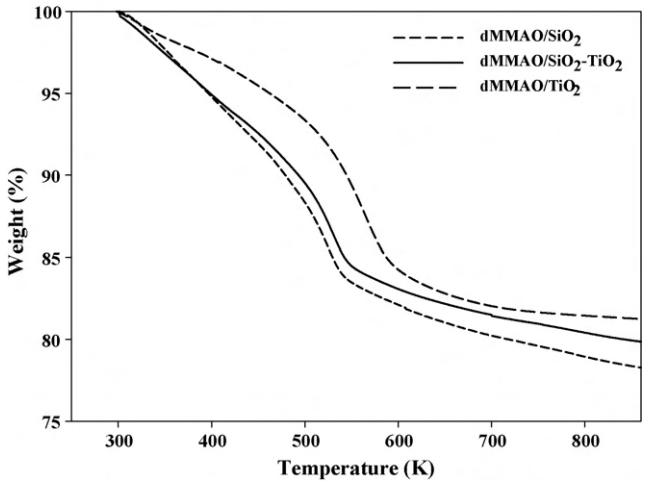

Fig. 6. TGA profiles of supported dMMAO on various supports.

and TiO_2, respectively. This indicated that $[Al]_{dMMAO}$ present on TiO_2 had the strongest interaction and thus the lowest observed polymerization activity. However, in the case of SiO_2–TiO_2 support, although it had stronger interaction than that of SiO_2, it exhibited higher polymerization interaction due to higher concentrations of $[Al]_{dMMAO}$ at surfaces as mentioned above. Besides, the presence of TiO_2 in SiO_2 as a spacer group was also responsible for higher activity.

In order to investigate the solvent effect on this polymerization system, we employed solvents having different dielectric constant (ε) values such as chlorobenzene for the corresponding polymerization system. The dielectric constant is in the order of CB (5.68) > toluene (2.38) [39]. The polymerization activity results in CB are also shown in Table 1. There was no significant change regarding activity for the homogeneous system when changing the solvent medium. However, the dramatic increases in activity were found in the supported system, especially with SiO_2 and SiO_2–TiO_2 supports, when CB was employed as the solvent medium. Such results indicated that the polymerization activities substantially increased with SiO_2 and SiO_2–TiO_2 supports in CB almost four times higher compared with those in toluene. The activity for TiO_2 support in CB only slightly increased compared to that in toluene. We propose that the different solvents can alter the nature of the catalyst in two ways: (i) changing the interaction between the support and cocatalyst and/or (ii) changing the form of active species i.e., active ion-pair and solvent-separated ion-pair as seen in the homogeneous systems reported by Nishii et al. [17] and Intaragamjon et al. [28]. It is worth noting that the dramatic increases in polymerization activities in CB compared to those in toluene can perhaps be attributed to increased propagation rate, presuming that the $[Al]_{dMMAO}$ species present on SiO_2 and SiO_2–TiO_2 supports were similar as shown by means of the XPS measurements. Nishii et al. [17] investigated the propylene polymerization using the Ti complex in various solvents having different dielectric constants in homogeneous systems. They reported that the high polarity of solvent resulted in increased activity due to the increased propagation rate. Such results revealed that the enhancement of the separation of the active metal cation and the MMAO-derived anion in the polar solvent occurred. It should be also noted that there was no solvent effect observed with the support having the strong interaction such as TiO_2, as seen in Table 1.

Table 3
Polymer characterization

System	Solvent	GPC Analysis (g mol^{-1})			T_m[a]
		M_w (10^4)	M_n (10^4)	MWD	
Homogeneous	Toluene	13.43	4.95	2.7	–[b]
SiO_2		36.37	13.80	2.6	–
SiO_2–TiO_2		36.60	16.02	2.3	–
TiO_2		6.91	4.25	1.6	–
Homogeneous	CB	27.24	8.11	3.4	–
SiO_2		50.98	26.52	1.9	–
SiO_2–TiO_2		37.86	9.64	4.0	–
TiO_2		18.16	6.50	2.8	–

[a] Melting temperature was measured by DSC analysis.
[b] Value not be detected from the measurement.

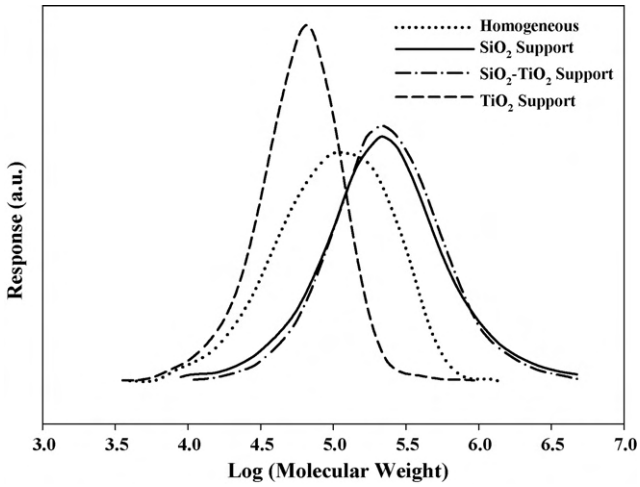

Fig. 7. Molecular weight distribution measured by GPC of EO copolymers obtained from various supports in toluene.

3.2. Characteristics of polymer

The various copolymers obtained were further characterized by means of GPC, DSC and ^{13}C NMR. The GPC was performed in order to determine the M_W, M_n and MWD of polymers. The GPC results are shown in Table 3. The GPC curves for EO copolymers using various supports in toluene and CB are shown in Figs. 7 and 8, respectively. They indicate that all copolymers obtained exhibited only the unimodal molecular weight distribution. If we consider polymerization in toluene, the supported systems (except for TiO_2 support) gave the higher M_W than that of the homogeneous system, however, without any significant changes in MWD. We suggest that using TiO_2 clearly promoted the chain transfer reaction, consequently resulting in lower M_W. The effect of TiO_2 support on the zirconocene/MAO system was also reported in our previous work [32]. However, it was obvious that the titanocene/dMMAO system gives much higher M_W. It can be observed that polymerization in CB exhibited higher M_W than those in

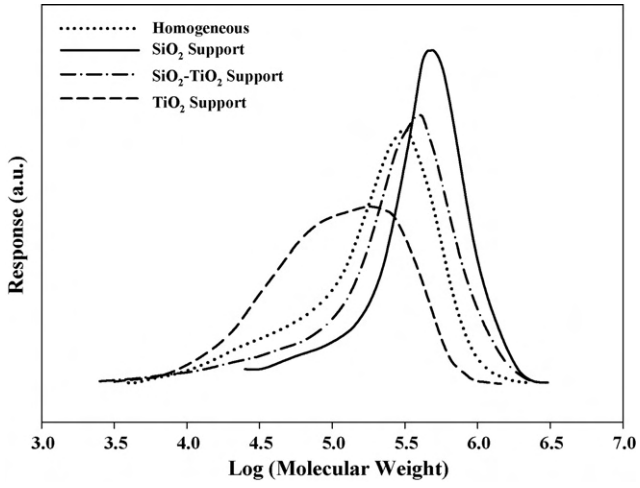

Fig. 8. Molecular weight distribution measured by GPC of EO copolymers obtained from various supports in CB.

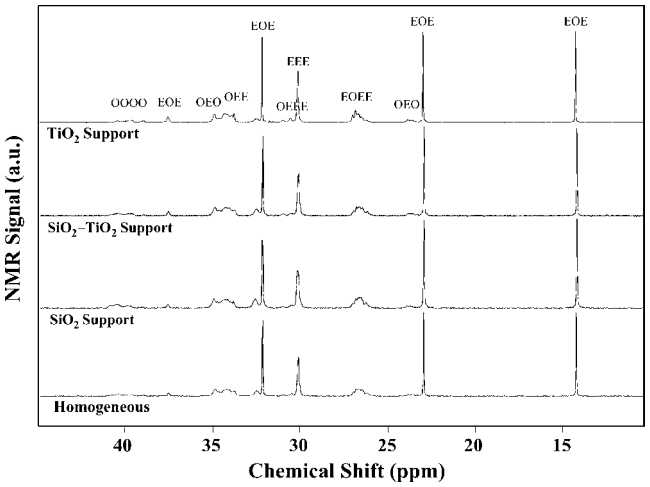

Fig. 9. ^{13}C NMR spectra of EO copolymers obtained from various supports in toluene.

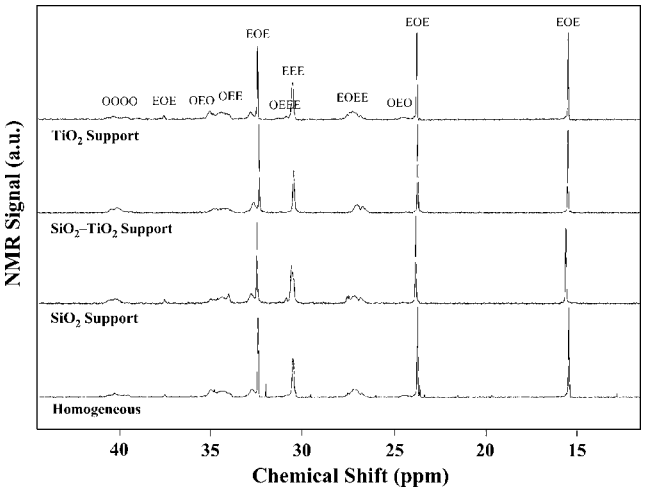

Fig. 10. ^{13}C NMR spectra of EO copolymers obtained from various supports in CB.

toluene without a significant change in MWD. The increased M_W in CB can be attributed to the solvent-separated ion-pair active species, which allowed inserting more monomers into the growing chain. Thus, the solvent-separated ion-pair can provide the high activity while also enhancing the insertion of monomer to the growing chain. The DSC was performed to measure the thermal properties of polymers. Results revealed that no melting temperature (T_m) was found, indicating a non-crystalline polymer is produced in this specified polymerization system. The non-crystalline polymers were attributed to the high degree of 1-octene insertion, which can be confirmed by ^{13}C NMR.

The quantitative analysis of triad distribution for all copolymers was conducted on the basic assignment of the ^{13}C NMR spectra of ethylene/1-octene copolymer [34]. The ^{13}C NMR spectra for EO copolymers using various supports in toluene and CB are shown in Figs. 9 and 10, respectively indicating the characteristic peaks of the typical EO copolymer. The triad distribution of all polymers is shown in Table 4. The incorporation of 1-octene increased with the CB system for the homogeneous system, the SiO_2–TiO_2, and TiO_2-suported systems. This indicated that the solvent-separated ion-pair obtained from CB exhibited less steric hindrance, thus enhancing the insertion of 1-octene in the growing polymer. However, for the SiO_2-supported system, a slight decrease in 1-octene incorporation was found when CB was employed. This was probably due to the inhibition arising from more steric hindrance in SiO_2-supported system. Nishii et al. [17] also investigated the effect of Ti-complex on the syndiospecificity of polypropylene in the homogeneous system. They reported that the presence of the solvent-separated ion-pairs allowed the growing chain to migrate between the two enantiomeric ligand sites on the Ti cation without monomer insertion. However, with the contact ion-pair obtained from the non-polar solvent, such migration of the growing chain was not allowed. Based on their work, we conclude that migration of the growing chain in different solvent mediums was the main factor for controlling the stereospecificity of polymer. However, in the present work, the copolymerization of ethylene/1-octene was conducted on both homogeneous and supported catalytic systems. Based on the ^{13}C NMR results, we observe that the microstructure of polymer was similar regardless of the solvents employed. Therefore, the migration of the growing chain did not occur as compared to the corresponding propylene polymerization system. Considering the triad distribution, we see that the polymers obtained from both solvent mediums were block polymers ($r_E r_O > 1$) indicating the large amounts of triblock (OOO) for the CB system and diblock (EOO) for the toluene system, as seen in Table 4.

Table 4
Triad distribution of copolymer obtained from ^{13}C NMR

System	Solvent	OOO	EOO	EOE	EEE	OEE	OEO	%Octene incorporation
Homogeneous	Toluene	0.107	0.481	0.096	0.184	0.015	0.117	68
SiO_2		0.295	0.436	0.067	0.102	0.012	0.087	80
SiO_2–TiO_2		0.140	0.487	0.082	0.181	0.011	0.098	71
TiO_2		0.027	0.415	0.140	0.125	0.133	0.160	58
Homogeneous	CB	0.223	0.558	0.045	0.102	0.010	0.062	83
SiO_2		0.498	0.162	0.085	0.247	0.008	0.000	75
SiO_2–TiO_2		0.610	0.346	0.000	0.014	0.030	0.000	96
TiO_2		0.268	0.442	0.054	0.093	0.009	0.134	76

4. Conclusions

In summary, the SiO_2–TiO_2-supported dMMAO with Ti-complex exhibited the highest activity towards ethylene/1-octene copolymerization in different solvent mediums due to decreased support interaction and steric hindrance. In particular, the dramatic increase in catalytic activity can be achieved using the high dielectric constant solvent medium such as chlorobenzene. We propose that the different solvents can alter the nature of catalyst in two ways: (i) changing the interaction between the support and cocatalyst and/or (ii) changing the form of active species i.e., active ion-pair and solvent-separated ion-pair, as seen in the homogeneous system. However, there was no significant change in the observed activity upon the different solvent mediums in the homogeneous system. The presence of CB also resulted in high M_W of polymer. In all cases, the block copolymer was obtained along with high insertion of 1-octene.

Acknowledgements

We thank the Thailand Research Fund (TRF) for the RMU50-B. Jongsomjit and the graduate school of CU for the financial support of this project. The guidance of the Ti-complex preparation by Professor Takeshi Shiono from Hiroshima University is greatly appreciated.

References

[1] P. Tait, I. Berry, Comp. Polym. Sci. 4 (1989) 575–579.
[2] H.-H. Brintzinger, D. Fischer, R. Mulhaupt, B. Rieger, R.M. Waymouth, Angew. Chem. Int. Ed. Engl. 34 (1995) 1143–1170.
[3] A.G. Simanke, G.B. Galland, L. Freitas, J.A.H. da Jornada, R. Quijada, R.S. Mauler, Polymer 40 (1999) 5489–5495.
[4] X.R. Xu, J.T. Xu, L.X. Feng, W. Chen, J. Appl. Polym. Sci. 77 (2000) 1709–1715.
[5] G.G. Hlatky, Chem. Rev. 100 (2000) 1347–1376.
[6] M. Dankova, R.M. Waymouth, Macromolecules 36 (2003) 3815–3820.
[7] M. Galimberti, F. Piemontesi, N. Mascellani, I. Camurati, O. Fusco, M. Destro, Macromolecules 32 (1999) 7968–7976.
[8] M.J. Schneider, J. Suhm, R. Mulhaupt, M.-H. Prosenc, H.-H. Brintzinger, Macromolecules 30 (1997) 3164–3168.
[9] A. Yano, S. Hasegawa, T. Kaneko, M. Sone, M. Sato, A. Akimoto, Macromol. Chem. Phys. 200 (1999) 1542–1553.
[10] M. Marques, A. Conte, F.C. De Resende, E.G. Chaves, J. Appl. Polym. Sci. 82 (2001) 724–730.
[11] G. Jacobs, T.K. Das, Y. Zhang, J. Li, G. Racoillet, B.H. Davis, Appl. Catal. A Gen. 233 (2002) 263–281.
[12] R. Quijada, J. Retuert, J.L. Gurvara, R. Rojas, M. Valle, P. Saavedra, H. Palza, G.B. Galland, Macromol. Symp. 189 (2002) 111–125.
[13] C.V. James, C.W.C. James, N.B. Caddam, A.N. Richard, J. Appl. Polym. Sci. Part A Polym. Chem. 32 (1994) 2049–2056.
[14] D. Coevoet, H. Cramail, A. Deffieux, Macromol. Chem. Phys. 197 (1996) 867–885.
[15] S.H. Yang, J. Huh, W.H. Jo, Macromolecules 38 (2005) 1402–1409.
[16] F. Forlini, E. Princi, I. Tritto, M.C. Sacchi, F. Piemontesi, Macromol. Chem. Phys. 203 (2002) 645–652.
[17] K. Nishii, T. Matsumae, E.O. Dare, T. Shiono, T. Ikeda, Macromol. Chem. Phys. 205 (2004) 363–369.
[18] K. Nishii, T. Shiono, T. Ikeda, Macromol. Rapid Commun. 25 (2004) 1029–1032.
[19] W. Kaminsky, A. Laban, Appl. Catal. A Gen. 222 (2001) 47–61.
[20] K. Soga, T. Uozumi, S. Nakamura, T. Toneri, T. Teranishi, T. Sano, T. Arai, T. Shiono, Macromol. Chem. Phys. 197 (1996) 4237–4251.
[21] T. Hasan, K. Nishii, T. Shiono, T. Ikeda, Macromolecules 35 (2002) 8933–8935.
[22] K. Nishii, H. Hagihara, T. Ikeda, M. Akita, T. Shiono, J. Organomet. Chem. 691 (2006) 193–201.
[23] K. Nishii, T. Ikeda, M. Akita, T. Shiono, J. Mol. Catal. A Chem. 231 (2005) 241–426.
[24] T. Hasan, T. Ikeda, T. Shiono, Macromolecules 38 (2005) 1071–1074.
[25] T. Hasan, T. Ikeda, T. Shiono, Macromolecules 37 (2004) 8503–8509.
[26] A. Ioku, T. Hasan, T. Shiono, T. Ikeda, Macromol. Chem. Phys. 202 (2002) 748–755.
[27] T. Shiono, S. Yoshida, H. Hagihara, T. Ikeda, Appl. Catal. A Gen. 200 (2000) 145–152.
[28] N. Intaragamjon, T. Shiono, B. Jongsomjit, P. Praserthdam, Catal. Commun. 7 (2006) 721–727.
[29] H. Hagihara, T. Shiono, T. Ikeda, Macromolecules 31 (1998) 3184–3188.
[30] A. Ioku, T. Shiono, T. Ikeda, Appl. Catal. A Gen. 226 (2002) 15–22.
[31] S.J. Conway, J.W. Falconer, C.H. Rochester, J. Chem. Soc. Faraday Trans. 185 (1989) 71–75.
[32] B. Jongsomjit, S. Ngamposri, P. Praserthdam, Catal. Lett. 100 (2005) 139–146.
[33] H. Hagimoto, T. Shiono, T. Ikeda, Macromol. Chem. Phys. 205 (2004) 19–26.
[34] J.C. Randall, J. Macromol. Sci. Rev. Macromol. Chem. Phys. C29 (1989) 201–315.
[35] B. Jongsomjit, C. Sakdamnuson, J.G. Goodwin Jr., P. Praserthdam, Catal. Lett. 94 (2004) 209–215.
[36] B. Jongsomjit, T. Wongsalee, P. Praserthdam, Mater. Chem. Phys. 97 (2006) 343–350.
[37] R. Riva, H. Miessuer, R. Vitali, G.D. Piero, Appl. Catal. A Gen. 196 (2000) 111–123.
[38] J.R. Severn, J.C. Chadwick, R. Duchateau, N. Friederichs, Chem. Rev. 105 (2005) 4073–4147.
[39] R. Kleinschmidt, Y. Griebenow, G. Fink, J. Mol. Catal. A Chem. 157 (2000) 83–90.

Journal of Molecular Catalysis A: Chemical 294 (2008) 1–7

Contents lists available at ScienceDirect

Journal of Molecular Catalysis A: Chemical

journal homepage: www.elsevier.com/locate/molcata

Effect of supports and solvents on ethylene polymerization with titanium complex consisting of phenoxy-imine ligands/dMMAO catalytic system

Sonthaya Srijumnong[a], Pattiya Suttipitakwong[b], Bunjerd Jongsomjit[a,*], Piyasan Praserthdam[a]

[a] Center of Excellence on Catalysis and Catalytic Reaction Engineering, Department of Chemical Engineering, Faculty of Engineering, Chulalongkorn University, Bangkok 10330, Thailand
[b] Innovation & Technology, PTT Chemical Public Company Limited, Tambon Map Ta Phut, Amphoe Mueang Rayong, Rayong 21150, Thailand

ARTICLE INFO

Article history:
Received 18 March 2008
Received in revised form 10 July 2008
Accepted 26 July 2008
Available online 3 August 2008

Keywords:
Phenoxy-imine
Ethylene polymerization
Titanium complex
Supports
Solvents

ABSTRACT

Ethylene polymerization by titanium complex having two phenoxy-imine with different supports and solvents has been investigated. It was found that the catalytic activity depended on supports used, and especially on the types of solvent medium. For the supported system, catalytic activities decreased in the following order: $TiO_2 > TiO_2–SiO_2 > SiO_2$. This can be attributed to the strong interaction of the TiO_2 with dried MMAO (dMMAO) and the larger amount of dMMAO present on the TiO_2 than other supports. Furthermore, the catalytic activity was significantly affected by the solvent medium. According to the homogeneous system, the catalytic activities increased in the order of: toluene > heptane > chlorobenzene ≫ dichloromethane up on difference solvent mediums. On the other hand, for the supported system, the catalytic activity was the highest when heptane was employed. In order to give a better explanation, the different types of ion-pairs formed was proposed. The properties of polymers were further discussed in more details.

1. Introduction

Nowadays, polymer and plastics are playing the important role on the material industry. This is because they exhibit many useful properties, such as low density, high strength, and resistance to chemical attack, as well as being cost-effective. Otherwise the demands for the plastics increase in huge quantities every year. Among synthetic polymers, polyethylene is the major polymer and the largest of production in plastic industry [1–3].

It is well known that research and development of high-performance olefin polymerization catalysts have contributed significantly to the advancement of organometallic chemistry and polymer chemistry and have made a dramatic impact on the polyolefin industry. A recent example is the discovery of group 4 metallocene catalysts, which displays very high ethylene polymerization activity [4–6]. More recently, other classes of transition metal complex have been investigated as precursor for a new generation of olefin polymerization catalyst [7–12]. Specifically, olefin polymerization catalysts have been developed from nickel or palladium complexes with diimine [7,8], iron or cobalt complexes with diimine–pyridine ligands [9,10], titanium with diamide ligands [11,12]. Furthermore, Fujita and his co-workers [13] have successfully established highly active titanium and zirconium catalysts using various substituted phenoxy-imine ligands for olefin polymerization, which were named as FI catalysts. Depending on the ligand design, the catalyst showed different behaviors in ethylene and propylene polymerization, and the ligands strongly influenced catalytic parameters such as activity, polymerization mechanism, and polymer properties such as molecular weight [14]. Now phenoxy-imine ligands greatly interest more and more researchers [15,16]. It was found that homogeneous catalytic system has two disadvantages; the lack of morphologies control of polymer produced and reactor fouling. Therefore, binding these catalysts onto inorganic supports can provide a promising way to overcome these drawbacks. It has been reported that many inorganic supports such as SiO_2, Al_2O_3, and $MgCl_2$ have been extensively studied [17,18].

In this present study, the effect of different supports/dMMAO with titanium complex having phenoxy-imine catalyst on ethylene polymerization was investigated. The supports such as TiO_2, SiO_2, and $TiO_2–SiO_2$ mixed oxide were employed. The effect of solvent mediums used in slurry polymerization of ethylene was also investigated. The solvent mediums such as heptane, toluene, chlorobenzene (CB), and dichloromethane (DCM) having different dielectric constant value (ε) were used. The catalytic activities during ethylene polymerization were monitored and further discussed. The microstructure of polymer obtained was also investigated.

* Corresponding author. Tel.: +66 2 218 6878; fax: +66 2 2186877.
E-mail address: bunjerd.j@chula.ac.th (B. Jongsomjit).

1381-1169/$ – see front matter © 2008 Elsevier B.V. All rights reserved.
doi:10.1016/j.molcata.2008.07.013

2. Experimental

2.1. Materials

All operations were handled under an argon atmosphere using glove box and/or standard Schlenk techniques. Ethylene (polymerization grade) was obtained from the National Petrochemical Co., Ltd., Thailand. 3-*tert*-Butylsalicylaldehyde was purchased from Aldrich Chemical Company, Inc., and used without further purification. $TiCl_4$ (99+%) was purchased from Aldrich Chemical Company., Ltd., and use without further purification. Aniline and tetrahydrofuran (Anhydrous grade) were purchased from Aldrich Chemical Company, Inc. Heptane and chlorobenzene were purchased from Fluka Chemie, A.G., Switzerland and purified by distilling over sodium under argon atmosphere before used. Modified methylaluminoxane, MMAO (1.86 M in toluene) was donated by Tosoh Akzo, Japan. Silica gel (Cariact P-10) came from Fuji Silysia Chemical, Ltd., Japan. Titanium(IV) oxide (pure anatase) was obtained from Aldrich Chemical Company. Toluene was donated by the Exxon Chemical, Thailand Co., Ltd. It was dried over dehydrated $CaCl_2$ and distilled over sodium/benzophenone. Ultra-high purify (UHP) argon (99.999%) was purchased from Thai Industrial Gas Co., Ltd., and was further purified by passing through molecular sieves 3 Å, BASF catalyst R3-11G, NaOH and phosphorus pentaoxide (P_2O_5) to remove traces oxygen and moisture.

2.2. Preparation of SiO_2–TiO_2 mixed oxide support

Each SiO_2–TiO_2 mixed oxide support [surface area of SiO_2 = 281 $m^2\,g^{-1}$ and TiO_2 = 70 $m^2\,g^{-1}$] was prepared according to the method described by Conway et al. [19]. In particular, 1 g of SiO_2–TiO_2 (4:1 by weight) [20] mixed oxide support was physically mixed by dispersing in toluene (ca. 20 mL). The mixture was stirred for 30 min, filtered, and then dried under vacuum.

2.3. Removal of trialkylaluminiums from MMAO

Removal of trialkylaluminiums from MMAO was carried out according to the reported procedure [21]. The toluene solution of MMAO was dried under vacuum for 6 h at room temperature to evaporate the solvent, $AlMe_3$, and Al(*i*Bu)$_3$. Then, we continued to dissolve the material with 100 mL of heptanes. Finally, the solution was evaporated under vacuum to remove the remaining $AlMe_3$ and Al(*i*Bu)$_3$. This procedure was repeated four times and the white powder of dried MMAO (dMMAO) was obtained.

2.4. Preparation of supported dMMAO

Silica-supported dMMAO (dMMAO/SiO_2) was prepared according to the literature [21]. SiO_2 was calcined at 573 K for 6 h. A toluene solution (100 mL) of dMMAO (15 g) was added into the SiO_2 slurry in toluene (20 g, 250 mL). The mixture was stirred for 30 min at room temperature. After the toluene was evaporated under vacuum, the mixture was washed with hexane (150 mL × 7) and finally dried under vacuum for 5 h to give SiO_2/dMMAO. Similarly, silica–titania mixed oxide-supported dMMAO (dMMAO/SiO_2–TiO_2) and titania-supported dMMAO (dMMAO/TiO_2) were prepared according to the method as described above.

2.5. Titanium complex synthesis

Titanium complex was synthesized by the reaction of $TiCl_4$ with two equivalents of salt of the corresponding phenoxy-imine ligands according to the literature [22].

2.6. Polymerization procedure

The ethylene polymerization reaction was carried out in a 100-mL semi-batch stainless steel autoclave reactor equipped with magnetic stirrer. First, the reactor was charged with solvent such as heptane, toluene, chlorobenzene, and dichloromethane (to make a total volume of 30 mL) follow by adding the desired amount of supported dMMAO. Then, a solution of catalyst in toluene was added into the reactor having the $[Al]_{dMMAO\text{-}support}/[Ti]_{cat}$ ratio of 250. The reactor was then immersed in liquid nitrogen. After that, it was evacuated to remove the argon. Then, the reactor was adjusted to the polymerization temperature at 323 K. Polymerization was started by feeding ethylene gas (total pressure 50 psi) until the consumption of ethylene 0.018 mol (6 psi was observed from pressure gaute) was completed. Ethylene pressure and temperature were kept constant during the polymerization, and the consumption rate of ethylene was monitored by a mass flow meter. Polymerization was terminated with acidic methanol. The polymer obtained was precipitated in acidic methanol, filtered, adequately washed with methanol, and finally dried under vacuum at 333 K for 6 h.

2.7. Characterization

2.7.1. Characterization of titanium complex catalyst

Nuclear magnetic resonance spectroscopy: The ^{1}H-NMR spectra were recorded at ambient probe temperature (298 K) using BRUKER AVANCE II 400 operating at 100 MHz with an acquisition time of 1.5 s and a delay time of 4 s. Ligands and titanium complex solution were prepared using tetramethylsilane as solvent and deuterated chloroform for an internal lock.

2.7.2. Characterization of supports and catalyst precursors

X-ray diffraction: XRD was performed to determine the bulk crystalline phases of samples. It was conducted using a SIEMENS D-5000 X-ray diffractometer with Cu Kα (λ = 1.54439 Å). The spectra were scanned at a range of 2.4° min^{-1} in the range 2θ = 20–80°.

Scanning electron microscopy and energy dispersive X-ray spectroscopy: SEM and EDX were used to determine the sample morphologies and elemental distribution throughout the sample granule, respectively. The SEM of JEOL mode JSM-5800LV was applied. EDX was performed using Link Isis series 300 program.

Thermogravimetric analysis: TGA was performed using a TA instruments SDT Q 600 analyzer. The samples of 10–20 mg and temperature ramping from 298 to 873 K at 5 K min^{-1} were used in the operation. The carrier gas was N_2 UHP.

Raman spectroscopy: The Raman spectra of the samples were collected by projecting a continuous wave YAG lasers of neodymium (Nd) red (810 nm) through the samples at room temperature. A scanning range of 100–1000 cm^{-1} with a resolution of 2 cm^{-1} was applied.

FTIR spectroscopy: FTIR was conducted on a NICOLET series 6700 instruments. The supports (1 mg) were mixed with 100 mg KBr. About 400 scans were accumulated for each spectrum in transmission with a resolution of 4 cm^{-1}. The spectrum of dried KBr was used as a background subtraction.

2.7.3. Characterization of polymer

Scanning electron microscopy and energy dispersive X-ray spectroscopy: SEM and EDX were performed to study morphologies of polymer produced. The same equipment as mentioned above was employed.

Differential scanning calorimetry: DSC thermal analysis measurements were performed using a PerkinElmer DSC P7 calorimeter. The DSC measurements reported here were recorded during the second heating/cooling cycle with the rate of 20 K min^{-1}. This procedure

ensured that the previous thermal history was erased and provided comparable conditions for all samples. Approximately 10 mg of sample was used for each DSC measurement.

3. Results and discussion

In this present study, the effects and roles of various supported-dMMAOs and solvents on catalytic activities using titanium complex having two phenoxy-imine catalyst systems are discussed as follows.

3.1. Characteristics of the different supports and supported-dMMAOs

First, the different supports before and after impregnation with dMMAO were characterized using many characterization techniques. It was observed that the XRD patterns of the pure TiO_2 indicated only the characteristic peaks of anatase TiO_2 at 25 (major), 37, 48, 55, 56, 62, 71, and 75°. It is apparent that the pure silica shown a broad XRD peak assigning to conventional amorphous silica. The XRD patterns of mixed TiO_2–SiO_2 supports exhibited the combination of mixed TiO_2–SiO_2 supports. Raman spectra of supports are shown in Fig. 1. It was found that the titania support exhibited the Raman band at 639, 516, and 397 cm^{-1} for titania in anatase form as seen in the literatures [23–25], whereas silica was Raman-insensitive over the scanning range applied. FTIR spectra of the different supports are shown in Fig. 2. Pure silica exhibited a typical spectrum of amorphous silica. The band at 1100 cm^{-1} was the asymmetrical vibration of the Si—O—Si bond in the tetrahedral SiO_4 unit of the SiO_2 matrixes [26]. A broad peak centered at around 650 cm^{-1} represented the presence of titanium oxide [27] appeared with the introduction of Ti species. A broad peak at 1100 cm^{-1} appeared for the mixed TiO_2–SiO_2 supports showed the combination of mixed TiO_2–SiO_2 supports. This band had been ascribed to the vibration involving a SiO_4 tetrahedron bonded to a titanium atom through Si—O—Ti bonds [28]. The presence of this band confirmed the presence of Si—O—Ti linkages in the TiO_2–SiO_2 mixed supported. In order to determine the morphologies and elemental distribution of the supports after impregnation with dMMAO, SEM and EDX were performed, respectively. The SEM and EDX mapping of the different supports are shown in Fig. 3. The EDX mapping of the supports can provide more information about the distribution on each supports. It can be observed that dMMAO was well distributed all over support granules. In addition, the EDX measurement was also used to determine the concentrations of $[Al]_{dMMAO}$ present on different supports with the EDX spectrum obtained as seen in Fig. 4. It was found that the average amount of $[Al]_{dMMAO}$ on TiO_2, TiO_2–SiO_2 and SiO_2 were 11.07, 10.29, and 9.11 wt.%, respectively. The larger amount of $[Al]_{dMMAO}$ present in the TiO_2 can be attributed to the strongest interaction among other supports.

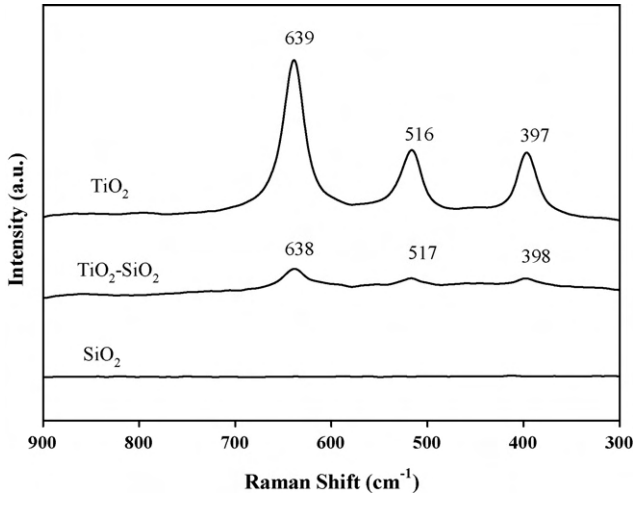

Fig. 1. Raman spectra of different supports before impregnation with dMMAO.

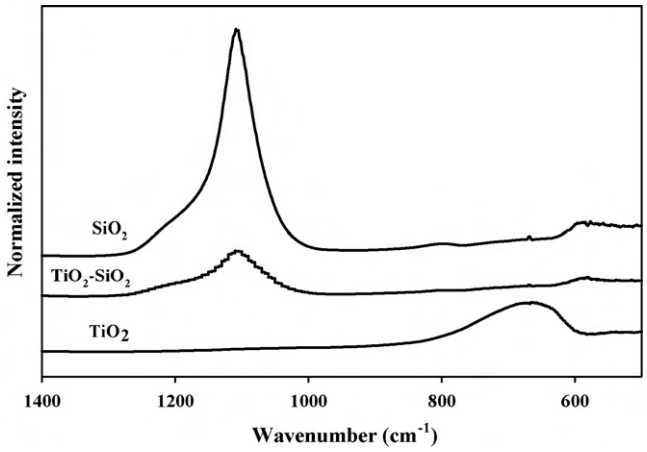

Fig. 2. FTIR spectra of different supports.

3.2. Effect of supports on the catalytic activity

For comparative studies, the catalytic activities towards the polymerization of ethylene upon different supported-dMMAOs were measured. The results are summarized in Table 1. The activities of the supported system were lower than the homogeneous one, as expected. However, considering only the supported system, it was found that activities were in the order of: TiO_2 > TiO_2–SiO_2 > SiO_2. It is well known that, the supported system exhibited lower activity than the homogeneous one due to the supporting effect. Among the supported system, the TiO_2 showed the highest activity (entry 2; 4286 kg PE/(mol cat h)), which was unusual for available literature reports. It was reported that the lowest polymerization activity obtained from zirconocene using the TiO_2 support was due to strong support interaction [21,25,29]. However, based on our results, the polymerization activity obtained from TiO_2 was the highest. This indicated that besides the surface concentration of $[Al]_{dMMAO}$, the interactions between the $[Al]_{dMMAO}$ and different support were quite important. In fact, the strong interaction of species with TiO_2 or other supports employed in this study was referred to the interaction between the support and the cocatalyst (dMMAO). Based on this study, dMMAO was dispersed by impregnation onto the support prior to polymerization. The degree of interaction between the support and dMMAO can be determined by the TGA measurement. In order to give a better understanding, we propose the interaction of support and dMMAO based on the review paper by Severn et al. [30]. They explained that the connection of the support and cocatalyst occurred via the $O_{support}$–$Al_{cocatalyst}$ linkage. In particular, the TGA can only provide useful information on the degree of interaction for the dMMAO bound to the support in terms of weight loss and removal temperature. The stronger interaction can result in decreased leaching of dMMAO bound to the different supports to react with the titanium complex catalyst during activation processes, leading to higher catalytic activity for polymerization. It has long been known that the TiO_2 support is known to have a strong interaction with species present on it. The TGA measurement was performed in order to prove interaction between the $[Al]_{dMMAO}$ and various supports as shown in Fig. 5. We can observe the similar profiles for different sup-

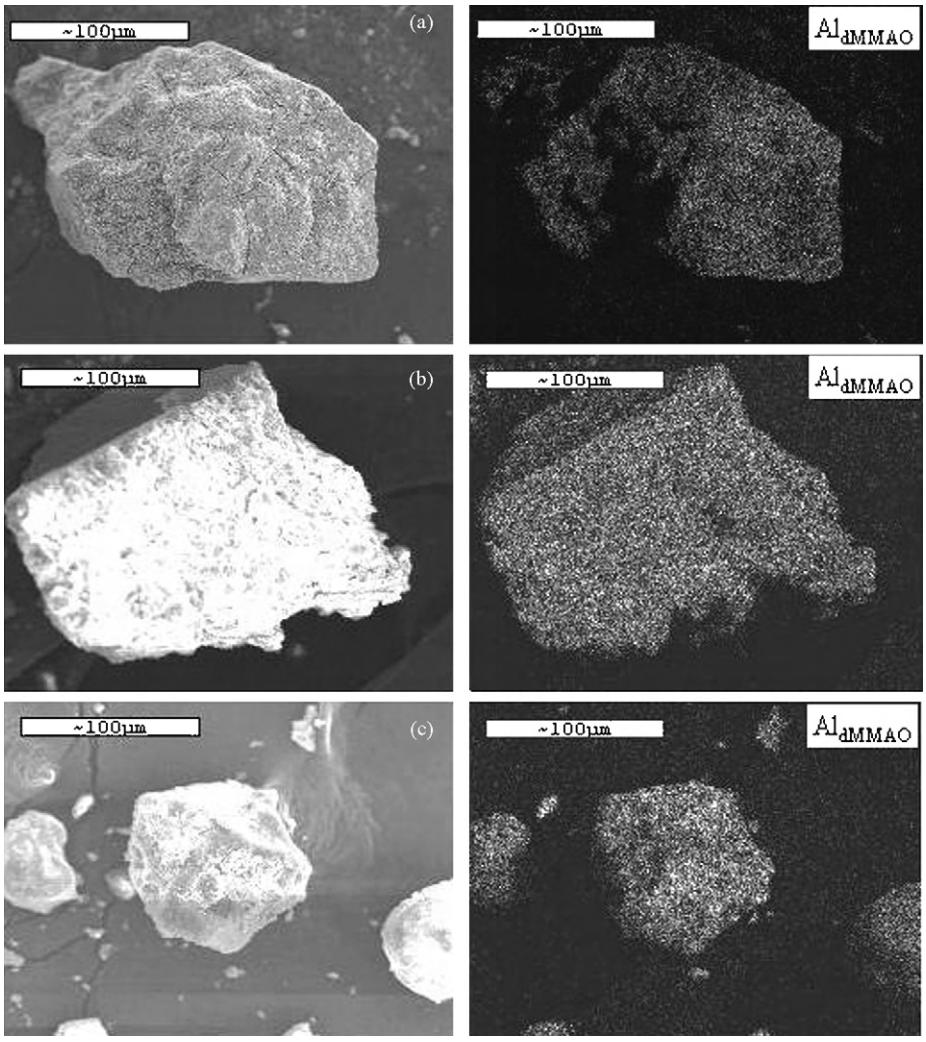

Fig. 3. SEM and EDX mapping of different supports: (a) TiO_2, (b) TiO_2–SiO_2, and (c) SiO_2.

ports. It demonstrated that the weight losses of $[Al]_{dMMAO}$ present on different supports were in order to of SiO_2 (22%) > TiO_2–SiO_2 (19.65%) > TiO_2 (16.36%). This indicated that $[Al]_{dMMAO}$ present on TiO_2 had the strongest interaction and thus, the highest observed polymerization activity. Morever, in the case of TiO_2–SiO_2 support, it had stronger interaction than that of SiO_2, therefore it exhibited higher polymerization interaction due to higher concentrations of $[Al]_{dMMAO}$ at surface as mentioned above. Besides, the presence of

Table 1
Polymerization[a] results

Entry	System	Solvent	Polymerization time (s)	Polymer Yield[b] (g)	Activity (kg PE/(mol cat h))	T_m[c] (K)
1	Homogeneous	Heptane	143	0.449	4521	409
2	TiO_2 support		150	0.446	4286	407
3	SiO_2–TiO_2 support		169	0.449	3828	406
4	SiO_2 support		174	0.407	3372	406
5	Homogeneous	Toluene	128	0.461	5186	406
6[d]	Homogeneous		151	0.452	4310	406
7	TiO_2 support		226	0.444	2828	406
8	SiO_2–TiO_2 support		244	0.470	2782	406
9	SiO_2 support		270	0.441	2350	406
10	Homogeneous	CB	290	0.444	2205	406
11	TiO_2 support		318	0.476	2156	407
12	SiO_2–TiO_2 support		400	0.480	1727	406
13	SiO_2 support		428	0.489	1646	406

[a] Polymerization condition: [Ti] = 2.5 μmol, $[Al]_{dMMAO}$/[Ti] = 250, temperature of polymerization = 323 K.
[b] The polymer yield was fixed by limiting the ethylene fed (0.018 mole equally).
[c] Melting temperature was measured by DSC analysis.
[d] Polymerization condition: [Ti] = 2.5 μmol, $[Al]_{MMAO}$/[Ti] = 250, temperature of polymerization = 323 K.

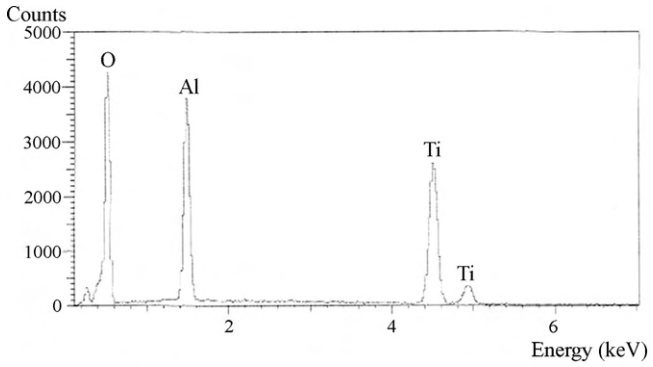

dMMAO/Supported	$[Al]_{dMMAO}$ (wt%) on the support
$dMMAO/TiO_2$	11.07
$dMMAO/TiO_2{-}SiO_2$	10.29
$dMMAO/SiO_2$	9.11

Fig. 4. A typical spectrum of the supported-dMMAO from EDX analysis used to measure the average $[Al]_{dMMAO}$ concentration on different supports.

TiO_2 in SiO_2 as a spacer group was also responsible for higher activity [20,31]. Furthermore, several researchers reported that TiO_2 had more active species being present during polymerization and removed residual hydroxyl groups from TiO_2 particles resulted in significant increases in catalytic activity of olefin polymerization [32]. Based on the observed polymerization activities, it is worth noting that in order to obtain the high polymerization activity, ones need to consider on high concentration of $[Al]_{dMMAO}$ present and the interaction between $O_{support}$ and $Al_{cocatalyst}$ linkage.

In order to obtain more detailed aspects on catalytic activity in the supported-dMMAO system, we consider the structure of titanium complex catalyst, which has large structure due to two phenoxy-imine ligands as shown on the review paper by Matsui et al. [33]. It is known that an active species of group 4 transition metal complexes for olefin polymerization is an alkyl cationic complex having two available *cis*-locate sites needed for polymerization [34]. It was generated by reaction of catalyst precursors such as dichloro complex with alkylaluminum compound. Therefore, the different supported-dMMAOs as catalyst precursors have shown remarkable effects on the catalytic activity of olefin polymerization. In contrast, we believe that the Al of dMMAO leached from different supports during activation processes caused the lesser amount of active species for polymerization. This hypothesis can be confirmed by the comparative study on catalytic activities between TiO_2 and SiO_2 supports, where the use of SiO_2 as support resulted in low catalytic activity due to more leached Al than that of TiO_2. Furthermore, Matsui et al. [33] reported that the high activity displayed by titanium complex resulted from the fact that a phenoxy-imine ligand possessed moderate electron donating properties and at the same time an active species of the complex had two available *cis* located sites needed for polymerization.

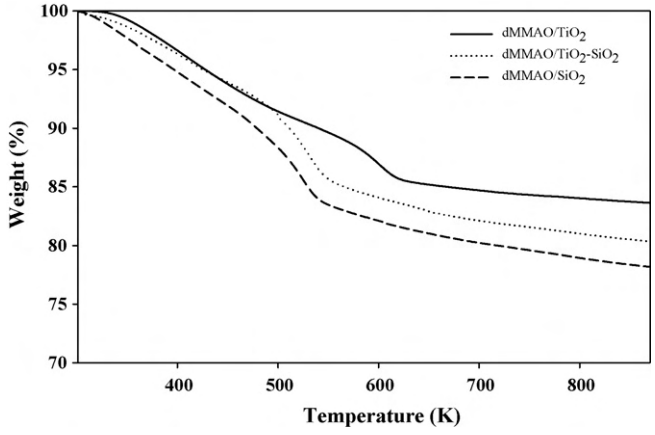

Fig. 5. TGA profiles of supported-dMMAO on different supports.

In order to compare the catalytic activity between MMAO and dMMAO, ethylene polymerization using different cocatalysts were conducted. It was observed that combination of titanium complex with dMMAO in toluene showed a higher catalytic activity than that with MMAO as shown in Table 1 (entry 5 and 6). Bryliakov et al. [35] reported that homogeneous polymerizations of α-olefins with the titanium FI-catalysts (titanium complex) were very sensitive towards trimethylaluminum (TMA), which was always included in the cocatalyst modified methylaluminoxane (MMAO). The amount of free TMA in the MMAO solution can be reduced by removing toluene from the cocatalyst to give a white powder (dMMAO). Additionally, Makio et al. [13] reported that FI-catalysts (titanium complex) were not only sensitive to the addition of TMA, but also to the triisobutylaluminum (TIBA), which was used as scavenger for water and impurities during polymerization. TIBA can attack the imine function of the ligands and reduce it to an amine. Dried modified methylaluminoxane (dMMAO) prepared from mixture of trimethylaluminum (TMA) and triisobutlyaluminum (TIBA) can also be used as an activator in case of titanium complex catalyst.

3.3. Effect of solvent on the catalytic activity

Ethylene polymerization was conducted in solvent medium that have different dielectric constant values (ε). The dielectric constant (ε) increases in the following order: heptane ($\varepsilon = 1.92$) < toluene ($\varepsilon = 2.38$) < chlorobenzene ($\varepsilon = 5.68$) < dichloromethane ($\varepsilon = 8.93$)

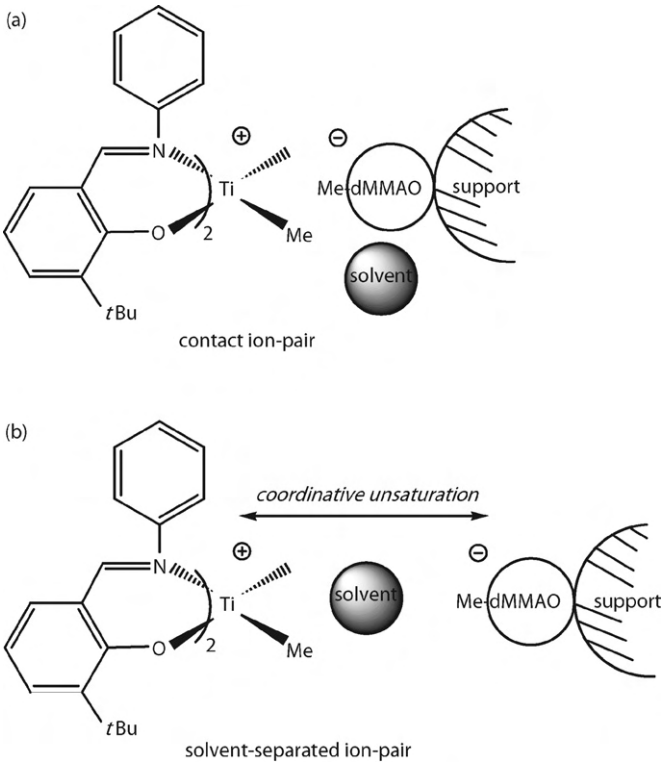

Scheme 1. A plausible scheme for the interaction between active species and solvent in the supported system: (a) active species in heptane and (b) active species in polar solvents.

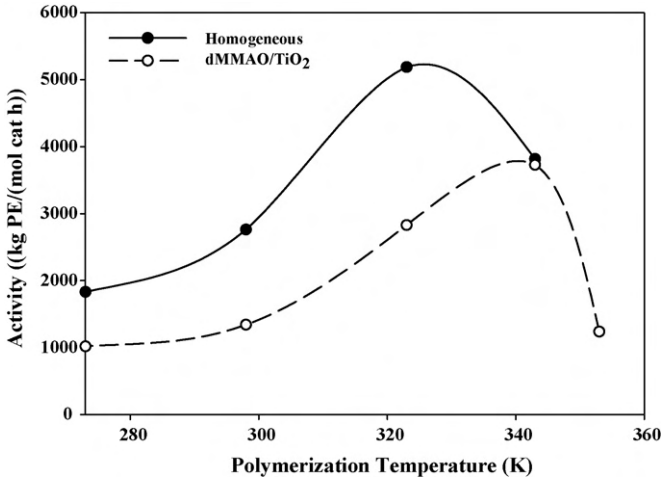

Fig. 6. Temperature dependence of polymerization activity obtained with titanium complex-dMMAO.

[36]. The catalytic activities based on polymer yield are shown in Table 1. For ethylene polymerization in homogeneous system, it was found that when using toluene as the polymerization medium, activity was the highest (entry 5; 5186 kg PE/(mol cat h)) followed by heptane (entry 1; 4521 kg PE/(mol cat h)) and chlolobenzene (entry 10; 2205 kg PE/(mol cat h)), respectively. No activity was observed when dichloromethane was employed. This indicated that the too high dielectric constant of solvent apparently resulted in such a low or no activity. Forlini et al., [37,38] also reported that the dielectric constant value of solvent could alter the polymerization behavior in other catalytic systems. In all cases, the polymerization did not proceed with the use of dichloromethane as a solvent medium. In the case of the supported system, activities are listed in Table 1. It was found that using heptane (entry 2; 4286 kg PE/(mol cat h)) as the polymerization medium gave the highest activity in all supports followed by toluene and dichlorobenzene, respectively.

It should be noted that the major factor to be considered besides the solvent polarity is the solubility of ethylene up on different solvents. Hence, the solubility of ethylene at polymerization temperature in different solvents was essentially important. Intaragamjon et al., [39] also reported that there was no variation in solubility of ethylene in the various solvents. Thus, the solubility of ethylene was not significant change regarding activity of ethylene polymerization in both homogeneous and supported systems. On the other hand, the catalytic activities observed were attributed to the solvent polarity itself.

In order to obtain more detailed aspects on effect of solvent on catalytic activity, the conceptual model of solvent effect was redrawn based on the work done by Ziegler group [40]. In general, in non-polar solvent, the dominant species is the contact ion-pair, whereas for the aromatic solvent, there are solvent separated ion-pair and solvent complexed cation. Based on the plausible reaction of the contact ion-pair model, the following considerations regarding to the solvent effect can be proposed: (i) considering in homogeneous system, the polarity of solvent greatly affected the polymerization activity. The solvent effect is based on the types of ion-pair formed. The higher activity observed in toluene was not only the reflex of ion-pair separation. In general, chlorinated

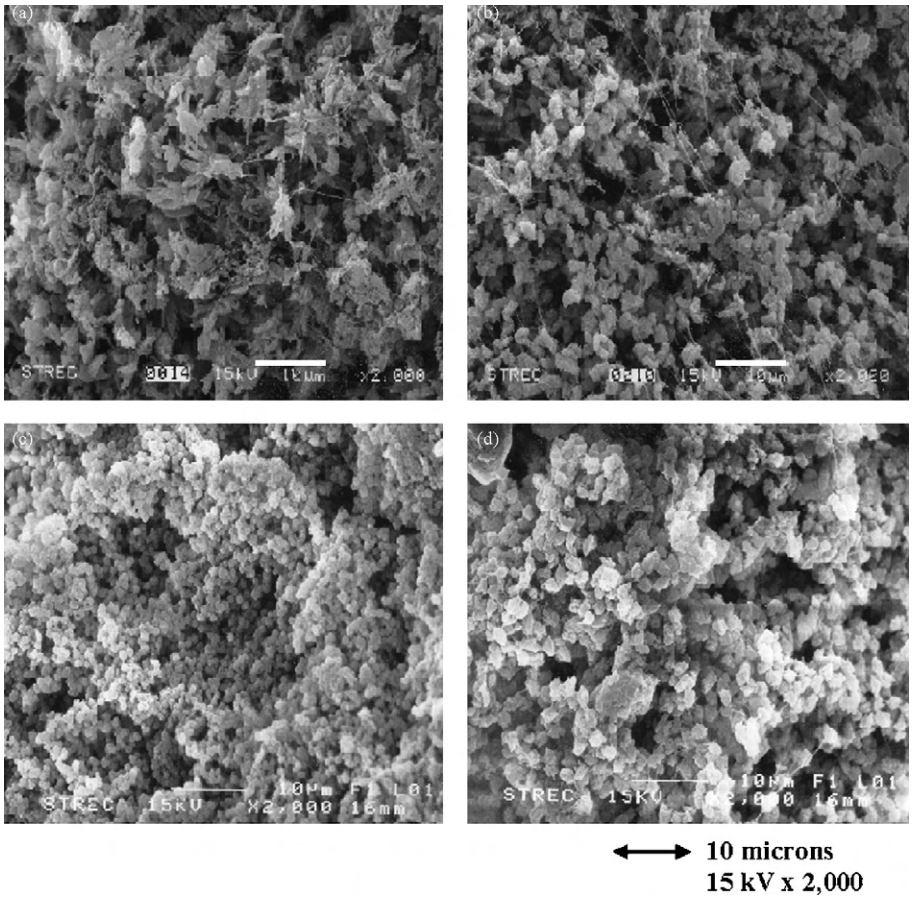

Fig. 7. SEM micrographs of polymers produced from: (a) homogeneous system, (b) TiO_2 support, (c) SiO_2 support, and (d) TiO_2–SiO_2 support.

solvents favor ion-pair separation. The reason why the activity in these solvents is lower is most probably due to solvent coordination. On the other hand, the lower activity in haptane may reflect the lower solubility of the cationic catalyst and may not be reduced to ion-pair separation, and (ii) for the supported system, heptane gave the highest activity since the interaction between cationic and solvent was less than the interaction between cationic, anionic and monomer in the system. Plausible scheme for the interaction between active species and solvent are shown in Scheme 1 indicating (a) active species in heptanes, which is shown the effect of contact ion-pair having low dielectric constant and (b) active species in polar solvents, which is shown the effect of solvent-separated ion-pair. Therefore, the less polarity of solvent resulted in high polymerization activity.

3.4. Effect of polymerization temperature on the catalytic activity

Fig. 6 shows the dependence of temperature on the catalytic activity. The effect of polymerization temperature via titanium complex with dMMAO was studied and the results obtained were compared with dMMAO/TiO_2-supported system. Profiles in Fig. 6 reveal that both homogeneous and supported systems exhibit a volcano shape. It indicated that the homogeneous system displayed higher catalytic activity than that of supported system in all temperature. This system gave maximum catalytic activity at polymerization temperature at 323 K (5186 kg PE/(mol cat h)). In contrast dMMAO/TiO_2-supported system exhibited the highest catalytic activity at 343 K (3727 kg PE/(mol cat h)). The catalytic activity decreased with increasing temperature probably due to the decomposition of the active species because of loss of the phenoxy-imine ligands from the titanium complex [13]. In fact, several mechanisms have been identified as decomposition pathways for cationic group 4 metal cations. Thus, based on this work it can be only concluded that the active species is thermaly unstable.

3.5. Properties of polymer

3.5.1. SEM of polymers

Fig. 7 reveals that the polyethylene produced by the titanium complex with different supports, displays morphologies with well-defined particles, whereas that obtained from the homogeneous system exhibits ill-defined polymer morphologies. This observation indicates that the titanium complex immobilized on the surface of the different supports and hence, the polymerization takes place on the solid surface. It is known that the morphology of the polymer particles can be controlled by shapes of the support used [41].

3.5.2. Thermal properties

Results of thermal behavior of polyethylene obtained from the differential scanning calorimetry (DSC) are shown in Table 1. These results suggested that for ethylene polymerization, the melting temperature (T_m) ranged between 407 and 409 K. It indicated that there was no significant change in melting temperature (T_m) upon different supports and solvents used.

4. Conclusion

In summary, we have demonstrated that the titanium complex having phenoxy-imine ligands (Ti–FI catalysts) can be activated using different supported-dMMAOs to give high-performance catalysts for the ethylene polymerization. It shows that the homogeneous catalyst displayed higher catalyst activity than that of the supported system. The Ti–FI catalysts are capable of producing the highest polymerization activity when TiO_2/dMMAO was employed. In addition, the Ti–FI catalysts can alter polymerization activity with different mediums employed. In order to give a better explanation, the contact ion-pair model under the typical polymerization condition was applied. There was no significant effect of different supports and solvents on the thermal properties of polymer obtained.

Acknowledgements

The authors gratefully acknowledge the Thailand Research Fund (TRF, RMU50-B. Jongsomjit), the graduate school of Chulalongkorn University and Bangkok Polyethylene Public Company Limited for the financial support of this work.

References

[1] K. Soga, T. Shiono, Prog. Polym. Sci. 22 (1997) 1503.
[2] S. Robinson, Chem. Ind. 12 (2001) 377.
[3] B.A. Krentsel, Y.V. Kissin, V.J. Kleiner, L.L. Stotskaya, Polymers and Copolymers of Higher α-Olefins, Hanser/Gardner Publication, Cincinnati, 1997.
[4] H. Sinn, W. Kaminsky, Adv. Organomet. Chem. 18 (1980) 99.
[5] H. Van der Heijden, B. Hessen, A.G. Orpen, J. Am. Chem. Soc. 120 (1998) 1112.
[6] P.J. Shapiro, W.D. Cotter, W.P. Schaefer, J.A. Labinger, J.E. Bercaw, J. Am. Chem. Soc. 116 (1994) 4623.
[7] L.K. Johnson, S. Mecking, M.S. Brookhart, J. Am. Chem. Soc. 118 (1996) 267.
[8] M. Killian, D.J. Temple, L.K. Johnson, S. Brookhart, J. Am. Chem. Soc. 118 (1996) 11664.
[9] B.L. Small, M.S. Brookhart, A.A. Bennett, J. Am. Chem. Soc. 120 (1998) 4049.
[10] G.J.P. Britovsek, V.C. Gibson, B.S. Kimberley, J. Maddox, S.J. McTavish, G.A. Solan, A.P. White, D. Williams, Chem. Commun. 7 (1998) 849.
[11] J.D. Scollard, D.H. McConville, N.C. Payne, J.J. Vital, Macromolecules 29 (1996) 5241.
[12] W.M. Davis, R.R. Schrock, J. Am. Chem. Soc. 119 (1997) 3830.
[13] H. Makio, N. Kashiwa, T. Fujita, Adv. Synth. Catal. 344 (2002) 477.
[14] S. Matsui, T. Fujita, Catal. Today 66 (2001) 61.
[15] L. Wang, W.H. Sun, L. Han, Z. Li, Y. Hu, C. He, C. Yan, J. Organomet. Chem. 650 (2002) 59.
[16] W.H. Sun, H. Yang, Z. Li, Y. Li, Organometallics 22 (2003) 3678.
[17] S. Jungling, S. Klotzenburg, R. Mulhaupt, J. Polym. Sci. A: Polym. Chem. 35 (1997) 1.
[18] G.G. Hlatky, D.J. Upton, Macromolecules 29 (1996) 8019.
[19] S.J. Conway, J.W. Falconer, C.H. Rochester, J. Chem. Soc., Faraday Trans. 185 (1989) 71.
[20] B. Jongsomjit, S. Ngamposri, P. Praserthdam, Catal. Lett. 100 (2005) 139.
[21] H. Hagimoto, T. Shiono, T. Ikeda, Macromol. Chem. Phys. 205 (2004) 19.
[22] J. Saito, M. Matita, S. Matsui, Y. Tohi, H. Makio, T. Nakano, H. Tanaka, N. Kashiwa, T. Fujita, Macromol. Chem. Phys. 203 (2002) 59.
[23] B. Jongsomjit, C. Sakdamnuson, J.G. Goodwin Jr., P. Praserthdam, Catal. Lett. 94 (2004) 209.
[24] B. Jongsomjit, T. Wongsalee, P. Praserthdam, Mater. Chem. Phys. 97 (2006) 343.
[25] C. Ketloy, B. Jongsomjit, P. Praserthdam, Appl. Catal. A: Gen. 327 (2007) 270.
[26] R.J. Davis, Z. Liu, Chem. Mater. 9 (1997) 2311.
[27] H. Yamashita, S. Kawasaki, Y. Ichihashi, M. Harada, M. Takeuchi, M. Anpo, G. Stewart, M.A. Fox, C. Louis, M. Che, J. Phys. Chem. B 102 (1998) 5870.
[28] M. Andrianainarivelo, R. Corriu, D. Leclercq, P.H. Mutin, A. Vioux, J. Mater. Chem. 6 (1996) 1665.
[29] R. Riva, H. Miessuer, R. Vitali, G.D. Piero, Appl. Catal. A: Gen. 196 (2000) 111.
[30] J.R. Severn, J.C. Chadwick, R. Duchateau, N. Friederichs, Chem. Rev. 105 (2005) 4073.
[31] B. Jongsomjit, S. Ngamposri, P. Praserthdam, Ind. Eng. Chem. Res. 44 (2005) 9059.
[32] M. Smit, X. Zheng, J. Loos, J.C. Chadwick, C.E. Koning, J. Polym. Sci. A 43 (2005) 2734.
[33] S. Matsui, T. Fujita, Catal. Today 66 (2001) 63.
[34] P.A. Deck, C.L. Beswick, T.J. Marks, J. Am. Chem. Soc. 120 (1998) 1772.
[35] K.P. Bryliakov, E.A. Kravtsov, D.A. Pennington, S.J. Lancaster, M. Bochmann, H.H. Brintzinger, E.P. Talsi, Organometallics 20 (2005) 5660.
[36] R. Kleinschmidt, Y. Griebenow, G. Fink, J. Mol. Catal. A: Chem. 157 (2000) 83.
[37] F. Forlini, Z.Q. Fan, I. Tritto, P. Locatelli, Macromol. Chem. Phys. 198 (1997) 2397.
[38] F. Forlini, E. Princi, I. Tritto, M.C. Sacchi, F. Piemontesi, Macromol. Chem. Phys. 203 (2002) 645.
[39] N. Intaragamjon, T. Shiono, B. Jongsomjit, P. Praserthdam, Catal. Commun. 7 (2006) 721.
[40] M.S.W. Chan, K. Vanka, C.C. Pye, T. Ziegler, Organometallics 18 (1999) 4624.
[41] G. Fink, B. Steinmetz, J. Zechlin, C. Przybyla, B. Tesche, Chem. Rev. 100 (2000) 1377.

Available online at www.sciencedirect.com
ScienceDirect
Catalysis Communications 9 (2008) 1426–1431
CATALYSIS COMMUNICATIONS
www.elsevier.com/locate/catcom

A comparative study of SiO_2- and ZrO_2-supported zirconocene/MAO catalysts on ethylene/1-olefin copolymerization

Tipawan Pothirat, Bunjerd Jongsomjit *, Piyasan Praserthdam

Center of Excellence on Catalysis and Catalytic Reaction Engineering, Department of Chemical Engineering, Faculty of Engineering, Chulalongkorn University, Bangkok 10330, Thailand

Received 5 September 2007; received in revised form 8 November 2007; accepted 11 December 2007
Available online 23 December 2007

Abstract

In this present study, the use of silica and zirconia as a support for zirconocene/MAO catalyst for copolymerization of ethylene/1-olefin (1-hexene, 1-octene, and 1-decene) was investigated. First, MAO as the cocatalyst was impregnated onto the support. Then, copolymerization of ethylene/1-olefin was performed. It was found that the use of zirconia support showed promising activities compared to those of the silica. Increased activities can be attributed to higher amount of $[Al]_{MAO}$ present on the zirconia support coupled with strong interaction between the $O_{support}$–$Al_{cocatalyst}$ linkage. In addition, the use of zirconia also resulted in higher degree of 1-olefin insertion and decreased T_m of copolymers produced.

Keywords: Silica; Zirconia; Zirconocene; MAO; Copolymerization; Metallocene

1. Introduction

The discovery of metallocene catalyst along with a methylaluminoxane (MAO) cocatalyst essentially led to the development of the highly active for homogeneous polymerization of α-olefin [1,2]. It is obvious that these active metallocene catalysts can compete with the conventional Ziegler–Natta catalysts. In particular, these catalysts are also capable of producing a variety of polyethylene copolymers, all with different chain compositions and architecture. However, to apply metallocene catalysts in the modern gas phase and slurry olefin polymerization processes, they need to be heterogenized on a support.

As known, the homogeneous metallocene catalysts have two major disadvantages; (i) the lack of morphology control and (ii) reactor fouling. Therefore, binding these metallocene catalysts onto inorganic supports as supported metallocene catalysts can overcome those drawbacks. Many inorganic supports such as SiO_2, Al_2O_3, TiO_2 and $MgCl_2$ have been investigated [3–14]. It has been reported that silica is perhaps the most attractive support employed for supported metallocene catalysts so far. However, the properties of silica itself may not be completely satisfied for all purposes based on the polymerization activity and properties of the obtained polymers. In order to increase an efficiency of supported metallocene catalysts, the modification of silica can be made [9,12] or alternative supports would be further investigated. Among various inorganic supports, zirconia (ZrO_2) has been widely used in many areas of chemistry such as in ceramics and catalysis. As catalysts, it was found that zirconia exhibited high catalytic activities for isomerization of olefins [15] and epoxides [16]. It was also used for isosynthesis via hydrogenation of CO as well [17]. The application of zirconia as a catalyst support has shown promising results in various catalytic reactions such as CO_2 hydrogenation [18], CO oxidation [19], and Fischer–Tropsch reaction [20–23]. Although the properties of zirconia as a catalytic support are promising in different areas of catalytic reaction, there has not been

* Corresponding author. Tel.: +662 2186869; fax: +662 2186877.
E-mail address: bunjerd.j@chula.ac.th (B. Jongsomjit).

1566-7367/$ - see front matter © 2007 Elsevier B.V. All rights reserved.
doi:10.1016/j.catcom.2007.12.005

the literature reported on the use of zirconia as a support for metallocene catalytic system so far.

In this present study, the use of zirconia as a support for zirconocene/MAO catalyst for ethylene/1-olefins (1-hexene, 1-octene, and 1-decene) copolymerization was investigated and compared with that obtained from the conventional silica support. The properties of supports were characterized using N_2 physisorption, X-ray diffraction (XRD), scanning electron microscopy (SEM)/energy dispersive X-ray spectroscopy (EDX), and thermal gravimetric analysis (TGA). The obtained copolymers were further characterized by means of SEM/EDX, ^{13}carbon nuclear magnetic resonance (^{13}C NMR), and differential scanning calorimetry (DSC).

2. Experimental

All chemicals [silica gel (Fuji Silasia, Cariact P-10), zirconium (IV) oxide powder (Aldrich), toluene (EXXON), *rac*-ethylenebis(indenyl) zirconium dichloride, *rac*-Et(Ind)$_2$-ZrCl_2) (Aldrich), methylaluminoxane, MAO, 2.667 M in toluene (Tosoh Akso), trimethylaluminum, TMA [Al$(CH_3)_3$] 2.0 M in toluene (Nippon Aluminum Alkyls), 1-hexene, 99% (Aldrich), 1-octene, 98% (Aldrich), and 1-decene, 98% (Fluka Chemie)] were manipulated under an inert atmosphere using a vacuum glove box and/or Schlenk techniques.

2.1. Materials

First, the support (SiO_2 and ZrO_2) was heated under vacuum at 400 °C for 6 h. Then, 1 g of the heated support was reacted with the desired amount of MAO in 10 ml of toluene at ambient temperature for 30 min. The solid part was separated and washed five times with 20 ml of toluene, followed by drying in vacuum at room temperature to obtain the catalyst support precursor MAO/SiO_2 and MAO/ZrO_2.

2.2. Polymerization

The ethylene/1-olefin [(1-hexene, EH), (1-octene, EO), and (1-decene, ED)] copolymerization reactions were carried out in a 100 ml semi-batch stainless steel autoclave reactor equipped with a magnetic stirrer. At first, 0.2 g of the supported MAO ($[Al]_{MAO}/[Zr]_{cat} = 2270$) and 0.018 mole of 1-olefin along with toluene (to make the total volume of 30 ml) were put into the reactor. The desired amount of Et(Ind)$_2$ZrCl_2 (5×10^{-5} M) and TMA ($[Al]_{TMA}/[Zr]_{cat} = 2500$) was mixed and stirred for 5 min aging at room temperature, separately, then was injected into the reactor. The reactor was frozen in liquid nitrogen to stop reaction for 15 min and then the reactor was evacuated to remove argon. The reactor was heated up to polymerization temperature (70 °C). By feeding the fixed amount of ethylene (0.018 mole $\sim$ 6 psi) into the reaction mixtures, the ethylene consumption can be observed corresponding to the ethylene pressure drop. The polymerization reaction was stopped and the reaction time used was recorded when all ethylene (0.018 mole) was totally consumed. After all ethylene was consumed, the reaction was terminated by addition of acidic methanol (0.1% HCl in methanol) and stirred for 30 min. After filtration, the obtained copolymers denoted as EH, EO, and ED (white powder) were washed with methanol and dried at room temperature.

2.3. Characterization

2.3.1. Characterization of supports

N_2 physisorption: Measurement of BET surface area, average pore diameter and pore size distribution of supports were determined by N_2 physisorption using a Micromeritics ASAP 2000 automated system.

X-ray diffraction: XRD was performed to determine the bulk crystalline phases of samples. It was conducted using a SIEMENS D-5000 X-ray diffractometer with Cu Kα ($\lambda = 1.54439$ Å). The spectra were scanned at a rate of 2.4° min^{-1} in the range $2\theta = 20$–80°.

Scanning electron microscopy and energy dispersive X-ray spectroscopy: SEM and EDX were used to determine the sample morphologies and elemental distribution throughout the sample granules, respectively. The SEM of JEOL mode JSM-5800LV was applied. EDX was performed using Link Isis series 300 program.

Thermal gravimetric analysis: TGA was performed to prove the interaction between the $[Al]_{MAO}$ and various supports. It was conducted using TA Instruments SDT Q 600 analyzer. The samples of 10–20 mg and temperature ramping from 50 to 600 °C at 5 °C min^{-1} were used in the operation. The carrier gas was N_2 UHP.

2.3.2. Characterization of polymer

Scanning electron microscopy: SEM was performed to study morphologies of polymers produced. The same equipment as mentioned above was employed.

Differential scanning calorimetry: The melting temperature of ethylene/1-olefin copolymer products was determined with a Perkin–Elmer diamond DSC. The analyses were performed at the heating rate of 20 °C min^{-1} in the temperature range of 50–150 °C. The heating cycle was run twice. In the first scan, sample was heated and then cooled to room temperature. In the second, sample was reheated at the same rate, but only the results of the second scan were reported because the first scan was influenced by the mechanical and thermal history of samples.

Nuclear magnetic resonance: ^{13}C NMR spectroscopy was used to determine comonomer incorporation and polymer microstructure. Comparison of the positions of peak in the ^{13}C NMR spectrum of polymer sample with characteristic leads to identification of the sequence of the comonomer incorporation. The ^{13}C NMR spectra were recorded at 100 °C using BRUKER magnet system 400 MHz/54 mm. The copolymer solutions were prepared using 1,2-dichlorobenzene as solvent and benzene-d_6 for an internal lock.

3. Results and discussion

The study revealed differences in catalytic activities during copolymerization of ethylene/1-olefins [1-hexene (EH), 1-octene (EO), 1-decene (ED)] upon the use of silica and zirconia as the support for zirconocene/MAO catalyst. The BET surface areas obtained from the N_2 physisorption of silica and zirconia employed were 193 and 17 $m^2\ g^{-1}$, respectively indicating that the silica had much higher surface area. The XRD patterns of the silica and zirconia supports prior to the MAO impregnation are shown in Fig. 1. It was observed that the silica exhibited a broad XRD peak between ca. 10° and 30° assigning to the conventional amorphous silica. The zirconia support exhibited the XRD patterns of traditional zirconia support having the characteristic peaks of zirconia at 28.2° and 31.5° assigning to monoclinic phase in zirconia [17]. After impregnation

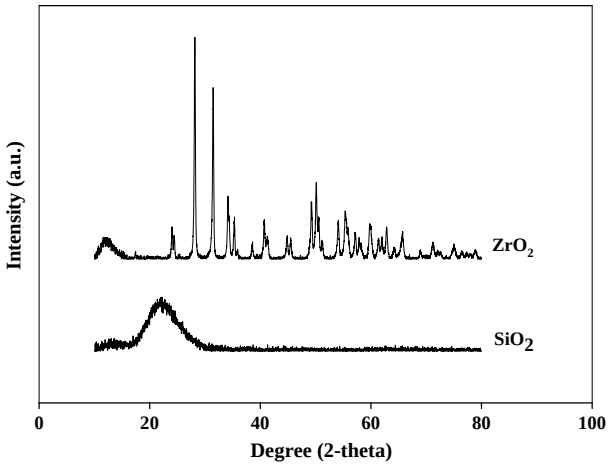

Fig. 1. XRD patterns of silica and zirconia supports prior to MAO impregnation.

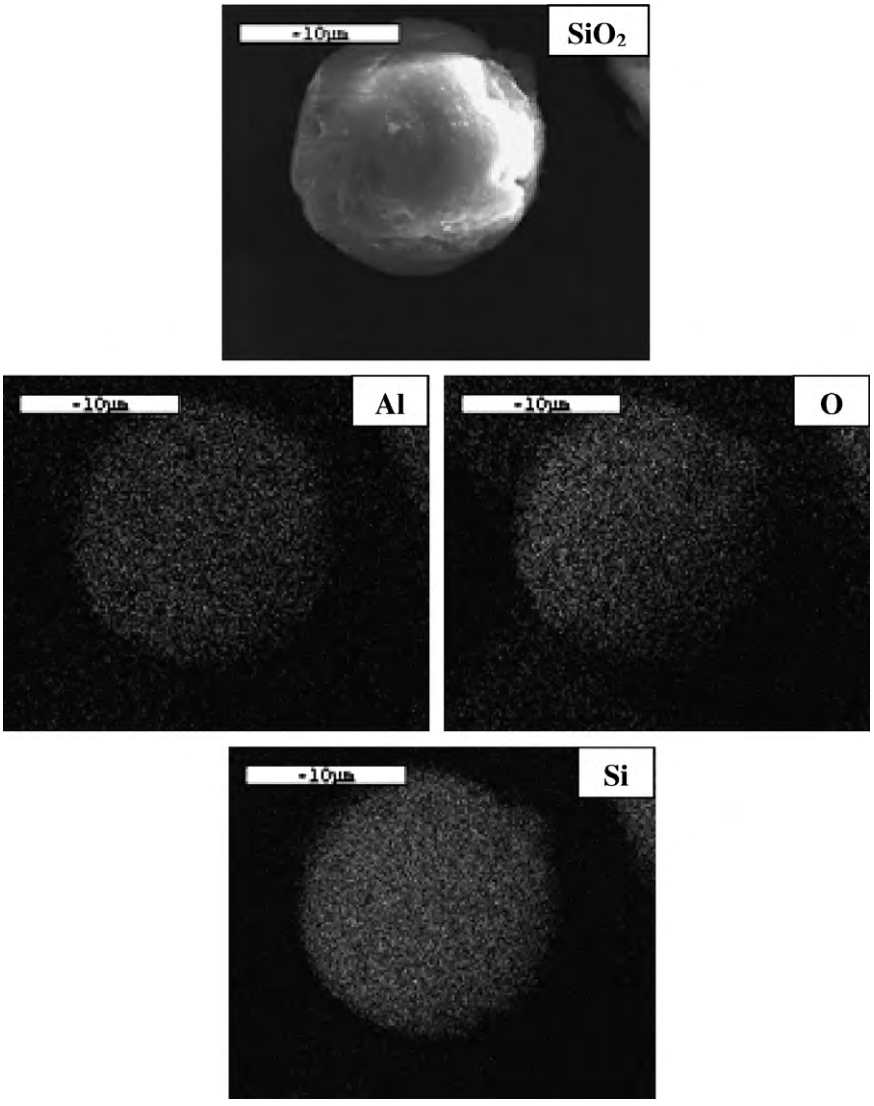

Fig. 2. EDX mapping of SiO_2-supported MAO.

with MAO, both supports also exhibited the similar XRD patterns as shown in Fig. 1 suggesting that MAO was well dispersed onto the supports. The morphologies and elemental distributions of the supports before and after impregnation with MAO were determined using SEM and EDX, respectively. The spherical shape for both supports was mainly observed. The distribution of all elements ($[Al]_{MAO}$, O, Si, or Zr) can be identified using the EDX mapping, especially to observe the distribution of $[Al]_{MAO}$ after impregnation. The EDX mapping of the SiO_2-supported MAO is shown in Fig. 2. It can be observed that the distribution for elements, especially for $[Al]_{MAO}$ was well dispersed all over the catalyst granule. The similar phenomenon was also found with the EDX mapping of the ZrO_2-supported MAO as seen in Fig. 3. In addition, the EDX measurement was also used to determine the concentration of $[Al]_{MAO}$ present on each support based on the EDX spectra. It was found that the amount of $[Al]_{MAO}$ present on the zirconia support (5.98 wt.%) was higher than that of the silica support (4.93 wt.%). This was suggested that the adsorption ability of MAO on zirconia was better than that on silica.

For a comparative study, the catalytic activities towards the copolymerization of ethylene/1-olefins upon the use of silica and zirconia supports were measured. The polymerization activities are shown in Table 1. It revealed that for all copolymers produced, the activities obtained from the zirconia support were higher than those obtained from the silica support about 10 times. The copolymerization of EO exhibited the highest activity among other comomers as also reported in our previous work [24] for the SiO_2-supported zirconocene/MAO. In the study, it was reported that for the in situ catalytic system, the copolymerization of ethylene with 1-octene resulted in the highest activity under similar polymerization condition used, suggesting that the optimum chain-size insertion was required. However, the effect of comomer used also depends on the support employed. It was found that with the use of mixed

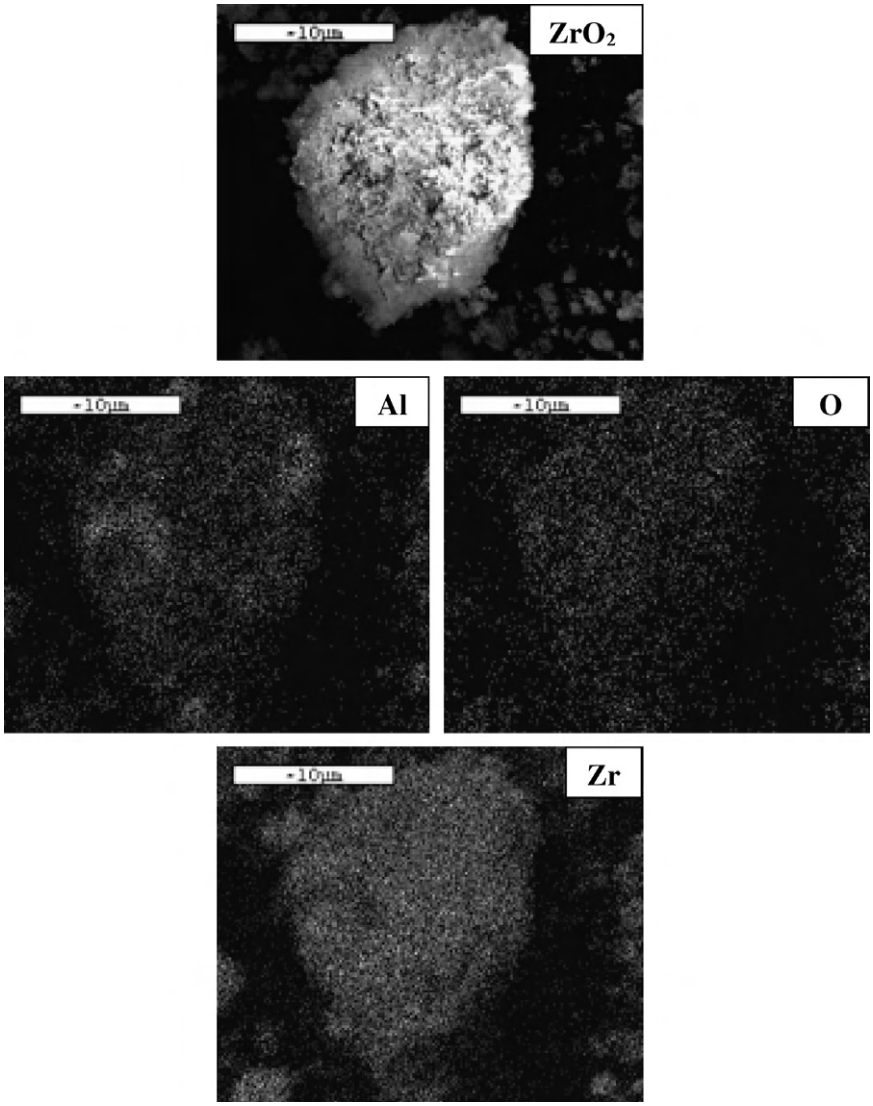

Fig. 3. EDX mapping of ZrO_2-supported MAO.

Table 1
Polymerization activities[a]

Support	Copolymer	Yield (g)	Polymerization time (sec)	Catalytic activity (kg polym mol^{-1} Zr h)
SiO_2	EH	0.5407	848	1530
	EO	0.6348	384	3968
	ED	0.8197	798	2465
ZrO_2	EH	1.2873	192	16091
	EO	1.2787	85	36104
	ED	1.5092	217	16692

[a] Activities were measured at polymerization temperature of 70 °C, [ethylene] = 0.018 mole, [1-olefin] = 0.018 mole, $[Al]_{MAO}/[Zr]_{cat}$ 2270, $[Al]_{TMA}/[Zr]_{cat} = 2500$, in toluene with total volume = 30 ml, and $[Zr]_{cat} = 5 \times 10^{-5}$ M.

SiO_2–TiO_2-supported zirconocene/MAO catalyst [25] under similar polymerization condition, the copolymerization of ethylene with 1-hexene exhibited the highest activity. This was due to more steric hindrance arising from the mixed oxide support. As the result, the short chain-size was preferred. The higher activities obtained from the zirconia support can be attributed to larger amount of MAO present on the support as measured by the EDX measurement. It should be noted that the amount of $[Al]_{MAO}$ on the zirconia support was only about 1.2 times higher than that on the silica support. However, the activities obtained from the zirconia support was dramatically higher (ca. 10 times) than those from the silica support. Thus, besides the high concentration of $[Al]_{MAO}$, it would be another factor that can enhance the catalytic activities for this specified system. It is worth noting that the interactions between $[Al]_{MAO}$ and the support are very important factor. Based on this study, $[Al]_{MAO}$ was dispersed onto both supports by impregnation method. The degree of interaction between the support and $[Al]_{MAO}$ can be determined using the TGA measurement [26]. To give a better understanding, we proposed the interaction of support and $[Al]_{MAO}$ based on the review paper by Severn et al. [27]. They explained that the connection of the support and cocatalyst occurred via the $O_{support}$–$Al_{cocatalyst}$ linkage. In particular, the TGA can only provide useful information on the degree of interaction for the $[Al]_{MAO}$ bound to the support in terms of weight loss and removal temperature. As a matter of fact, too strong interaction can result in it being more difficult for the $[Al]_{MAO}$ bound to the support to react with metallocene catalyst during activation processes, leading to low activity for polymerization. In contrast, the leaching of $[Al]_{MAO}$ can occur due to very weak interaction resulting in low activity as well. Hence, the optimum interaction between the $O_{support}$–$Al_{cocatalyst}$ linkage is crucial. Experimentally, the TGA measurement was performed to prove the interaction between the $[Al]_{MAO}$ and each support. The TGA profiles of $[Al]_{MAO}$ on each support are shown in Fig. 4 indicating the similar profiles for each support. We observed that the weight loss of $[Al]_{MAO}$ present on each support was in the order of SiO_2 (12.4%) > ZrO_2 (7.0%). This indicated that $[Al]_{MAO}$ present on the ZrO_2 support exhibited the stronger interaction than that on the SiO_2 support. Thus, based on the observed polymerization activities as listed in Table 1, it is worth noting that the higher activities obtained from the zirconia support can be attributed to both larger amount of $[Al]_{MAO}$ present coupled with stronger interaction between the $O_{support}$–$Al_{cocatalyst}$ linkage.

The obtained copolymers were further characterized using SEM, ^{13}C NMR, and DSC measurements. The typical SEM micrographs of polymers are shown in Fig. 5 indi-

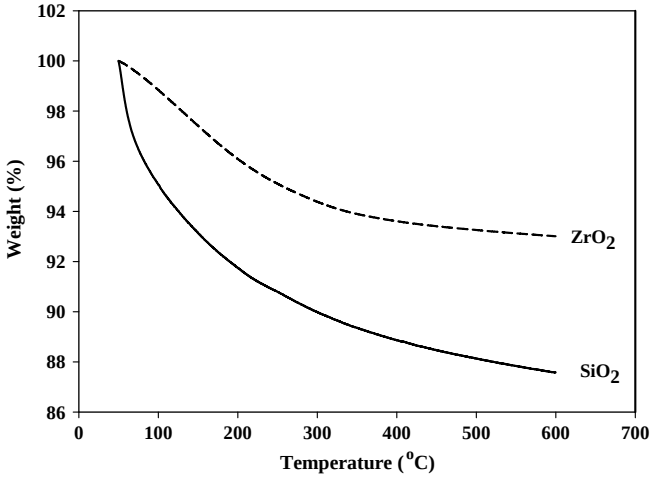

Fig. 4. TGA profiles of SiO_2- and ZrO_2-supported MAO.

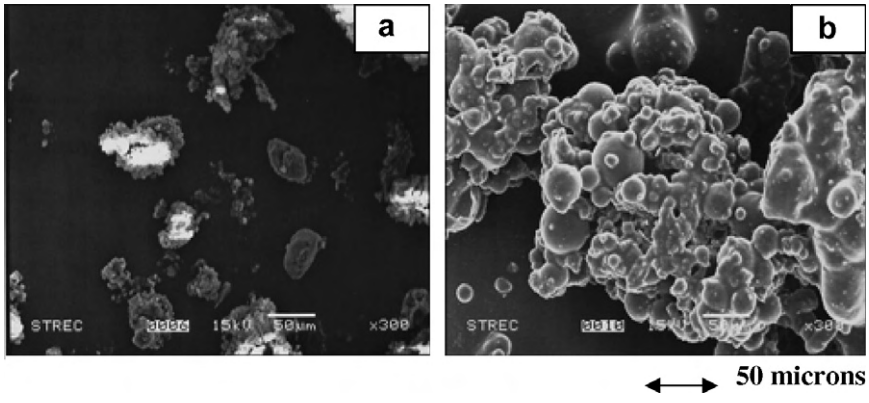

Fig. 5. SEM micrographs of EH copolymers obtained from (a) SiO_2 and (b) ZrO_2 supports.

Table 2
Triad distribution of EC copolymers[a] and their melting temperature (T_m)[b]

Support	Copolymer	CCC	ECC	ECE	EEE	CEE	CEC	%C insertion	T_m (°C)
SiO_2	EH	0	0	.107	.816	.077	0	10.6	89
	EO	0	0	.043	.855	.102	0	4.3	97
	ED	0	0	.061	.803	.136	0	6.1	92
ZrO_2	EH	0	0	.105	.717	.173	.005	12.2	75
	EO	0	0	.128	.637	.214	.021	13.7	84
	ED	0	0	.125	.587	.269	.019	12.5	N.o.[c]

[a] Obtained from ^{13}C NMR where C refers to the corresponding comonomer; H, O, and D.
[b] Obtained from DSC.
[c] Not observed.

cating the morphologies of EH copolymers obtained from the SiO_2 (a) and ZrO_2 (b). In fact, the copolymers obtained from the zirconia support seemed to agglomerate more. The quantitative analysis of triad distribution for all copolymers was conducted on the basis assignment of the ^{13}C NMR spectra [28]. The triad distribution for all copolymers is shown in Table 2. All copolymers produced from each support exhibited the similar distribution having the majority for the triad of EEE. Based on ^{13}C NMR, it was suggested that the microstructure of copolymers was not affected by the use of SiO_2 or ZrO_2 supports. However, considering the insertion of 1-olefins (Table 2), it was found that the use of zirconia apparently yielded higher degree of 1-olefin insertion. This was probably due to decreased steric hindrance for the zirconia support. In addition, the melting temperature (T_m) of copolymers was evaluated using DSC as also shown in Table 2. It revealed that T_m of copolymer trended to decrease with the use of zirconia as a support. The decreased T_m of copolymers was attributed to the increased degree of 1-olefin insertion, which was in agreement with the ^{13}C NMR results.

4. Conclusions

The use of zirconia as a support for a zirconocene/MAO catalyst under specified condition was promising based on increased polymerization activities. In particular, increased activities can be attributed to the high amount of $[Al]_{MAO}$ coupled with strong interaction between the $O_{support}$–$Al_{cocatalyst}$ linkage. The use of zirconia support also resulted in increased degree of 1-olefin insertion by means of ^{13}C NMR. This was probably due to a decrease in steric hindrance. In addition, the decreased T_m for copolymers obtained from the zirconia support was also observed, which was in agreement with the results obtained from ^{13}C NMR.

Acknowledgments

The authors thank the Thailand research fund (TRF) for RMU50-B. Jongsomjit, the National Research Council of Thailand (NRCT) and Thailand–Japan Technology Transfer Project (TJTTP-JBIC) for the financial support of this work. We extend our thankful to Professor Takeshi Shiono at Hiroshima University, Japan for his kind advice of this project.

References

[1] W. Kaminsky, M. Miri, H. Sinn, R. Woldt, Macromol. Chem. Rapid Commun. 4 (1983) 417.
[2] JA. Ewen, J. Am. Chem. Soc. 106 (1984) 6355.
[3] A.M. Uusitalo, T.T. Pakkanen, E.I. Iskola, J. Mol. Catal. A: Chem. 177 (2002) 179.
[4] K. Soga, M. Kaminaka, Macromol. Chem. 194 (1993) 1745.
[5] Y.S. Ko, T.K. Han, J.W. Park, S.I. Woo, Macromol. Rapid Commun. 17 (1996) 749.
[6] M. Margue, A. Conte, J. Appl. Polym. Sci. 86 (2002) 2054.
[7] P.G. Belelli, M.L. Ferreira, D.E. Damiani, Appl. Catal. A: Gen. 228 (2002) 132.
[8] A. Koppl, H.G. AH, J. Mol. Catal. A: Chem. 165 (2001) 23.
[9] B. Jongsomjit, P. Prasertham, P. Kaewkrajang, Mater. Chem. Phys. 86 (2004) 243.
[10] T. Rai, J.T. Ban, T. Uozumi, K. Soga, Macromol. Chem. Phys. 198 (1997) 229.
[11] P.H. Lee, K.B. Yoon, S.K. Noh, Macromol. Rapid Commun. 18 (1997) 427.
[12] B. Jongsomjit, P. Kaewkrajang, P. Praserthdam, Catal. Lett. 94 (2004) 205.
[13] B. Jongsomjit, S. Ngamposri, P. Praserthdam, Molecules 10 (2005) 603.
[14] B. Jongsomjit, S. Ngamposri, P. Praserthdam, Catal. Lett. 100 (2005) 139.
[15] Y. Nakono, T. Iizuka, H. Hattori, K. Tanabe, H. Hideshi, T. Kozo, J. Catal. 157 (1979) 1.
[16] K. Arata, K. Kato, K. Tanabe, Bull. Chem. Soc. Jpn. 49 (1976) 663.
[17] W. Khaodee, B. Jongsomjit, S. Assabumrungrat, P. Praserthdam, Catal. Commun. 8 (2007) 548.
[18] J.H. Bitter, K. Sechan, J.A. Lercher, J. Catal. 171 (1997) 279.
[19] W.P. Dow, T.J. Huang, J. Catal. 147 (1994) 322.
[20] G.K. Chuah, Catal. Today 49 (1999) 131.
[21] L. Bruce, J.F. Mathews, Appl. Catal. A: Gen. 4 (1982) 353.
[22] D.I. Enache, M. Roy-Auberger, R. Revel, Appl. Catal. A: Gen. 268 (2004) 51.
[23] J. Panpranot, N. Taochaiyaphum, B. Jongsomjit, P. Praserthdam, Catal. Commun. 7 (2006) 192.
[24] B. Jongsomjit, P. Kaewkrajang, T. Shiono, P. Praserthdam, Ind. Eng. Chem. Res. 43 (2004) 7959.
[25] B. Jongsomjit, S. Ngamposri, P. Praserthdam, Ind. Eng. Chem. Res. 44 (2005) 9059.
[26] C. Ketloy, B. Jongsomjit, P. Praserthdam, Appl. Catal. A: Gen. 327 (2007) 270.
[27] J.R. Severn, J.C. Chadwick, R. Duchateau, N. Friedeichs, Chem. Rev. 105 (2005) 4073.
[28] J.C. Randall, J. Macromol. Sci. Rev. Macromol. Chem. Phys. C29 (1989) 201.

Catalysis Communications 10 (2008) 118–122

Contents lists available at ScienceDirect

Catalysis Communications

journal homepage: www.elsevier.com/locate/catcom

Copolymerization of ethylene/1-octene via different pore sized silica-based-supported zirconocene/dMMAO catalysts

Pongsathorn Wongwaiwattanakul, Bunjerd Jongsomjit *

Center of Excellence on Catalysis and Catalytic Reaction Engineering, Department of Chemical Engineering, Faculty of Engineering, Chulalongkorn University, Bangkok 10330, Thailand

ARTICLE INFO

Article history:
Received 3 March 2008
Received in revised form 7 August 2008
Accepted 8 August 2008
Available online 14 August 2008

Keywords:
Metallocene
Polymerization catalyst
LLDPE
Silica
Pore size

ABSTRACT

Here, the copolymerization of ethylene/1-octene with zirconocene/dMMAO catalyst using different pore sized silica-based supports was investigated. It revealed that the large pored silica [SiO_2 (LP)] exhibited the highest polymerization activity due to both highest amount of available active sites present along with the moderate interaction between dMMAO and the support. The strong interaction between dMMAO and the support as proven by TGA analysis apparently resulted in dramatically decreased polymerization activity for the bimodal pored silica–alumina [Si–Al (BP)]. The copolymers produced were further characterized by means of DSC and ^{13}C NMR. Although they exhibited the similar triad distribution, the degree of 1-octene insertion was different.

1. Introduction

Copolymerization of ethylene and 1-olefins such as 1-butene, 1-hexene, and 1-octene using metallocene catalyst has been extensively studied for the production of elastomers and linear low-density polyethylene (LLDPE). As known, LLDPE is one of the most important commercial polyolefins in petrochemical industry. Thus, it has been consumed consistently [1]. In fact, LLDPE produced by metallocene catalysts exhibits a narrow molecular weight distribution (MWD). However, it also has limitation in polymer processing due to the uniform chemical composition distributions (CCDS) or stereospecificity [2–4]. It is known that the heterogeneous metallocene catalyst system has advantages such as being able to control polymer morphologies, use in gas-phase and slurry polymerization, which is suitable for production of polyolefins on industrial scales, and also prevent a reactor fouling and slower deactivation [5,6].

Significant effort has also focused into heterogenizing the catalyst system by supporting the metallocene and cocatalyst onto mostly inorganic supports. The most common support materials are simple metal oxides, such as alumina, silica and titania, although zirconia and ceria also find applications [7]. The supports have been studied and modified continuously [8–12]. The different supports could vary the catalytic behaviors during reaction as well [13–17]. The influence of supported metallocene catalysts on polymer tacticity was investigated by Kaminsky and Winkelbach [18]. They reported that the silica-supported zirconocene exhibited the lower syndiotactic polypropylene compared with that obtained from the homogeneous system. A remarkable number of methods have been developed to prepare supported metallocene catalyst. In general, this fall in three classes [19]: (i) supporting the activator followed by reaction with the metallocene; (ii) supporting the metallocene, then reacting with the cocatalyst; and (iii) reacting a metallocene–cocatalyst mixture with the support. The former of supporting method is claimed to fix the activator onto the support, avoiding leaching into solution [20]. In order to maintain high catalytic activity for the zirconocene system, it was suggested that the cocatalyst should be first impregnated on the support and the zirconocene catalyst was then injected into the solution mixture [10,15].

Generally, the activity and selectivity of the polymerization catalyst are markedly dependent on their pore structure of support. In the slurry polymerization, effects of the support pore size have been studied [21–24]. The support with large surface area, however, usually contains small pore size, which results in poor intra-pellet diffusion efficiency of reactants and products, slow transportation of reactants and products [25]. Nevertheless, a catalyst with large pore size has a small specific surface area and is not beneficial to disperse support metal, leading to low metal dispersion. The distinct bimodal pore structure support, which contains large pores and small pores at the same time, provides pathways for rapid molecular transportation contributing to high diffusion efficiency as theoretically expressed by Levenspiel by the large pores [26] and contributes to higher dispersion of supported metal by the small pores, which enlarged the surface area

* Corresponding author. Tel.: +66 2 2186869; fax: +66 2 2186877.
E-mail address: bunjerd.j@chula.ac.th (B. Jongsomjit).

1566-7367/$ - see front matter © 2008 Elsevier B.V. All rights reserved.
doi:10.1016/j.catcom.2008.08.007

of the support. Furthermore, it is able to diminish the diffusion resistance by its large pores. In polymerization, the geometrical shapes of the nano-channels of support affect the pattern and activity of monomer insertion. Thus, the arrangement of polymer chain and polymer morphology can be controlled.

The present study has focused on effect of different pore sizes of silica supports used for the supported dMMAO with zirconocene catalyst for copolymerization of ethylene/1-octene. The different silica supports having large pore, small pore and bimodal pore of silica–alumina were studied. The copolymers produced were further characterized by means of DSC and ^{13}C NMR and discussed in more details.

2. Experimental

2.1. Materials

All chemicals and polymerization were operated under an argon atmosphere, using a glove box and/or Schlenk techniques. The small pore silica gel [Cariact P-10, denoted as SiO_2 (SP)] and large pore silica gel [Cariact Q-50, denoted as SiO_2 (LP)] were donated by Fuji Silasia Chemical Ltd., Japan. Aluminium nitrate and polyethylene glycol (PEG) were purchased by Aldrich Chemical Company, Inc. Toluene was dried over dehydrated $CaCl_2$ and distilled over sodium/benzophenone before use. The *rac*-ethylenebis (indenyl) zirconium dichloride (*rac*-Et[Ind]$_2$ZrCl$_2$) was supplied from Aldrich Chemical Company, Inc. Modified methylaluminoxane (MMAO) in hexane was donated by Tosoh (Akso, Japan). In this study, the dMMAO (dried MMAO) was employed since it gave higher activity than MMAO with zirconocene catalyst. Trimethylaluminum (TMA, 2 M in toluene) was supplied by Nippon Aluminum Alkyls, Ltd., Japan. Ultrahigh purity argon was further purified by passing it through columns that were packed with BASF catalyst R3-11G (molecular-sieved to 3 Å), sodium hydroxide (NaOH), and phosphorus pentaoxide (P_2O_5) to remove traces of oxygen and moisture. Ethylene gas (99.96% pure) was donated by the National Petrochemical Co., Ltd., Thailand. 1-octene (d = 0.715) was purchased from Aldrich Chemical Company, Inc.

2.2. Preparation of silica–alumina (Si–Al) bimodal pore supports

The Si–Al bimodal pore support denoted as Si–Al (BP) was synthesized according to the method described by Zhang et al. [27,28]. The Si–Al (BP) support was obtained by the incipient-wetness impregnation of the solution of aluminium nitrate. First, aluminium nitrate was dissolved in a 0.3 mol/l polyethylene glycol aqueous solution stirring at 353 K for 1 h. The solution was impregnated into silica gel (Cariact Q-50). The amount of alumina loading was 15 wt%. The support was dried at 383 K for 12 h and calcined in air at 673 K for 2 h.

2.3. Preparation of dried MMAO (dMMAO)

Removal of TMA from MMAO was carried out according to the reported procedure Ref. [29]. The toluene solution of MMAO was dried under vacuum for 6 h at room temperature to evaporate the solvent, TMA, and Al(iBu)$_3$ (TIBA). Then, continue to dissolve with 100 ml of heptane and the solution was evaporated under vacuum to remove the remaining TMA and TIBA. This procedure was repeated four times and the white powder of dried MMAO (dMMAO) was obtained.

2.4. Preparation of supported dMMAO

The support was reacted with the desired amount of dMMAO in 20 ml of toluene at room temperature for 30 min. The solvent was then removed from the mixture by evacuation. This procedure was done only once with toluene (20 ml × 1) and three times with hexane (20 ml × 3). Then, the solid part was dried under vacuum at room temperature. The white powder of supported cocatalyst (dMMAO/support) was then obtained.

2.5. Polymerization

Ethylene/1-octene copolymerization was carried out in a 100 ml semi-batch stainless steel autoclave reactor equipped with magnetic stirrer. In the glove box, the desired amounts of *rac*-Et[Ind]$_2$ZrCl$_2$ and TMA were mixed and stirred for 5 min aging. Then, toluene (to make a total volume of 30 ml) and desired amount of dMMAO/support were introduced into the reactor. After that, the mixture of *rac*-Et[Ind]$_2$ZrCl$_2$ and TMA were injected into the reactor. The reactor was frozen in liquid nitrogen to stop reaction and then 0.018 mol of 1-octene was injected into the reactor. The reactor was evacuated to remove argon. Then, it was heated up to polymerization temperature (343 K) and the polymerization was started by feeding ethylene gas (total pressure 50 psi in the reactor) until the consumption of ethylene 0.018 mol (6 psi was observed from the pressure gauge) was reached. The reaction of polymerization was terminated by addition of acidic methanol. The time of reaction was recorded for purpose of calculating the activity. The precipitated polymer was washed with methanol and dried at room temperature.

2.6. Characterization

2.6.1. Characterization of supports and catalyst precursor

N_2 physisorption: Measurement of BET surface area, average pore diameter and pore size distribution were determined by N_2 physisorption using a Micromeritics ASAP 2000 automated system.

X-ray diffraction: XRD was performed to determine the bulk crystalline phases of samples. It was conducted using a SIEMENS D-5000 X-ray diffractometer with CuK_α (λ = 1.54439 Å). The spectra were scanned at a rate of 2.4° min^{-1} in the range of 2θ = 10–80°.

Scanning electron microscopy and energy dispersive X-ray spectroscopy: SEM and EDX were used to determine the morphologies and elemental distribution throughout the sample granules, respectively. The SEM of JEOL mode JSM-6400 was applied. The EDX was performed using Link Isis series 300 program.

Thermogravimetric analysis: TGA was performed using TA Instruments SDT Q 600 analyzer. The samples of 10–20 mg and a temperature ramping from 298 to 500 K at 2 K min^{-1} were used in the operation. The carrier gas was N_2 UHP.

2.6.2. Characterization of polymer

^{13}C NMR spectroscopy: ^{13}C NMR spectroscopy was used to determine the triad distribution and 1-octene insertion indicating the copolymer microstructure. Chemical shift were referenced internally to the $CDCl_3$ and calculated according to the method described by Randall [30]. Sample solution was prepared by dissolving 50 mg of copolymer in 1,2,4-trichlorobenzene and $CDCl_3$. ^{13}C NMR spectra were taken at 333 K using BRUKER AVANCE II 400 operating at 100 MHz with an acquisition time of 1.5 s and a delay time of 4 s.

Differential scanning calorimetry (DSC): Thermal analysis measurements were performed using a Perkin-Elmer DSC P7 calorimeter. The DSC measurements reported here were recorded during the second heating/cooling cycle with the rate of 20 K min^{-1}. This procedure ensured that the previous thermal history was erased and provided comparable conditions for all samples. Approximately 10 mg of sample was used for each DSC measurement.

3. Results and discussion

3.1. Characteristics of supports and polymerization activity

In the present study, the different pore sized SiO_2-based supports were employed as supports for the supported zirconocene/dMMAO catalysts used for copolymerization of ethylene/1-octene. First, the different SiO_2 supports such as SiO_2 (LP), SiO_2 (SP) and Si–Al (BP) were prepared and characterized as mentioned in the experimental part. The surface areas, average pore diameter and pore volume for all different supports are listed in Table 1. The surface areas were ranged 72, 127, and 257 m^2/g for the SiO_2 (LP), Si–Al (BP), and SiO_2 (SP), respectively, corresponding to the average pore size of 33.8 nm for SiO_2 (LP), 3.8 and 33.6 nm for Si–Al (BP) and 13.7 nm for SiO_2 (SP). In order to identify the characteristics of pore size all supports, the pore size distribution profiles obtained from the N_2 physisorption are illustrated in Fig. 1. It was obvious that the SiO_2 (SP) and SiO_2 (LP) exhibited the unimodal pore size distribution, whereas the bimodal pore size distribution for Si–Al (BP) was evident. The XRD patterns (not shown) for all different supports before and after impregnation with dMMAO exhibited the similar XRD patterns indicating only a board peak between 20° and 30°, as seen typically for the conventional amorphous silica. No XRD peaks of dMMAO were observed after impregnation due to its highly dispersed form. After impregnation with dMMAO, the $[Al]_{dMMAO}$ content was also measured using EDX. The amounts of $[Al]_{dMMAO}$ were 18.9, 12.9, and 12.2 wt% for the SiO_2 (LP), SiO_2 (SP) and Si–Al (BP), respectively. Results showed that the SiO_2 (LP) exhibited the highest amount of $[Al]_{dMMAO}$ among other supports. The typical EDX mappings for distribution of $[Al]_{dMMAO}$ on different supports are shown in Fig. 2. As seen, all samples exhibited good distributions of Al without any changes in the support morphology.

Table 1
Characteristics of different SiO_2 supports

Support	BET surface area (m^2/g)	Average small pore diameter (nm)	Average large pore diameter (nm)	Pore volume(cm^3/g)
SiO_2 (LP)	72	–	33.8	0.26
SiO_2 (SP)	257	13.7	–	1.50
Si–Al (BP)	127	3.8	33.6	0.30

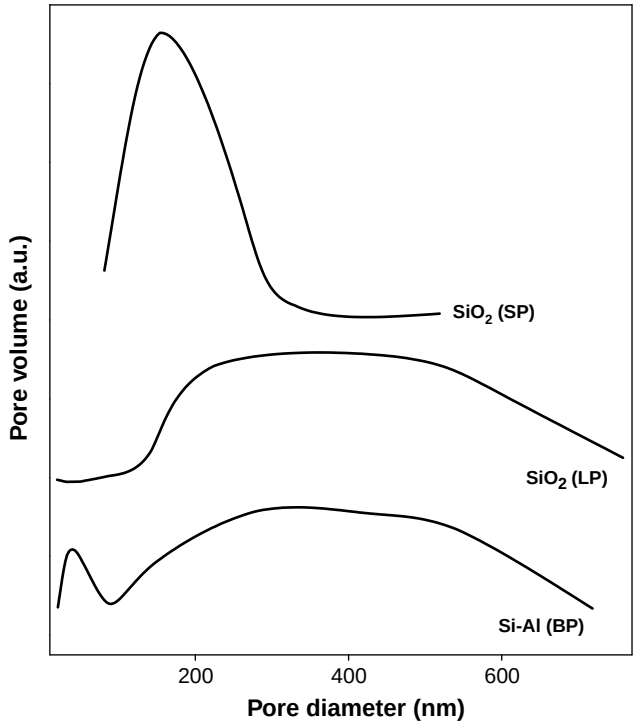

Fig. 1. Pore size distribution of different supports.

For comparative studies, the polymerization activities towards copolymerization of ethylene/1-octene upon the presence of different supports were measured. During polymerization, the $[Al]_{dMMAO}/[Zr]_{cat}$ ratio was kept at 1135 by fixing the amount of catalyst and varying the amount of dMMAO/support used based on the amount of $[Al]_{dMMAO}$ present as measured by EDX. Thus, increased activity can be attributed to more available active sites rather than more amounts of $[Al]_{dMMAO}$ being present. The polymerization activities of the homogeneous and the different supported systems are listed in Table 2. The polymerization activities were in the order of homogeneous system > SiO_2 (LP) > SiO_2 (SP) > Si–Al (BP). As known, the activities of the supported system were apparently lower than homogeneous one due to supporting effect [31]. Among the supported systems, the polymerization activity obtained from the SiO_2 (LP) was the highest. This was presumably due to more available active sites present on the support. It is known that the greater amounts of dMMAO resulted in more active species being present during polymerization [32–34]. It was proposed that dMMAO possibly had many functions, such as alkylating agent, a stabilizer for a cationic metallocene alkyl and/or counter-ion, an ionizing and/or reducing agent for the transition element, and a scavenger for the metallocene catalytic system. However, one of the most important roles of this alkylaluminoxane is apparently to prevent the formation of $ZrCH_2CH_2Zr$ species, which is formed via a bimolecular process [35]. The polymerization activities obtained from the SiO_2 (SP) and Si–Al (BP) exhibited lower activities due to fewer amounts of available active sites. It should be noted that although the Si–Al (BP) had the same amount of $[Al]_{dMMAO}$ as the SiO_2 (SP), the polymerization activity obtained from the former was much lower (almost three times). Thus, the lower polymerization activity can not be only attributed to the available active sites, but also to other factor, such as the interaction between the $[Al]_{dMMAO}$ and the support [36]. Based on this study, dMMAO was dispersed by impregnation onto the different supports prior to polymerization. The degree of interaction between the support and dMMAO can be determined by the TGA measurement. In order to give a better understanding, we propose the interaction of support and dMMAO based on the review paper by Severn et al. [37]. They explained that the connection of the support and cocatalyst occurred via the $O_{support}–Al_{cocatalyst}$ linkage. In particular, the TGA can only provide useful information on the degree of interaction for the dMMAO bound to the support in terms of weight loss and removal temperature. The stronger interaction can result in it being more difficult for the dMMAO bound to the support to react with metallocene during activation processes, leading to lower polymerization activity for polymerization. The TGA profiles of $[Al]_{dMMAO}$ on different supports are shown in Fig. 3, indicating similar profiles for all supports. We observed that the weight losses of $[Al]_{dMMAO}$ present on various supports were in the order of SiO_2 (LP) [21.4%] > SiO_2 (SP) [20.8%] > Si–Al (BP) [13.7%]. This indicated that $[Al]_{dMMAO}$ present on the Si–Al (BP) had the strongest interaction and thus the lowest observed polymerization activity. In our previous work, we also used the pure bimodal pore SiO_2 (as MCM-41) [38]. It was found that the bimodal pure MCM-41 exhibited higher catalytic activity than the unimodal one. However, in this present study, the alumina-silica bimodal was used in order to investigate the chemical

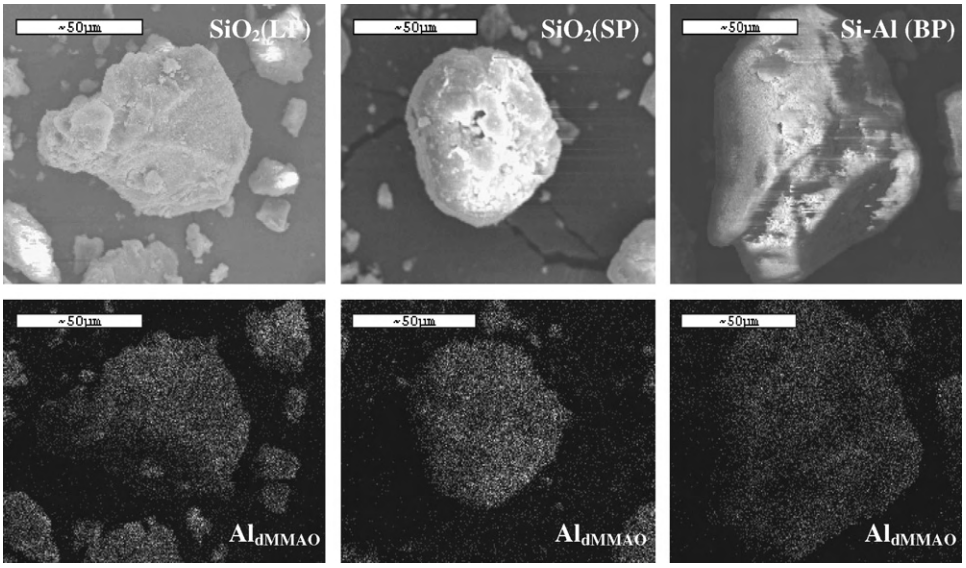

Fig. 2. SEM and EDX mapping for $[Al]_{dMMAO}$ of different supports.

Table 2
Polymerization activities for different SiO_2 supports

Support	Polymerization time (s)	Polymerization yield[a] (g)	Catalytic activity[b] (kg Pol.mol. $Zr^{-1}.h^{-1}$)
Homogeneous	128	1.4665	27496
SiO_2 (LP)	134	1.3899	24893
SiO_2 (SP)	202	1.0956	13017
Si–Al (BP)	307	0.6052	4731

[a] The polymer yield was fixed [limited by ethylene fed and 1-octene used (0.018 mol equally)].
[b] Activities were measured at polymerization temperature of 343 K, [ethylene] = 0.018 mol, $[Al]_{dMMAO}$ /$[Zr]_{cat}$ = 1135, $[Al]_{TMA}/[Zr]_{cat}$ = 2500, in toluene with total volume = 30 ml and $[Zr]_{cat} = 5 \times 10^{-5}$ M.

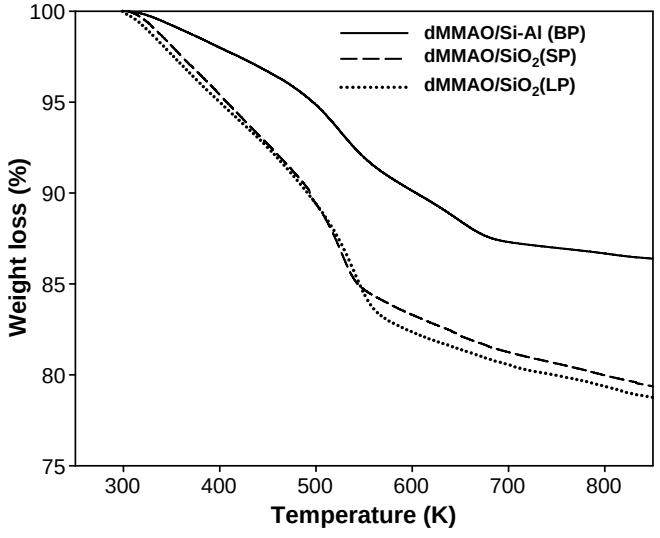

Fig. 3. TGA profiles of dMMAO dispersed on different supports.

effect of alumina being present in the Si–Al (BP) support. It was found that Al can result in the increased interaction between the dMMAO and support. As the result, the catalytic activity obtained from the Si–Al (BP) was the lowest due to strong support interaction. It should be noted that under the weaker strength interaction of the dMMAO and the support, the leaching of dMMAO to the liquid phase might occur. However, based on the work done by Harrison et al. [39], they reported that a variety of evidence indicates that leaching of active catalyst from the supports occurs to a minor extent under slurry conditions, particularly at higher temperatures in the presence of additional aluminoxane. At lower temperatures, this does not occur to an appreciable extent. In this study, the polymerization temperature was 70 °C under slurry condition. Thus, the leaching of dMMAO can be negligible under this condition. It should be also mentioned that if the leaching of dMMAO occurs, the system can not be treated as the homogeneous system. This is due to the deactivation of the leached dMMAO after bound with the support.

3.2. Polymer characteristics

The various copolymers obtained were further characterized by means of DSC and ^{13}C NMR. The DSC was performed to measure the thermal properties of copolymers. The melting temperature (T_m) obtained from the DSC measurement is listed in Table 3. Results revealed that no melting temperature was observed for the copolymers obtained from SiO_2 (LP) and SiO_2 (SP) supports indicating non-crystalline copolymers produced. The non-crystalline copolymers were attributed to the high degree of 1-octene insertion, which can be confirmed by ^{13}C NMR. Only the copolymer obtained from the Si–Al (BP) exhibited the melting temperature at 367 K suggesting lower degree of 1-octene insertion. The quantitative analysis of triad distribution for all copolymers was conducted on the basis assignment of the ^{13}C NMR spectra of ethylene/1-octene (EO) copolymer [30]. The characteristics of ^{13}C NMR spectra (not shown) for all copolymers were similar indicating the copolymer of ethylene/1-octene. The triad distribution of all polymers is also shown in Table 3. It was found that ethylene incorporation in all systems gave copolymers with similar triad distribution. It was also shown a little probability to produce the dyad of OO, which is the characteristic of this zirconocene in homogeneous system [38]. No triad of EOO in the copolymers was found. Only the random copolymers can be produced in all systems. In addition, the 1-octene incorporations in both SiO_2 (LP) and SiO_2 (SP) supports were 18 and 21 mol%, which was similar to that in the homogeneous system (22 mol%). Apparently, the copolymer obtained from the Si–Al (BP) support exhibited the lowest degree of 1-octene inser-

Table 3
Characteristics of polymer obtained

Support	Triad distribution[a]						1-octene[a] insertion (mol%)	T_m[b] (K)
	OOO	EOO	EOE	EEE	OEO	OEE		
Homogeneous	0	0	0.157	0.590	0.101	0.152	22	n.o.
SiO_2 (LP)	0	0	0.149	0.471	0.070	0.310	18	n.o.
SiO_2 (SP)	0	0	0.158	0.418	0.110	0.314	21	n.o.
Si–Al (BP)	0	0	0.063	0.790	0	0.147	6	367

[a] Obtained from ^{13}C NMR, where E refers to ethylene monomer and O refers to 1-octene comonomer.
[b] Obtained from DSC measurement.

tion resulting in the observation of T_m based on DSC measurement. Thus, increased crystallinity of the polymer was obtained with the Si–Al (BP) support.

4. Conclusions

It was found that the polymerization activity obtained from the large pored silica [SiO_2 (LP)] was the highest among other small pored silica [SiO_2 (SP)] and bimodal pored silica–alumina [Si–Al (BP)] supports. The high activity can be attributed to more available active sites present coupled with moderate interaction between the dMMAO and support. The strong interaction of dMMAO and Si–Al (BP) was the major factor that caused the decrease in polymerization activity. It is worth noting that all copolymers produced exhibited the similar triad distribution, but had different degree of 1-octene insertion.

Acknowledgements

We thank the Thailand Research Fund (TRF) for RMU50-B. Jongsomjit and the National Research Council of Thailand (NRCT) for the financial support of this project.

References

[1] M.L. Britto, G.B. Galland, J.H.Z. dos Santos, M.C. Forte, Polymer 42 (2001) 6355.
[2] J.D. Kim, J.B.P. Soares, G.L. Rempel, J. Polym. Sci. Part A: Pol. Chem. 37 (1999) 331.
[3] J.D. Kim, J.B.P. Soares, Macromol. Rapid Commun. 20 (1999) 347.
[4] H.W. Park, J.S. Chung, S.H. Baeck, I.K. Song, J. Mol. Catal. A: Chem 255 (2006) 69.
[5] K.S. Lee, C.-G. Oh, S.-K. Yim, J. Ihm, J. Mol. Catal. A: Chem. 159 (2000) 301.
[6] J. Tian, S. Wang, Y. Feng, J. Li, S. Collins, J. Mol. Catal. A: Chem. 144 (1999) 137.
[7] K.P. De Jong, J.W. Geus, Catal. Rev-Sci. Eng. 42 (2000) 481.
[8] H. Rahiala, I. Beurroies, T. Eklund, K. Hakala, R. Gougeon, P. Trens, J.B. Rosenholm, J. Catal. 188 (1999) 14.
[9] R. Van Grieken, A. Carrerc, I. Suarez, B. Paredes, Eur. Polym. J. 43 (2007) 1267.
[10] B. Jongsomjit, S. Ngamposri, P. Paserthdam, Ind. Eng. Chem. Res. 44 (2005) 9059.
[11] S.J. Kim, W.Y. Lee, Y. Park, W. Huh, Y.G. Ko, Polym. Eng. Sci. 43 (2003) 1011.
[12] P. Kumkaew, L. Wu, P. Praserthdam, S.E. Wanke, Polymer 44 (2003) 4791.
[13] A.M. Uusitalo, T.T. Pakkenen, E.I. Iskola, J. Mol. Catal. A: Chem. 177 (2002) 179.
[14] Y.S. Ko, T.K. Han, J.W. Park, S.I. Woo, Macromol. Rapid Commun. 17 (1996) 749.
[15] B. Jongsomjit, S. Ngamposri, P. Paserthdam, Catal. Lett. 100 (2005) 139.
[16] M.D.V. Marques, A. Conte, J. Appl. Polym. Sci. 86 (2002) 2054.
[17] B. Jongsomjit, J. Panpranot, J.G. Goodwin Jr., J. Catal. 204 (2001) 98.
[18] W. Kaminsky, H. Winkelbach, Topics Catal. 7 (1999) 61.
[19] G.G. Hlatky, in: J. Scheirs, W. Kaminsky (Eds.), Metallocene-based Polyolefins, John Wiley & Sons Ltd., Chichester, 2000, p. 203.
[20] G.B. Jacobsen, L. Spencer, P.W. Wauteraerts, PCT Int. Appl. 96 (1996) 16092.
[21] T. Sano, K. Doi, H. Hagomoto, Z. Wang, T. Uozumi, K. Soga, Chem. Commun. (1999) 733.
[22] T. Sano, K. Doi, H. Hagomoto, Z. Wang, T. Uozumi, K. Soga, Stud. Surf. Sci. Catal. 125 (1999) 777.
[23] T. Sano, H. Hagimoto, J. Jin, Y. Oumi, T. Uozumi, K. Soga, Macromol. Rapid Commun. 21 (2000) 1191.
[24] T. Sano, H. Hagimoto, S. Sumiya, Y. Naito, Y. Oumi, T. Uozumi, K. Soga, Micropor. Mesopor. Mat. 44 (2001) 557.
[25] E. Iglesia, S.C. Reyes, R.J. Madon, J. Catal. 129 (1991) 238.
[26] O. Levenspiel (Ed.), Chemical Reaction Engineering, Wiley, New York, 1972, p. p. 496.
[27] Y. Zhang, Y. Yoneyama, N. Tsubaki, Chem. Commun. 11 (2002) 1216.
[28] Y. Zhang, M. Koike, N. Tsubaki, Catal. Lett. 91 (2005) 193.
[29] H. Hagimoto, T. Shiono, T. Ikeda, Macromol. Chem. Phys. 205 (2004) 19.
[30] J.C. Randall, J. Macromol. Sci. Rev. Macromol. Chem. Phys. C29 (1989) 201.
[31] W. Wang, Z. Fan, L. Feng, Eur. Polym. J. 41 (2005) 2380.
[32] B. Jongsomjit, E. Chaichana, P. Praserthdam, Chem. Eng. Sci. 62 (2007) 899.
[33] B. Jongsomjit, J. Panpranot, P. Praserthdam, Mater. Lett. 61 (2007) 1376.
[34] C. Desharun, B. Jongsomjit, P. Praserthdam, Catal. Commun. 9 (2008) 522.
[35] B. Jongsomjit, P. Kaewkrajang, T. Shiono, P. Praserthdam, Ind. Eng. Chem. Res. 43 (2004) 7959.
[36] C. Ketloy, B. Jongsomjit, P. Praserthdam, Appl. Catal. A. Gen. 327 (2007) 270.
[37] J.R. Severn, J.C. Chadwick, R. Duchateau, N. Friderichs, Chem. Rev. 105 (2005) 4073.
[38] S. Bunchongturakarn, B. Jongsomjit, P. Praserthdam, Catal. Commun. 9 (2008) 789.
[39] D. Harrison, M. Coulter, S. Wang, S. Nistala, B.A. Kuntz, M. Pigeon, J. Tian, S. Collins, J. Mol. Catal. A: Chem. 128 (1998) 65.

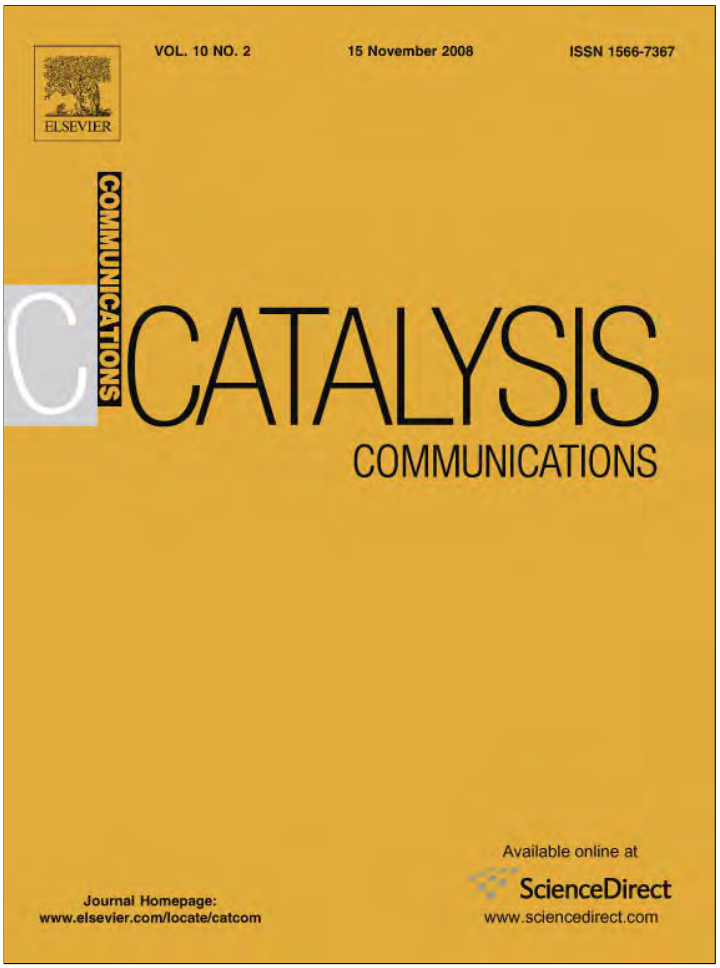

Catalysis Communications 10 (2008) 232–236

Contents lists available at ScienceDirect

Catalysis Communications

journal homepage: www.elsevier.com/locate/catcom

Synthesis of cobalt on cobalt-aluminate via solvothermal method and its catalytic properties for carbon monoxide hydrogenation

Sirirat Rojanapipatkul, Bunjerd Jongsomjit *

Center of Excellence on Catalysis and Catalytic Reaction Engineering, Department of Chemical Engineering, Faculty of Engineering, Chulalongkorn University, Bangkok 10330, Thailand

ARTICLE INFO

Article history:
Received 9 January 2008
Received in revised form 27 August 2008
Accepted 28 August 2008
Available online 2 September 2008

Keywords:
Cobalt-aluminate
Cobalt catalyst
CO hydrogenation
Solvothermal
Alumina

ABSTRACT

The study focused on synthesis of cobalt on cobalt-aluminate catalyst in one-pot via the solvothermal process. The obtained catalysts apparently exhibited higher activities than that prepared from the conventional solvothermal-derived alumina-supported cobalt catalyst without any changes in product selectivity during methanation. Enhanced activities can be attributed to the smaller amount of non-reducible cobalt-aluminate formed (at temperature <800 °C. Increased Co/Al molar ratios (1.0 and 2.0) also resulted in increased activities whereas the holding time during solvothermal synthesis had only little effect.

1. Introduction

At present, the rapid increase of using fossil fuels or crude oil and environmental concerns are attentive problems. Fischer-Tropsch synthesis (FTS) has been considered as a part of gas-to-liquid technology, which converts natural gas that is the basis for a number of large-scale chemical industrial processes to more valuable middle distillates and clean transportation fuels. Natural gas is first transformed into synthesis gas, which is a mixture of carbon monoxide and hydrogen as the starting material to produce heavy hydrocarbons or synthetic fuels, which generally contain negligible sulfur and aromatic compounds compared to gasoline or diesel from crude oil, through carbon monoxide hydrogenation or FTS [1].

Many transition metals of Group VIII can be used as catalysts for FTS such as iron (Fe), cobalt (Co), nickel (Ni), and ruthenium (Ru) [2–4]. However, supported cobalt catalysts are preferred for FTS because of their high activities for FTS based on natural gas [5], high selectivity for linear hydrocarbons, and low activity for the competitive water-gas shift (WGS) reaction [6,7]. To increase their activities, cobalt is usually deposited on a high surface area support to obtain a high metal dispersion. Many inorganic supports such as SiO_2, Al_2O_3, TiO_2 and zeolites [8–11] have been extensively studied for supported Co catalyst for years. It is known that in general, the catalytic properties depend on reaction conditions, catalyst composition, metal dispersion, and types of inorganic supports used. Furthermore, the catalytic performance of all FT catalysts strongly depends on the methods of catalyst preparation. The preparation of cobalt supported catalysts involves choice of the appropriate catalyst support, deposition of active phase, its promotion, oxidative and reductive treatments. The deposition of the precursor on the support surface is a complex phenomenon, which involves physical or chemical interactions between the precursor and the support. However, compound formation between cobalt and the supports such as cobalt-aluminate, cobalt-silicate can occur during the catalyst activation and/or reaction conditions resulting in irreversible catalyst deactivation [12].

The main objective of this present research was to investigate the influences of conditions to synthesize cobalt on cobalt-aluminate catalyst using single step synthesis on the characteristics and catalytic properties during CO hydrogenation. The great benefit of this study is that the cobalt on cobalt-aluminate can be prepared in only single step via the solvothermal process, plus the cobalt-aluminate as cobalt-support compound formation (Co-SCF) [12] is not formed further due to the limitation of Co/Al ratio upon stoichiometry to form cobalt-aluminate. The catalysts were characterized using various characterization techniques and tested in order to evaluate the catalytic properties during CO hydrogenation.

2. Experimental

2.1. Catalyst preparation

Cobalt on cobalt-aluminate was synthesized by solvothermal method. It was prepared using the mixture of aluminium isopropoxide (AIP, $[(CH_3)_2CHO]_3Al$), 15.0 g (0.07344 mole) and appropriate

* Corresponding author. Tel.: +662 2186869; fax: +662 2186877.
E-mail address: bunjerd.j@chula.ac.th (B. Jongsomjit).

1566-7367/$ - see front matter © 2008 Elsevier B.V. All rights reserved.
doi:10.1016/j.catcom.2008.08.026

amount of cobalt (II) acetylacetonate [$(CH_3COCH{=}COCH_3)_2Co$] that depended on the Co/Al molar ratios employed. The starting materials were suspended in 100 mL of toluene in a beaker, and then set up in 1000 mL autoclave. In the gap between the beaker and autoclave wall, toluene (40 mL) was added. After the autoclave completely purged with nitrogen, the suspension was heated to 300 °C at the rate of 2.5 °C /min and was hold at that temperature for 1 and 2 h. The synthesis was performed at different Co/Al molar ratios (0.5, 1.0 and 2.0). Autogenous pressure during the reaction gradually increased as temperature was raised. Then the autoclave was cooled to room temperature. After the autoclave was cooled, the resulting product was washed repeatedly with methanol by centrifugation and dried at 110 °C for 24 h. The calcination of the obtained product was carried out in a furnace. The product was heated at the rate of 10 °C/min at 300 °C for 1 h.

2.2. Catalyst characterization

2.2.1. N_2 physisorption

The specific surface area of catalysts was performed using Micromeritic Chemisorb 2750. It was calculated based on nitrogen uptake at liquid-nitrogen temperature using the Brunauer–Emmett–Teller (BET) equation by the single point method.

2.2.2. X-ray diffraction

XRD was performed to determine the bulk crystalline phases of catalyst. It was conducted using a SIEMENS D-5000 X-ray diffractometer with CuK_α ($\lambda = 1.54439$ Å). The spectra were scanned at a rate of 2.4 deg/min in the range $2\theta = 20{-}80^\circ$.

2.2.3. Scanning electron microscopy and energy dispersive X-ray spectroscopy

SEM and EDX were used to determine the catalyst morphologies and elemental distribution throughout the catalyst granules, respectively. The SEM of JEOL mode JSM-5410LV was applied using the secondary electron mode at 15 kV. EDX was performed using Link Isis series 300 program.

2.2.4. Transmission electron microscopy

The morphology and size of the catalysts were determined using a JEOL-TEM 200CX transmission electron spectroscopy operated at 100 kV. In fact, the sample was dispersed in ethanol to obtain the uniform dispersion of sample. The scans were done many times in different areas as much as possible until the good representative image for all areas was obtained.

2.2.5. Temperature-programmed reduction

TPR was used to determine the reduction behaviors of the samples. It was carried out using 20 mg of a sample and a temperature ramp from 35 to 800 °C at 10 °C/min. The carrier gas was 5% H_2 in Ar. A cold trap was placed before the detector to remove water produced during the reaction. A thermal conductivity detector (TCD) was used to determine the amount of H_2 consumed during TPR.

2.3. Reaction study

CO hydrogenation (H_2/CO = 10/1) was performed to measure the overall activity of the catalyst samples. Hydrogenation of CO was carried out at 220 °C and 1 atm. A flow rate of H_2/CO/Ar = 20/2/8 cc/min in a fixed-bed flow micro-reactor [stainless steel with 30 cm × 1 cm (id)] under non-adiabatic differential condition was used. A relatively high H_2/CO ratio was used to minimize deactivation due to carbon deposition during reaction. Typically, 0.2 g of a catalyst sample was reduced in situ in flowing H_2 (30 cc/min) at 350 °C for 3 h prior to the reaction. Reaction effluent samples were taken at 1 h intervals and analyzed by GC. In all cases, steady-state was reached within 6 h.

2.4. Catalyst nomenclature

The nomenclature used for the catalyst samples in this study is as follows:

- Co/Al_a_b.
- Co/Al_2O_3_b.

Co/Al refers to the cobalt on cobalt-aluminate catalyst using single step synthesis.

Co/Al_2O_3 refers to the alumina-supported cobalt catalyst using the conventional impregnation method having 25%wt of cobalt.

a refers to the Co/Al ratio.

b refers to the holding time during synthesis.

3. Results and discussion

The present study focused on synthesis of the cobalt on cobalt-aluminate using the solvothermal process. The excess cobalt precursor was added in order to obtain the cobalt oxides on cobalt-aluminate after calcination of samples. Therefore, the Co/Al molar ratios (0.5, 1.0, and 2.0) and the holding times (1 and 2 h) during solvothermal process were varied. After solvothermal synthesis, all samples were calcined at 300 °C for 1 h prior to characterization and reaction study.

After calcination, all catalyst samples were characterized by means of N_2 physisorption, XRD, SEM/EDX, TEM, and TPR. The BET surface areas of samples obtained from N_2 physisorption are listed in Table 1. It can be observed that increased Co/Al molar ratios apparently resulted in decreased surface areas of samples. However, the holding time during solvothermal process showed only little effect on surface areas of samples. The decreased surface areas of samples with increased Co/Al molar ratios can be attributed to agglomeration of the larger amounts of cobalt oxide formed. Thus, the decreased surface areas of samples were evident when the Co/Al ratios increased. The XRD patterns for all samples are shown in Fig. 1. All samples exhibited the similar short-broaden XRD peaks at 31, 37, 46, 59, and 65° assigned to Co_3O_4 and $CoAl_2O_4$ species, which were overlapped [12–15]. This was suggested that all crystallite species were in the highly dispersed form. SEM and EDX were performed to study the morphologies of catalyst samples and the elemental distribution on the external surface of the catalyst granule. It was found that no significant change in morphologies upon different Co/Al molar ratios and holding time during solvothermal process was observed. A typical SEM micrograph and EDX mapping for cobalt on cobalt-aluminate are shown in Fig. 2. It can be also observed that cobalt was well distributed on the catalyst granule. In order to determine the dispersion of cobalt oxide species and crystallite size of them, the more powerful technique, such as TEM was performed. The TEM micrographs for Co/

Table 1
BET surface area

Samples	BET surface area (m^2/g)
Co/Al_0.5_1h	139
Co/Al_0.5_2h	139
Co/Al_1.0_1h	131
Co/Al_1.0_2h	137
Co/Al_2.0_1h	100
Co/Al_2.0_2h	103
Impregnated Co/Al_2O_3_1h	84

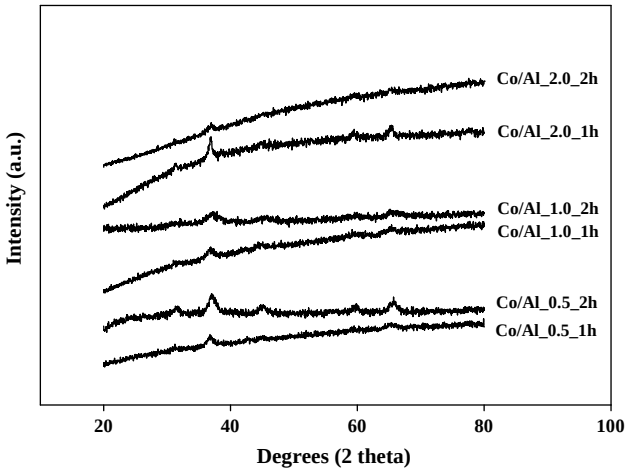

Fig. 1. XRD patterns of the calcined cobalt on cobalt-aluminate catalysts.

Al_1.0_1h and Co/Al_1.0_2h samples are shown in Fig. 3. The dark spots represented the cobalt species dispersing on the catalyst granule. It was found that the degree of dispersion apparently decreased with increased holding time during solvothermal process as well as increased Co/Al ratios (not shown) due to increased cobalt species. Based on TEM micrographs, all samples exhibited the agglomeration of cobalt species.

TPR was performed in order to determine the reduction behaviors. The TPR profiles for all catalyst samples are shown in Fig. 4. It was found that mostly the one reduction peak below 400 °C was observed and assigned to the overlap of two step reduction of Co_3O_4 to CoO and, then to Co metal [12–15]. Upon the TPR conditions, the two-step reduction may or may not be observed. In fact, the TPR peak locations are affected by reduction kinetics. The kinetics of reduction can be affected by a wide range of variables, including particle size, support interaction, and reduction gas composition [12,16]. The effects of particle size and support interaction can be superimposed on each other. Thus, while a decrease in metal oxide particle size can result in faster reduction due to greater surface area/volume ratio, smaller particles may interact more with the support, slowing reduction. Based on the TPR profiles of sample, the reduction peak at high temperature (ca. above 600 °C) was also observed. This peak can be assigned to the reduction of non-stoichometric cobalt-aluminate, which is more difficult

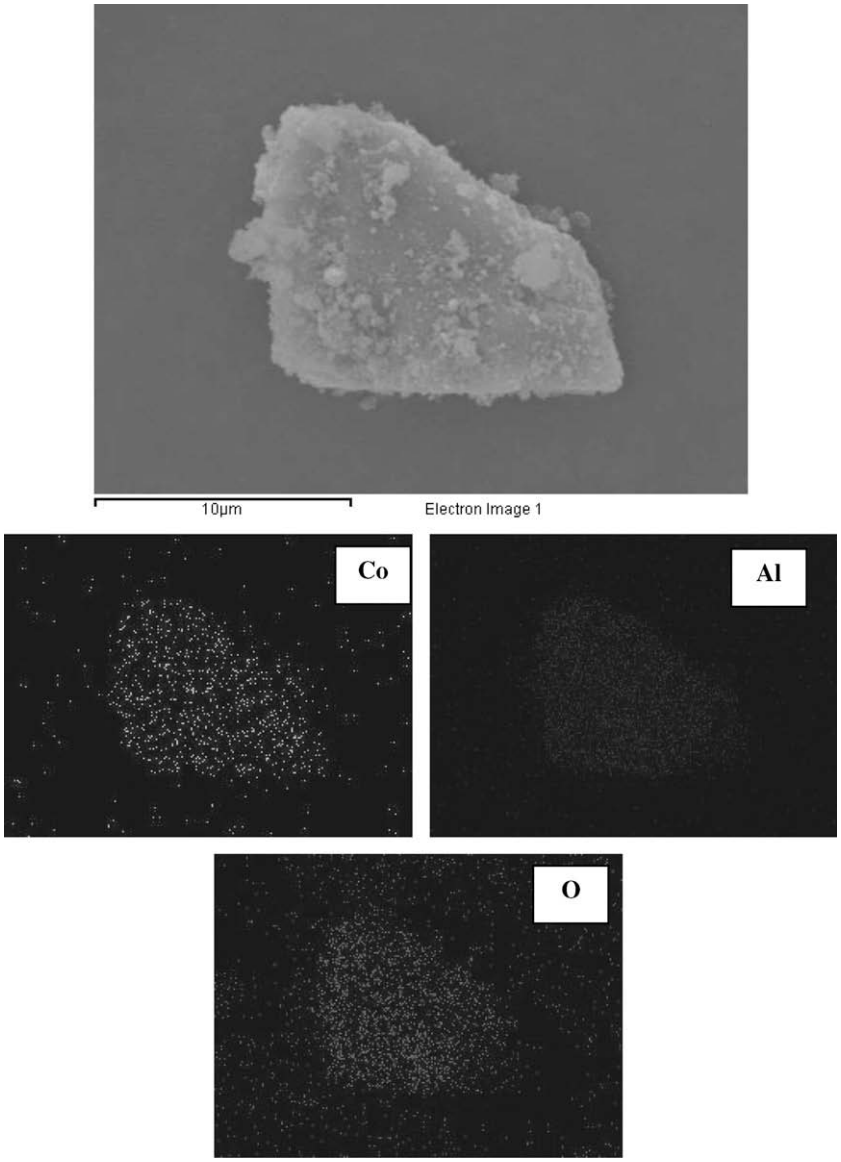

Fig. 2. A typical SEM micrograph and EDX mapping for the calcined cobalt on cobalt-aluminate catalysts.

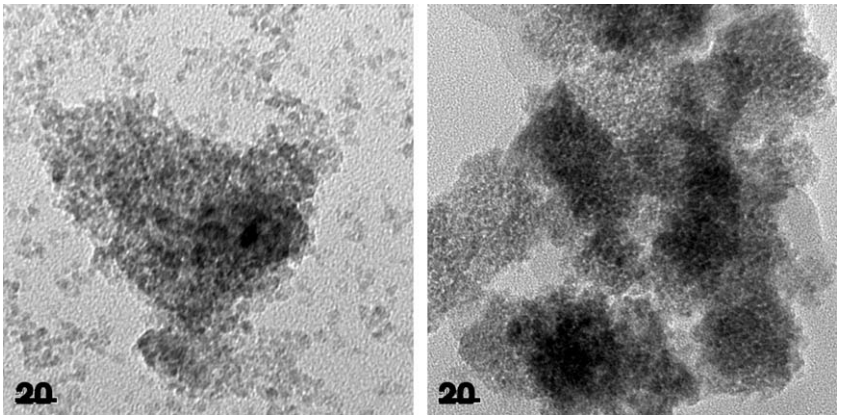

Fig. 3. A typical TEM micrograph of the calcined cobalt on cobalt-aluminate catalysts left (Co/Al_1.0_1h) and right (Co/Al_1.0_2h).

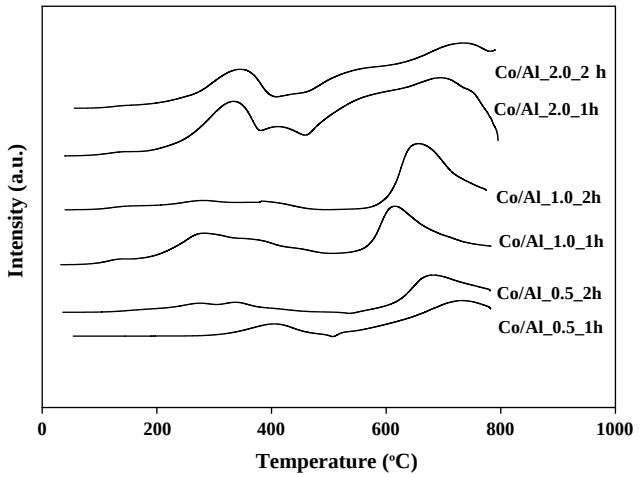

Fig. 4. TPR profiles for different cobalt on cobalt-aluminate catalyst samples.

than the reduction of Co_3O_4 species [12]. According to the TPR results, it can be concluded that increased Co/Al molar ratios resulted in increased Co_3O_4 species, which facilitated the reduction behavior of catalyst samples. Thus, the larger reduction peaks at low reduction temperature (ca. below 400 °C) for Co/Al_2.0_1h and Co/Al_2.0_2h samples were evident. No significant change on the reduction behaviors upon changing the holding time during solvothermal process was observed.

In order to determine the catalytic behaviors of the samples having different Co/Al ratios and holding time during solvotnermal synthesis, CO hydrogenation (H_2/CO = 1) was performed to determine the overall activity and product selectivity of the samples.

Table 2
Reaction study

Samples	Rate		Selectivity	
	($\times 10^2$gCH$_2$/g.cat.h)	(x10^4gCH$_2$/m^2.cat.h)[a]	CH_4 (%)	C_2-C_4 (%)
Co/Al_0.5_1h	29.5	21.2	99.4	0.6
Co/Al_0.5_2h	21.0	15.1	99.8	0.2
Co/Al_1.0_1h	30.3	23.1	99.4	0.6
Co/Al_1.0_2h	30.1	22.0	99.7	0.3
Co/Al_2.0_1h	33.3	33.3	99.6	0.4
Co/Al_2.0_2h	32.6	31.7	99.8	0.2
Impregnated Co/Al_2O_3_1h	25.8	30.7	99.7	0.3

[a] Based on BET surface area.

In fact, hydrogenation of CO under methanation condition was carried out at 220 °C at atmospheric pressure. A flow rate of H_2/CO/Ar = 20/2/8 cc/min in a fixed-bed flow reactor was used. The relatively high H_2/CO ratio was employed to minimize deactivation due to carbon deposition during reaction. The resulted reaction study is shown in Table 2 (based on g. cat and BET surface area of cat.). For a comparative study, the activity and selectivity for the conventional solvothermal-derived alumina-supported cobalt catalyst having 25 wt% of cobalt was also measured as listed in Table 2. It was found that increased Co/Al molar ratios of cobalt on cobalt-aluminate catalysts apparently resulted in increased activity without changing the product selectivity. Increased activities can be attributed to more reducible cobalt oxide species at lower reaction temperature with increased Co/Al molar ratios as mentioned in the TPR results. The holding time during solvothermal synthesis seemed to have only little effect on activity for the samples having Co/Al molar ratios of 1.0 and 2.0. However, the holding time during solvothermal synthesis was found to have a significant effect on the catalyst sample having Co/Al molar ratio of 0.5 where the activities dramatically decreased with increasing the holding time. This was probably due to more non-reducible cobalt-aluminate formed resulting in lower amount of the reducible cobalt oxide species as also seen in Fig. 4 during the TPR measurement. On the other word, the longer holding time, the larger amount of non-reducible cobalt-aluminate was formed. Considering the activity of the conventional solvothermal-derived alumina-supported cobalt catalyst having 25 wt% of cobalt, it exhibited lower activity due to the formation of non-reducible cobalt-aluminate (at temperature <800 °C) [12,16,17]. It is worth noting that the catalyst activity tests performed under methanation condition are acceptable at this stage of catalyst development. However, to obtain the real picture of catalyst performance data from long-term tests under Fischer-Tropsch conditions are necessary in the near future.

4. Conclusions

In summary, the cobalt on cobalt-aluminate catalyst can be synthesized in one-pot via solvothermal process. The obtained catalysts exhibited higher activities than that obtained from the conventional solvothermal-derived alumina-supported cobalt catalyst without changing the product selectivity. It was found that increased Co/Al molar ratios apparently resulted in increased activities during methanation, whereas the holding time during solvothermal synthesis seemed to have only little effect on the activities upon the high molar ratios of Co/Al. However, at low molar ratio of Co/Al (0.5), the increased holding time can result in dra-

matically decreased activity due to increased amount of non-reducible cobalt-aluminate formed based on the TPR study.

Acknowledgements

We thank the Thailand Research Fund (TRF for the RMU50-B. Jongsomjit) for the financial support of this project.

References

[1] T. Mochizuki, T. Hara, N. Koizumi, M. Yamada, Appl. Catal. A. 317 (2007) 97.
[2] H.J. Wan, B.S. Wu, C.H. Zhang, H.W. Xiang, Y.W. Li, B.F. Xu, F. Yi, Catal. Com. 8 (2007) 1538.
[3] N.O. Elbashir, P. Dutta, A. Manivannan, M.S. Seehra, C.B. Roberts., Appl, Catal. A. 285 (2005) 169.
[4] S.A. Hosseini, A. Taeb, F. Feyzi, Catal. Com. 6 (2005) 233.
[5] A.P. Steynberg, M.E. Dry, B.H. Davis, B.B. Breman, in: Fischer-Tropsch Technology Study, Surface Science and Catalysis 152 (2004) 64.
[6] E. Iglesia, Appl. Catal. 161 (1997) 59.
[7] R.C. Brady, R.J. Pettie, J. Am. Chem. Soc. 103 (1981) 1287.
[8] A. Martinez, C. Lopez, F. Marquez, I. Duaz, J. Catal. 220 (2003) 486.
[9] T. Das, G. Jacobs, P.M. Patterson, W.A. Coner, J.L. Li, B.H. Davis, Fuel 82 (2003) 215.
[10] J.L. Li, G. Jacobs, T. Das, B.H. Davis, Appl. Catal. A. 233 (2002) 255.
[11] X.H. Li, K. Asami, M.F. Luo, K. Michiki, N. Tsubaki, K. Fujimoto, Catal. Today 84 (2003) 59.
[12] B. Jongsomjit, J. Panpranot, J.G. Goodwin, J. Catal. 204 (2001) 98.
[13] B. Jongsomjit, C. Sakdamnuson, J.G. Goodwin Jr., P. Praserthdam, Catal. Lett. 94 (2004) 209.
[14] B. Jongsomjit, C. Sakdamnuson, P. Praserthdam, Mater. Chem. Phy. 89 (2005) 395.
[15] B. Jongsomjit, T. Wongsalee, P. Praserthdam, Catal. Commun. 6 (2005) 705.
[16] B. Jongsomjit, J.G. Goodwin Jr., Catal. Today 77 (2002) 191.
[17] B. Jongsomjit, J. Panpranot, J.G. Goodwin Jr., J. Catal. 215 (2003) 66.

Catal Lett (2008) 121:266–273
DOI 10.1007/s10562-007-9327-y

Effect of Zr-Modified SiO_2-Supported Metallocene/MAO Catalyst on Copolymerization of Ethylene/1-Octene

Tipawan Pothirat · Bunjerd Jongsomjit · Piyasan Praserthdam

Received: 29 August 2007 / Accepted: 18 October 2007 / Published online: 17 November 2007

Abstract The study revealed enhancement (four to seven times) of catalytic activities for ethylene/1-octene copolymerization via the Zr-modified SiO_2-supported the metallocene/MAO catalyst. Increased activity can be attributed to an increase in absorption ability of MAO on the modified support. In addition, the strong interaction between MAO and the support was also considered.

Keywords Metallocene · Copolymerization · Zirconocene catalyst · Zr modification

1 Introduction

The discovery of metallocene catalyst along with a methylaluminoxane (MAO) cocatalyst essentially led to the development of the highly active for homogeneous polymerization of α-olefin [1, 2]. It is obvious that these active metallocene catalysts can compete with the conventional Ziegler-Natta catalysts. In particular, these catalysts are also capable of producing a variety of polyethylene copolymers, all with different chain compositions and architecture. However, in order to apply metallocene catalysts in the modern gas phase and slurry olefin polymerization processes, they need to be heterogenized on a support.

As known, the homogeneous metallocene catalysts have two major disadvantages; (a) the lack of morphology control and (b) reactor fouling. Therefore, binding these metallocene catalysts onto inorganic supports as supported metallocene catalysts can overcome those drawbacks. Many inorganic supports such as SiO_2, Al_2O_3, and $MgCl_2$ have been investigated [3–9]. It was reported that silica is perhaps the most attractive support so far. However, the properties of silica itself may not be completely satisfied for all purposes based on the polymerization activity and the properties of obtained polymer. Thus, the modification of silica properties is necessary in order that it can be used more efficiently. It has been reported that the immobilization method of introducing a spacer group between the support and metallocene was found to enhance the catalytic activity [10, 11]. In our previous study, the use of silane-modified silica-supported MAO with $Et[Ind]_2ZrCl_2$ catalyst for ethylene/α-olefin copolymerization was investigated [12]. It was found that silane modification resulted in increased activities for ethylene/1-hexene copolymerization. In addition, the copolymerization of ethylene/α-olefin via mixed TiO_2/SiO_2-supported zirconocene/MAO catalyst was also studied [13, 14]. It was found that mixed TiO_2/SiO_2 supports apparently resulted in increased polymerization activity as well. It was reported that zirconia can be used as a modifier for supports such as silica [15] and alumina [16]. It revealed that some catalytic properties increased with the zirconia modification due to increased dispersion of active species. Therefore, it would be interesting to investigate the impact of zirconia modification on the supported metallocene catalytic systems.

In this work, the impact of zirconia modification on the silica-supported metallocene catalyst was investigated. Experimentally, the Zr-modified silica was prepared by impregnation of a zirconium precursor onto the silica, then subsequently reacted with MAO. The modified support was employed for the copolymerization of ethylene/1-octene.

T. Pothirat · B. Jongsomjit (✉) · P. Praserthdam
Center of Excellence on Catalysis and Catalytic Reaction Engineering, Department of Chemical Engineering, Faculty of Engineering, Chulalongkorn University, Bangkok 10330, Thailand
e-mail: bunjerd.j@chula.ac.th

The characteristics of the modified support and catalyst precursors were investigated by means of X-ray diffraction (XRD), scanning electron microscopy (SEM), energy-dispersive X-ray spectroscopy (EDX), thermal gravimetric analysis (TGA) and N_2 physisorption. The obtained polymers were also further characterized using SEM, differential scanning calorimetry (DSC) and ^{13}C nuclear magnetic resonance (^{13}C NMR).

2 Experimental

All chemicals [zirconium (IV) propoxide, 70 wt.% solution in 1- propanol (Aldrich, St. Louis, MO, USA), silica gel (Fuji Silasia, Cariact P-10), toluene (EXXON), *rac*-ethylenebis(indenyl) zirconium dichloride, *rac*-$Et(Ind)_2ZrCl_2$) (Aldrich), methylaluminoxane, MAO, 2.667 M in toluene (Tosoh Akso), trimethylaluminum, TMA [$Al(CH_3)_3$] 2.0 M in toluene (Nippon Aluminum Alkyls), and 1-octene, 98% (Aldrich)] including the preparation of MAO/supports and polymerization were manipulated under an argon atmosphere using a vacuum glove box and/or Schlenk techniques.

2.1 Materials

2.1.1 Preparation of the Zr-Modified Silica Support

The Zr-modified silica supports were prepared by the sequential impregnation method as referred in [16]. First, Zr was impregnated onto silica using a solution of zirconium (IV) n-propoxide to produce Zr-modified supports having 1, 2, and 5 wt.% of Zr in the support. The mixture was dried in oven at 100 °C overnight.

2.1.2 Preparation of MAO/Modified Support

The modified support was heated under vacuum at 400 °C for 6 h., then, 2 g of the calcined support was reacted with the desired amount of MAO in 10 ml of toluene at room temperature for 30 min. The solid part was separated and washed five times with 20 ml of toluene, followed by drying in vacuum at room temperature to obtain the catalyst support precursor MAO/modified support.

2.2 Polymerization

The ethylene/1-octene copolymerization reaction was carried out in a 100 ml semi-batch stainless steel autoclave reactor equipped with a magnetic stirrer. At first, 0.2 g of the supported MAO ($[Al]_{MAO}/[Zr]_{cat} =$ 2,270) and 0.018 mole of 1-octene along with toluene (to make the total volume of 30 ml) were put into the reactor. The desired amount of $Et(Ind)_2ZrCl_2$ (5×10^{-5} M or 1.5×10^{-6} mole in 30 ml of solution mixture) and TMA (3.75×10^{-3} mole corresponding to $[Al]_{TMA}/[Zr]_{cat} = 2{,}500$) was mixed and stirred for 5 min aging at room temperature, separately, then was injected into the reactor. The reactor was frozen in liquid nitrogen to stop reaction between the catalyst and cocatalyst for 15 min and then the reactor was evacuated to remove argon. The reactor was heated up to polymerization temperature (70 °C). By feeding the fixed amount of ethylene (0.018 mole–6 psi) into the reaction mixtures, the ethylene consumption can be observed corresponding to the ethylene pressure drop. The polymerization reaction was stopped and the reaction time used was recorded when all ethylene (0.018 mole) was totally consumed. After all ethylene was consumed, the reaction was terminated by addition of acidic methanol (0.1% HCl in methanol) and stirred for 30 min. After filtration, the obtained copolymer (white powder) was washed with methanol and dried at room temperature.

2.3 Characterization

2.3.1 Characterization of Supports and Catalyst Precursors

X-ray diffraction. XRD was performed to determine the bulk crystalline phases of samples. It was conducted using a SIEMENS D-5000 X-ray diffractometer with CuK_α ($\lambda = 1.54439$ Å). The spectra were scanned at a rate of 2.4 degree/min in the range $2\theta = 20$–$80°$.

Scanning Electron Microscopy and Energy Dispersive X-ray Spectroscopy. SEM and EDX were used to determine the sample morphologies and elemental distribution throughout the sample granules, respectively. The SEM of JEOL mode JSM-5800LV was applied. EDX was performed using Link Isis series 300 programs.

Thermal Gravimetric Analysis. TGA was performed to prove the interaction between the $[Al]_{MAO}$ and various supports. It was conducted using TA Instrument SDT Q 600 analyzer. The samples of 10–20 mg and temperature ramping from 50 to 600 °C at 5 °C/min were used in the operation. The carrier gas was N_2 UHP.

N_2 Physisorption. Measurement of BET surface area, average pore diameter and pore size distribution of supports were determined by N_2 physisorption using a Micromeritics ASAP 2000 automated system.

2.3.2 Characterization of Polymer

Scanning Electron Microscopy. Scanning electron microscopy was performed to study morphologies of polymers produced. The same equipment as mentioned above was employed.

Differential Scanning Calorimeter. The melting temperature of ethylene/1-octene copolymer products was determined with a Perkin-Elmer diamond DSC. The analyses were performed at the heating rate of 20 °C/min in the temperature range of 50–150 °C. The heating cycle was run twice. In the first scan, samples were heated and, then cooled to room temperature. In the second scan, samples were reheated at the same rate, but only the results of the second scan were reported because the first scan was influenced by the mechanical and thermal history of samples.

Nuclear Magnetic Resonance. ^{13}C NMR spectroscopy was used to determine comonomer incorporation and polymer microstructure. Comparison of the positions of peak in the ^{13}C NMR spectrum of polymer sample with characteristic leads to identification of the sequence of the comonomer incorporation. The ^{13}C NMR spectra were recorded at 100 °C using BRUKER magnet system 400 MHz/54 mm. The copolymer solutions were prepared using 1,2 dichlorobenzene as solvent and benzene-d_6 for an internal lock.

3 Results and Discussion

The present study showed the impact of zirconia modification on silica- supported metallocene catalyst via ethylene/1-octene copolymerization. The modified supports containing various amounts of zirconia loading on silica were characterized using XRD measurement. The XRD patterns of the silica and Zr-modified silica supports are shown in Fig. 1. It was observed that the pure silica exhibited a broad XRD peak between *ca.* 10° and 30° assigning to the conventional amorphous silica. The Zr-modified silica supports having 1, 2, and 5 wt.% of Zr exhibited the similar XRD patterns of pure silica plus a small sharp peak at 30° indicating the presence of zirconia in the tetragonal phase for the Zr-modified support [17]. Furthermore, it can be seen that the intensity of XRD characteristic peaks for the modified supports was changed based on the amounts of zirconia loading where the tetragonal phase peak at 30° apparently increased with increasing the amounts of zirconia in the silica support. In addition, the width of the line is about 0.5° which corresponds to a ZrO_2 crystal size of 15 nm or more. The particles with sizes of 15 nm are not considered to be well dispersed. The surface areas determined by N_2

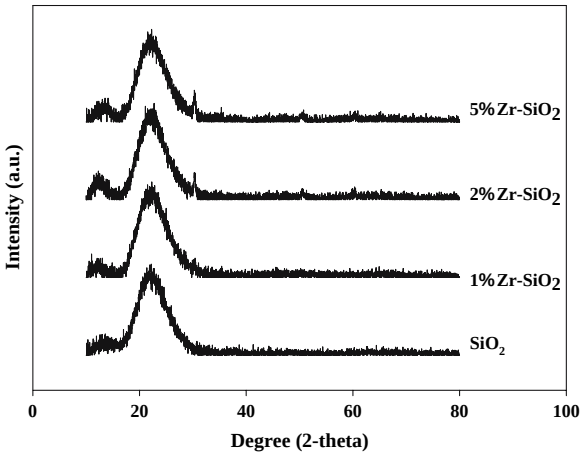

Fig. 1 XRD patterns of various Zr-modified silica supports prior to the MAO impregnation

physisorption of the modified supports decreased from 193 to 160 m^2/g upon increasing the amounts of zirconia loading. The morphologies and elemental distributions of the supports before and after MAO impregnation were determined using SEM and EDX, respectively. The SEM micrographs of the supports prior to MAO impregnation are shown in Fig. 2 indicating similar morphologies of the various supports. After MAO impregnation, the morphologies of the various supports were also determined and shown in Fig. 3. It can be observed that after impregnation with MAO, we obtained the larger size of supports due to the adsorption of MAO on the support. The typical EDX mapping image for Zr-modified silica-supported MAO at the external surface is shown in Fig. 4. The distribution of all elements ($[Al]_{MAO}$, O, Si, and Zr) was similar in all samples indicating well distribution for all elements, especially for the $[Al]_{MAO}$. In order to determine the $[Al]_{MAO}$ distribution inside the support granule, the particle was cut or microtomed, then the EDX mapping was performed at the cross-sectional area as shown in Fig. 5. It also indicated the good distribution of $[Al]_{MAO}$ inside the support granule. In addition, the EDX measurement was also used to determine the concentrations of $[Al]_{MAO}$ present on various supports with the EDX spectrum obtained as seen in Fig. 6. The concentrations of $[Al]_{MAO}$ present on various supports are also listed below. It indicated that the amounts of $[Al]_{MAO}$ apparently increased with zirconia modification from 4.93 to 7.37 wt.% upon increased amounts of zirconia loading. This was suggested that the adsorption of MAO on silica can be enhanced with zirconia modification.

For comparative studies, the catalytic activities toward the copolymerization of ethylene/1-octene upon various supports were measured. The polymerization activities are shown in Table 1. As seen, the polymerization activities were in the order of 1%Zr–SiO_2–2%Zr–SiO_2 > 5%

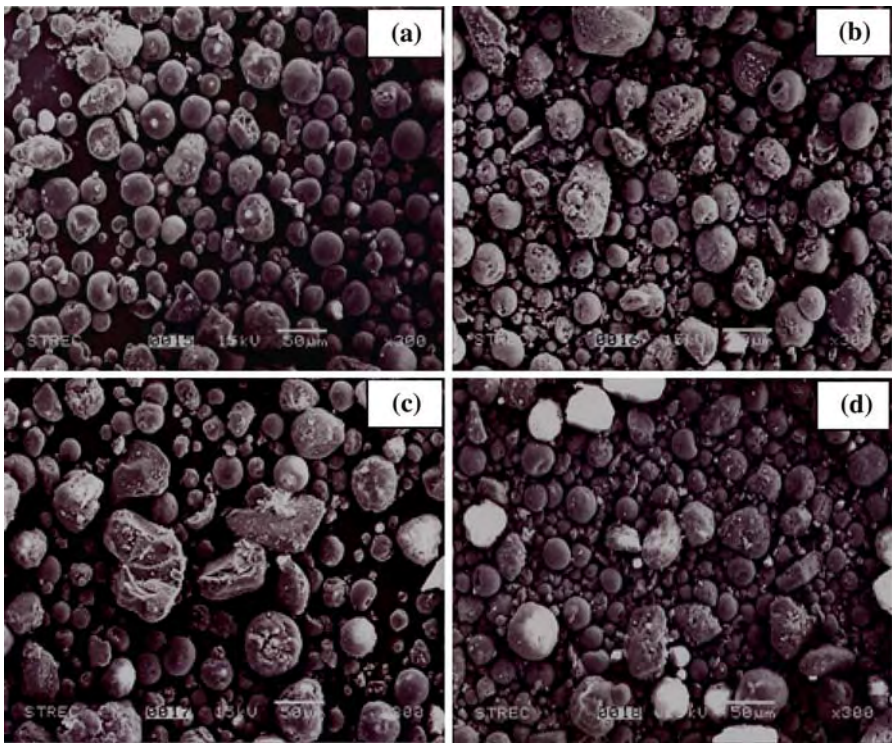

Fig. 2 SEM micrographs of various Zr-modified silica supports prior to the MAO impregnation; (**a**) SiO_2, (**b**) 1%Zr–SiO_2, (**c**) 2%Zr–SiO_2, and (**d**) 5%Zr–SiO_2

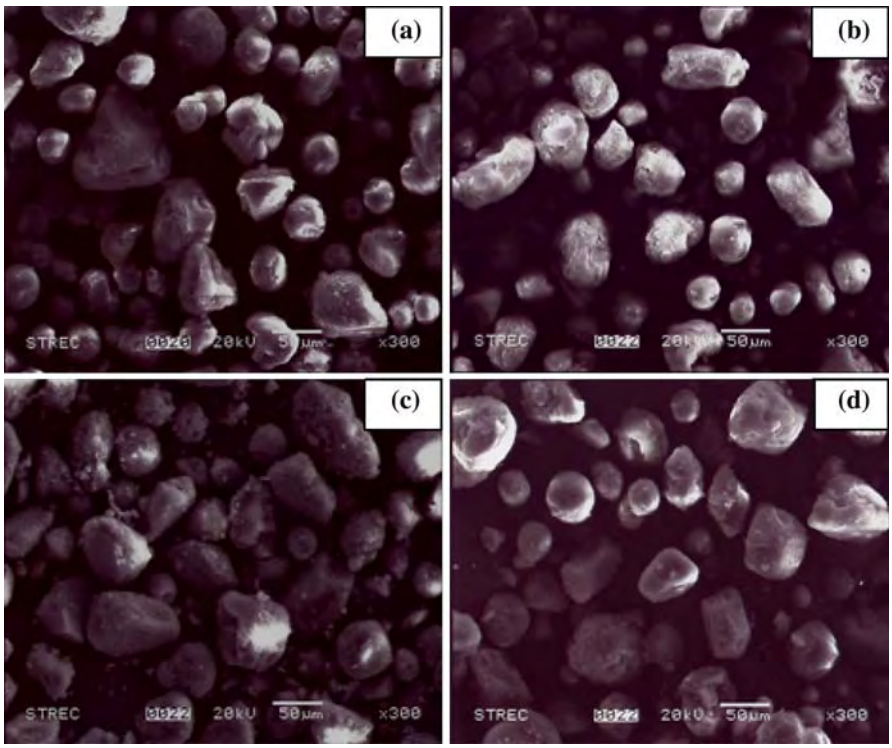

Fig. 3 SEM micrographs of various Zr-modified silica supports after the MAO impregnation; (**a**) SiO_2, (**b**) 1%Zr–SiO_2, (**c**) 2%Zr–SiO_2, and (**d**) 5%Zr–SiO_2

$Zr–SiO_2 > SiO_2$. Apparently, the SiO_2 support exhibited the lowest activity due to the lowest amount of $[Al]_{MAO}$ being present. It was also obvious that the zirconia modification on silica support essentially resulted in increased activities about four to seven times. Considering only the silica supports with zirconia modification, it can be observed that the catalytic activities dramatically decreased with increasing the amounts of zirconia loading, especially

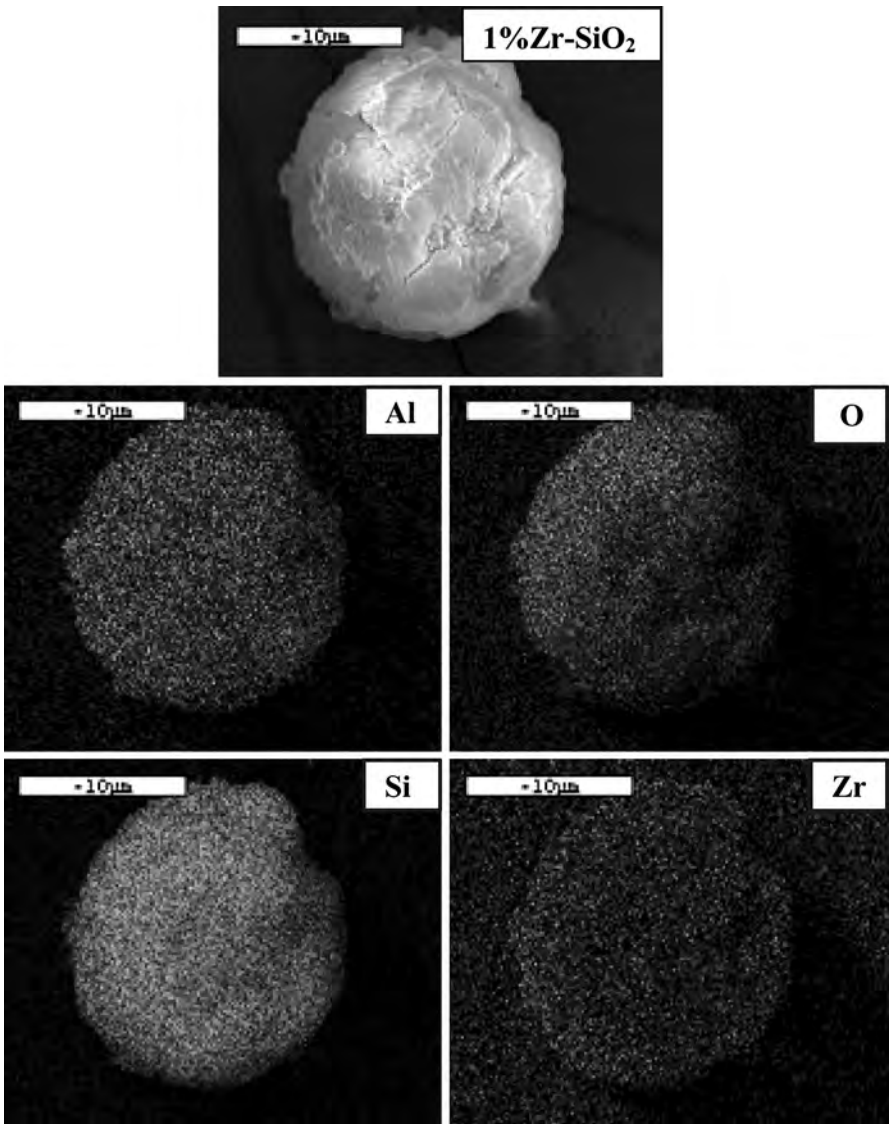

Fig. 4 A typical SEM/EDX mapping (external surface) of Zr-modified silica supports after the MAO impregnation

up to 5 wt.% of Zr. From the EDX measurement as mentioned before, the amount of $[Al]_{MAO}$ (7.37 wt.%) for the 5%Zr–SiO_2 support was the highest among other supports. Thus, based on the amount of $[Al]_{MAO}$ present in the support, one might argue that the polymerization activity for the 5%Zr–SiO_2 support should be the highest due to the largest amount of $[Al]_{MAO}$ adsorbed. This indicated that besides the concentrations of $[Al]_{MAO}$, the interactions between $[Al]_{MAO}$ and the support were very important. Based on this study, $[Al]_{MAO}$ was dispersed by impregnation onto the various supports prior to polymerization. The degree of interaction between the support and $[Al]_{MAO}$ can be determined by the TGA measurement [18]. In order to give a better understanding, we propose the interaction of support and $[Al]_{MAO}$ based on the review paper by Severn et al. [19]. They explained that the connection of the support and cocatalyst occurred via the $O_{support}$–$Al_{cocatalyst}$ linkage. In particular, the TGA can only provide useful information on the degree of interaction for the $[Al]_{MAO}$ bound to the support in terms of weight loss and removal temperature. As a matter of fact, too strong interaction can result in it being more difficult for the $[Al]_{MAO}$ bound to the support to react with the metallocene catalyst during activation processes, leading to low activity for polymerization. Conversely, the leaching of $[Al]_{MAO}$ can occur due to very weak interaction resulting in low activity as well. Therefore, the optimum interaction between the $O_{support}$–$Al_{cocatalyst}$ linkage is necessary. Here, the TGA measurement was performed to prove the interaction between the $[Al]_{MAO}$ and various supports. The TGA profiles of $[Al]_{MAO}$ on various supports are shown in Fig. 7 indicating similar profiles for various supports. We observed that the

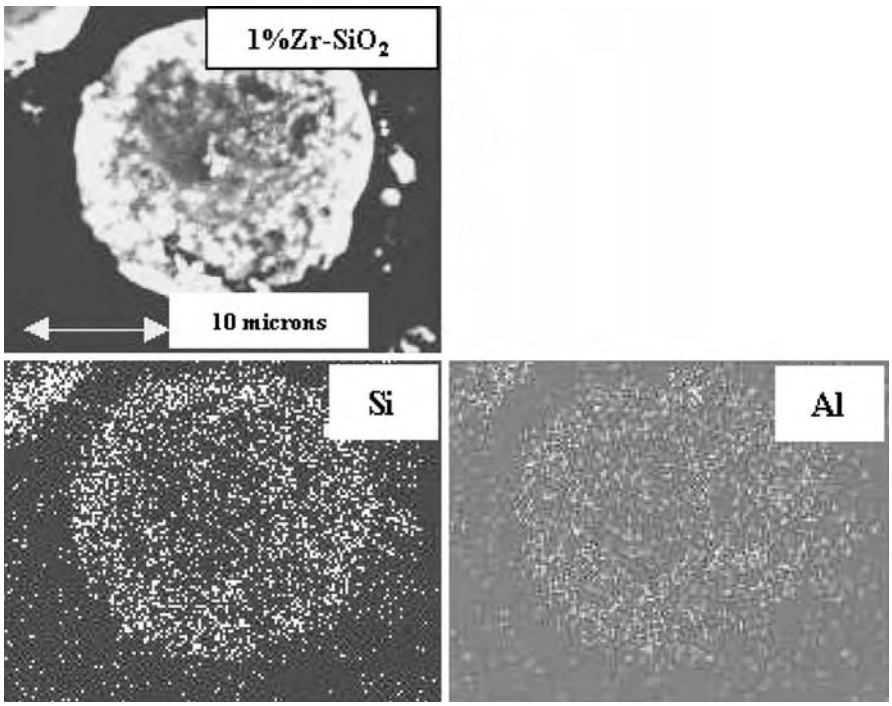

Fig. 5 A typical SEM/EDX mapping of (cross-sectional area) of Zr-modified silica supports after the MAO impregnation

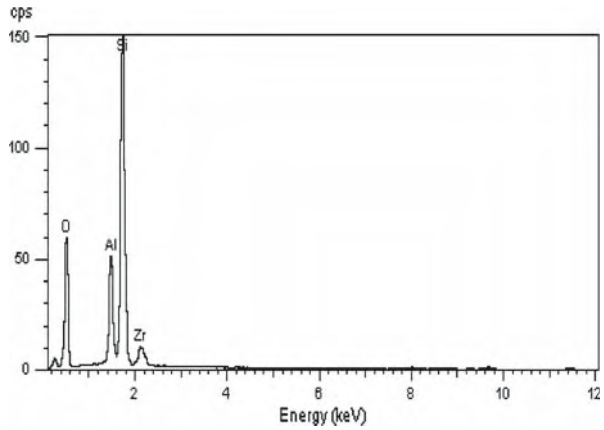

Supported MAO	$[Al]_{MAO}$ (wt%) on the support
MAO/SiO_2	4.93
$MAO/1\%Zr\text{-}SiO_2$	6.63
$MAO/2\%Zr\text{-}SiO_2$	6.78
$MAO/5\%Zr\text{-}SiO_2$	7.36

Fig. 6 A typical spectrum of the supported MAO from EDX analysis used to measure the average $[Al]_{MAO}$ concentration on various supports

weight loss of $[Al]_{MAO}$ present on various supports was in order of $5\%Zr\text{–}SiO_2$ (12.6%)–SiO_2 (12.4%) > $1\%Zr\text{–}SiO_2$ (10.8%) > $2\%Zr\text{–}SiO_2$ (10.0%). This indicated that $[Al]_{MAO}$ present on $5\%Zr\text{–}SiO_2$ support had the weakest interaction among other supports. Although it had the highest amount of $[Al]_{MAO}$ among other Zr-modified supports, it exhibited the lower activity. This should be due to the weak interaction as mentioned before. Based on the observed polymerization activities, it is worth noting that

Table 1 Polymerization activities[a]

Samples	Yield (g)	Polymerization Time (sec)	Catalytic Activity (kg of polymer/molZr h)
SiO_2	0.6348	384	3,968
$1\%Zr\text{–}SiO_2$	1.7586	156	27,055
$2\%Zr\text{–}SiO_2$	1.7757	167	25,519
$5\%Zr\text{–}SiO_2$	1.0644	180	14,192

[a] Activities were measured at polymerization temperature of 70 °C, [ethylene] = 0.018 mole, [1-octene] = 0.018 mole, $[Al]_{MAO}/[Zr]_{cat}$ 2,270, $[Al]_{TMA}/[Zr]_{cat} = 2{,}500$, in toluene with total volume = 30 ml, and $[Zr]_{cat} = 5 \times 10^{-5}$ M

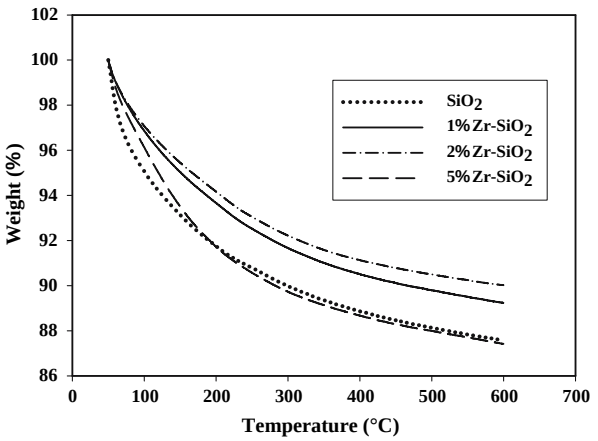

Fig. 7 TGA profiles of $[Al]_{MAO}$ on various Zr-modified silica supports

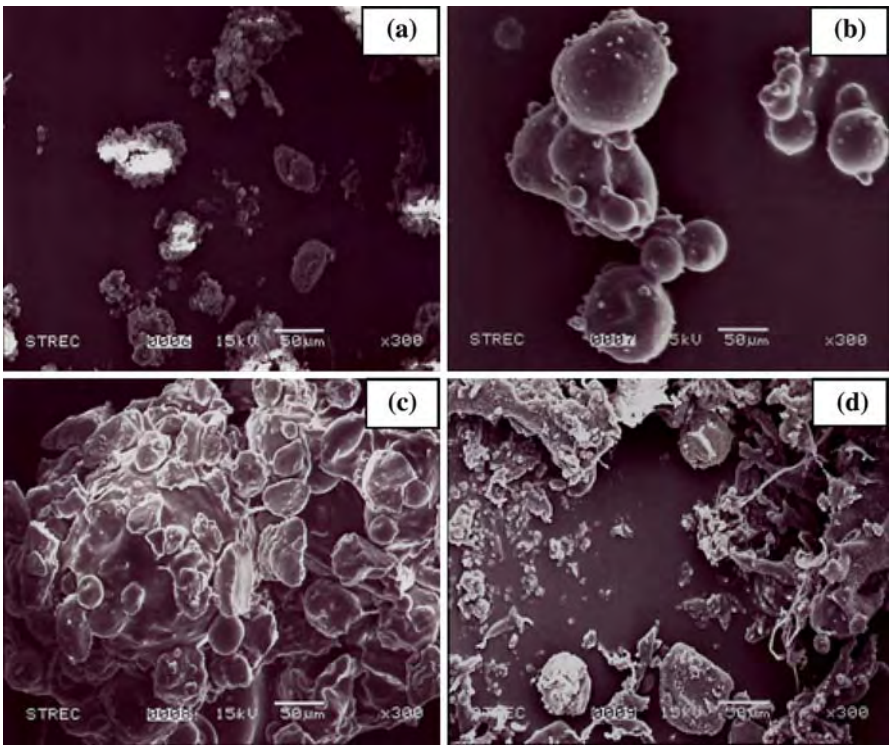

Fig. 8 SEM micrographs of ethylene/1-octene copolymers obtained from various Zr-modified silica supports; (**a**) SiO_2, (**b**) 1%Zr–SiO_2, (**c**) 2%Zr–SiO_2, and (**d**) 5%Zr–SiO_2

Table 2 Triad distribution of EO copolymers[a] and their melting temperature (T_m)[b]

Polymer samples obtained from	OOO	EOO	EOE	EEE	OEE	OEO	Mol. %O insertion	T_m (°C)
SiO_2	0.000	0.000	0.043	0.855	0.102	0.000	4.3	97
1%Zr–SiO_2	0.000	0.000	0.078	0.719	0.201	0.002	7.8	86
2%Zr–SiO_2	0.000	0.000	0.125	0.615	0.234	0.026	12.8	88
5%Zr–SiO_2	0.000	0.000	0.104	0.683	0.198	0.015	10.4	94

[a] Obtained from ^{13}C NMR

[b] Obtained from DSC

in order to obtain the high polymerization activity, one needs to consider on both high concentration of $[Al]_{MAO}$ present and the interaction between the $O_{support}$–$Al_{cocatalyst}$ linkage. A wide range of variables including the concentration of $[Al]_{MAO}$ and support interaction between the $O_{support}$–$Al_{cocatalyst}$ linkage can affect the polymerization activity. These effects of both $[Al]_{MAO}$ concentration and interaction of $O_{support}$–$Al_{cocatalyst}$ linkage can be superimposed on each other. Thus, an increase in the amount of $[Al]_{MAO}$ can result in weaker interaction (as seen for the 5%Zr–SiO_2 support) leading to lower polymerization activity compared to other Zr-modified supports.

The obtained copolymers were further characterized using SEM, ^{13}C NMR and DSC measurements. The SEM micrographs of polymers are shown in Fig. 8 indicating the typical morphologies of copolymers obtained from this catalytic system [9, 14]. There was no significant change in copolymer morphologies upon various supports employed. The quantitative analysis of triad distribution for all copolymers was conducted on the basic assignment of the ^{13}C NMR spectra [20]. The triad distribution for all copolymers is shown in Table 2. All copolymers produced from different supports exhibited the similar triad distribution having the majority triad of EEE without the triad of OOO. Based on ^{13}C NMR, it was suggested that the zirconia modification did not affect the microstructure of copolymers. However, considering the insertion of 1-octene (Table 2), it was found that zirconia modification resulted in an increase in 1-octene insertion. This was probably due to decreased steric hindrance in Zr-modified silica supports. It should be mentioned that the amounts of polyethylene products which should have been produced based on the 1-octene insertion (4.3–12.8 mol.%) obtained from the ^{13}C NMR

results as listed in Table 2 is about 0.6–0.8 g. However, the obtained polymer yields as seen in Table 1 are higher. This should be probably due to the presence of high MW polyoctene or some impurities, which cannot be dissolved using the 1,2 dichlorobenzene prior to the ^{13}C NMR measurement. Therefore, the degree of 1-octene insertion obtained from ^{13}C NMR was less than that calculated from the polymer yield obtained. In addition, the melting temperatures (T_m) of copolymers were evaluated using DSC as also shown in Table 2. It revealed that T_m of copolymers trended to decrease with zirconia modification on the support. The decreased T_m of copolymers can be attributed to the increased degree of 1-octene insertion, which can be confirmed by ^{13}C NMR as mentioned before.

4 Conclusions

The zirconia modification on the silica support was found to enhance the catalytic activity for ethylene/1-octene copolymerization using the zirconocene/MAO catalyst. The increased activities can be attributed to the larger amounts of $[Al]_{MAO}$ present on the modified support coupled with stronger interaction between the $O_{support}$–$Al_{cocatalyst}$ linkage. The zirconia modification can also increase the degree of 1-octene insertion without any significant change in polymer microstructure. Increased degree of 1-octene insertion consequently resulted in decreased T_m of copolymers obtained.

Acknowledgments The authors thank the Thailand Research Fund (TRF) for RMU50-B. Jongsomjit, the National Research Council of Thailand (NRCT) and Thailand-Japan Technology Transfer Project (TJTTP-JBIC) for the financial support of this work. We also extend our thankful to Professor Takeshi Shiono at Hiroshima University, Japan for his kind advice of this project.

References

1. Kaminsky W, Miri M, Sinn H, Woldt R (1983) Macromol Chem Rapid Commun 4:417
2. Ewen JA (1984) J Am Chem Soc 106:6355
3. Uusitalo AM, Pakkanen TT, Iskola EI (2002) J Mol Catal A Chem 177:179
4. Soga K, Kaminaka M (1993) Macromol Chem 194:1745
5. Ko YS, Han TK, Park JW, Woo SI (1996) Macromol Rapid Commun 17:749
6. Margue M, Conte A (2002) J Appl Polm Sci 86:2054
7. Belelli PG, Ferreira ML, Damiani DE (2002) Appl Catal A Gen 228:132
8. Koppl A, AH HG (2001) J Mol Catal A Chem 165:23
9. Jongsomjit B, Prasertham P, Kaewkrajang P (2004) Mater Chem Phys 86:243
10. Rai T, Ban JT, Uozumi T, Soga K (1997) Macromol Chem Phys 198:229
11. Lee PH, Yoon KB, Noh SK (1997) Macromol Rapid Commun 18:427
12. Jongsomjit B, Kaewkrajang P, Praserthdam P (2004) Catal Lett 94:205
13. Jongsomjit B, Ngamposri S, Praserthdam P (2005) Molecules 10:603
14. Jongsomjit B, Ngamposri S, Praserthdam P (2005) Catal Lett 100:139
15. Ali S, Chen B, Goodwin JG Jr (1995) J Catal 157:35
16. Jongsomjit B Panpranot J, Goodwin JG Jr (2003) J Catal 215:66
17. Khaodee W, Jongsomjit B, Assabumrungrat S, Praserthdam P (2007) Catal Commun 8:548
18. Ketloy C, Jongsomjit B, Praserthdam P (2007) Appl Catal 327:270
19. Severn JR, Chadwick JC, Duchateau R, Friedeichs N (2005) Chem Rev 105:4073
20. Randall JC (1989) J Macromol Sci Rev Macromol Chem Phys C29:201

Catal Lett (2009) 128:119–126
DOI 10.1007/s10562-008-9698-8

A Study on Characteristics and Catalytic Properties of Co/ZrO_2-B Catalysts Towards Methanation

Nithinart Chitpong · Piyasan Praserthdam · Bunjerd Jongsomjit

Received: 15 January 2008 / Accepted: 1 February 2008 / Published online: 15 October 2008

Abstract The B modification (0.5–3 wt%) on zirconia was found to increase the catalytic activities of Co catalyst during methanation. The B modification resulted in (i) preventing the agglomeration of Co oxide species, and (ii) increasing the dispersion of Co oxide species. Only a slight decrease in C_2–C_4 selectivity was observed.

Keywords Cobalt catalyst · Zirconia · Support · Boron modification · Methanation

1 Introduction

In general, supported catalysts usually consist of three components; (i) a catalytic phase, (ii) a promoter, and (iii) a support or carrier. In fact, the catalytic properties apparently depend on the components as mentioned above. The catalytic phase can be metals, metal oxides, and other metal compounds. These can be employed under the specified catalytic reactions. The catalytic performance can be effectively improved by using a promoter such as a noble metal. Besides the catalytic phase and promoter, it is worth noting that a support could play a crucial role for altering the catalytic performance. Basically, a support material acts as a carrier for the catalytic phase to be well dispersed on it. However, due to the supporting effect along with dispersion of the catalytic phase, the properties of a catalyst could be altered with various supports used. It is reported that many inorganic supports such as silica (SiO_2) [1], alumina (Al_2O_3) [1–5], titania (TiO_2) [1, 6–11], zirconia (ZrO_2) [5, 6], and zeolites have been extensively studied for years. During recent years zirconia has received much attention from researchers in the fields of heterogeneous catalysis as a support material as well as a catalyst because it is more chemically inert than the classical supports and it may possess different chemical properties such as acidity, basicity, reducing, or oxidizing ability [5, 6, 12–14]. However, it should be noted that the properties of zirconia itself may not be suitable as a sole support for the supported cobalt catalyst. Hence, the modification of the zirconia support would be necessary. It has been reported that some metals, such as boron were used to modify the properties of other supports such as alumina or titania [15–19]. It shows a significant enhancement of catalytic activity of cobalt due to increased cobalt dispersion.

In the present study, the effect of boron modification of zirconia on the characteristics and catalytics properties of zirconia-supported cobalt catalyst during CO hydrogenation was investigated. Experimentally, the boron-modified zirconia was prepared by impregnation of boric acid as the source of boron onto the zirconia support. The amounts of boron loading were varied in the range of 0.5 to 3 wt%. After calcination of the modified support, cobalt nitrate was impregnated onto the modified supports. Then, the catalyst samples were characterized using various techniques. The reaction study on carbon monoxide (CO) hydrogenation was performed in order to evaluate the catalytic activity and selectivity of products.

N. Chitpong · P. Praserthdam · B. Jongsomjit (✉)
Center of Excellence on Catalysis and Catalytic Reaction Engineering, Department of Chemical Engineering, Faculty of Engineering, Chulalongkorn University, Bangkok 10330, Thailand
e-mail: bunjerd.j@chula.ac.th

2 Experimental

2.1 Materials

2.1.1 B-Modified ZrO_2 Support

The B-modified ZrO_2 supports were prepared by the incipient impregnation method. First, boron was impregnated on the ZrO_2 support [from Aldrich(<5 μmicron, 99.99%)] using a solution of boric acid (99.99%, Aldrich) to produce B-modified ZrO_2 supports having 0.5, 1, and 3 wt% of B. Then, the B-modified ZrO_2 supports were calcined at 500 °C for 4 h prior to impregnation of cobalt.

2.1.2 Co/B-Modified ZrO_2 Catalyst

Cobalt nitrate [$Co(NO_3)_2{\cdot}6H_2O$] was dissolved in deionized water and impregnated on the support as derived above to give a final catalyst with 20 wt% of cobalt. The catalyst precursor was dried at 110 °C for 12 h and calcined in air at 500 °C for 4 h.

2.2 Catalyst Nomenclature

The nomenclature used for the support and catalyst samples in this study is as follows:

ZrB-0: ZrO_2 support without B modification
ZrB-*i*: B-modified ZrO_2 having *i* wt% of B
Co/support: supported cobalt catalyst on various supports as derived above

2.3 Catalyst Characterization

2.3.1 BET Surface Area

BET surface area of the samples after calcination was performed to determine if the total surface area changes upon the various B loadings. It was determined using N_2 adsorption at 77 K in a Micromeritics ASAP 2010.

2.3.2 X-ray Diffraction

XRD was performed to determine the bulk crystalline phases of catalyst following different B loadings. It was conducted using a SIEMENS D-5000 X-ray diffractometer with CuK_α (λ = 1.54439 Å). The spectra were scanned at a rate of 2.4° min^{-1} in the range 2θ = 20–80°.

2.3.3 Temperature-Programmed Reduction

TPR was used to determine the reduction behaviors of the samples. It was carried out using 50 mg of a sample and a temperature ramp from 35 to 800 °C at 5 °C/min. The carrier gas was 5%H_2 in Ar. A cold trap was placed before the detector to remove water produced during the reaction. A thermal conductivity detector (TCD) was used to determine the amount of H_2 consumed during TPR [20, 21].

2.3.4 Scanning Electron Microscopy and Energy Dispersive X-ray Spectroscopy

The catalyst granule morphology and elemental distribution were obtained using a Hitachi S-3500N scanning electron microscopy (SEM). The SEM was operated using the back scattering electron (BSE) mode at 20 kV and a working distance (the distance between the sample and the electron beam) of 20 mm. After the SEM micrographs were taken, EDX was performed to determine the elemental concentration distribution on the catalyst granules using INCA software.

2.3.5 Transmission Electron Microscopy

The dispersion of cobalt oxide species on the various supports was determined using a JEOL-TEM 200CX transmission electron microscopy operated at 200 kV with 25 k magnification.

2.3.6 Hydrogen Chemisorption

Static H_2 chemisorption at 100 °C on the reduced samples [at 350 °C for 10 h in H_2 (30 cc/min)] was used to determine the number of reduced surface cobalt metal atoms. This is related to the overall activity of the samples during CO hydrogenation. Gas volumetric chemisorption at 100 °C was performed using the method described by Reuel and Bartholomew [22]. The experiment was performed in a Micromeritics ASAP 2010 using ASAP 2010C V3.00 software.

2.4 Reaction Study

Methanation (H_2/CO = 10/1) was performed to determine the overall activity of the catalyst samples reduced at various conditions. Methanation was carried out at 220 °C and 1 atm. A flowrate of H_2/CO/Ar = 20/2/8 cc min^{-1} in a fixed-bed flow reactor was used. A relatively high H_2/CO ratio was used to minimize deactivation due to carbon deposition during reaction. Typically, 20 mg of a catalyst sample was reduced in situ in flowing H_2 (30 cc min^{-1}) at 350 °C for 10 h prior to the reaction. Reactor effluent samples were taken at 1 h intervals and analyzed by GC. In all cases, steady-state was reached within 5 h.

3 Results and Discussion

The present study focused on the effect of boron (B) modification on zirconia-supported cobalt catalysts for methanation. The BET surface area and cobalt oxide crystallize size obtained from the XRD measurement using Scherrer's equation [22] are listed in Table 1. The BET surface areas of B-modified zirconia supports decreased from 2.6 to 1.1 m^2/g upon increasing the amounts of boron loading. The pore size distributions of the unmodified and B-modified zirconia support are shown in Fig. 1. In fact, the slightly bimodal pore size distribution for the unmodified zirconia support was observed. However, with the B modification, the unimodal pore size distribution of the B-modified zirconia supports was evident. It indicated that B was presumably located in the small pore of zirconia support resulting in the disappearance of the small pore portion as seen in Fig. 1. Considering the surface areas of the zirconia-supported cobalt catalysts with B modification, they apparently increased from 1.8 to 12.6 m^2/g with increasing the amounts of B loading in the zirconia supports. This was suggested that the B modification could prevent the agglomeration of Co oxide species resulting in increased surface areas of the catalyst samples. The XRD patterns for different zirconia supports consisting of various amounts of boron loading are shown in Fig. 2. The unmodified zirconia support exhibited the strong XRD peaks at 29° and 32° assigning to the ZrO_2 in the monoclinic phase, and the strong XRD peak at 50° indicating the ZrO_2 in the tetragonal phase. In addition, the strong XRD peak at 29° (overlap with the XRD peak for the monoclinic phase of ZrO_2) was detected for the zirconia supports with B modification also assigning to the B_2O_3 species [24]. Figure 3 shows the XRD patterns of different zirconia-supported cobalt catalysts consisting of

Table 1 Characteristics of supports and catalysts

Samples	BET Surface Area (m^2/g)[a]	XRD Co oxide crystallize size[b] (nm)	TEM Co oxide particle size[c] (nm)
ZrB-0	2.6	–	–
ZrB-0.5	1.8	–	–
ZrB-1	1.3	–	–
ZrB-3	1.1	–	–
20-Co/ZrB-0	1.8	59.6	259
20-Co/ZrB-0.5	6.8	55.0	236
20-Co/ZrB-1	12.4	32.1	207
20-Co/ZrB-3	12.6	11.6	159

[a] Measurement error is ±5%

[b] Determined by XRD line broadening using Scherrer's equation [23]

[c] Derived from the measurement of average particle size as seen by TEM micrographs

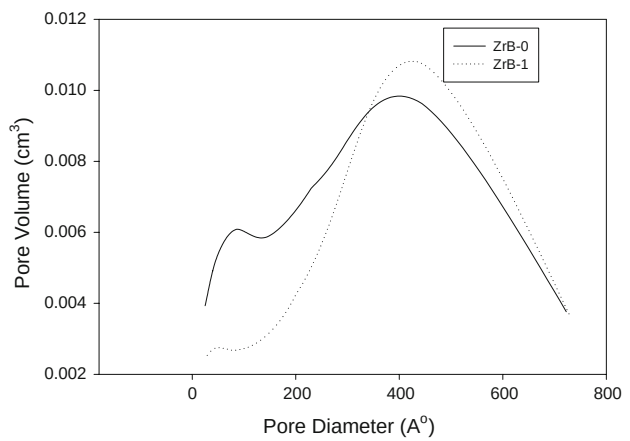

Fig. 1 Pore size distribution of supports

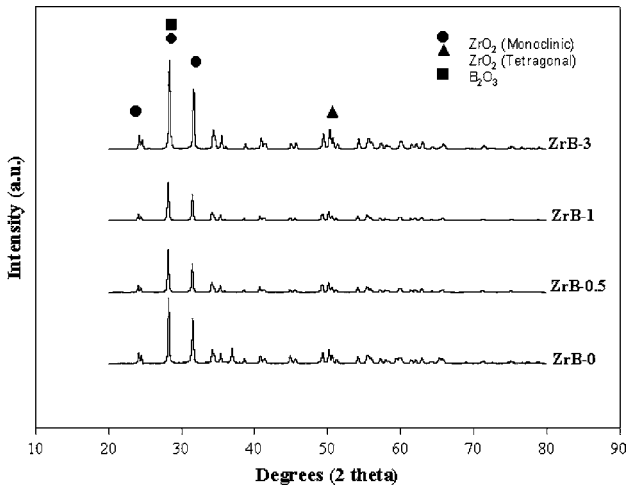

Fig. 2 XRD patterns for different ZrO_2 supports consisting of various amounts of boron loading

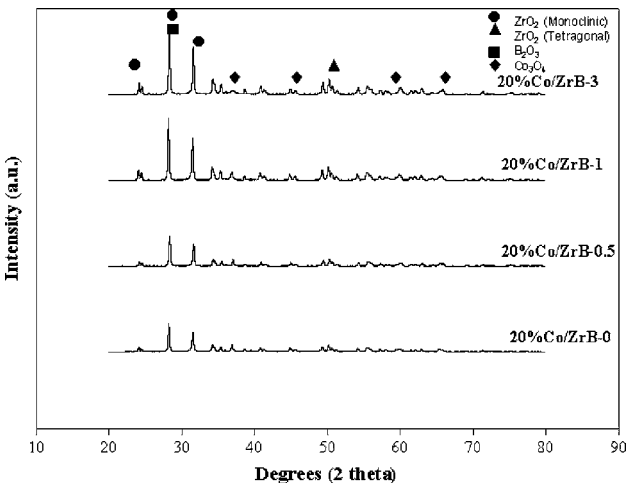

Fig. 3 XRD patterns for different Co/ZrO_2 catalysts with various amounts of boron modification on zirconia support

various amounts of B loading in the zirconia supports. The catalyst samples exhibited XRD peaks at 36°, 45°, 60° and 65° indicating the presence of Co_3O_4 species. The XRD crystallize size of cobalt catalysts decreased from 59.6 to 11.6 nm upon increasing the amounts of B loading indicating high Co oxide dispersion with the B modification on zirconia support. This result was in accordance with the obtained surface areas as mentioned above.

In order to study the morphologies and elemental distribution of the catalyst samples, SEM and EDX were performed, respectively. The SEM micrograph and the elemental distribution for Co, Zr, and O for the unmodified zirconia-supported Co catalyst are shown in Fig. 4 whereas the typical SEM micrograph and the elemental distribution for the B-modified zirconia-supported Co catalyst are shown in Fig. 5. For both figures, it was found that the distribution of Co oxide species was well distributed all over the catalyst granule. In order to determine the dispersion and crystallite size of Co oxides species dispersed on the various supports employed, the high resolution TEM was used. The TEM micrographs for the unmodified and B-modified zirconia supports are shown in Fig. 6. There was no significant change in morphologies of the zirconia supports upon B modification. The dispersion of Co oxide species on various zirconia supports is illustrated in Fig. 7. It can be observed that the dispersion of Co oxide species apparently increased with increasing the amounts of B loading in the zirconia support resulting in the smaller size of the Co oxides present. The TEM results were in agreement with we have found using the XRD measurement as mentioned before. As seen from Table 1, the crystallite size obtained from XRD measurement of the Co oxide species decreased from 59.6 to 11.6 nm upon increasing the amount of B loading from 0.5 to 3 wt% into the zirconia support. Considering the Co oxide sizes obtained from the TEM measurement as also listed in Table 1, they apparently ranged between 159 and 259 nm. The Co oxide sizes also decreased with the B modification as observed by XRD. However, when compared the Co oxide sizes obtained from XRD and TEM measurement, it was found that the sizes obtained from the TEM were much larger (about an order of magnitude). This was due to the agglomeration of the primary particles into the secondary particles as seen by the TEM used in this study.

The TPR measurement was performed in order to determine the reduction behaviors of Co oxides species on various samples. The TPR profiles of various zirconia-supported Co catalysts with and without B modification on zirconia supports are shown in Fig. 8 and the reduction temperatures are listed in Table 2. Basically, only two reduction peaks can be observed. The peaks can be assigned to the two-step reduction of Co_3O_4 to CoO and then to Co^0 [21, 25]. Upon the TPR conditions, the two reduction peaks based on two-step reduction may or may

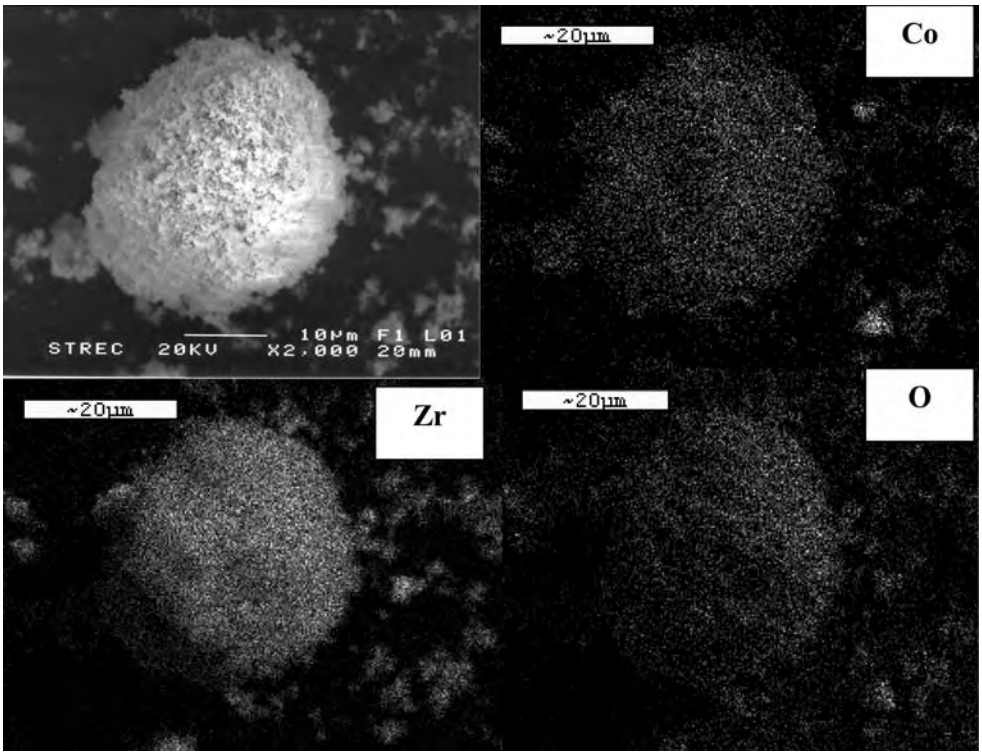

Fig. 4 A typical SEM micrograph and EDX mapping for 20-Co/ZrB-0 sample

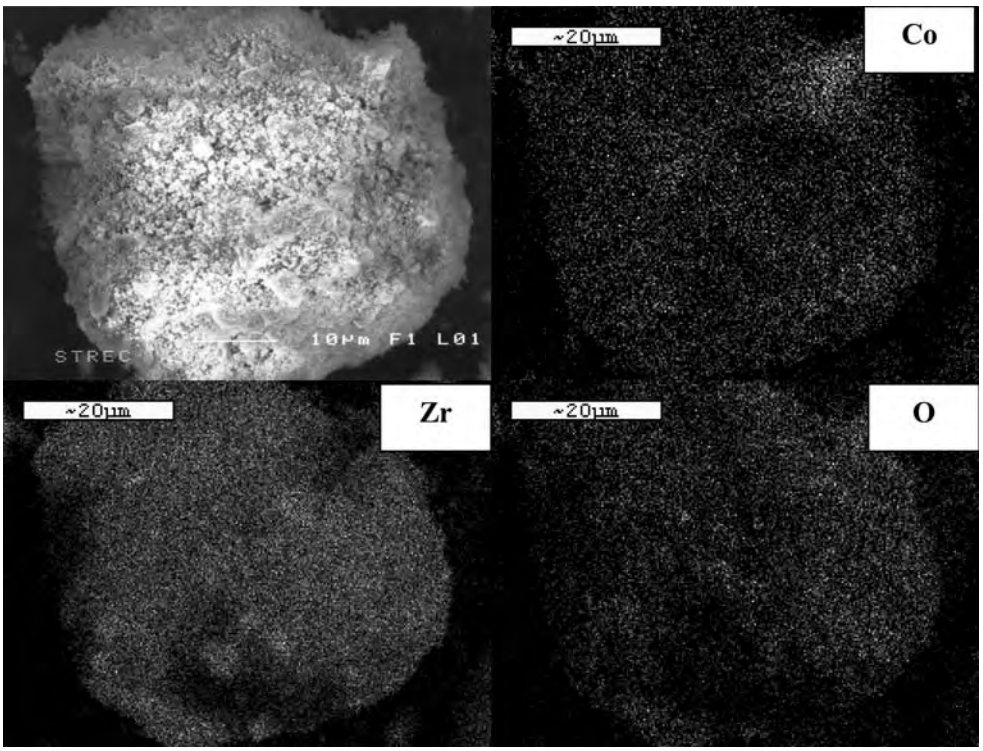

Fig. 5 A typical SEM micrograph and EDX mapping for 20-Co/ZrB-3 sample

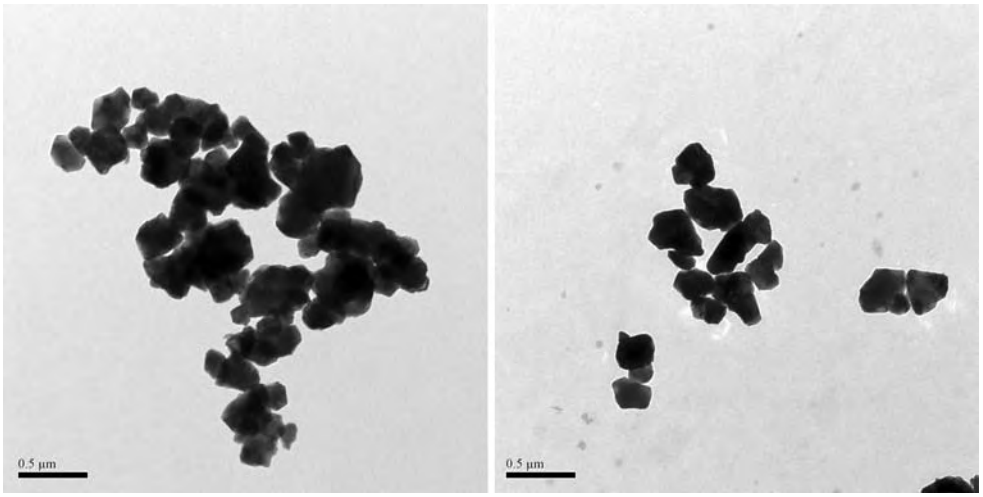

Fig. 6 TEM micrographs for different ZrO_2 supports consisting of various amounts of boron loading; ZrB-0 (Left) and ZrB-3 (Right)

not be observed. Here, for the unmodified zirconia-supported Co catalyst, the broad reduction peak (ca.230–490 °C) having a little shoulder (ca. 300 °C) can be observed assigning to the overlap of two-step reduction. However, with the B modification we found that the reduction peaks were shifted to the higher reduction temperatures. The reducibility during TPR (30–800 °C) as also shown in Table 2 were in the range of 18.9 to 22.3%. It was suggested that the B-modification can result in lower degree of reduction, especially with high amounts (3 wt%) of B loading on the zirconia supports. The smaller size of Co oxide species, the more difficult of them to be reduced. However, it should be noted that TPR conditions were different from the standard reduction used prior to reaction. Therefore, the H_2 chemisorption was performed in order to determine the number of reduced cobalt metal surface atoms. It is known that the active form of cobalt catalysts for CO hydrogenation is cobalt metal (Co^0). Thus,

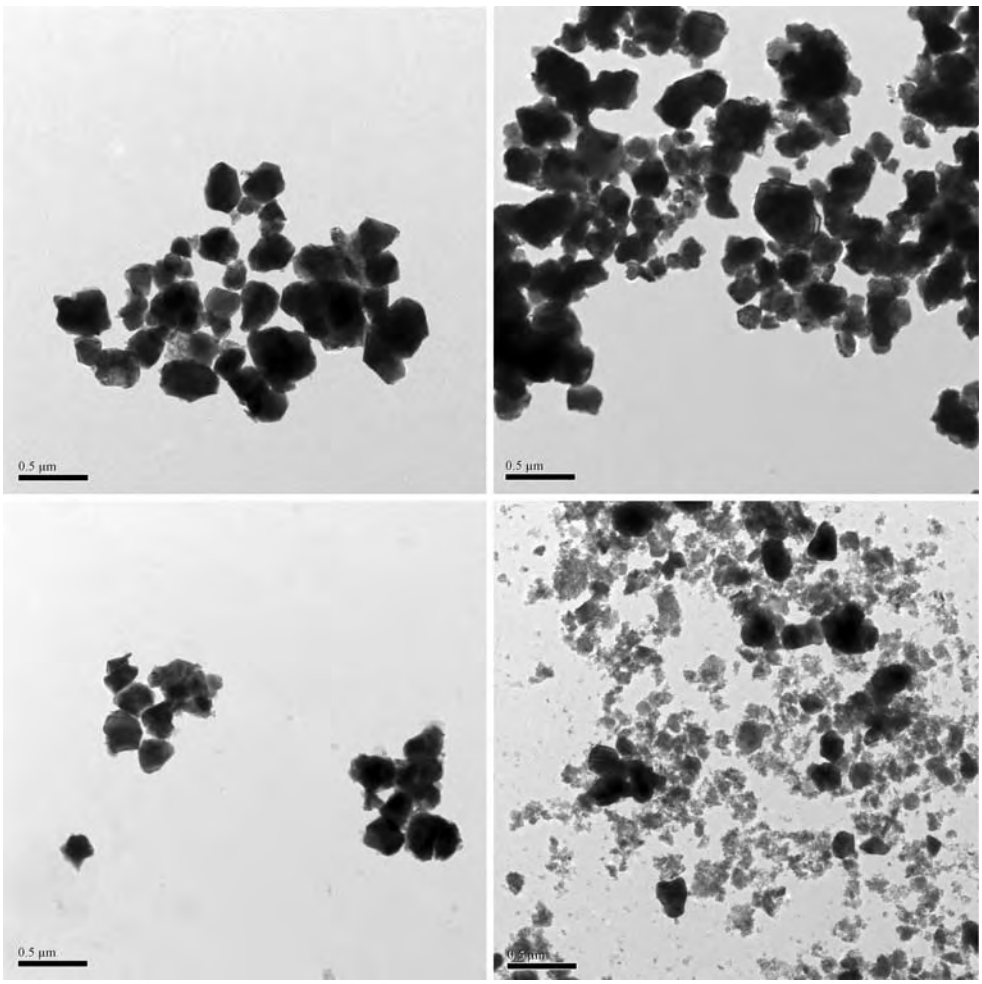

Fig. 7 TEM micrographs for different Co/ZrO_2 catalysts with various amounts of boron modification on zirconia support; 20Co/ZrB-0 (Top-Left), 20Co/ZrB-0.5 (Top-Right), 20Co/ZrB-1 (Bottom-Left) and 20Co/ZrB-3 (Bottom-Right)

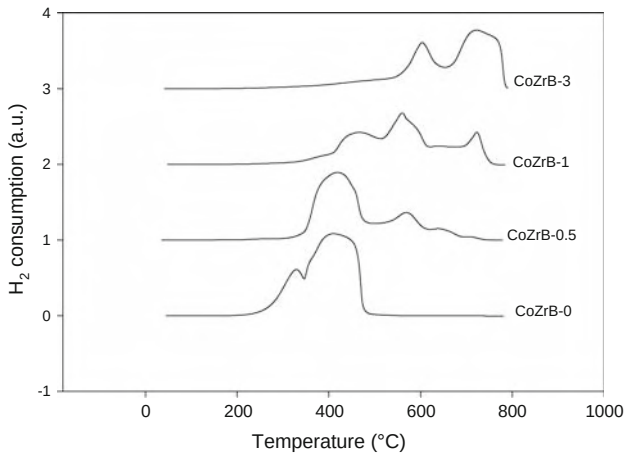

Fig. 8 TPR profiles for different Co/ZrO_2 catalysts with various amounts of boron modification on zirconia support

reduction of cobalt oxide species is essentially performed in order to transform cobalt oxides obtained after calcination process into the active cobalt metal atoms for

Table 2 Reduction temperature of catalyst samples

Catalyst samples	Reduction temperature (°C)			% Reducibility during TPR (30–800 °C)[a]
	Initial	Final	Maximum	
20-Co/ZrB-0	230	490	420	22.3
20-Co/ZrB-0.5	330	760	450	19.8
20-Co/ZrB-1	350	770	570	18.9
20-Co/ZrB-3	560	800	750	19.8

[a] Based on the peak areas below TPR curve

Table 3 H_2 chemisorption and % cobalt dispersion

Catalyst samples	Total H_2 chemisorption (μmol H_2/g cat)	Cobalt dispersion (%)
20-Co/ZrB-0	0.33	1.9
20-Co/ZrB-0.5	0.44	2.6
20-Co/ZrB-1	0.47	2.8
20-Co/ZrB-3	0.34	2.0

Table 4 Activities and selectivity of various catalysts during CO hydrogenation

Catalyst samples	CO conversion (%)	Steady-state rate[a] ($x10^2 gCH_2/g$ cat h)	CH_4 selectivity (%)	C_2–C_4 selectivity (%)	TOF_H[b] (s^{-1})
20-Co/ZrB-0	8	3.0	96.5	3.5	0.36
20-Co/ZrB-0.5	54	20.2	99.0	1.0	1.82
20-Co/ZrB-1	68	25.2	99.0	1.0	2.13
20-Co/ZrB-3	61	22.7	98.9	1.1	2.66

[a] Methanation was carried out at 220 °C, 1 atm and $H_2/CO/Ar = 20/2/8$. The steady-state was reached after 5 h

[b] Based on the H_2 chemisorption

catalyzing the reaction. Hence, the static H_2 chemisorption on the reduced cobalt samples (at the same condition used to reduce the catalyst samples prior to reaction) was used to determine the number of cobalt metal surface atoms. This is usually related to the overall activity of the catalyst during CO hydrogenation. The H_2 chemisorption results are shown in Table 3 indicating increased Co dispersion upon the B modification.

The reaction study under methanation was also investigated in order to measure the activity and selectivity of catalysts. The reaction study results are listed in Table 4. The CO conversion ranged between 8 and 68% upon the B modification. It was obvious that the catalytic activities of the zirconia-supported Co catalyst dramatically increased about 6–8 times with B-modification on the zirconia supports. Increased activities upon B-modification can be attributed to increased dispersion of Co oxide species as seen from the XRD and TEM measurements. This was suggested that the higher degree dispersion of Co oxide species could facilitate the reduction of Co oxides giving the higher number of the Co metal surface atoms for catalyzing the reaction. However, it should be carefully noted that too small crystallite sizes of Co oxides, i.e., 11.6–32.1 nm (obtained from the XRD measurement), which were corresponding to the amounts of B loading of 0.5 and 3 wt%, respectively essentially decreased the degree of reduction resulting in a slight decrease in activity. It was interesting to note that the rate increased from 20-Co/ZrB-0 to 20-Co/ZrB-0.5, but the rate was more constant for 20-Co/ZrB-0.5, 20-Co/ZrB-1, and 20-Co/ZrB-3. However, the Co oxide sizes (based on XRD) decreased from 55 nm for 20-Co/ZrB-0.5 to 32 nm for 20-Co/ZrB-1, and to 11.6 nm for 20-Co/ZrB-3. It should be mentioned that XRD was used to measure the size of Co oxide species, not the reduced Co metal atoms. This suggested that the sizes of Co oxide species was the only factor that insured larger number of reduced Co metal atoms [10]. In fact, the kinetics of reduction can be affected by a wide range of variables, including crystallite size, support interaction, and reduction gas composition [2–4]. The effects of crystallite size and support interaction can be superimposed on each other. Thus, while a decrease in metal oxide crystallite size can result in faster reduction due to greater surface area/volume ratio, smaller particles may interact more with the support, slowing reduction. The similar phenomenon was also discussed for the dispersion of Co oxide species on titania supports consisting of various ratios of anatase and rutile phases [9, 10, 26]. Thus, this was also confirmed that highly dispersed forms of Co oxide species were not only the factor to insure larger number of reduced Co metal surface atoms. Considering the product selectivity upon methanation condition as seen in Table 4, it was found that the selectivity to C_2–C_4 products slightly decreased with the B modification on the zirconia supports. The TOF values (0.36–2.66 s^{-1}) calculated on the basis of H_2 chemisorption for all samples are also shown in Table 4. It indicated that the enhanced activities during methanation for the catalyst samples with B modification were apparently attributed to increased TOF values (about an order of magnitude). Yamasaki et al. [27] reported on the use of Ni/ZrO_2 catalysts under similar methanation condition. They found that the TOF values ranged between 0.73 and 5.43 s^{-1}. These were similar to the TOF values reported in this work, which were typical for the cobalt catalyst under this condition.

4 Conclusions

It appeared that B modification on the zirconia supports resulted in increased activities based on methanation without a dramatic change in the product selectivity. The increased activities can be attributed to higher dispersion of Co oxide species on the support. It was suggested that the role of B modification could be drawn based on (i) preventing the agglomeration of Co oxide species and (ii) increasing the dispersion of the Co oxide species, then facilitating reduction of Co oxides to Co metal surface atoms for catalyzing the reaction.

Acknowledgments We thank the Thailand Research Fund (TRF) for RMU50-B. Jongsomjit and the graduate school at Chulalongkorn University (90th Anniversary of CU under the Golden Jubilee Fund) for financial support of this project.

References

1. Jacobs G, Das T, Zhang Y, Li J, Racoillet G, Davis BH (2002) Appl Catal A: Gen 233:263
2. Jongsomjit B, Panpranot J, Goodwin JG Jr (2001) J Catal 204:98
3. Jongsomjit B, Goodwin JG Jr (2002) Catal Today 77:191
4. Jongsomjit B, Panpranot J, Goodwin JG Jr (2003) J Catal 215:66
5. Enache DI, Auberger MR, Revel R (2004) Appl Catal A: Gen 268:51
6. Kraum M, Baerns M (1999) Appl Catal A: Gen 186:189
7. Madikizela NN, Coville NJ (2002) J Mol Catal A: Chem 181:129
8. Jongsomjit B, Sakdamnuson C, Goodwin JG Jr, Praserthdam P (2004) Catal Lett 94:209
9. Jongsomjit B, Sakdamnuson C, Praserthdam P (2005) Mater Chem Phys 89:395
10. Jongsomjit B, Wongsalee T, Praserthdam P (2005) Mater Chem Phys 92:572
11. Wongsalee T, Jongsomjit B, Praserthdam P (2006) Catal Lett 108:55
12. Panpranot J, Taochaiyaphum N, Praserthdam P (2005) Mater Chem Phys 89:395
13. Panpranot J, Taochaiyaphum N, Jongsomjit B, Praserthdam P (2006) Catal Commun 7:192
14. Soisuwan P, Praserthdam P, Panpranot J, Trimm DL (2006) Catal Commun 7:761
15. Stranick MA, Houalla M, Hercules DM (1987) J Catal 104:396
16. Li J, Coville NJ (1999) Appl Catal A: Gen 181:201
17. Li J, Coville NJ (2002) Catal Today 71:403
18. Li J, Jacobs G, Zhang Y, Das T, Davis BH (2002) Appl Catal A: Gen 223:195
19. Brik Y, Kacimi M, Verduraz FB, Ziyad MJ (2002) J Catal 211:470
20. Kogelbaue A, Weber JC, Goodwin JG Jr (1995) Catal Lett 34:269
21. Zhang Y, Wei D, Hammache S, Goodwin JG Jr (1999) J Catal 188:281
22. Reuel RC, Bartholomew CH (1984) J Catal 85:63
23. Klug HP, Alexander LE (1974) X-ray diffraction procedures for polycrystalline amorphous, 2nd edn. Wiley, New York
24. Tupabut P, Jongsomjit B, Praserthdam P (2007) Catal Lett 118:195
25. Schanke D, Vada S, Blekkan EA, Hilmen A, Hoff A, Holmen A (1995) J Catal 156:85
26. Jonsomjit B, Wongsalee T, Praserthdam P (2005) Catal Commun 6:705
27. Yamasaki M, Habasaki H, Asami K, Izumiya K, Hashimoto K (2006) Catal Commun 7:24

Materials Chemistry and Physics 112 (2008) 954–961

Contents lists available at ScienceDirect

Materials Chemistry and Physics

journal homepage: www.elsevier.com/locate/matchemphys

A comparative study on synthesis of LLDPE/TiO_2 nanocomposites using different TiO_2 by *in situ* polymerization with zirconocene/dMMAO catalyst

Wathanyoo Owpradit, Bunjerd Jongsomjit*

Center of Excellence on Catalysis and Catalytic Reaction Engineering, Department of Chemical Engineering, Faculty of Engineering, Chulalongkorn University, Bangkok 10330, Thailand

ARTICLE INFO

Article history:
Received 13 February 2008
Received in revised form 26 June 2008
Accepted 9 July 2008

Keywords:
Zirconocene catalyst
Cocatalyst
Catalyst characterization
Polymer nanocomposite
Titania

ABSTRACT

The present study revealed the effect of different TiO_2 nanoparticles employed on catalytic and characteristic properties of LLDPE/TiO_2 nanocomposites synthesized by the *in situ* polymerization with zirconocene/dMMAO catalyst. It was found that the presence of rutile phase in titania apparently resulted in decreased activities due to low intrinsic activity of active sites being present. Based on ^{13}C NMR results, all LLDPE/TiO_2 samples exhibited the random copolymer having different degree of 1-hexene insertion. The highly dispersion of titania can enhance the degree of 1-hexene insertion resulting in decreased crystallinity.

1. Introduction

The development of metallocene technologies has led to the synthesis of new polymers with different structures and properties to feed up the progressive demand of modern industry. According to the olefin polymerization, metallocenes are crucial since they can control the properties of polyolefins. Metallocene catalysts are often used in the heterogeneous form based on the most existent technologies such as gas phase and slurry polymerization. Therefore, they are supported on an insoluble carrier prior to the polymerization. The reasons for the heterogenization of the metallocene are to slower the deactivation of the metallocene, employ less cocatalyst required, protect the reactor fouling, control the polymer morphologies and fulfil the requirements of the commercial polymerization processes [1–3]. It has been known that polyethylene such as linear low-density polyethylene (LLDPE) is obtained via the copolymerization of ethylene with various alpha olefins. They have grown in importance because of the specific properties that can be obtained by varying comonomer content and polymerization condition.

Recently, polymer nanocomposites have attracted a great deal of interest from material scientists since their applications have dramatically improved material properties in engineering plastics. These characteristics usually resulted from the synergistic effect arising from the addition of the nanofillers. Depending on the composition and microstructure, the effects of different nanoparticles on the properties of polymers are different. The most commonly used inorganic nanoparticles are SiO_2 [4,5], TiO_2 [6–8], Al_2O_3 [9], and ZrO_2 [10]. In addition, TiO_2 nanoparticles were used as fillers in order to produce new materials. Due to many interesting properties of TiO_2 such as anti-bacterial with photocatalysis technique (when exposed to light radiation, the pairs of electron-cavity are formed on TiO_2, and consequently the oxygen and water absorbed in the surface of TiO_2 are radicalized). Hydroxyl (OH) excited by light plays an important role in catalysis reaction. It attacks the microorganisms and makes them lose activity [7] and optical properties (absorption of UV light up to the proximity of visible wavelengths, transparency at visible wavelengths, and very high refractive index) [6]. In general, polymer nanocomposites can be prepared by three methods, such as: (i) a melt mixing [11–13], (ii) a solution blending [14] and (iii) *in situ* polymerization [15–17]. Due to the direct synthesis via polymerization along with the presence of fillers, the *in situ* polymerization is perhaps considered the most promising technique to produce polymer nanocomposites with homogeneous distribution of the nanoparticles inside the polymer matrix. Although LLDPE/TiO_2 nanocomposites have been investigated by some authors [6,7], only the melt mixing or solution blending processes were employed to synthesize those polymer samples.

In this work, LLDPE/TiO_2 nanocomposites were synthesized by *in situ* polymerization of ethylene/1-hexene with zirconocene/dMMAO catalyst. The various TiO_2 nanofillers were employed. In general, they had different phases and crystallite sizes. The catalytic activity and properties of polymer nanocom-

* Corresponding author. Tel.: +66 2 2186869; fax: +66 2 2186877.
E-mail address: bunjerd.j@chula.ac.th (B. Jongsomjit).

0254-0584/$ – see front matter © 2008 Elsevier B.V. All rights reserved.
doi:10.1016/j.matchemphys.2008.07.050

posites obtained were further investigated and discussed in more details.

2. Experimental

2.1. Materials

All chemicals and polymerization were handled under an argon atmosphere using a glove box and/or Schlenk techniques. The TiO_2 nanoparticles [100.0% of anatase designated as TiO_2 (A) and 100.0% of rutile designated as TiO_2 (R)] were purchased from Aldrich Chemical Company, Inc. The mixed phases of anatase and rutile TiO_2 nanoparticles [90.7% of anatase and 9.3% of rutile designated as TiO_2 (D) and 80.4% of anatase and 19.6% of rutile designated as TiO_2 (J)] were donated from Degussa and Japan Reference Catalyst, respectively. They were heated at 673 K under vacuum for 6 h prior to impregnation with dMMAO. Toluene was dried over dehydrated $CaCl_2$ and distilled over sodium/benzophenone before use. The *rac*-ethylenebis (indenyl) zirconium dichloride (*rac*-Et[Ind]$_2$$ZrCl_2$) was supplied from Aldrich Chemical Company, Inc. Modified methylaluminoxane (MMAO) in hexane was donated by Tosoh (Akso, Japan). Trimethylaluminum (TMA, 2 M in toluene) was supplied by Nippon Aluminum Alkyls, Ltd., Japan. Ultrahigh purity argon was further purified by passing it through columns that were packed with BASF catalyst R3-11G (molecular-sieved to 3 Å), sodium hydroxide (NaOH), and phosphorus pentaoxide (P_2O_5) to remove traces of oxygen and moisture. Ethylene gas (99.96%) was donated by the National Petrochemical Co., Ltd., Thailand. 1-Hexene (99+%, $d = 0.673\ g\ mL^{-1}$) was purchased from Aldrich Chemical Company, Inc.

2.2. Preparation of dried MMAO (dMMAO)

Removal of TMA from MMAO was carried out according to the reported procedure [18]. The toluene solution of MMAO was dried under vacuum for 6 h at room temperature to evaporate the solvent, TMA and TIBA. Then, continue to dissolve with 100 mL of heptane and the solution was evaporated under vacuum to remove the remaining TMA and TIBA. This procedure was repeated four times and the white powder of dried MMAO (dMMAO) was obtained.

2.3. Preparation of dMMAO impregnated on TiO_2 nanoparticles (dMMAO/TiO_2)

The dMMAO (concentration of Al = 5.6 wt.% 1.00 g or 16.3 mmol) was impregnated on TiO_2 (1.30 g or 12.5 mmol) in 20 mL of toluene at room temperature. The mixture was stirred for 30 min. The solvent was then removed from the mixture by evacuated. This procedure was done only once with toluene (20 mL × 1) and three times with hexane (20 mL × 3). Then, the solid part was evaporated and dried under vacuum at room temperature. The gray powder of dMMAO/TiO_2 was then obtained.

2.4. Polymerization reaction

The copolymerization of ethylene/1-hexene was carried out in a 100 mL semi-batch stainless steel autoclave reactor equipped with magnetic stirrer. In the glove box, the desired amount of *rac*-Et[Ind]$_2$$ZrCl_2$ and TMA was mixed and stirred for 5 min aging to affect alkylation of the zirconocene catalyst. Then, toluene (to make a total volume of 30 mL) and 0.4 g of dMMAO/TiO_2 corresponding to the $[Al]_{dMMAO}/[Zr]_{cat}$ ratios of 2270 were introduced into the reactor for each run. After that, the mixture of *rac*-Et[Ind]$_2$$ZrCl_2$ and TMA was injected into the reactor. The reactor was frozen in liquid nitrogen to stop reaction and then 0.018 mol of 1-hexene was injected into the reactor. The autoclave was evacuated to remove the argon. Then, the reactor was heated up to polymerization temperature (343 K) and the polymerization was started by feeding ethylene gas (total pressure 50 psi in the reactor) until the consumption of ethylene at 0.018 mol (decreased ethylene pressure of 6 psi was observed) was reached. The reaction of polymerization was terminated by addition of acidic methanol (0.1% HCl in methanol). The reaction time was recorded for purpose of calculating the activity. The precipitated polymer was washed with methanol and dried at room temperature.

2.5. Characterization procedures

2.5.1. Characterization of the TiO_2 nanofillers

2.5.1.1. X-ray diffraction. XRD was performed to determine the bulk crystalline phases of samples. It was conducted using a SIEMEN D-5000 X-ray diffractometer with Cu Kα (λ = 1.54439 Å). The spectra were scanned at a rate of 2.4° min^{-1} in the range $2\theta = 10–80°$.

2.5.1.2. Transmission electron microscopy. TEM was used to determine the shape and size of TiO_2 nanoparticles. The sample was dispersed in ethanol before using TEM (JEOL JEM-2010) for microstructural characterization.

2.5.1.3. Thermal gravimetric analysis. TGA was performed using a TA Instruments SDT Q-600 analyzer. The samples of 10–20 mg and a temperature ramping from 298 to 873 K at 2 K min^{-1} were used in the operation. The carrier gas was N_2 UHP.

Table 1
Characteristics of different TiO_2 nanoparticles

Types of filler	Surface area ($m^2\ g^{-1}$)	Crystallite size[a] (nm)	% Anatase[b]	% Rutile[b]
TiO_2 (A)	240	6.1	100	0
TiO_2 (J)	50	23.1	80.4	19.6
TiO_2 (D)	47	21.2	90.7	9.3
TiO_2 (R)	160	6.9	0	100

[a] Based on XRD measurement.
[b] Calculated from equation based on Ref. [29].

2.5.1.4. Scanning electron microscopy and energy dispersive X-ray spectroscopy. SEM and EDX were used to investigate the sample morphologies and elemental distribution throughout the nanofillers. The SEM of JEOL mode JSM-5800 LV scanning microscope was employed. EDX was further performed using Link Isis series 300 program.

2.5.2. Characterization of polymer

2.5.2.1. Scanning electron microscopy and energy dispersive X-ray spectroscopy. SEM and EDX were performed to study the morphologies of polymer and elemental distribution within polymer matrix. The same equipment as mentioned above was employed.

2.5.2.2. Transmission electron microscopy. TEM was used to determine the dispersion of TiO_2 nanofillers in LLDPE. The same equipment as mentioned above was employed.

2.5.2.3. Differential scanning calorimetry. The melting temperature of ethylene/1-hexene copolymer products was determined with a Perkin-Elmer diamond DSC. The analyses were performed at the heating rate of 10 K min^{-1} in the temperature range of 283–423 K. The heating cycle was run twice. In the first scan, sample was heated and cooled to 283 K. In the second scan, sample was reheated at the same rate, but only the result of the second scan was reported because the first scan was influenced by the mechanical and thermal history of sample.

2.5.2.4. ^{13}C NMR spectroscopy. ^{13}C NMR spectroscopy was used to determine the 1-hexene incorporation and copolymer microstructure. Chemical shifts were referenced internally to the $CDCl_3$ and calculated according to the method described by Randall [19]. Each sample solution was prepared by dissolving 50 mg of copolymer in 1,2-dichlorobenzene and $CDCl_3$. The ^{13}C NMR spectra were taken at 373 K using a BRUKER AVANCE II 400 operating at 100 MHz with an acquisition time of 1.5 s. The pulse angle was 90° and 5000 scans were accumulated in pulse repetition of 4 s.

3. Results and discussion

In the present study, the synthesis of LLDPE/TiO_2 nanocomposites using different TiO_2 nanoparticles [TiO_2 (A), TiO_2 (J), TiO_2 (D), and TiO_2 (R) as listed in Table 1 having different phase com-

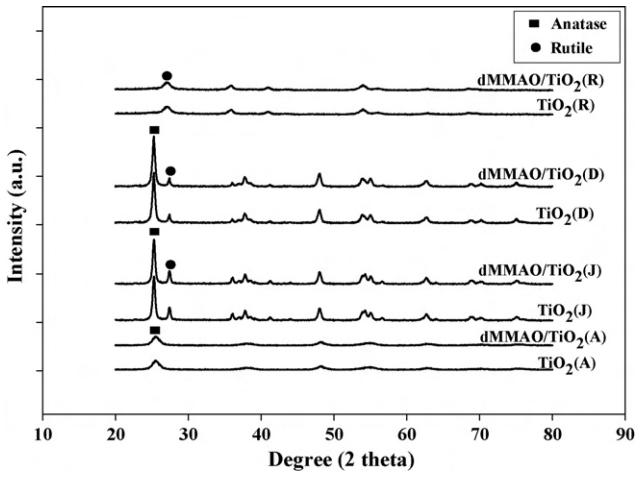

Fig. 1. XRD patterns of different TiO_2 nanoparticles before and after impregnation with dMMAO.

positions and crystallite sizes] by the *in situ* polymerization of ethylene/1-hexene with zirconocene/dMMAO catalyst was investigated. First, the TiO_2 nanoparticles before and after impregnation with dMMAO were characterized using various techniques. The XRD patterns of TiO_2 samples before and after impregnation with dMMAO are shown in Fig. 1 indicating the characteristic peaks for the anatase form of TiO_2 (A) at 25° (major) and the rutile form of TiO_2 (R) at 27° (major). The average crystallite sizes for the TiO_2 (A) and TiO_2 (R) calculated from the Sherrer's equation were 6.1 and 6.9 nm, respectively. The XRD patterns for the TiO_2 (J) and TiO_2 (D) revealed the mixed phases of anatase and rutile having the crystallite sizes of 23.1 and 21.2 nm, respectively. No significant changes were observed upon the dMMAO impregnation onto the TiO_2 nanoparticles suggesting well dispersion of dMMAO. More details of the characteristics of different TiO_2 nanoparticles are also listed in Table 1.

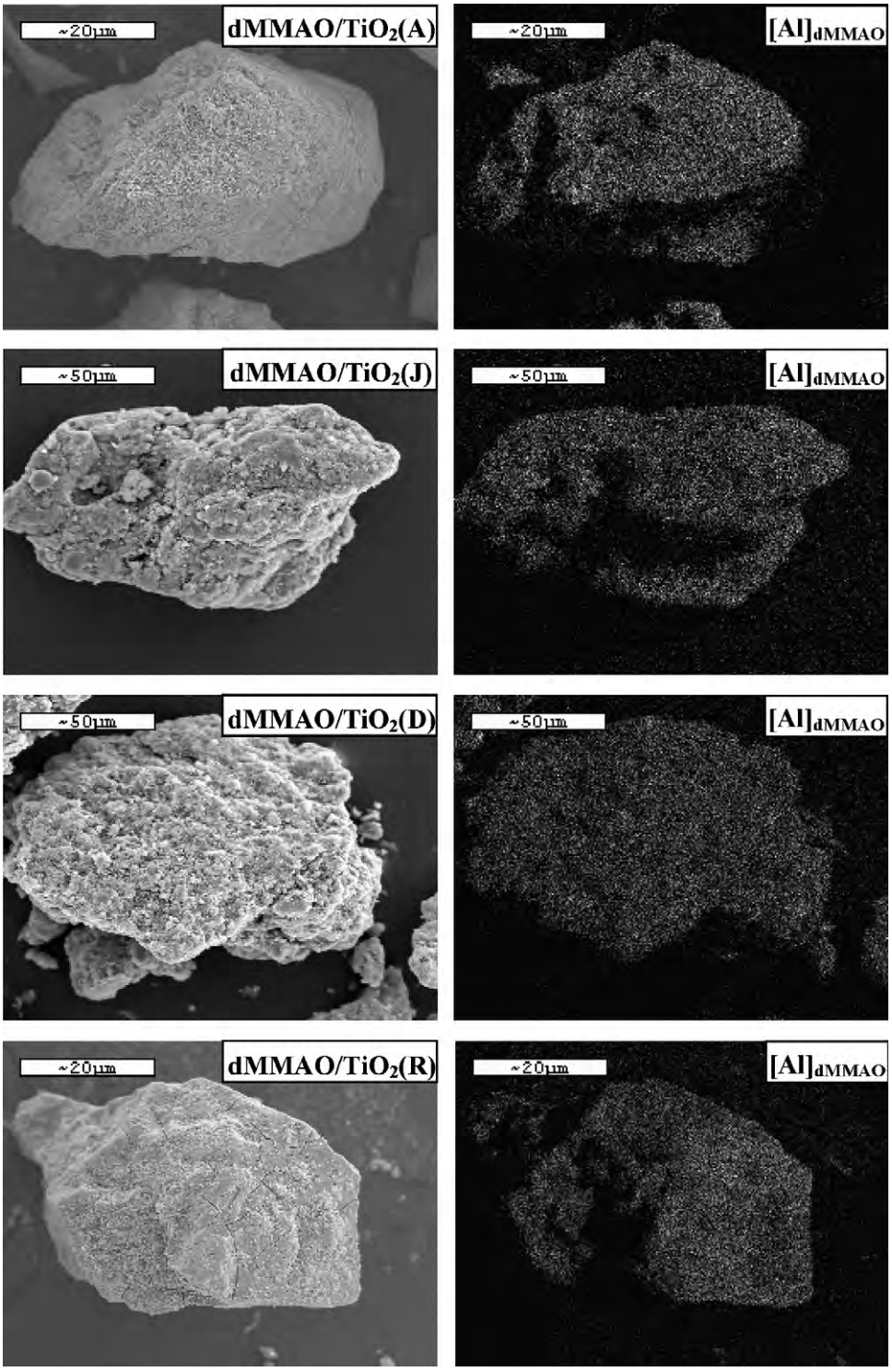

Fig. 2. SEM micrographs and EDX mapping for different dMMAO/TiO_2 nanofillers.

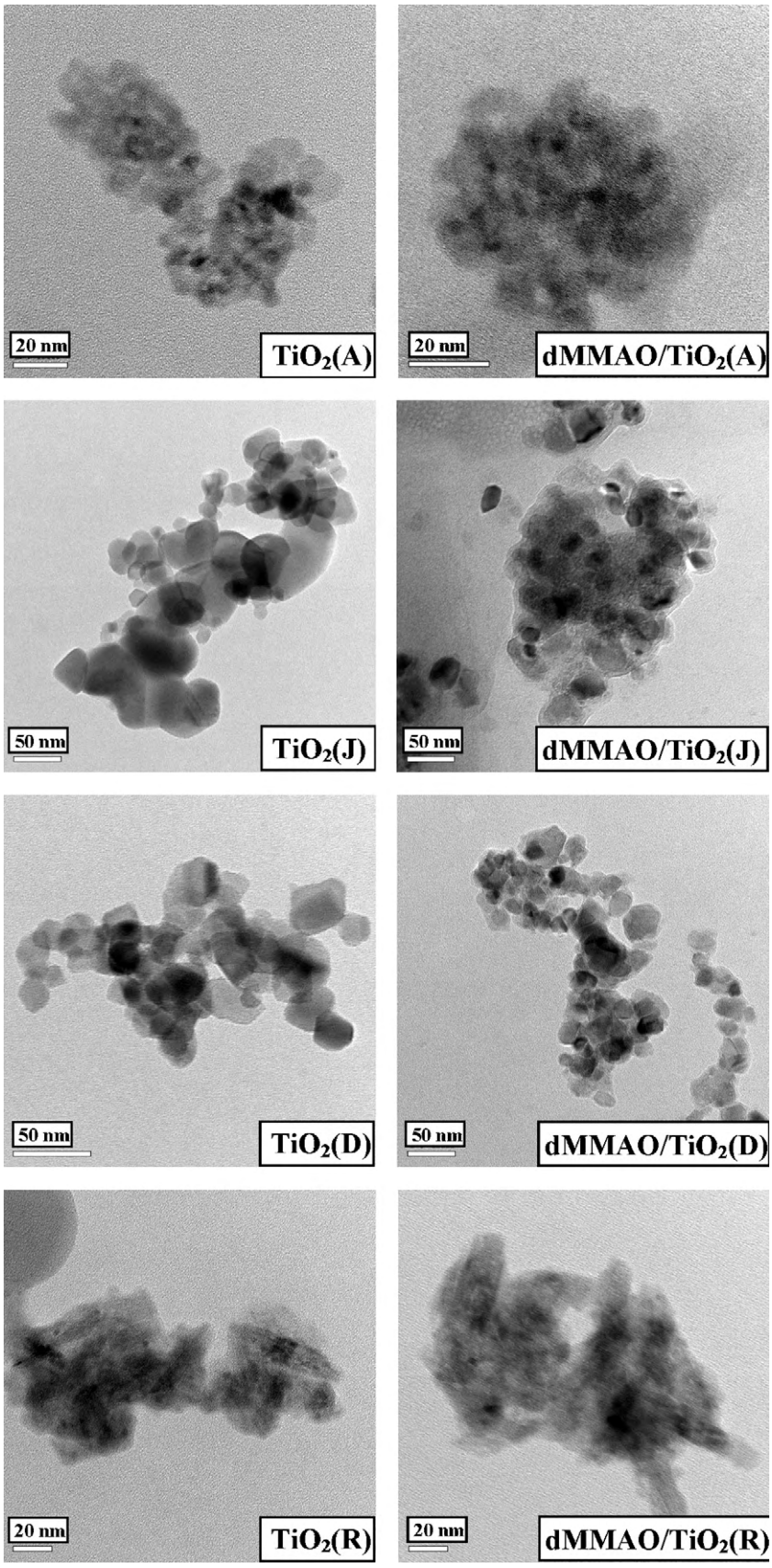

Fig. 3. TEM micrographs of different TiO_2 nanoparticles before and after impregnation with dMMAO.

SEM and EDX were performed in order to study the morphologies and distribution of dMMAO onto the different TiO_2 nanoparticles, respectively. The SEM micrographs and EDX mapping for the dMMAO/TiO_2 samples are shown in Fig. 2. All samples apparently exhibited the similar morphologies. It can be observed that the dMMAO was well distributed all over the TiO_2 granules as seen by the EDX mapping. Based on the EDX measurement, the amounts of $[Al]_{dMMAO}$ present on the TiO_2 samples can be also determined. They were in the range of 12.5, 11.8, 10.4, and 10.2 wt.% for TiO_2 (A), TiO_2 (J), TiO_2 (D), and TiO_2 (R), respectively. The largest amount of $[Al]_{dMMAO}$ present in the TiO_2 (A) can be attributed to largest surface area for the TiO_2 (A) coupled with the absence of rutile phase. It can be also observed that the presence of rutile phase apparently resulted in decreased amounts of $[Al]_{dMMAO}$ being present on the TiO_2 nanoparticles. In order to determine the dispersion of TiO_2 before and after dMMAO impregnation, a more powerful technique such as TEM was applied to all samples. The TEM micrographs of all TiO_2 nanoparticles before and after impregnation with dMMAO are shown in Fig. 3. It indicated that the TiO_2 (A), TiO_2 (J), and TiO_2 (D) crystals appeared in the spherical-like shape, whereas the TiO_2 (R) crystals were in the needle-like shape. It appeared that the crystal size of primary particle obtained from the TEM measurement was below 50 nm for all samples. However, only the TiO_2 (A) and TiO_2 (R) exhibited the sizes below 20 nm.

After impregnation with dMMAO to obtain the dMMAO/TiO_2, the *in situ* polymerization of ethylene/1-hexene was performed with the presence of dMMAO/TiO_2 using zircocene catalyst in order to produce the LLDPE/TiO_2 nanocomposites. Based on the EDX measurement, the amounts of $[Al]_{dMMAO}$ were varied on each sample. Therefore, the amount of dMMAO/TiO_2 used for polymerization was not equal in order to keep the $[Al]_{dMMAO}/[Zr]_{cat}$ ratio being constant at 2270 during each run. The resulted polymerization activities obtained from dMMAO/TiO_2 (A), dMMAO/TiO_2 (J), dMMAO/TiO_2 (D) and, dMMAO/TiO_2 (R) with same ratio of $[Al]_{dMMAO}/[Zr]_{cat}$ are summarized in Table 2. It was found that the polymerization activities obtained from the dMMAO/TiO_2 (A) exhibited pronouncedly highest activities among those from the dMMAO/TiO_2 (J), dMMAO/TiO_2 (D), and dMMAO/TiO_2 (R). The highest activity obtained from the TiO_2 (A) was likely due to the high intrinsic activity and/or high stability of the active sites present on the TiO_2 (A). It was proposed that the dMMAO possibly had many functions, such as an alkylating agent, a stabilizer for a cationic metallocene alkyl and/or counter-ion, an ionizing and/or reducing agent for the transition element, and a scavenger for the metallocene catalytic system. However, one of the most important roles of this alkylaluminoxane is apparently to prevent the formation of $ZrCH_2CH_2Zr$ species, which is formed via a bimolecular process [20].

Besides the concentration of $[Al]_{dMMAO}$ being present on the TiO_2 nanoparticles (this was not the case for this study since the ratio of $[Al]_{dMMAO}/[Zr]_{cat}$ was constant), the interactions between the $[Al]_{dMMAO}$ and TiO_2 nanoparticles were also important to consider. In fact, the strong interaction of the active species with TiO_2 nanoparticles employed in this study was essentially referred to the interactions between the TiO_2 nanoparticles and the dMMAO cocatalyst. Based on this study, the dMMAO was impregnated onto the TiO_2 nanoparticles prior to polymerization. The degree of interactions between the TiO_2 nanoparticles and dMMAO can be possibly determined by the TGA measurement. In order to give a better understanding, we propose the interactions of TiO_2 nanoparticles and dMMAO based on the review paper by Severn et al. [21]. They explained that the connection of the support and cocatalyst occurred via the $O_{filler}–Al_{cocatalyst}$ linkage. In particular, the TGA can only provide useful information on the degree of interactions for the dMMAO bound to the TiO_2 nanoparticles in terms of the weight loss and removal temperature. The stronger interaction can result in it being more difficult for the dMMAO bound to the TiO_2 nanoparticles to react with Zr-complex during activation processes, leading to lower catalytic activity for polymerization [22]. The TGA measurement was performed in order to possibly prove the interaction between the $[Al]_{dMMAO}$ and TiO_2 nanoparticles. The TGA profiles of all dMMAO/TiO_2 samples are given in Fig. 4. The weight loss of $[Al]_{dMMAO}$ present on TiO_2 nanoparticles was in the order of TiO_2 (J) (26.6%) > TiO_2 (A) (20.0%) > TiO_2 (R) (18.8%) > TiO_2 (D) (18.1%). However, based on this study the relation between the interaction and TGA might be difficult to explain. In fact, TGA only shows the thermal stability of dMMAO on the support. Thus, it is proper to use the word "stability" instead of "interaction" according to the TGA measurement. Based on TGA results, it can be observed that the dMMAO/TiO_2 (J) exhibited low polymerization activity due to less stability of the dMMAO compared to other samples. Considering the dMMAO/TiO_2 (A), dMMAO/TiO_2 (D) and dMMAO/TiO_2 (R) samples, they had the similar stability of the dMMAO. However, the TiO_2 (A) showed the highest activity. This can be also attributed to the smaller crystallite size (6.1 nm, as shown in Table 1) for the TiO_2 (A) compared to that of TiO_2 (D) (21.1 nm, as also shown in Table 1). The small particles are highly dispersed resulting in high activity observed. However, the low activity obtained from the TiO_2 (R) can be attributed to low intrinsic activity of the active sites being present.

Then, the LLDPE/TiO_2 nanocomposites obtained were further characterized by means of SEM/EDX, TEM, ^{13}C NMR, and DSC. In order to study the morphologies and TiO_2 distribution inside the polymer matrix of LLDPE/TiO_2 nanocomposites, SEM/EDX were performed. The SEM micrographs and EDX mapping for Ti of all samples are shown in Fig. 5. There was no significant change in

Table 2
Polymerization activities of LLDPE/TiO_2 nanocomposites synthesized by *in situ* polymerization with *rac*-Et(Ind)$_2ZrCl_2$/dMMAO catalysts

Types of filler	Time[a] (s)	Polymer yield[b] (g)	Catalytic activity (kg polymer (mol Zr h)$^{-1}$)
TiO_2 (A)	171	1.01	14,123
TiO_2 (J)	242	0.70	6,905
TiO_2 (D)	204	0.39	4,596
TiO_2 (R)	266	0.41	3,667

[a] A period of time used for the total 0.018 mol of ethylene to be consumed.

[b] Measurement at polymerization temperature of 343 K, [Ethylene] = 0.018 mol, $[Al]_{dMMAO}/[Zr]_{cat}$ = 2270, $[Al]_{TMA}/[Zr]_{cat}$ = 2500, in toluene with total volume = 30 mL, and $[Zr]_{cat} = 5 \times 10^{-5}$ M.

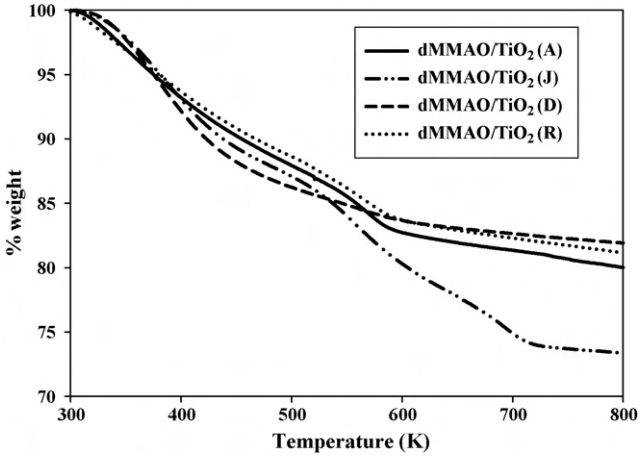

Fig. 4. TGA profiles of $[Al]_{dMMAO}$ on different TiO_2 nanoparticles.

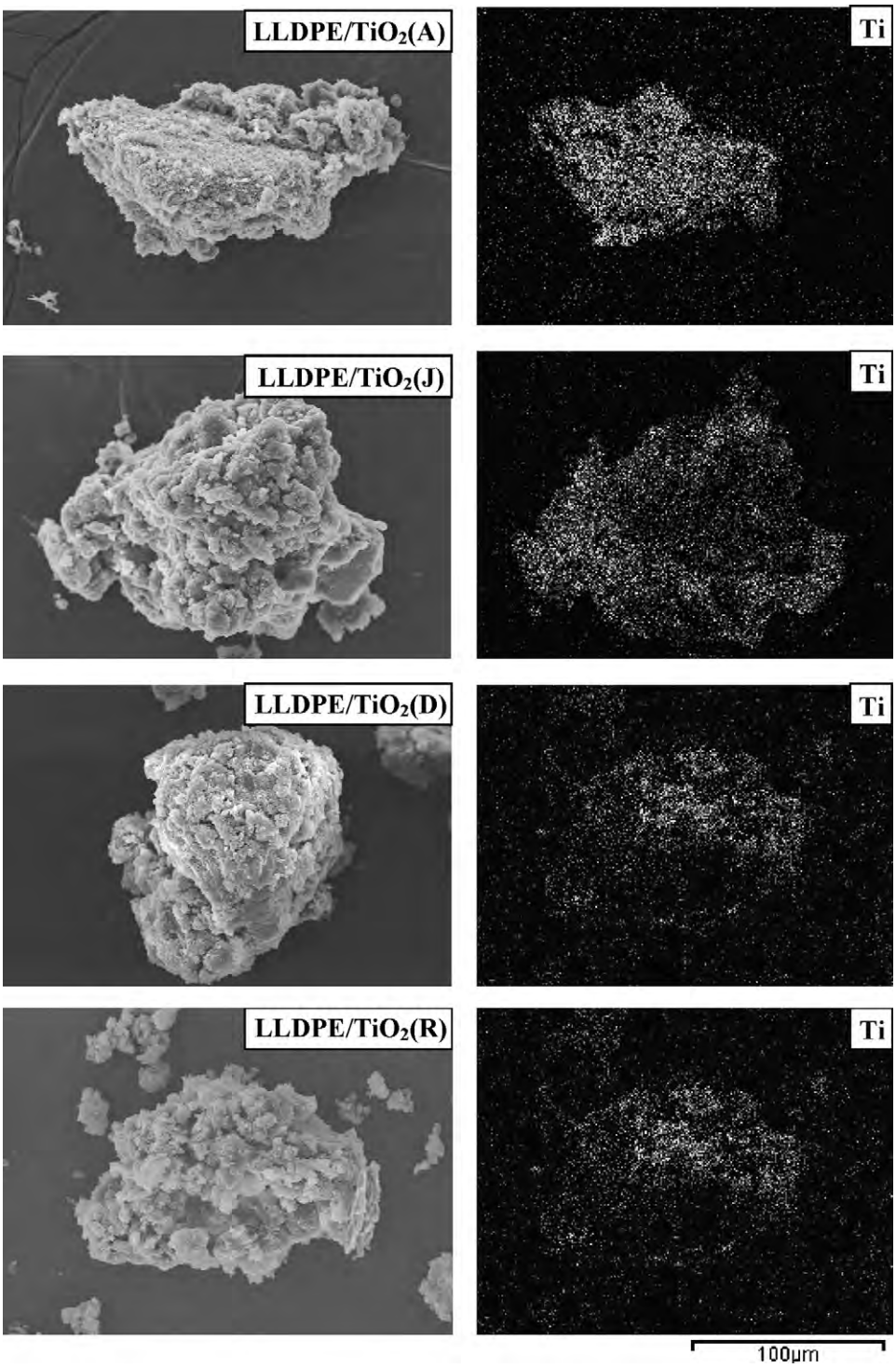

Fig. 5. SEM micrographs of LLDPE/TiO_2 nanocomposites and Ti distribution obtained from EDX upon different TiO_2 nanoparticles.

morphologies for all samples upon the different TiO_2 nanoparticles employed. Based on the EDX mapping, it revealed good distribution of the TiO_2 nanoparticles inside the polymer matrix. As known, the images from high-resolution transmission electron microscopy (TEM) are essential components of nanoscience and nanotechnology, therefore TEM was performed in order to determine the dispersion of TiO_2 nanoparticles inside the polymer matrix. The TEM micrographs for the dispersion of TiO_2 in all LLDPE/TiO_2 samples are shown in Fig. 6. In general, all TiO_2 nanoparticles apparently exhibited good dispersion inside the polymer matrix without any changes in crystal morphologies.

The ^{13}C NMR is one of the most powerful techniques used to identify the polymer microstructure, especially for polyolefins. The resulted ^{13}C NMR spectra are shown in Fig. 7 for all LLDPE/TiO_2 samples, which were assigned typically to the LLDPE obtained from copolymerization of ethylene/1-hexene. The triad distribution was identified based on the method described by Randall [19]. It can be observed that all LLDPE/TiO_2 nanocomposites exhibited similar

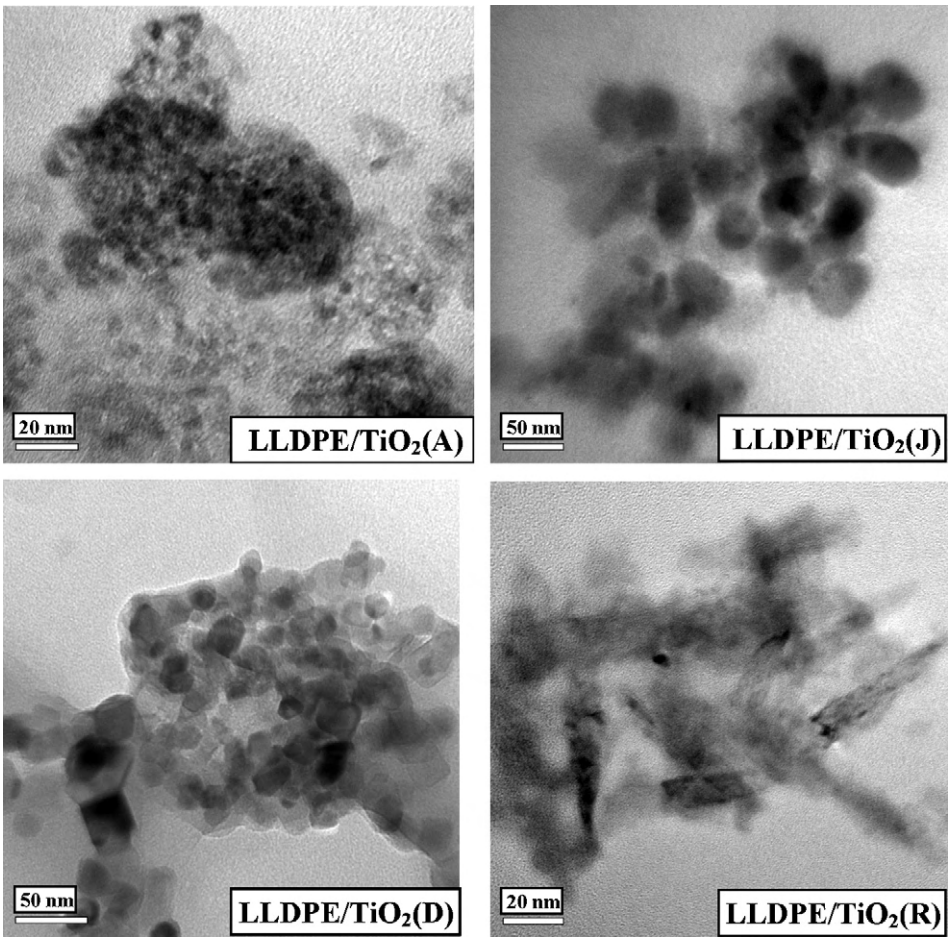

Fig. 6. TEM micrographs of LLDPE/TiO_2 nanocomposites and Ti distribution obtained from EDX upon different TiO_2 nanoparticles.

Table 3
Triad distribution of LLDPE/TiO_2 nanocomposites obtained from ^{13}C NMR analysis

Types of filler	EEE	HEE + EEH	HEH	EHE	EHH + HHE	HHH	1-Hexene incorporation (%)
TiO_2 (A)	0.433	0.205	0.063	0.112	0.107	0.080	29.9
TiO_2 (J)	0.592	0.188	0.016	0.108	0.095	0.000	20.3
TiO_2 (D)	0.769	0.128	0.004	0.062	0.037	0.000	10.0
TiO_2 (R)	0.716	0.140	0.006	0.073	0.065	0.000	13.8

E refers to ethylene and H refers to 1-hexene.

^{13}C NMR patterns indicating similar molecular structure of polymer. Based on calculations described by Randall [19] and Galland et al. [23], the triad distributions of ethylene (E) and 1-hexene (H) incorporation are listed in Table 3. It indicated that all LLDPE/TiO_2 nanocomposites obtained from different TiO_2 nanoparticles were random copolymer having different degrees of 1-hexene incorporation. It was found that the incorporation of 1-hexene in LLDPE/TiO_2 (A) nanocomposites was the highest among other samples. It is worth noting that it must be very difficult to determine the exact mechanism of 1-hexene insertion upon different TiO_2 employed. Thus, differences in 1-hexene insertion can be only attributed to the different steric hindrance arising from varied crystallite sizes and phase compositions of TiO_2. The DSC analysis was also used to measure the thermal properties of LLDPE/TiO_2 nanocomposites obtained. The DSC results are shown in Table 4. It was found that the increased degree of 1-hexene incorporation basically decreased the crystallinity of samples. This was in agreement with the results obtained from ^{13}C NMR as mentioned before. Thus, the highest crystallinity for the LLDPE/TiO_2 (D) nanocomposites was evident. The crystallinity of LLDPE can be decreased with a higher degree of 1-olefin (1-hexene) insertion [24–26] along with the larger amount of TiO_2 being present [27,28]. As reported, when the larger amounts of the TiO_2 nanoparticles are employed, they may locate themselves in the interlamellar spaces, which leave little room for additional crystallization. So, the presence of these nanoparticles may even inhibit crystallization.

Table 4
Thermal properties of LLDPE/TiO_2 nanocomposites obtained from DSC measurement

Types of filler	T_m (K)	ΔH_m (J g^{-1})	Crystallinity (%)
TiO_2 (A)	–[a]	–[a]	–[a]
TiO_2 (J)	351.7	5.16	1.8
TiO_2 (D)	364.9	19.58	6.9
TiO_2 (R)	354.9	17.98	6.3

[a] Value not be detected from the measurement.

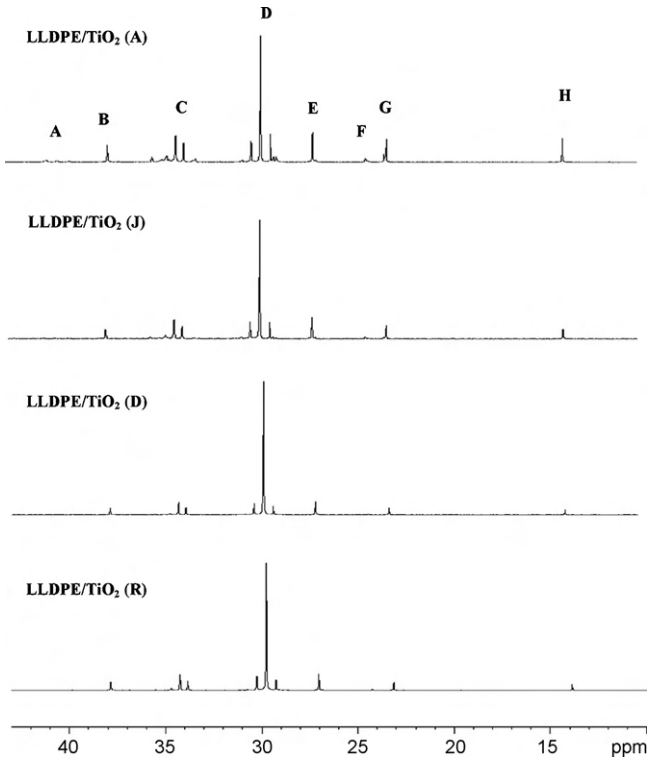

Fig. 7. ^{13}C NMR spectra of LLDPE/TiO_2 nanocomposites obtained from different TiO_2 nanoparticles, where the observed n-ads are assigned based on Ref. [19] as follows: A = [HHHH, HHHE + EHHH, EHHE], B = [EHE], C = [EHH + HHE, HHH, EHE + EHH + HHE + HHH, EHEH + HEHE, HHEH + HEHH, EHEE + EEHE, HHEE + EEHH], D = [HEEH, HEEE + EEEH, (EEE)*n*, EHE + EHH + HHE + HHH], E = [EHEE + EEHE, HHEE + EEHH], F = [HHEHH, HHEHE + EHEHH, EHEHE], G = [H], and H = [H].

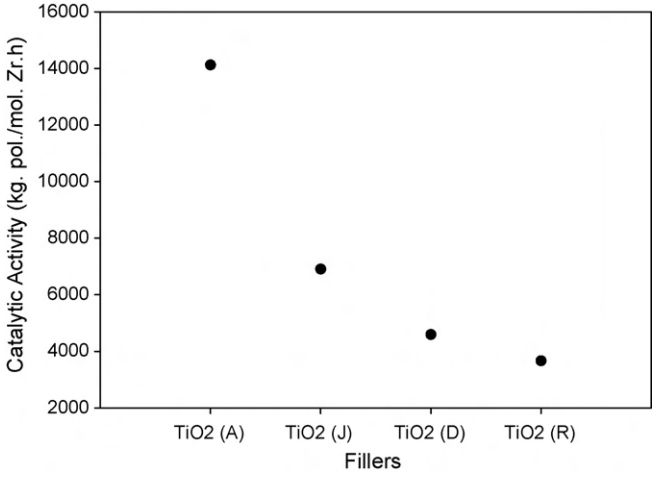

Fig. 8. Catalytic activity of different TiO_2 fillers.

4. Summary

The LLDPE/TiO_2 nanocomposites were produced using different TiO_2 nanoparticles via *in situ* polymerization of ethylene/1-hexene with zirconocene/dMMAO catalyst. The polymerization activities were in the order of TiO_2 (A) > TiO_2 (J) > TiO_2 (D) > TiO_2 (R) as shown in Fig. 8. It was found that the presence of rutile phase can result in decreased activities due to low intrinsic activity of active sites being present. Besides the presence of rutile phase the stability of dMMAO on TiO_2 were considered. Low stability of dMMAO also caused the decreased activities. All LLDPE/TiO_2 nanocomposites obtained were random copolymer having different triad distribution. The results obtained from ^{13}C NMR was in agreement with those from DSC where the higher degree of 1-hexene insertion apparently resulted in lower crystallinity of samples.

Acknowledgements

The authors gratefully acknowledge the Commission on Higher Education (CHE) for the financial support of this research. We also extend our thankful to The Thailand Research Fund (TRF) for RMU50-B. Jongsomjit project.

References

[1] J.P.J. Turunen, T.T. Pakkanen, J. Mol. Catal. A: Chem. 263 (2006) 1.
[2] M.R. Ribeiro, A. Deffieux, M.F. Portela, Ind. Eng. Chem. Res. 36 (1997) 1224.
[3] J.C.W. Chien, Top. Catal. 7 (1999) 23.
[4] E. Kontou, M. Niaounakis, Polymer 47 (2006) 1267.
[5] K.T. Li, C.L. Dai, C.W. Kuo, Catal. Commun. 8 (2007) 1209.
[6] R.J. Nussbaumer, W.R. Caseri, P.T. Tervoort, Macromol. Mater. Eng. 288 (2003) 44.
[7] Z. Wang, G. Li, X.Z. Zhang, Macromol. Chem. Phys. 206 (2005) 258.
[8] X.D. Chen, Z. Wang, Z.F. Liao, Y.L. Mai, M.Q. Zhang, Polym. Test. 26 (2007) 202.
[9] M.C. Kuo, C.M. Tsai, J.C. Huang, M. Chen, Mater. Chem. Phys. 90 (2005) 185.
[10] B. Jongsomjit, J. Panpranot, M. Okada, T. Shiono, P. Praserthdam, Iran. Polym. J. 15 (2006) 431.
[11] R. Nawang, I.D. Danjaji, U.S. Ishiaku, H. Ismail, Z.A.M. Ishak, Polym. Test. 20 (2001) 167.
[12] C.J.R. Verbeek, Mater. Lett. 52 (2002) 453.
[13] Y. Haung, Y.Q. Zhang, Y.Q. Hua, J. Mater. Sci. Lett. 22 (2003) 997.
[14] G.B. Rossi, G. Beaucage, T.D. Dang, R.A. Vaia, Nano Lett. 2 (4) (2002) 319.
[15] W. Cheng, Z. Wang, C. Ren, H. Chen, T. Tang, Mater. Lett. 61 (2007) 3193.
[16] B. Jongsomjit, J. Panpranot, P. Praserthdam, Mater. Lett. 61 (2007) 1376.
[17] B. Jongsomjit, S. Ngamposri, P. Praserthdam, Molecules 10 (2005) 672.
[18] H. Hagimoto, T. Shiono, T. Ikeda, Macromol. Chem. Phys. 205 (2004) 19.
[19] J.C. Randall, J. Macromol. Sci. Rev. Macromol. Chem. Phys. C 29 (1989) 201.
[20] C. Desharun, B. Jongsomjit, P. Praserthdam, Catal. Commun. 9 (2008) 522.
[21] J.R. Severn, J.C. Chadwick, R. Duchateau, N. Friederichs, Chem. Rev. 105 (2005) 4073.
[22] C. Ketloy, B. Jongsomjit, P. Praserthdam, Appl. Catal. A: Gen. 327 (2007) 270.
[23] G.B. Galland, P. Quijada, R.S. Mauler, S.C. de Menezes, Macromol. Rapid Commun. 17 (1996) 607.
[24] R.G. Alamo, L. Mandelkern, Macromolecules 22 (1989) 1273.
[25] R.G. Alamo, B.D. Viers, L. Mandelkern, Macromolecules 26 (1993) 5740.
[26] A.G. Simanke, G.B. Galland, L.L. Treitas, J.A.H. Jornada, R. Quijada, Macromol. Chem. Phys. 202 (2001) 172.
[27] A.S. Luyt, J.A. Molefi, H. Krump, Polym. Degrad. Stab. 91 (2006) 1629.
[28] E. Chaichana, B. Jongsomjit, P. Praserthdam, Chem. Eng. Sci. 62 (2007) 899.
[29] B. Jongsomjit, T. Wongsalee, P. Praserthdam, Catal. Commun. 6 (2005) 705.

Iranian Polymer Journal
16 (8), 2007, 549-559

Available online at: http://journal.ippi.ac.ir

Effect of Boron-modified MCM-41-supported dMMAO/Zirconocene Catalyst on Copolymerization of Ethylene/1-Octene for LLDPE Synthesis

Supaluk Jiamwijitkul, Bunjerd Jongsomjit*, and Piyasan Praserthdam

Center of Excellence on Catalysis and Catalytic Reaction Engineering,
Department of Chemical Engineering, Faculty of Engineering
Chulalongkorn University, Bangkok-10330, Thailand

Received 16 July 2007; accepted 29 August 2007

ABSTRACT

In this work, the boron (B) modification of MCM-41-supported dMMAO/zirconocene catalysts showed a promising increase (almost twice) in catalytic activity in ethylene/1-octene copolymerization. The enhanced activity can be attributed to the decreased interaction between the support and dMMAO with boron modification as was proved by TGA. It was proposed that boron acted as a spacer anchoring the support and dMMAO. However, at high boron loading (ca. 5 wt%), the activity slightly decreased due to the migration of dMMAO into boron layer resulting in less surface concentration of $[Al]_{dMMAO}$ which was measured by XPS. The inhibition of chain transfer reaction during polymerization apparently occurred upon the boron modification providing higher MW polymer. It was also suggested that boron modification has rendered more uniform catalytic sites which was leading to narrower MWD of the polymer observed. Based on ^{13}CNMR, boron modification did not affect the microstructure of copolymers obtained. However, the insertion of 1-octene increased with boron modification probably due to decreased steric hindrance of the MCM-41 support.

Key Words:

supports;
boron-modification;
metallocene catalyst;
copolymerization;
polyolefins.

(*) To whom correspondence to be addressed:
E-mail: bunjerd.j@chula.ac.th

INTRODUCTION

During the past years, metallocene catalysts have had great impact on both the academic research works and polymer industry. Metallocene catalysts have revolutionized olefin polymerization catalysis because of the tailor-made polymer properties. They provide higher activity and narrower molecular weight distribution (MWD) when compared to the conventional Ziegler-Natta (ZN) catalysts. Furthermore, these catalysts also produce a very uniform polymer due to their single-site catalytic nature. However, it was found that the homogeneous metallocene catalytic systems have two major disadvantages: (1) the lack of morphology control of polymer which causes the reactor foul-

ing and (2) the limitation of its use in solution process whereas the existing technologies are mainly based on gas phase and slurry processes. Therefore, binding these metallocene catalysts onto inorganic supports can provide a promising route to overcome these drawbacks.

In general, the heterogeneous metallocene catalytic system (or supported system) apparently has a lower activity than its corresponding homogeneous type under similar conditions. However, it is able to control the polymer morphology due to the support employed, avoid the fouling effect, and the sticking of the formed polymer to the reactor wall [1]. Supported metallocene catalysts are widely used in olefin polymerization [2-15]. Some scientists have carried out this polymerization by using the regular arranged mesoporous silica materials such as MCM-41 as the support of metallocene catalysts [16,17]. Since its discovery in 1992 [18], MCM-41 and related mesoporous molecular sieves have attracted much attention. As it is known, MCM-41 possesses unidirectional channel-like pores of rather uniform size which are arranged in a regular hexagonal pattern. The pores diameters are adjustable in the range 15 to 100 Å depending on the synthesis conditions [19]. Many scientists have investigated MCM-41 materials in which a catalytically active component was introduced. Several elements, such as Al [3,4] and B [20-22] have been incorporated into the catalyst structure in order to generate potential catalytic activity. Therefore, modification of the MCM-41 may provide an alternative strategy to obtain suitable supports to maintain high activity as in the homogeneous system for the supported metallocene catalysts.

In the present study, the effect of B-modification was investigated on the MCM-41-supported dMMAO/zirconocene catalyst during ethylene/1-octene copolymerization. In fact, the boron-modification was chosen based on its promising property as a support modifier as mentioned above. Besides, up to the present time, there has not been any literature reporting about the effect of boron-modification on MCM-41 support for the supported metallocene catalysts via ethylene/1-olefin copolymerization. In particular, we have proposed that boron-modification on MCM-41 probably alters the polymerization activities of the supported metallocene catalysts based on the changes in the interactions between the support and catalyst. Experimentally, the amounts of boron loading onto the MCM-41 support were also varied. The characterization of different supports was performed by means of N_2 physisorption, XRD, Raman spectroscopy, SEM/EDX, TGA, and XPS techniques. The polymer obtained was further analyzed using SEM, ^{13}CNMR, and GPC techniques in order to determine the effect of boron-modification on molecular weight (MW) and MWD.

EXPERIMENTAL

Materials

All chemicals and polymerization were manipulated under argon atmosphere, using a glove-box and/or Schlenk techniques. Toluene was dried over dehydrated $CaCl_2$ and distilled over sodium/benzophenone before use. The *rac*-ethylenebis (indenyl) zirconium dichloride (*rac*-Et[Ind]$_2$ZrCl_2) was supplied from Aldrich. Modified methylaluminoxane (MMAO) in hexane was donated by Tosoh (Akso, Japan). Trialkylaluminium (TMA, 2 M in toluene) was supplied by Nippon Aluminum Alkyls, Ltd., Japan. Ultra-high purity argon was further purified by passing it through columns that were packed with BASF catalyst R3-11G (molecular-sieved to 3 Å), sodium hydroxide (NaOH), and phosphorus pentaoxide (P_2O_5) to remove traces of oxygen and moisture. Ethylene gas (99.96% pure) was donated by National Petrochemical Co., Ltd., Thailand. 1-Octene (d = 0.715) was purchased from Aldrich.

Preparation of MCM-41 Support

The MCM-41 support was synthesized according to the method described by Panpranot et al. [23] using the gel composition of CTABr: NH_3: SiO_2: Na_2O: H_2O= 1:0.3: 4:1:200 (by mole), where CTABr denotes cetyltrimethyl ammonium bromide. Briefly, 20.03 g of colloidal silica Ludox HS 40% (Aldrich) was mixed with 22.67 g of 11.78% sodium hydroxide solution. Another mixture comprised of 12.15 g of CTABr (Aldrich) in 36.45 g of deionized water, and 0.4 g of an aqueous solution of 25% NH_3. Both of these mixtures were stirred by agitator (125 RPM) for 30 min, and then heated statically at 373 K for 5 days. The obtained solid material was filtered, washed with deionized water until no base was detected, and then dried at 373 K. The sample was then calcined in the flowing nitrogen up to 823 K (1-2 K/min) in order to remove the CTABr template, then in

air at the same temperature for 5 h. After preparation, the MCM-41 support had pore diameter of 3 nm and surface area of 864 m^2/g.

Preparation of Boron-modified MCM-41 Support

Boron-modified MCM-41 supports were prepared by an incipient wetness impregnation on the support. The desired amount of the aqueous solution of boric acid (99.99% H_3BO_3, Aldrich) was added onto the support to yield a final loading of approximately 1 and 5 wt% of boron. The supports were dried overnight at 383 K and then calcined in the air at 773 K for 4 h.

Preparation of Dried-MMAO

MMAO solution (100 mL) in hexane was evacuated and washed with toluene (100 mL × 2) to remove impurities. Then washing was continued with heptane 6-8 times in order to remove TMA and TIBA from MMAO solution to obtain a dried MMAO (dMMAO) as a white solid.

Preparation of Boron-modified MCM-41-supported dMMAO

The boron-modified MCM-41 support was reacted with the desired amount of dMMAO in 20 mL of toluene at room temperature for 30 min. The solvent was then removed from the mixture by evacuation. This procedure is done once with 20 mL of toluene (20 mL × 1) and 3 times with hexane (20 mL × 3). Then, the solid part was dried under vacuum at room temperature. Finally, the white powder of supported cocatalyst (dMMAO/support) was obtained.

Polymerization

The ethylene and 1-octene copolymerization reaction was carried out in a 100 mL semi-batch stainless steel autoclave reactor equipped with magnetic stirrer. In the glove-box, the amount of *rac*-Et$[Ind]_2ZrCl_2$ and TMA were mixed and stirred for 5 min for aging process. Then, toluene (to make a total volume of 30 mL) and 100 mg of dMMAO/support were introduced into the autoclave. After that, the mixture of *rac*-Et$[Ind]_2ZrCl_2$ and TMA were injected into the reactor. The reactor was frozen in liquid nitrogen to stop reaction and then 0.018 mol of 1-octene was injected into the reactor. The autoclave was evacuated to remove the argon. Then, the reactor was heated up to polymerization temperature (343 K) and the polymerization was started by feeding ethylene gas (total pressure 50 psi in the reactor) until the consumption of ethylene 0.018 mol (reading 6 psi on pressure gauge). The reaction of polymerization was terminated by addition of acidic methanol. The time length of reaction was recorded for purpose of calculating the activity. The precipitated polymer was washed with methanol and dried at room temperature.

CHARACTERIZATION

Characterization of Support and dMMAO/support

N_2 Physisorption

Measurement of BET surface area, average pore diameter, and pore size distribution of MCM-41 support were determined by N_2 physisorption using a Micromeritics ASAP 2000 automated system.

X-ray Diffraction

XRD was performed to determine the bulk crystalline phases of samples. This was conducted using a Siemens D-5000 X-ray diffractometer with CuK_α (λ = 1.54439 Å). The spectra were scanned at a rate of 2.4°/min in the range 2θ = 10-80°.

Raman Spectroscopy

The Raman spectra of the samples were collected by projecting a continuous wave YAG laser of Nd (810 nm) through the samples at room temperature. A scanning range of 100-1000 cm^{-1} with a resolution of 8 cm^{-1} was applied.

X-ray Photoelectron Spectroscopy

XPS was used to determine the binding energies (BE) and surface concentration of samples. It was carried out using the Shimazu Amicus with VISION 2-control software. Spectra were recorded at room temperature in high-resolution mode (0.1 eV step, 23.5 eV pass energy) for Al 2p core-level region. The samples were mounted on an adhesive carbon tape as pellets. The energy reference for Ag metal (368.0 eV for $3d_{5/2}$) was used for this study.

Scanning Electron Microscopy and Energy Dispersive X-ray Spectroscopy

SEM and EDX were used to determine the sample morphologies and elemental distribution throughout the

sample granules, respectively. The SEM of Jeol mode JSM-5800LV was applied. EDX was performed using Link Isis series 300 program.

Thermal Gravimetric Analysis

TGA was performed using TA Instruments SDT Q 600 analyzer. The samples of 10-20 mg and a temperature ramping from 303 to 873 K at 5 K/min were used in the operation. The carrier gas was N_2 UHP.

Characterization of Polymer

Scanning Electron Microscopy

SEM was performed to study morphologies of polymers produced. The same equipment, as mentioned above was employed.

Gel Permeation Chromatography

The molecular weight and molecular weight distribution of polymer was determined using gel permeation chromatography (GPC, PL-GPC-220). Samples were prepared having approximately concentration of 1 to 2 mg/mL in trichlorobenzene (mobile phase) by using the sample preparation unit (PL-SP 260) with filtration system at a temperature 423 K. The dissolved and filtered samples were transferred into the GPC instrument at 423 K. The calibration was conducted using the universal calibration curve based on narrow polystyrene standards.

^{13}CNMR Spectroscopy

^{13}CNMR spectroscopy was used to determine the triad distribution and 1-octene insertion indicating the copolymer microstructure. Chemical shifts were referenced internally to the $CDCl_3$ and calculated according to the method described by Randall [24]. Sample solution was prepared by dissolving 50 mg of copolymer in 1,2,4-trichlorobenzene and $CDCl_3$. ^{13}CNMR spectra were taken at 333 K using Bruker Avance II 400 operating at 100 MHz with an acquisition time of 1.5 s and a delay time of 4 s.

RESULTS AND DISCUSSION

In this study, the catalytic activity of boron-modified MCM-41-supported dMMAO with a zirconocene catalyst was investigated during ethylene/1-octene copolymerization. In fact, the MCM-41 support having BET surface area 863 m^2/g was prepared, and then sequentially it was modified with boron. The supports containing approximately 1 and 5 wt% of boron were designated as 1B-MCM-41 and 5B-MCM41, respectively. The boron-modified MCM-41 supports were then characterized using XRD and Raman spectroscopy techniques.

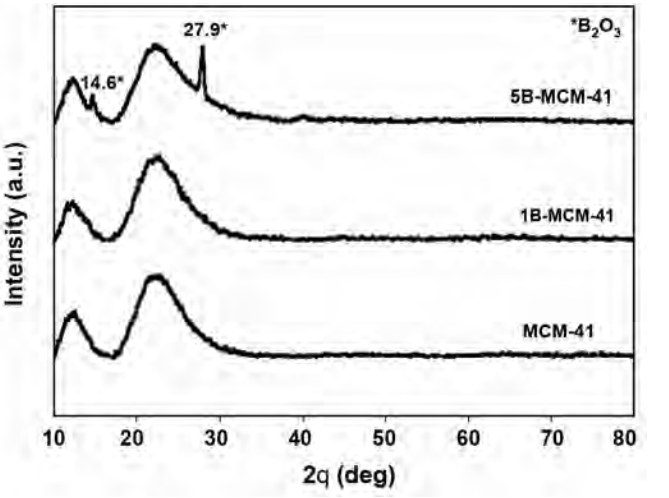

Figure 1. XRD Patterns of unmodified and boron-modified MCM-41 supports.

The XRD patterns of the unmodified MCM-41 and boron-modified MCM-41 supports are shown in Figure 1. It can be seen that the unmodified MCM-41 support exhibit the characteristic broad peaks of the amorphous silica at ca. 10° to 30°. After modification with 1 wt% of boron, the support still exhibited the similar XRD patterns as the unmodified sample. This indi-

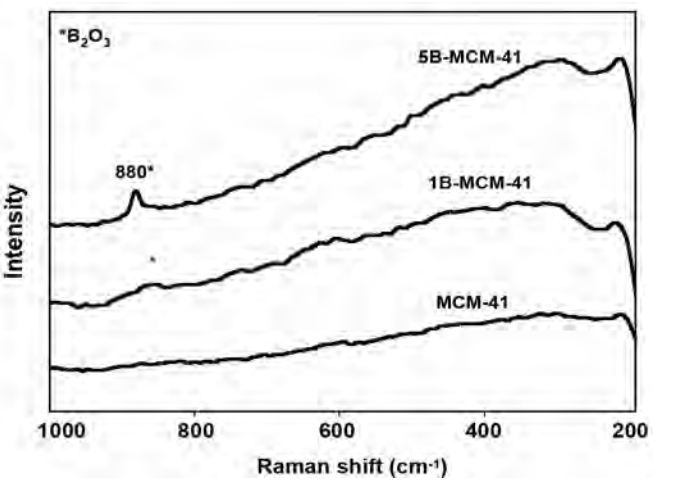

Figure 2. Raman spectra of unmodified and boron-modified MCM-41 supports.

cated that B_2O_3 was highly dispersed which was invisible by XRD technique. However, when the boron loading was increased to 5 wt%, the XRD peaks of B_2O_3 could be detected at ca. 14.6° (weak) and 27.9° (strong). Raman spectra of supports with and without boron-modification are shown in Figure 2. No significant Raman bands were observed for the unmodified MCM-41 support between 200 and 1000 cm^{-1}. However, the strong Raman band for B_2O_3 was observed at ca. 880 cm^{-1} for 5B-MCM-41. For the low boron loading sample (1 wt%), the characteristic Raman band at 880 cm^{-1} was just slightly observed. It should be noted that Raman spectroscopy is a rather surface technique. Therefore, the observation of boron at low loading on the surface could be possible and is not the same for the bulk in the case of XRD technique. The morphologies obtained from SEM of the MCM-41 support with and without boron-modification are shown in Figure 3. Any significant change in morphologies of the support was not found upon boron-modification. After dMMAO impregnation of the support, the distribution of elements, especially in $[Al]_{dMMAO}$ was determined using EDX technique. It was found that the $[Al]_{dMMAO}$ was well distributed all over the support granules. The typical EDX mapping for dMMAO/MCM-41 support is illustrated in Figure 4.

After the impregnation of dMMAO onto the unmodified and boron-modified MCM-41 supports, the ethylene/1-octene copolymerization with *rac*-Et$[Ind]_2ZrCl_2$ catalyst was performed in the presence of supports at the same condition for a comparative study in regards to the catalytic activities derived from different supports. In fact, the activation of a zirconocene catalyst with methylaluminoxane compound has been reported elsewhere [25]. The activities of catalyst via various supports are listed in Table 1. It was obvious that the homogeneous catalytic system provided the highest activity among the supported catalytic systems due to the absence of support interaction. Considering the supported system, it can be observed that the boron-modified MCM-41 exhibited higher activity, almost twice the unmodified MCM-41, for both the 1B-MCM-41 and 5B-MCM41 supports. It should be noted that an increase in the amount of boron loading apparently resulted in a slight decrease in the catalytic activity.

In order to determine the effect of boron-modification, XPS measurements were conducted on various

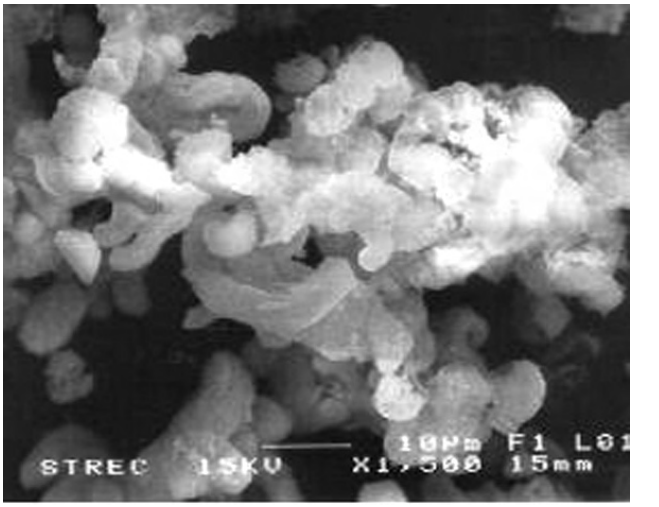

(a)

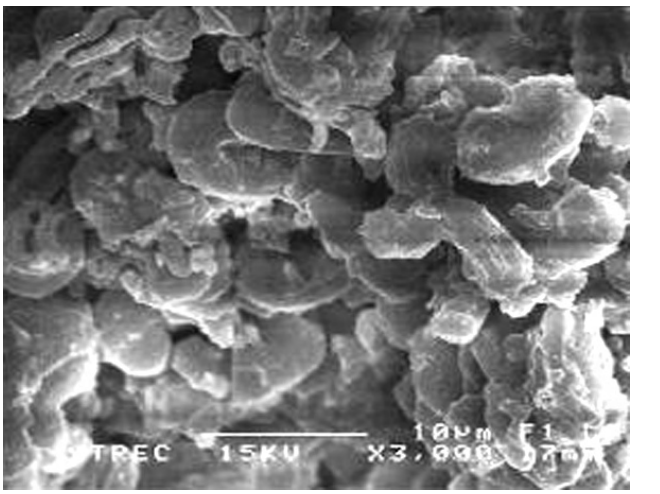

(b)

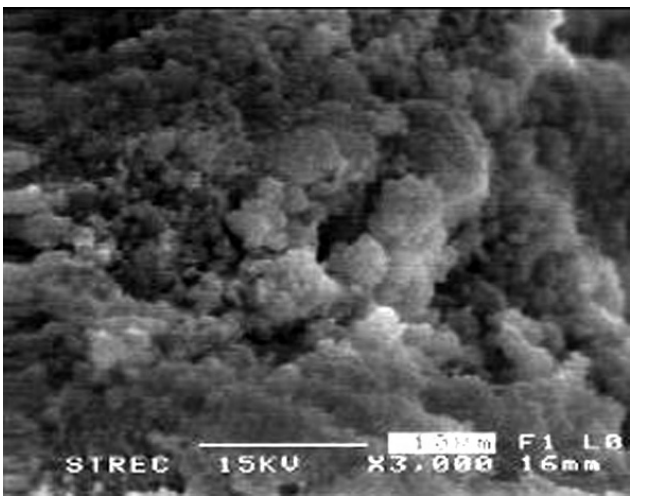

(c)

Figure 3. SEM micrographs of: (a) MCM-41, (b) 1B-MCM-41, and (c) 5B-MCM-41.

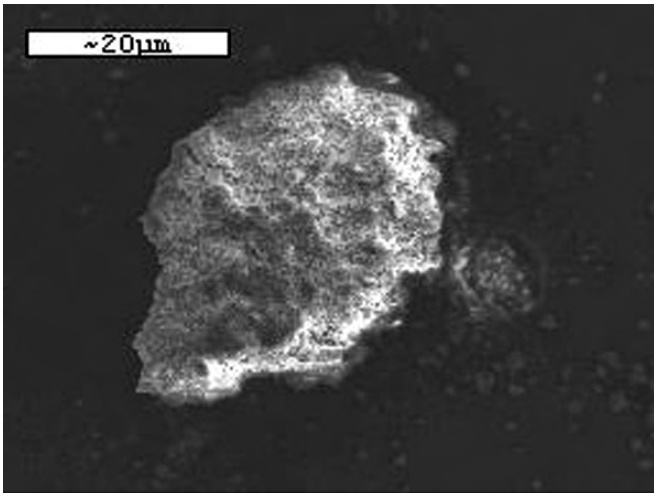

(a)

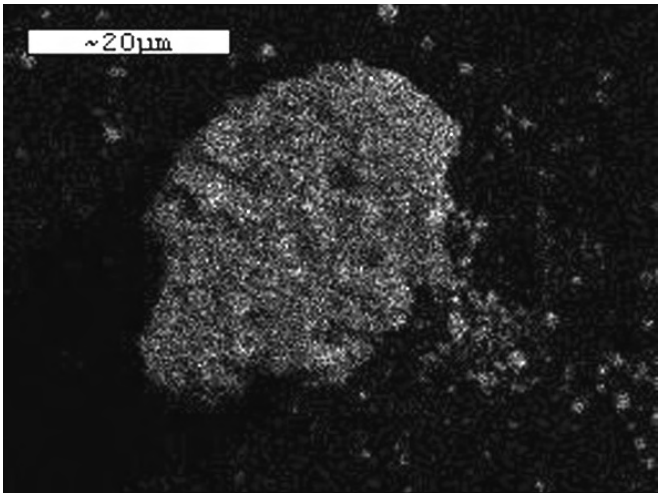

(b)

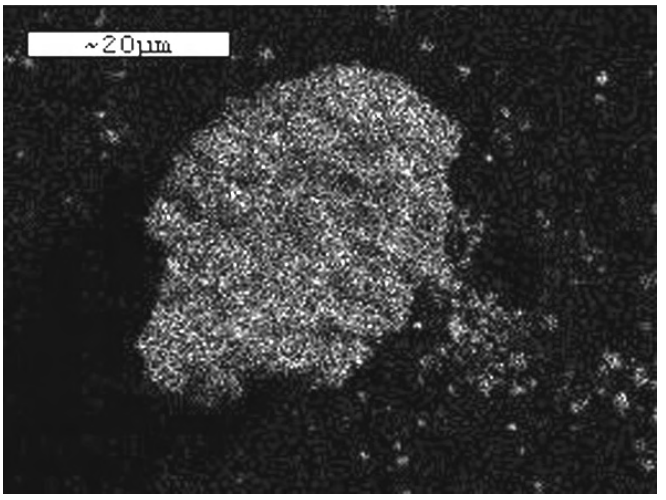

(c)

Figure 4. A typical SEM/EDX mapping of: (a) dMMAO/MCM-41 support, (b) Si distribution, and (c) $[Al]_{dMMAO}$ distribution.

Table 1. Catalytic activities of the boron-modified MCM-41-supported dMMAO with zirconocene catalyst during ethylene/1-octene copolymerization.

System	B in support (wt%)	Polymer yield[a] (g)	Catalytic activity[b] ($x10^{-4}$ kg Pol. mol.$Zr^{-1}.h^{-1}$)
Homogeneous	0	1.68	4.9
MCM-41	0	1.43	2.2
1B-MCM-41	1	1.47	3.8
5B-MCM-41	5	1.35	3.6

[(a)] The polymer yield was fixed [limited by ethylene fed and 1-octene used (0.018 mol equally)]. [(b)] Activities were measured at polymerization temperature of 343 K, [Ethylene] = 0.018 mol, $[Al]_{dMMAO}/[Zr]_{cat}$ = 1135, $[Al]_{TMA}/[Zr]_{cat}$ = 2500, in toluene with total volume = 30 ml and $[Zr]_{cat} = 5x10^{-5}$ M.

supports. The binding energies (BE) were measured for B 1s and Al 2p along with the surface concentrations of $[B]_{Support}$ and $[Al]_{dMMAO}$. The XPS profiles (not shown) for typical B 1s (BE ~ 192.5-192.8 eV) and Al 2p (BE ~ 74.6-74.8 eV) on various supports are similar in this study. It should be mentioned that the BE of Al 2p is also in accordance with those on silica reported by Shiono group [26]. It is suggested that no significant change has happened in the oxidation state of B (support) and Al (dMMAO) upon the various supports employed. The surface concentrations of $[B]_{Support}$ and $[Al]_{dMMAO}$ measured by XPS technique are shown in Table 2. Considering the surface concentrations of boron in different modified supports, it is found that in case of 1B-MCM-41, boron (~ 1.2 wt% at surface) has been mostly located on the surface of MCM-41, whereas in case of 5B-MCM-41 most borons are located in the bulk. This indicates that only one forth of boron (only 1.3 wt%) has been located at the surface. The surface concentrations of Al as shown in Table 2 are also varied upon different supports employed.

It can be observed that the surface concentrations for the unmodified and 1B-MCM-41 supports were similar (~26.5-26.8 wt%). Although they had the equal amount of Al concentration at the surface, the 1B-MCM-41 exhibited dramatically higher activity almost twice the unmodified MCM-41 support. This indicated that boron-modification would result in decreased interaction between the support and dMMAO. As a result, activity has strikingly increased with boron-modifica-

Table 2. XPS Results for different supports.

Support	BE for B 1s (eV)	BE for Al 2p[a] (eV)	Mass concentration (%)	
			B	Al
dMMAO/MCM-41	-	74.7	-	26.5
dMMAO/1B-MCM-41	192.5	74.8	1.2	26.8
dMMAO/5B-MCM-41	192.8	74.8	1.3	19.4

(a) Al 2p from dMMAO

tion. However, with the increase of boron loading in the support (5B-MCM-41) the surface concentration of Al has decreased significantly. This was presumably due to the migration of Al into the boron layer. The lesser amount of surface concentrations of Al would be the main reason for the decreased activity observed in the 5B-MCM-41 support compared to the 1B-MCM-41 support. It is worth noting that even though the surface concentration of $[Al]_{dMMAO}$ for the unmodified MCM-41 support is essentially higher than that of the 5B-MCM-41, the unmodified MCM-41 support, however, has exhibited such an extent of lower activity. It is suggested that the stronger support interaction in the unmodified MCM-41 support played more important role on the decreased activity than the amount of dMMAO at the surface. Hence, the unmodified MCM-41 gave lower activity than the 5B-MCM-41 (lesser amount of $[Al]_{dMMAO}$ on the surface). On the other hand, strong support interaction was the key factor (not the surface concentrations of $[Al]_{dMMAO}$) to determine the catalytic activity of this catalytic system. It may be suggested that boron can act as a spacer to anchor the support and dMMAO which leads to the fewer interactions. In order to give a better understanding of the effect of boron-modification on the surface concentrations and strong support interaction as mentioned earlier, the proposed model is shown in Scheme I. The TGA measurement was performed to prove the interaction between the $[Al]_{dMMAO}$ and various supports. It is worth noting that the interactions between $[Al]_{MAO}$ and support are very important factors. Based on this study, $[Al]_{dMMAO}$ was dispersed onto the supports by impregnation method. The degree of interaction between support and $[Al]_{dMMAO}$ can be determined using the TGA

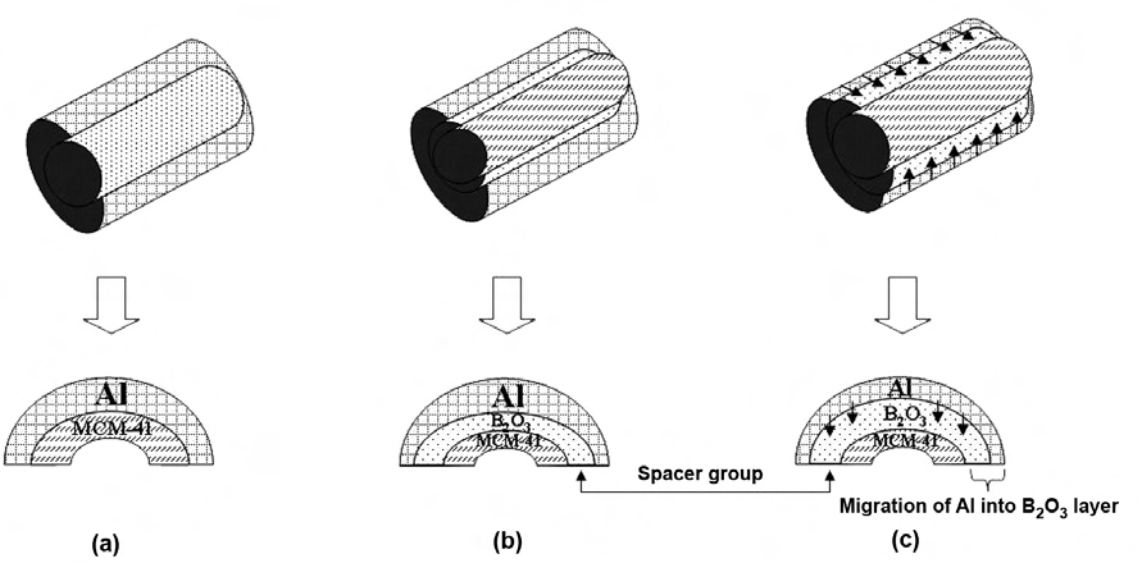

Scheme I. Suggested model for effect of B loading on the surface concentrations of $[Al]_{dMMAO}$ determined by XPS measurement; (a) dMMAO/MCM-41, (b) dMMAO/1B-MCM-41, and (c) dMMAO/5B-MCM-41.

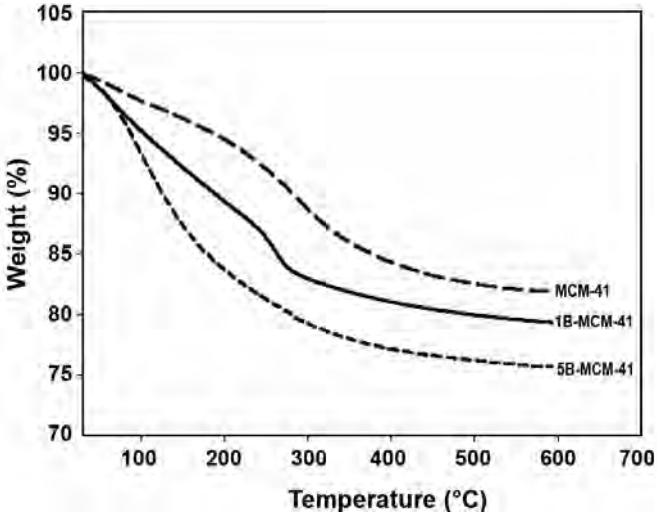

Figure 5. TGA curves of unmodified and boron-modified MCM-41 supports.

measurement [27]. In order to give a better understanding, we proposed the interaction of support and $[Al]_{dMMAO}$ based on the review paper by Seven et al. [28]. They have explained that the interconnection between support and cocatalyst occurred via the $O_{support}$-$Al_{cocatalyst}$ linkages. In particular, the TGA can only provide useful information on the degree of interaction between the $[Al]_{dMMAO}$ and support in terms of weight loss and removal temperature. As a matter of fact, too strong interaction can bind $[Al]_{dMMAO}$ stronger to the support to react with metallocene catalyst during activation processes, leading to lower activity for polymerization. In contrast, leaching of $[Al]_{dMMAO}$ can occur due to very weak interactions resulting in low activity as well. Hence, optimum interaction between the $O_{support}$-$Al_{cocatalyst}$ linkage is crucial.

The TGA profiles of $[Al]_{dMMAO}$ on various supports are shown in Figure 5 indicating the similar profiles for various supports. It was observed that the weight losses of $[Al]_{dMMAO}$ present on various supports were in the order of 5B-MCM-41 (20%) > 1B-MCM-41 (17%) > MCM-41 (13%). The species having strong interactions with supports were removed at ca. 553, 563, and 606 K for 5B-MCM-41, 1B-MCM-41, and MCM-41, respectively. This indicates that $[Al]_{dMMAO}$ present on MCM-41 without boron-modification had the strongest interaction, and hence, lowest polymerization activity.

Besides the effect of boron-modification on the catalytic activity, it would be very interesting to further investigate how this affect the polymer properties in terms of molecular weights (MW), molecular weight distribution (MWD), morphologies, and percentage insertion of 1-octene. As known, the MW and MWD are two of the most important properties used to classify the application of polymers. The MW and MWD of polymer obtained from different supports are shown in Table 3. Based on the GPC curve (not shown), only the uni-modal molecular weight distribution of polymer has been obtained. It can be observed that boron-modification apparently results in a slight increase in MW of polymer produced. This has suggested that inhibition of chain transfer reaction during polymerization could be achieved by boron-modification on MCM-41 support. Furthermore, it is worth noting that the narrower MWD is also evident for boron-modification indicating more uniform catalytic sites have been formed.

Table 3. Molar weight (MW) and molecular weight distribution (MWD) of polymers obtained via boron-modified MCM-41-supported-MMAO with zirconocene catalyst.

System	MW[a] (x 10^{-4} g.mol^{-1})	Mn[a] (x 10^{-4} g.mol^{-1})	MWD[a]
Homogeneous	2.13	0.63	3.4
MCM-41	2.15	0.63	3.4
1B-MCM-41	2.61	1.02	2.6
5B-MCM-41	2.42	1.45	1.7

(a) Obtained from GPC and MWD was calculated from MW/M_n

The morphologies of the obtained copolymers are shown in Figure 6 indicating the similar morphologies for the supported system, but different from the homogeneous system. The quantitative analysis of triad distribution for all copolymers has been conducted on the assignment basis of the ^{13}CNMR spectra [24]. The triad distributions for all copolymers are shown in Table 4. All copolymers produced from each support have exhibited similar distributions having the majority for the triad of EEE. Based on ^{13}CNMR, it has been suggested that the microstructure of copolymers was not affected by boron-modification. However, considering the insertion of 1-octene **(**Table 4**)**, it was found that using boron-modification has apparently yielded higher degree of 1-olefin insertion. This may probably be due to the decreased steric hindrance of the MCM-41 support.

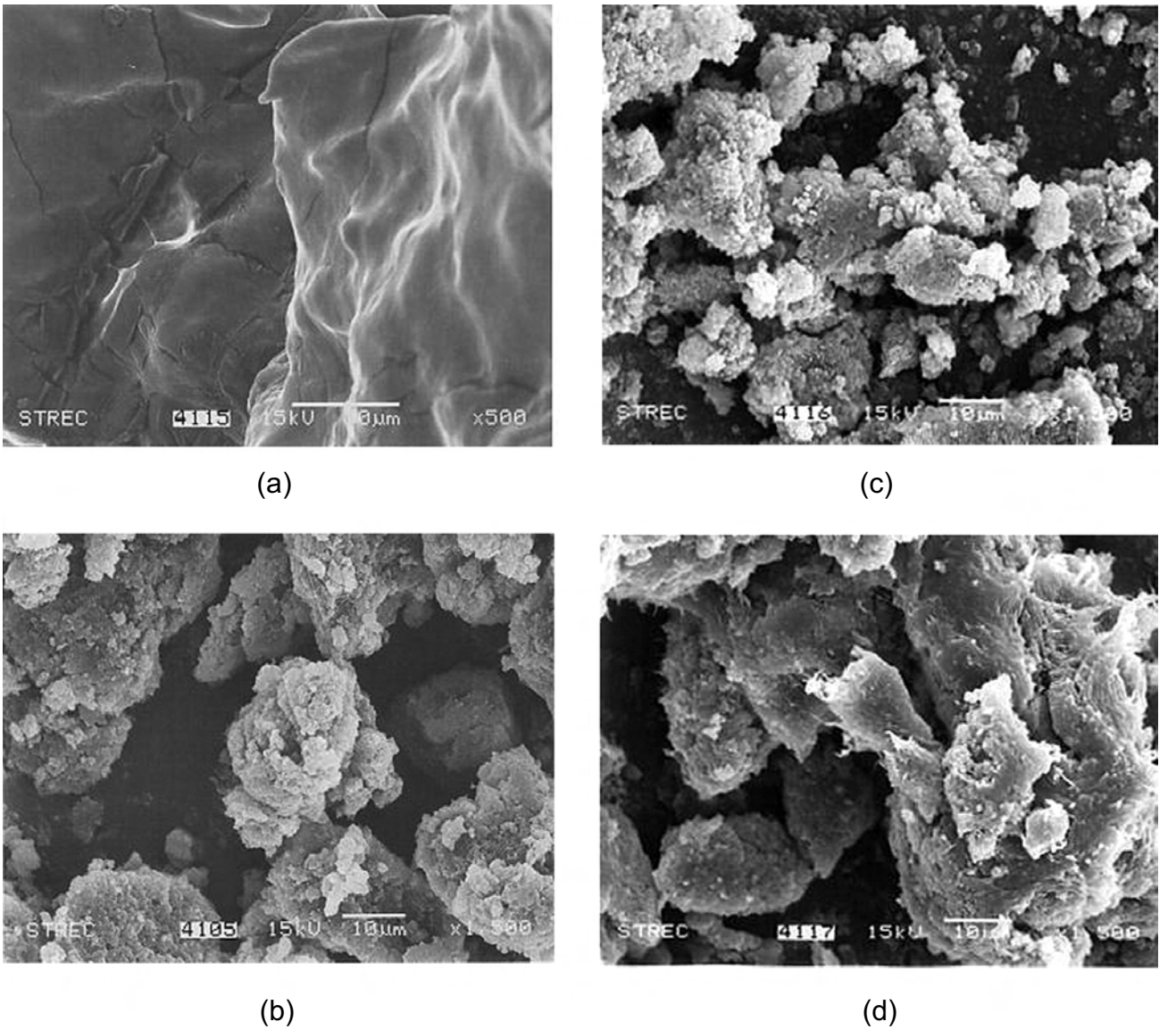

Figure 6. SEM Micrographs of the EO copolymer obtained by the (a) homogeneous system, (b) dMMAO/MCM-41, (c) dMMAO/1B-MCM-41, and (d) dMMAO/5B-MCM-41.

Table 4. ^{13}CNMR Analysis of ethylene/1-octene copolymer.

System	Triad distribution of copolymer						O in copolymer (mol%)
	OOO	EOO	EOE	EEE	OEE	OEO	
Homogeneous	0	0.099	0.153	0.477	0.226	0.045	25
MCM-41	0	0.024	0.126	0.577	0.241	0.032	15
1B-MCM-41	0	0.074	0.125	0.591	0.171	0.039	20
5B-MCM-41	0	0.074	0.134	0.588	0.172	0.032	21

E: ethylene monomer and O: 1-octene comonomer

CONCLUSION

Based on the present study, it can be concluded that the enhanced catalytic activity may be achieved via boron-modified MCM-41 support for the supported dMMAO/zirconocene catalyst during ethylene/1-octene copolymerization. Boron can act as a spacer to anchor the support and dMMAO which leads to lower interaction. However, larger amounts of boron loading turned to a slight decrease in activity due to the migration of Al (dMMAO) into boron layer. In addition, the MW of polymer was found to increase slightly with the boron-modification due to inhibition of chain transfer reaction during polymerization. Besides, a narrower MWD of polymer which has been obtained with boron-modification would be an indication of greater single site nature of the catalytic system. Based on ^{13}CNMR, boron-modification did not affect the microstructure of the copolymers obtained. However, the insertion of 1-octene increased with boron-modification, probably due to the decreased steric hindrance of the MCM-41 support.

ACKNOWLEDGEMENTS

We thank Thailand Research Fund (TRF) of RMU50-B. Jongsomjit, National Research Council of Thailand (NRCT), and the financial support from the graduate school at Chulalongkorn University. Guidance of the MCM-41 preparation by Dr. Panpranot is greatly appreciated.

REFERENCES

1. Kaminsky W., Laban A., Metallocene catalysis, *Appl. Catal. A*., **222**, 47-61, 2001.
2. Galland G.B., Seferin M., Mauler R.S., Dos Santos J.H.Z, Linear low-density polyethylene synthesis promoted by homogeneous and supported catalysts, *Polym. Int.,* **48**, 660-664, 1999.
3. Rahiala H., Beurroies I., Eklund T., Hakala K., Gougeon R., Trens P., Rosenholm J.B., Preparation and characterization of MCM-41 supported metallocene catalysts for olefin polymerization, *J. Catal*., **188**, 14-23, 1999.
4. Lee K.-S., Oh C.-G., Yim J.-H., Ihm S.-K., Characteristics of zirconocene catalysts supported on Al-MCM-41 for ethylene polymerization, *J. Mol. Catal. A-Chem*., **159**, 301-308, 2000.
5. Galland G.B., Seferin M., Guimarães R., Rohrmann J.A., Stedile F.C., Dos Santos J.H.Z., Evaluation of silica-supported zirconocenes in ethylene/1-hexene copolymerization, *J. Mol. Catal. A-Chem*., **189**, 233-240, 2002.
6. Quijada R., Retuert J., Guevara J.L., Rojas R., Valle M., Saavedra P., Palza H., Galland G.B., Results coming from homogeneous and supprted metallocene catalysts in the homo- and copolymerization of olefins, *Macromol. Symp.,* **189**, 111-125, 2002.
7. Jongsomjit B., Kaewkrajang P., Wanke S.E., Praserthdam P., A comparative study of ethylene/α-olefin copolymerization with silane-modified silica-supported MAO using zirconocene catalysts, *Catal. Lett*., **94**, 205-208, 2004.
8. Jongsomjit B., Praserthdam P., Kaewkrajang P., A comparative study on supporting effect during copolymerization of ethylene-1-olefin with silica-supported zirconocene/MAO catalyst, *Mater. Chem. Phys*., **86**, 243-246, 2004.
9. Jongsomjit B., Kaewkrajang P., Shiono T., Praserthdam P., Supporting effects of silica-supported methylaluminoxane (MAO) with zirconocene catalyst on ethylene/1-olefin copolymerization behaviors for linear low-density polyethylene (LLDPE) production, *Ind. Eng. Chem. Res.,***43**, 7959-7963, 2004.
10. Britcher L., Rahiala H., Hakala K., Mikkola P., Rosenholm J.B., Preparation, characterization, and activity of silica supported metallocene catalysts, *Chem. Mater*. , **16**, 5713-5720, 2004.
11. Jongsomjit B., Ngamposri S., Preserthdam P., Role of titania in TiO_2-SiO_2 mixed oxides-supported metallocene catalyst during ethylene/1-octene copolymerization, *Catal. Lett*., **100**, 139-146, 2005.
12. Jongsomjit B., Ngamposri S., Preserthdam P., Catalytic activity during copolymerization of ethylene and 1-hexene via mixed TiO_2-SiO_2-supported MAO with *rac*-Et[Ind]$_2$ZrCl_2 metallocene catalyst, *Molecules*.**, 10,** 603-609, 2005.
13. Jongsomjit B., Khotdee A., Praserthdam P., Behaviors of ethylene/norbornene copolymerization with zirconocene catalysts, *Iran. Polym. J.*, **14**, 559-564, 2005.

14. Jongsomjit B., Panpranot J., Okada M., Shiono T., Praserthdam P., Characteristics of LLDPE/ZrO_2 nanocomposite synthesized by in situ polymerization using a zirconocene/MAO catalyst, *Iran. Polym. J*., **15**, 433-439, 2006.
15. Pipatpratanporn P., Jongsomjit B., Praserthdam P., Impact of process variables on properties of polypropylene derived from the supported ziegler-natta and metallocene catalysts, *Iran. Polym. J*., **16**, 123-131, 2007.
16. Ko Y.S., Woo S.I., Copolymerization of ethylene and α-olefin using Et[Ind]$_2$$ZrCl_2$ entrapped inside the regular and small pores of MCM-41, *Macromol. Chem. Phys.,* **202**,739-744, 2001.
17. Dong X., Wang L., Wang, W., Yu H., Wang J., Chen T., Zhao Z., Preparation of nano-polyethylene fibers and floccules using MCM-41-supported metallocene catalytic system under atmospheric pressure, *Eur. Polym. J*., **41**, 797-803, 2005.
18. Beck J.S., Vartuli J.C., Roth W.J., Leonowicz M.E., Kresge C.T., Schmitt K.D., Chu C.T-W., Olson D.H., Sheppard E.W., McCullen S.B., Higgins J.B., Schlenker J.L., A new family of mesoporous molecular sieves prepared with liquid crystal templates, *J. Am. Chem. Soc.,* **114**, 10834-10843, 1992.
19. Oberhagemann U., Jeschke M., Papp H., Synthesis of highly ordered boron-containing B-MCM-41 and pure silica MCM-41, *Micropor. Mesopor. Mater.,* **33**, 165-172, 1999.
20. Sayari A., Danumah C., Moudrakovski I.L., Boron-modified MCM-41 mesoporous molecular sieves, *Chem. Mater*., **7**, 813-815, 1995.
21. On T.D., Joshi P.N., Kaliaguine S., Synthesis, stability and state of boron in boron-substituted MCM-41 mesoporous molecular sieves, J. *Phys. Chem*., **100**, 6743-6748, 1996.
22. Charoenchaidet S., Chavadej S., Gulari E., Borane-functionalized silica supports in situ activated heterogeneous zirconocene catalysts for MAO-free ethylene polymerization, *J. Mol. Catal. A-Chem*., **185**, 167-177, 2002.
23. Panpranot J., Pattamakomsan K., Goodwin Jr, J.G., Praserthdam P., A comparative study of Pd/SiO_2 and Pd/MCM-41 catalysts in liquid-phase hydrogenation, *Catal. Commun.,* **5**, 583-590, 2004.
24. Randall J.C., A review of high resolution liquid ^{13}carbon nuclear magnetic resonance characterizations of ethylene-based polymers, *Sci. Rev. Macromol. Chem. Phys*., **C29**, 201-315, 1989.
25. Jongsomjit B., Ngamposri S., Praserthdam P., Application of silica/titania mixed oxide-supported zirconocene catalysts for synthesis of linear low-density polyethylene, *Ind. Eng. Chem. Res*., **44**, 9059-9063, 2005.
26. Hagimoto H., Shiono T., Ikeda T., Supporting effects of methylaluminoxane on living polymerization of propylene with a chelating (diamide)dimethyl titanium complex, *Macromol. Chem. Phys*., **205**, 19-26, 2004.
27. Ketloy K., Jongsomjit, B., Praserthdam P., Characteristics and catalytic properties of [t-BuNSiMe_2Flu]TiMe_2/dMMAO catalyst dispersed on various supports towards ethylene/1-octene copolymerization, *Appl. Catal. A-Gen*., **327**, 270-277, 2007.
28. Seven J.R., Chadwick J.C., Duchateau R., Friederichs N., "Bound but not gagged"-Immobilizing single-site α-olefin polymerization catalysts, *Chem. Rev*., **105**, 4073-4147, 2005.

Catalysis Communications 10 (2009) 1319–1323

Contents lists available at ScienceDirect

Catalysis Communications

journal homepage: www.elsevier.com/locate/catcom

Catalytic behaviors of SiO_2-supported various aluminoxanes as coactivator in $MgCl_2$/DEP/$TiCl_4$–TEA catalysts for propylene polymerization

Kitti Tangjituabun, Bunjerd Jongsomjit *, Piyasan Praserthdam

Center of Excellence on Catalysis and Catalytic Reaction Engineering, Department of Chemical Engineering, Faculty of Engineering, Chulalongkorn University, Bangkok 10330, Thailand

ARTICLE INFO

Article history:
Received 16 January 2009
Received in revised form 17 February 2009
Accepted 18 February 2009
Available online 26 February 2009

Keywords:
Ziegler-Natta catalyst
Methylaluminoxane
Propylene polymerization
Silica support
Interaction

ABSTRACT

The study showed that the use of silica-supported aluminoxanes as coactivator can alter the catalytic behaviors of $MgCl_2$/diethylphthalate (DEP)/$TiCl_4$ catalyst with triethylaluminum (TEA) as an activator for propylene polymerization. It was found that the catalytic activities were ranged between 380 and 760 kg PP/mol.Ti.h within the order of dMMAO/SiO_2 > MAO/SiO_2 > MMAO/SiO_2 > dMMAO > no coactivator > SiO_2. The TGA analysis revealed that the strong interaction between aluminoxane compounds and support apparently resulted in a decreased catalytic activity. Based on the polymer microstructure, it indicated that an enhanced activity can be attributed to the increase in active site concentration.

1. Introduction

The Ziegler-Natta catalyst, which comprises of $TiCl_4$, $MgCl_2$ and an electron donor, constitutes the majority of global polyolefin production during the past several decades [1]. The discovery of $MgCl_2$-supported $TiCl_4$ catalyst in the late 1960s leads not only to the substantial enhancement of catalyst activity, but also results in polymers with morphology control [2]. In particular, the use of spherical $MgCl_2$ adducts as the catalyst support afforded significant progress in controlling polymer morphology as spherical particles and brought about revolutionary industrial developments [3,4]. Afterwards, various generations of electron donor (Lewis base) including monoester, diester, alkoxysilane, diether and succinates were sequentially developed and now become the most promising compound, which is indispensable for producing polymer with high stereoregularity so that highly isotactic polypropylene could be achieved [5]. However, highly active Ziegler-Natta catalyst is still the important issue for catalyst research. Modification of catalyst supports [6] and introduction of other components such as Grignard reagent [7,8] have been applied to enhance polymerization activity. Recently, trimethylaluminum-free methylaluminoxane (MAO) together with a certain amount of an alkylaluminum showed a notable effect on activity improvement for propylene polymerization at high temperature [9,10]. In fact, MAO is a particularly prominent activator for metallocene catalyst system. The formation of active sites undergoes by alkylation of transition metal complexes subsequent to methyl anion abstraction to yield cationic transition metal species which is active for olefin polymerization [11,12]. Nevertheless, alkylaluminum cocatalyst serves as alkylating agent in a similar way as MAO, but greater capability. Moreover, it further reduces Ti oxidation state to lower valence species and possibly form bimetallic complexes with Ti species [13,14]. Therefore, the activation mechanism of the combination between aluminoxane compound and alkylaluminum component might differ from the conventional activation process and it perhaps generates new active species, which gives high activity and novel polymer properties.

In this study, several SiO_2-supported alkylaluminums, such as MAO, modified MAO (MMAO), dried-MMAO (dMMAO) and unsupported dMMAO were prepared and used as coactivator to perform propylene polymerization using $MgCl_2$/DEP/$TiCl_4$ catalyst in combination with triethylaluminum (TEA) as an activator. The influence of the supported aluminoxanes on the catalytic activity and polymer properties were investigated and discussed further.

2. Experimental

2.1. Chemicals

Polymerization-grade propylene and triethylaluminum (TEA), donated from PTT Chemical Plc., were used as received. Methylaluminoxane (MAO) and modified methylaluminoxane (MMAO) in toluene were donated by Tosoh Akzo Corp. Cariact P-10 Silica gel (specific surface area 300 m^2/g), supplied by Fuji Silasia Chemical, was heated at 400 °C under vacuum for 6 h before use. $TiCl_4$ was

* Corresponding author. Tel.: +66 2 218 6869; fax: +66 2 218 6877.
E-mail address: bunjerd.j@chula.ac.th (B. Jongsomjit).

1566-7367/$ - see front matter © 2009 Elsevier B.V. All rights reserved.
doi:10.1016/j.catcom.2009.02.012

purchased from Merck Ltd. Anhydrous $MgCl_2$ was supplied from Sigma–Aldrich Inc., Phthalic anhydride, diethylphthalate (DEP, used as an internal donor), *n*-heptane, *n*-decane and 2-ethyl-1-hexanol were purchased from Fluka Chemie A.G. Switzerland. *n*-Hexane and toluene were donated by Exxon Chemical Thailand Ltd. and were purified by refluxing over sodium/benzophenone under argon atmosphere prior to use. Ultra high purity argon (99.999%) was obtained from Thai Industrial Gas Co., Ltd. and was further purified by passing through molecular sieves 3 Å, ASF catalyst R3-11G, NaOH and phosphorus pentoxide (P_2O_5) in order to remove traces of oxygen and moisture. All chemicals and catalyst preparation were carried out under an inert atmosphere of argon using a vacuum glove box and/or standard Schlenk techniques.

2.2. Catalyst preparation

A catalyst of type $MgCl_2$/DEP/$TiCl_4$ was synthesized according to a reported procedure [15]. Under an argon atmosphere and magnetic stirring, a mixture of 0.476 g (5 mmol) of anhydrous $MgCl_2$ and 2.5 ml of *n*-decane were treated with 2.34 ml (15 mmol) of 2-ethyl-1-hexanol at 130 °C for 2 h then added 0.1089 g (0.74 mmol) of phthalic anhydride and held at the temperature for one more hour. After the system was cooled to −20 °C, about 20 ml (182.2 mmol) of $TiCl_4$ was injected dropwise before heating slowly to 110 °C followed by treatment of the solution in the presence of 0.26 ml (1.3 mmol) of diethylphthalate (DEP) at 110 °C for 2 h. The resulting solid product was separated by filtration and the addition of 20 ml of $TiCl_4$ was repeated at room temperature. After heating and keeping the solution at 120 °C for 2 h, the liquid was siphoned off and the solid part was washed twice with 10 ml of *n*-decane and three portions of *n*-hexane 10 ml, respectively. The obtained solid catalyst was vacuum dried at 40 °C for 30 min and contained 3% Ti by means of ICP analysis.

2.3. Preparation of SiO_2-supported aluminoxanes

Silica gel was heated under vacuum at 400 °C for 6 h. Then, 1 g of heated silica was reacted with 40 ml of MAO or MMAO in additional 10 ml of toluene for 30 min at room temperature. The solid part was washed twice with toluene and then dried under vacuum to obtain MAO/SiO_2 or MMAO/SiO_2 powder. For preparation of dMMAO/SiO_2, dMMAO was carried out according to the method as described in the literature [16]. The toluene solution of 40 ml MMAO was vacuum dried at ambient temperature for 6 h followed by dissolving with *n*-heptane and dried under vacuum for removing the residue of TMA and *i*-Bu_3Al (TIBA). Based on this technique, only about 40% of TMA was removed [16]. After repeat this procedure for 4 times, the obtained solid particle (dMMAO) was treated with 1 g of SiO_2 in toluene solution for 30 min and again evacuated to give a final white powder of dMMAO/SiO_2.

2.4. Propylene polymerization

Propylene polymerization was carried out in a 100 ml stainless steel autoclave reactor equipped with a magnetic stirrer. The prescribed amount of hexane (30 ml), TEA (Al/Ti molar ratio = 167), the selected SiO_2-supported aluminoxanes (MAO/SiO_2, MMAO/SiO_2, dMMAO/SiO_2) or dMMAO with the $Al_{aluminoxane}$/Ti mole ratio of 13 and catalyst were respectively added into the reactor. Polymerization was initiated by continuous feeding of propylene at constant pressure of 60 psi and temperature of 60 °C. After 30 min of polymerization, the reaction was then terminated by the addition of acidified methanol and the product was precipitated with a large amount of methanol. The resulting polymer was then filtered off and dried under vacuum at 60 °C for 6 h.

2.5. Characterization

2.5.1. Characterization of supported aluminoxanes

2.5.1.1. N_2 physisorption. Measurement of BET surface area, average pore diameter and pore size distribution of SiO_2-supported aluminoxanes were determined by N_2 physisorption using a Micromeritics ASAP 2000 automated system.

2.5.1.2. Scanning electron microscopy and energy dispersive X-ray spectroscopy. SEM and EDX were used to determine the morphologies and elemental distribution throughout the supported SiO_2, respectively. The SEM of JEOL mode JSM-6400 was applied. The EDX was performed using Link Isis series 300 program.

2.5.1.3. Thermogravimetric analysis. TGA was performed using TA Instruments SDT Q 600 analyzer. The samples of 10–20 mg and a temperature ramping from 40 to 800 °C at 10 °C/min were used in the operation. The carrier gas was N_2 UHP.

2.5.2. Characterization of polymer

2.5.2.1. ^{13}C NMR spectroscopy. ^{13}C NMR spectroscopy was used to determine the *mmmm* pentad of polymer obtained. Sample solution was prepared by dissolving 70 mg of polymer in 1,2,4-trichlorobenzene and benzene-d_6. The spectra were taken at 110 °C using BRUKER AVANCE II 400 operating at 100 MHz with an acquisition time of 1.5 s and a delay time of 4 s.

2.5.2.2. Differential scanning calorimetry. DSC (Perkin–Elmer DSC7) was used to examine melting temperatures and crystallinity of polymers at a ramping rate of 10 °C/min in temperature range of 30–200 °C. The thermogramme was recorded in the second heating run in order to remove the thermal history.

3. Results and discussion

The characteristics of different silica-supported aluminoxanes, such as $[Al]_{aluminoxanes}$ content, surface area, and number of Al atoms/nm^2 are shown in Table 1. As seen, the Al contents based on EDX measurement in various supported coactivators apparently increased in the following order: MAO/SiO_2 < MMAO/SiO_2 < dMMAO/SiO_2. These behaviors could be due to the adsorption ability between the different aluminoxanes and the silica support employed. Since the surface hydroxyl groups of SiO_2 have high reactivity towards exchange reaction, thus it results in high capability to be tailored by interaction with the external agents. In these regards, it is possible for the aluminoxane compounds to be able to bind on the SiO_2 surface by reactions with the hydroxyl groups [17]. As also shown in Table 1, the heterogenization caused

Table 1
Characteristics of different silica-supported aluminoxane and activity.

System	% Al[a]	Surface area (m^2/g)	Number of Al[b] (atoms/nm^2)	Activity[c] (kg PP/mol.Ti.h)
SiO_2	–[d]	211	–[d]	380
MAO/SiO_2	7.3	282	6	630
MMAO/SiO_2	8.7	250	8	560
dMMAO/SiO_2	10.2	254	9	760
dMMAO	20.1	–[d]	–[d]	500
No coactivator	–[d]	–[d]	–[d]	430

[a] Determined by EDX analysis.
[b] Calculated by Al contents and specific surface area of final support.
[c] Measured for propylene polymerization using catalyst = 10 mg, cocatalyst (Al_{TEA}/Ti) = 167, $Al_{aluminoxane}$/Ti = 13, solvent = n-hexane (30 ml), *P* = 60 psi, *T* = 60 °C, and polymerization time = 30 min.
[d] Not applicable.

a favorable effect on increasing a specific surface area accompanied by a drastic drop of an average pore size diameter and narrowing its distribution (Fig. 1). In fact, surface area has a pronounced influence on the determination of dispersion states of the supported aluminoxane. The calculation of the supported Al amounts on the silica surface (Al atoms/nm^2) indicated the highly dispersed aluminoxane species on the support ranging from 6 to 9 atoms of Al/nm^2. Moreover, the increase of the numbers of Al adsorption species per surface area followed a similar trend as mentioned earlier for the increase of surface aluminum contents, which was detected by EDX. It should be also mentioned that EDX only measures the concentrations in a layer less than 1 micrometer from the surface. Hence, EDX does not measure the Al concentration in the pores of particles. As a matter of fact, for whole particles, EDX measures the concentration on external surface of the particles.

For the confirmation of the homogeneous dispersion of all aluminoxane compounds employed in this study, the typical EDX mapping images were also applied on each modified SiO_2 as shown in Fig. 2. It was obviously seen that all aluminoxanes were well distributed onto the external surface of the silica support. However, SEM micrographs demonstrated that the impregnation of dMMAO brought about an altering in the SiO_2 morphology and surface characteristics. These results were in agreement with the remarkable decrease of pore size diameter and its distribution of dMMAO/SiO_2 as also seen in Fig. 1. One of the interesting features of the immobilized SiO_2 is the degree of interaction between aluminoxanes and silica. Severn et al. [18] have reported that these two compounds were possibly linked to each other via O–Al bonding. We also have investigated the correlation between these interactions and the catalytic activity towards ethylene/α-olefin copolymerization using metallocene catalyst [19,20]. In this study, TGA analysis was performed to identify the interaction degree in terms of weight loss and removal temperature. For MAO/SiO_2, MMAO/SiO_2 and dMMAO/SiO_2, it is apparent from Fig. 3 that there was only a single temperature indicating the removal of aluminoxane compounds from the support at ca. 277 °C. As seen in Fig. 3, the decomposition pattern of the unsupported dMMAO (inserted figure) is similar to the SiO_2-supported dMMAO and other SiO_2-supported aluminoxane compounds. So, all patterns would reflect to the decomposition of the aluminoxane compounds. Besides, no such significant different patterns were observed indicating the undetectable impurities. However, the dMMAO showed the weight loss at 360 °C due to the decomposition of Al from dMMAO. The heated silica exhibited no weight loss due to the absence of adsorbed species. The typical weight loss for all cases were in the order of dMMAO (39.8%) > dMMAO/SiO_2 (19.2%) > MAO/SiO_2 (18.6%) > MMAO/SiO_2 (16.9%). This indicated that the MMAO/SiO_2 exhibited the strongest interaction among other samples.

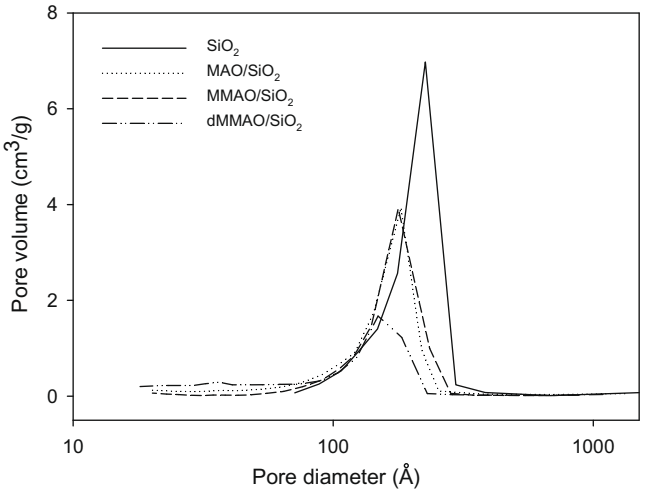

Fig. 1. Pore size distribution of different SiO_2-supported aluminoxanes.

Further study has also been performed in order to evaluate effects of different silica-supported aluminoxanes on the catalytic activities and polymer properties towards the $MgCl_2$/DEP/$TiCl_4$–TEA system via propylene polymerization. First, propylene polymerization was carried out with the addition of different aluminoxane compounds supported on SiO_2 as coactivatior. For a comparative study, the polymerization with and without SiO_2 was also tested and denoted as SiO_2 and no coactivator, respectively. The polymerization activities are also shown in Table 1 indicating the dependence of polymerization activity upon the different silica-supported aluminoxanes. It can be seen that the activities were in the range of 380–760 kg PP/mol.Ti.h. in the following order: dMMAO/SiO_2 > MAO/SiO_2 > MMAO/SiO_2 > dMMAO > no coactivator > SiO_2. It was demonstrated that the addition of sole SiO_2 resulted in a decreased catalytic activity, whereas the introduction of the SiO_2-supported aluminoxanes as coactivator enhanced the catalytic activities. As compared to the work done by García et al. [21], they found that the modified microsized-silica with a silane coupling agent can be added to prevent catalyst deactivation. We also reported that the addition of metal oxide, such as CaO (Ca/Ti = 6) during *in situ* propylene polymerization can improve the activity due to reduction of Ti^{4+} [22]. This might be attributed to the fact that active sites were sensitive to the hydroxyl species, which can remove chlorine atoms from the coordination sphere of titanium species. Therefore, hydroxyl moieties remained on the silica surface was more likely to play an important role for the catalyst deactivation.

It revealed that the dMMAO/SiO_2 rendered the highest polymerization activity while unsupported dMMAO possessed the low catalytic activity. This phenomenon was due to the supporting effect, which perhaps increased the reactivity of dMMAO towards titanium active species. It is known that three various titanium valances; Ti^{4+}, Ti^{3+}, and Ti^{2+} are formed by reacting $TiCl_4$ with an alkylaluminum. The Ti^{3+} species is considerably active for the polymerization of both ethylene and propylene while over-reduction of Ti^{3+} to Ti^{2+} leads to ethylene polymerization only [23,24]. It is generally accepted that during the activation process the alkyl aluminum cocatalysts, i.e. trimethylaluminum (TMA), triethylaluminum (TEA) and triisobutylaluminum (TIBA), are the key components for the alkylation and reduction of Ti species to form catalytic active centers. For instant, it is well known that TEA has higher reduction power than TIBA. So the Ti species reacting with TEA may have lower oxidation state than TIBA. On the other hand, TEA has higher Lewis acidity and lower steric hindrance than TIBA, making its association with the active sites easier [25]. Therefore, the high Lewis acidic property with less steric hindrance provides a high reducing power as listed in the order: TMA > TEA > TIBA based on structure. For the supported system, it should be noted that MAO contained free TMA, whereas the MMAO contained both free TMA and TIBA, which possibly took part in the activation of active sites for some extent. However, here large amount of TEA was consumed as an activator, thus we believed that the major influences of the additional aluminoxane compounds came from their nature and structure. From this point of view, the higher activity of dMMAO compared to MMAO could be attributed to higher actual amount of alkylaluminum-free MMAO existed on the silica support. Moreover, MAO was more active than MMAO as a cocatalyst [26].

It was however, still unclear that how it could activate active species, which was active for propylene polymerization. Zhong et al. [9] reported that alkylaluminum-free MAO was not active for propylene polymerization at high temperature, but a

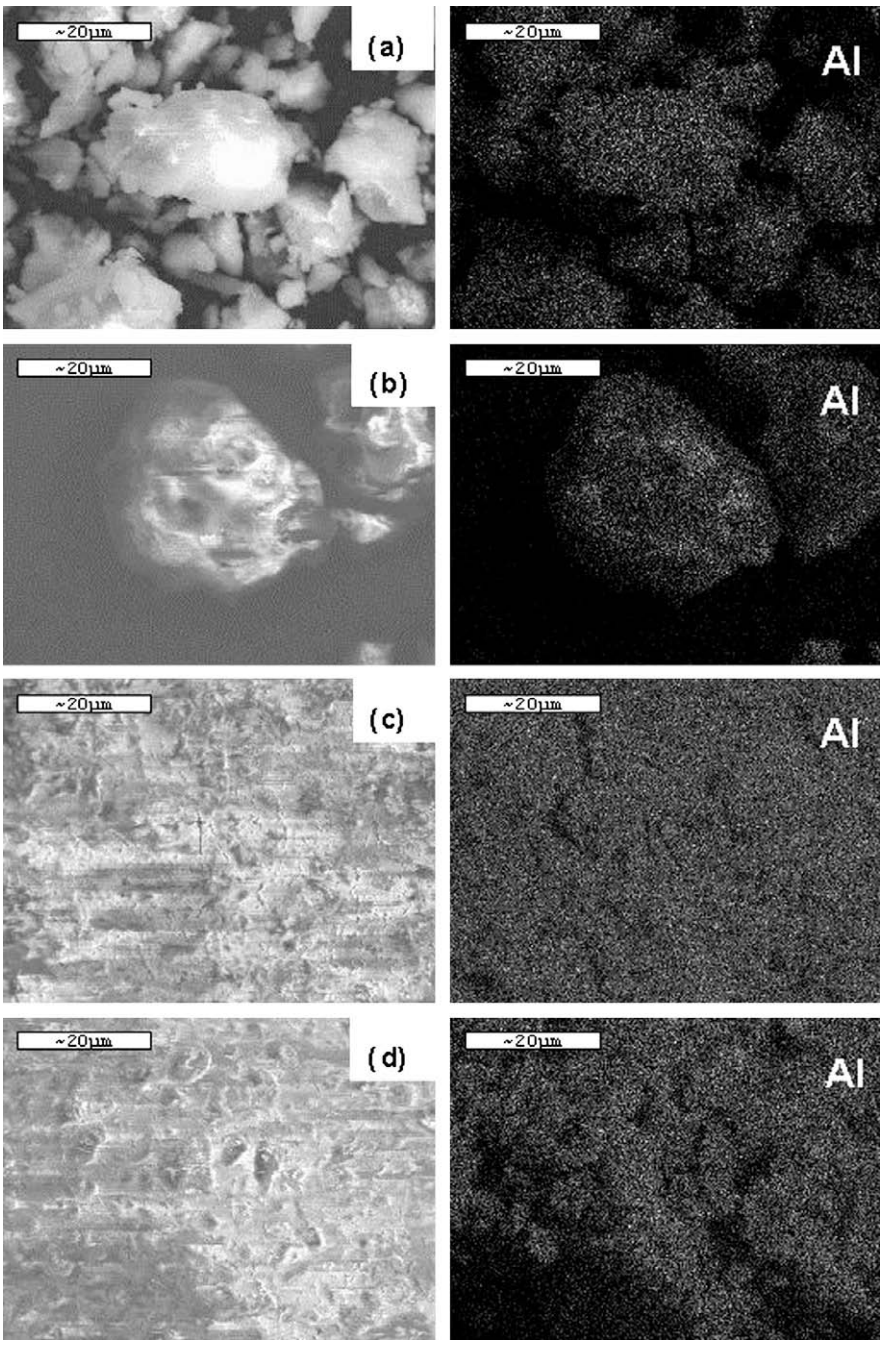

Fig. 2. SEM micrograph and EDX mapping for Al distributions of various supported aluminoxanes; (a) MAO/SiO_2, (b) MMAO/SiO_2, (c) dMMAO/SiO_2, (d) dMMAO.

combination of that with small amount of various alkyaluminums increased catalytic activity resulted from separated ion pairs formation of active species. Nath et al. [27] stated that in $CoCl_2$ catalyst system, TMA is indispensable for alkylation of $CoCl_2$, and then MAO abstracts the methyl anion from the alkylated cobalt compound to generate the cationic cobalt species. In this case, further investigation of the polymerization behavior in the absence of TEA were carried out with the same aluminoxanes/Ti molar ratio = 13 (MAO/SiO_2, MMAO/SiO_2, dMMAO/SiO_2, dMMAO). It was found that no polymerization occurred in the use of only aluminoxane compounds. This confirms that the aluminoxane compounds can not act as a polymerization activator in this system, but only a combination with alkylaluminum could efficiently activate propylene polymerization.

Furthermore, it was very interesting to disclose that the order of activating power of the silica-supported aluminoxanes was in accordance with the degree of interaction (Fig. 3). In other word, the stronger interaction present, the lower polymerization takes place. It was feasible that strong interaction decreased its reactivity towards Ti species in the course of activation process, resulted in relative decrease of catalyst activity for polymerization.

The properties of polymer obtained with various coactivators are listed in Table 2. The polymer crystallinity (X_c), *mmmm* pentad and melting temperature (T_m) were almost constant with the addition of modified SiO_2. In general, the most important factor affecting activity promotion comes from an increase in active site concentration [C*] or propagation rate constant (k_p). In addition, a number of relevant contributions have reported that k_p of

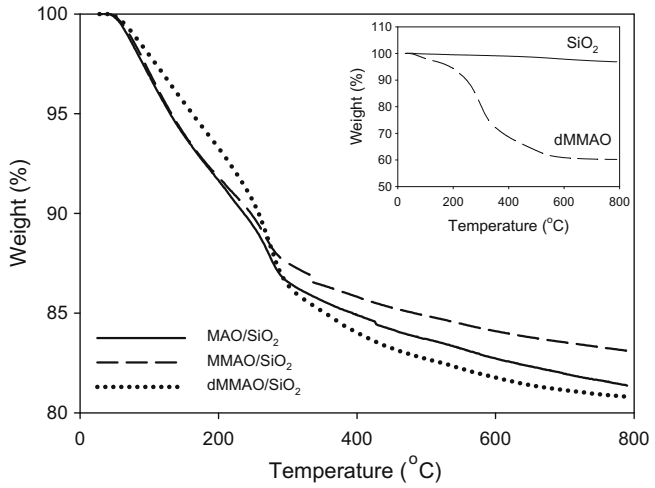

Fig. 3. TGA thermogrammes of several SiO_2-supported aluminoxanes.

Table 2
Characterization of polymer.

System	*mmmm*[a]	T_m (°C)[b]	X_c[b]
SiO_2	78	160.9	28.0
MAO/SiO_2	76	160.9	30.3
$MMAO/SiO_2$	77	160.3	28.5
$dMMAO/SiO_2$	78	160.9	29.9
dMMAO	75	159.7	27.5
No coactivator	77	159.5	24.7

[a] Obtained by ^{13}C NMR.
[b] Measured by DSC.

isospecific sites is much more higher than k_p of aspecific sites [28,29]. Although different trialkylaluminums were employed for the activation process of ZN catalyst, the identical active species formation, which possessed a comparable k_p value with varying in active site concentrations took place [30]. In this view point, the presence of aluminoxane compounds might generate the active centers, which are similar to that of trialkylaluminum. Thus, the number of active centers increased at constant of *mmmm* pentad indicating that there was no change in propagation rate constant.

4. Conclusions

The effects of different silica-supported aluminoxane compounds were investigated in propylene polymerization with $MgCl_2$/DEP/$TiCl_4$–TEA catalysts. In fact, TEA was used as an activator while MAO/SiO_2, $MMAO/SiO_2$, $dMMAO/SiO_2$ and dMMAO were employed as coactivator. The impregnated support showed high surface area and high Al dispersion. All aluminoxane compounds were active in the polymerization. The catalyst activities were improved in the order: $dMMAO/SiO_2$ > MAO/SiO_2 > $MMAO/SiO_2$ > no coactivator > SiO_2, which was in a reverse trend as the degree of interaction measured by TGA. Therefore, the strong interaction caused a decrease in catalytic activity. In addition, the constant of *mmmm* pentad suggested that an increase in a number of active centers plays an important role in activity enhancement.

Acknowledgements

The authors gratefully acknowledge the Thailand Research Fund (TRF) under RMU50-B. Jongsomjit and Royal Golden Jubilee program for the financial support.

References

[1] E. Moore, Polymerization, Characterization, Properties, Processing and Applications, Polypropylene Handbook, Hanser-Gardner, Cincinnati, OH, 1996.
[2] N. Kashiwa, H. Fujimura, Y. Tokuzumi, JP Patent 1031698.
[3] M. Covezzi, Macromol. Symp. 89 (1995) 577.
[4] L. Wu, D.T. Lynch, S.E. Wanke, Macromolecule 32 (1999) 7990.
[5] E.P. Moore Jr., The Rebirth of Polypropylene: Supported Catalysts, Hanser, Minich, 1998.
[6] K.S. Kang, M.A. Ok, S.I. Ihm, J. Appl. Polym. Sci. 40 (1990) 1303.
[7] K. Mahino, K. Tsuda, M. Takaki, Polym. Bull. 26 (1991) 371.
[8] A. Munoz-Escalona, H. Grica, A. Albornaz, J. Appl. Polym. Sci. 34 (1987) 977.
[9] C.F. Zhong, M.Z. Gao, B. Mao, Catal. Commun. 6 (2005) 173.
[10] C.F. Zhong, M.Z. Gao, B. Mao, J. Mol. Catal. A: Chem. 243 (2006) 198.
[11] R.F. Jordan, Adv. Organomet. Chem. 32 (1991) 325.
[12] R.F. Jordan, C.S. Bajgur, R.R. Willet, B. Scott, J. Am. Chem. Soc. 108 (1986) 7410.
[13] T. Nitta, B. Liu, H. Nakatani, M. Terano, J. Mol. Catal. A: Chem. 180 (2002) 25.
[14] B. Liu, T. Nitta, H. Nakatani, M. Terano, Macromol. Chem. Phys. 204 (2003) 395.
[15] Aust. Pat. 181 018/81 (1983).
[16] H. Hagimoto, T. Shiono, T. Ikeda, Macromol. Chem. Phys. 205 (2004) 19.
[17] M. Kaminaga, K. Soga, Macromol. Chem. Rapid Commun. 12 (1991) 1603.
[18] J.R. Severn, J.C. Chadwick, R. Duchateau, N. Friederichs, Chem. Rev. 105 (2005) 4073.
[19] C. Ketloy, B. Jongsomjit, P. Praserthdam, Appl. Catal. A: Gen. 327 (2007) 270.
[20] S. Bunchongturakarn, B. Jongsomjit, P. Praserthdam, Catal. Commun. 9 (2008) 789.
[21] M. García, W.E. van Zyl, M.G.J. ten Cate, J.W. Stouwdam, H. Verweij, M.S. Pimplapure, G. Weickert, Ind. Eng. Chem. Res. 42 (2003) 3750.
[22] K. Tangjituabun, B. Jongsomjit, P. Praserthdam, Catal. Lett. 109 (2006) 147.
[23] N. Kashiwa, J. Yoshigate, Macromol. Chem. 185 (1984) 1133.
[24] K. Soga, T. Sano, R. Ohnishi, Polym. Bull. 4 (1981) 157.
[25] Q. Dong, Z. Fu, J. Xu, Z. Fan, Eur. Polym. J. 43 (2007) 3442.
[26] N. Intaragamjon, T. Shiono, B. Jongsomjit, P. Praserthdam, Catal. Commun. 7 (2006) 721.
[27] D.C.D. Nath, T. Shiono, T. Ikeda, Appl. Catal. A: Gen. 238 (2003) 193.
[28] H. Mori, K. Tashino, M. Terano, Macromol. Chem. Phys. 197 (1996) 895.
[29] K. Soga, M. Ohgizawa, T. Shiono, Macromol. Chem. Rapid Commun. 10 (1984) 503.
[30] H. Nori, H. Iguchi, K. Hasebe, M. Terano, Macromol. Chem. Phys. 198 (1997) 1249.

Catal Lett (2009) 130:583–587
DOI 10.1007/s10562-009-9915-0

Observation on Different Turnover Number in Two-phase Acid-catalyzed Esterification of Dilute Acetic Acid and 1-Heptanol

Supareak Praserthdam · Bunjerd Jongsomjit

Received: 17 January 2009 / Accepted: 19 February 2009 / Published online: 25 March 2009

Abstract This paper reports on the two-phase acid-catalyzed esterification of dilute acetic acid and 1-heptanol. It reveals larger turnover number of the Amberlyst 15 than sulfuric acid. It indicates that adsorbed water on protonated sites is replaced by acetic acid, then moving into the organic phase to promote the reaction.

Keywords Acetic acid · Heptanol · Acid catalyst · Esterification · Turnover number

1 Introduction

It has been known that dilute acetic acid is considered as the waste of many important processes, such as in the production of cellulose esters and dimethyl terphthalate [1]. For instant, in the destructive distillation of wood, the acetic acid content obtained from this process is about 1–8 wt% [1]. For purification of desired products, it is required to remove or recovery the dilute acetic acid efficiently. The basic separation process, such as distillation and extraction consume large amounts of energy and solvents. Therefore, a promising way to separate the dilute acetic is to perform reaction via esterification. It is well known that esterification is a reaction between carboxylic acid and alcohol to obtain the corresponding ester as a main product. It is necessary to select the suitable alcohol having high molecular weight to react with acetic acid in the aqueous phase. Normally, the high molecular weight alcohols from C_4^+ and their ester products are insoluble in aqueous phase. In fact, the acetic acid in water can dissolve in high molecular weight alcohols and the reaction takes place in organic phase [2]. Normally, esterification is catalyzed by an acid catalyst, such as sulfuric acid, sulfonic acid or phosphoric acid [3–5]. Due to the toxicity, corrosion and difficult removal, these homogeneous acid catalysts need to be replaced with environmental friendly solid catalysts.

However, in most case, the homogeneous acid catalysts exhibit higher overall activity than the heterogeneous one. It is worth noting that many reaction parameters, such as types of catalyst, reaction condition, single-phase or two-phase system, and dilution of carboxylic acid can affect on the catalytic nature. In this present study, we have disclosed the advantage of using a solid acid catalyst, such as the Amberlyst 15 over sulfuric acid for the two-phase acid-catalyzed esterification of dilute acetic acid with 1-heptanol. In fact, 1-heptanol was employed to elucidate the effect of solubility of product in an aqueous phase. It is proposed that adsorbed water molecules on the solid catalyst can be replaced by adsorption of acetic acid molecules, then promoting the reaction in the organic phase. More information is further discussed.

2 Experimental

2.1 Chemicals and Characterization

1-heptanol (>99.0% from MERCK), dilute acetic acid (5 w/v%, 99.9% from Mallinckrodt Chemical), concentrated sulfuric acid (98% from Univar), and the Amberlyst

S. Praserthdam · B. Jongsomjit (✉)
Center of Excellence on Catalysis and Catalytic Reaction Engineering, Department of Chemical Engineering, Faculty of Engineering, Chulalongkorn University, Bangkok 10330, Thailand
e-mail: bunjerd.j@chula.ac.th

S. Praserthdam
Chulalongkorn University Demonstration Secondary School, Faculty of Education, Chulalongkorn University, Bangkok 10330, Thailand

15 (from Fluka) were used in this study. The acid strength in terms of H^+ for the Amberlyst 15 was determined using ion-exchange technique [6], where 0.2 g of sample was mixed and stirred in a conical flask with 10 mL of 3.42 M NaCl in aqueous solution for 30 h. Then, it was filtered and analyzed by titration with 0.05N NaOH using methyl orange as an indicator. The amounts of H^+ were known (sulfuric acid = 203.9 H^+ mol/g cat and Amberlyst 15 = 41.5 H^+ mol/g cat) and converted into weight of the catalyst used in each run.

The desorption characteristics of acetic acid, water and 1-heptanol on the surface of Amberlyst 15 catalyst were determined using thermal gravimetric analysis (TGA). It was performed using the SDT analyzed model Q600 from TA instruments. The catalyst was first dried at 110 °C under vacuum prior to adsorption to remove water and impurities. No deactivation of the catalyst after drying was observed based on XRD and FTIR measurement (not shown). It was reported that the catalyst is easily deactivated upon heating up to 120 °C for a long period of time [3, 7]. The dried catalyst was immersed in the first adsorbed species, and then it was filtered prior to adsorption with the second species. Then, the adsorbed catalyst was tested from 30 to 100 °C in nitrogen atmosphere with the ramp rate at 10 °C/min.

2.2 Esterification

Esterification of 1-heptanol and acetic acid was carried out in the three-neck flask heated to 90 °C (using oil-bath) and connected to a condenser (cooled by cooling water at 5 °C in order to prevent the evaporation of reaction mixtures), where the desired amounts of acetic acid and the acid catalyst (sulfuric acid or Amberlyst 15) having the identical amount of H^+ were introduced first [the concentration of sulfuric was 50 wt% (with regards to the same amount of H^+ for Amberlyst 15) of acetic acid used]. When the temperature was reached 90 °C, the desired amount of 1-heptanol (alcohol:acetic acid = 6) was added. The reaction time was 4 h and the stirring speed was 350 rpm (to avoid mass transfer effect) under batch operation. After reaction, the amounts of acetic acid left in both phases were determined by titration with 0.1 M NaOH in aqueous solution using phenolphthalein as an indicator. The number of moles of acetic acid converted was calculated based on the initial moles of acetic acid used subtracted with the moles of acetic acid remain in both aqueous and organic phases. The turnover number (TON) of catalysts was calculated as follows;

$$\mathrm{TON} = \frac{\text{Mole of acetic acid converted}}{(\text{Mole of } H^+ \text{ present})\,(\text{Reaction time})}$$

3 Results and Discussion

In this study, the two-phase acid-catalyzed esterification of dilute acetic acid with 1-heptanol using liquid (sulfuric acid) and solid (Amberlyst 15) catalysts was investigated. In order to compare the catalytic activity for both systems, the identical amount of H^+ being present in the both types of catalyst was employed. The obtained TON was calculated based on mole of acetic acid converted per mole of H^+ per reaction time (h). The TON for each catalyst under different conditions is shown in Table 1. It was found that the Amberlyst 15 exhibited higher TON than sulfuric acid under two-phase system with dilute acetic acid. In order to compare the results, we also performed this reaction using the concentrated (glacial) acetic acid as also seen in Table 1. It can be observed that the use of glacial acetic acid apparently resulted in remarkably increased in TON for both sulfuric acid and Amberlyst 15 catalysts. This can be attributed to the water effect [8]. In contrast to the dilute acetic acid system, sulfuric acid absolutely yielded much higher TON than Amberlyst 15.

For comparison, the single-phase esterification was also performed using dilute acetic acid and ethanol. The resulted TON is also shown in Table 1. The single-phase esterification exhibited higher intrinsic activity than the two-phase system as expected. In fact, the two-phase system gave remarkably low TON because there is a transfer of a molecule to a different phase. Considering the TON from the single-phase, it was found that the TON obtained from sulfuric acid was slightly higher than that of Amberlyst 15. In addition, increased agitation would have effect more in the two-phase system than in the single-phase system as also mentioned by Ataya et al. [9, 10]. With the use of sulfuric acid, the activity increased with stirring speed. This is due to the reduction of mass transfer film resistance. Ataya et al. [9, 10] also investigated the effect of mass transfer during the transesterification reaction of canola oil with methanol to form fatty acid methyl ester (FAME) using sodium hydroxide as a base catalyst. They postulated

Table 1 Comparative TON for sulfuric acid and Amberlyst 15 under different conditions

Reactants	TON ($\times 10^{-2}$ h^{-1})[a]	
	H_2SO_4	Amberlyst 15
5 wt% acetic acid and 1-heptanol (2-phase)	10.7	13.3
5 wt% acetic acid and ethanol (1-phase)	65.8	61.8
Glacial acetic acid and 1-heptanol (2-phase)	2,890	1,806

[a] TON is calculated based on the reaction condition; alcohol:acetic acid = 6, reaction temperature = 90 °C, reaction time = 4 h and stirring speed = 350 rpm

that the reaction occurred at interface and the reaction rate increased with increasing stirring speed. Other effect of mass transfer limitations during the transesterification of canola oil were also further investigated by Ataya et al. [11, 12]. We observed that the stirring speed had no effect on activity obtained from the Amberlyst 15 for both single- and two-phase system. This is because it needs only a certain force to go into the organic phase and, then fall back vigorously to aqueous phase by gravitational force.

It was also reported by Goodwin group [6, 8] that in the single-phase esterification of acetic acid with methanol, sulfuric acid exhibited higher activity than the solid catalyst. They also found that the acid strength of sulfuric acid was reduced by water. This is due to the solvation of protons [13, 14]. Rived et al. [15] stated that multiple water molecules can form strong hydrogen bond network, which changed species can be delocalized and stabilized. Pines and Fleming [16] also proposed that protons can be easily accommodated inside the water network. The similar effect on esterification reaction of a solid catalyst was also reported by Liu et al. [8]. They found that the solid catalyst was less deactivated than sulfuric acid. Nusterer et al. [17] explained that water solvation of protons hindered by the support matrix compared with solvation of free protons in aqueous phase. The similar results were observed in our two-phase system. Bianchi et al. [1] reported that for the two-phase system consisting of organic phase and aqueous phase, which occurs when the alcohols used have high molecular weight, then insoluble in an aqueous phase. The reaction occurs at the interface for sulfuric acid and at the organic phase for solid catalysts. This phenomenon can be applied to the two-phase system used in this study towards esterification of the dilute acetic acid and 1-heptanol.

Since there are very large amounts of water surrounding the protonated sites of solid catalyst in dilute acetic acid and ethanol, the positive hindrance of the catalyst support matrix can be negligible. In contrast, for the two-phase system, higher TON obtained was probably due to the reaction only occurred in the organic phase. Therefore, an additional experiment was performed by using the water-treated and untreated Amberlyst 15 for the esterification of glacial acetic acid with 1-heptanol. It indicates the similar activity profiles towards the reaction times. This is suggested that upon the presence of large amount of acetic acid (high concentration), the adsorbed water on the catalyst surface can be replaced by acetic acid. Hence, the solvation of proton can be eliminated consistently. To verify this phenomenon, a set of experiment of TGA was conducted in order to give a better understanding on the adsorbed and desorbed species on the surface of Amberlyst 15. Experimentally, Amberlyst 15 was separately adsorbed by water, acetic acid, 1-heptanol, water followed by acetic acid, acetic acid followed by water, 1-heptanol followed by water, and water followed by 1-heptanol. First, the catalyst was dried at 110 °C under vacuum prior to adsorption in order to remove water and impurities. After 5 min of adsorption for each species as mentioned above, the sample was filtered. Then, the TGA was performed with a temperature ramp of 10 °C/min from 30 to 100 °C under nitrogen atmosphere. The TGA profiles for all samples are illustrated in Fig. 1. It was found that at 100 °C about 40, 20, and 20 wt% of water (a), acetic acid (b), and 1-heptanol (c), respectively, can be desorbed from Amberlyst 15 surface. TGA results showed that water (Fig. 1a) desorbed very fast compared to acetic acid (Fig. 1b) and 1-heptanol (Fig. 1c). Thus, the adsorption of water was weak and can be replaced by acetic acid. Considering the adsorption of water followed by acetic acid adsorption (d), the TGA profile is similar to that of acetic acid (b). Thus, acetic acid can replace adsorbed water. This is also similar to the sample adsorbing acetic acid followed by water (e), where the TGA profile is identical to the one with water adsorption (a). Thus, acetic acid and water can replace each other for adsorption on Amberlyst 15 surface. Based on the TGA results, it can be concluded that water can replace adsorbed 1-heptanol (e), but 1-heptanol can not replace adsorbed water (g).

Many researchers [18–24] proposed a mechanism for esterification of carboxylic acid with alcohol using homogeneous and heterogeneous catalysts as shown in Scheme 1. The catalyst donates proton to carboxylic acid molecule. After the proton transfer, the carboxylic acid molecule is accessible for a nucleophilic attack by the hydroxyl group from the alcohol, in bulk liquid to form ester and water. It also believes that the proton-donating step is usually rapid, whereas the nucleophilic substitution is slow. With all

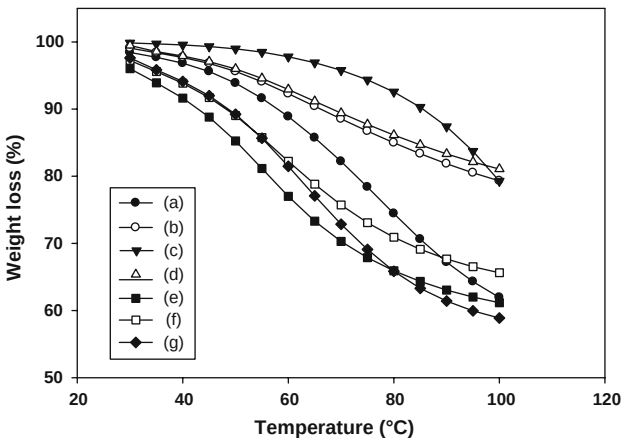

Fig. 1 TGA profiles of various treated Amberlyst 15; (*a*) water adsorption, (*b*) acetic acid adsorption, (*c*) 1-heptanol adsorption, (*d*) water followed by acetic acid adsorption, (*e*) acetic acid followed by water adsorption, (*f*) 1-heptanol followed by water adsorption, and (*g*) water followed by 1-heptanol adsorption

Scheme 1 Proposed mechanism for esterification of carboxylic acid with alcohol with acid catalyst; redrawn based on ref. [18–24]

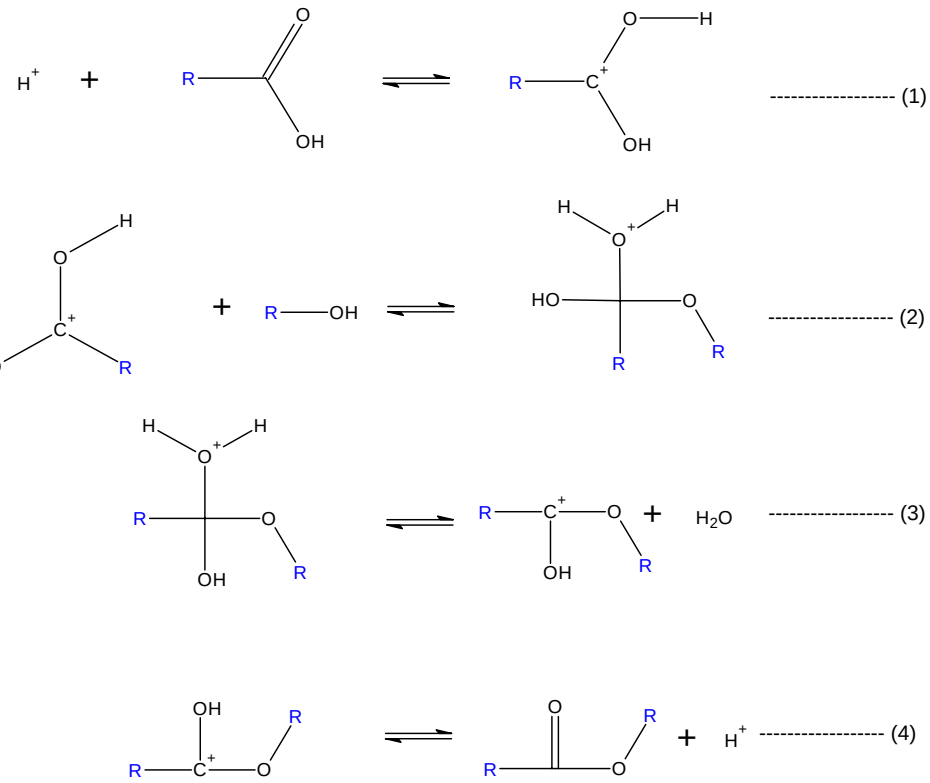

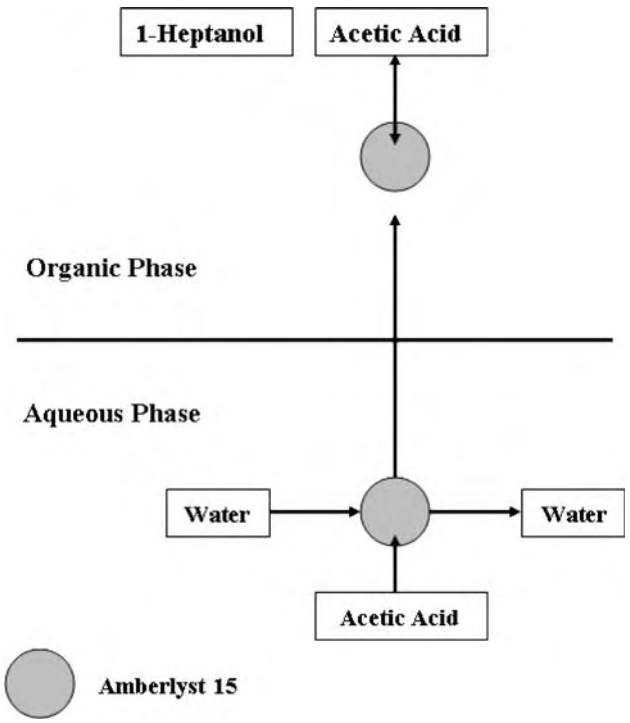

Scheme 2 Proposed mechanism for esterification of dilute acetic acid and 1-heptanol with Amberlyst 15

information, the mechanism for two-phase system of dilute acetic acid with 1-heptanol can be proposed as shown in Scheme 2. In aqueous phase, water adsorbs on the surface of solid catalyst, and then the solvation of protonated site occurs. The solid catalysts move into the organic phase by agitator. Acetic acid in the organic phase adsorbs on acid site and reacts with 1-heptanol dispersing in organic phase to form hepthyl acetate. In addition, some acetic acid can replace the adsorbed water (based on TGA) remaining on the protonated sites. Therefore, increased the TON of catalyst was observed. Then, the catalyst returns back to the aqueous phase, while the solvation of proton still occurs. This phenomenon gives benefits for the two-phase system with dilute acetic acid. The other advantage of solid catalyst (Amberlyst 15) is its reusable (at least five times) without a significant change in activity.

4 Summary

It is of great benefit to perform the two-phase esterification using a solid acid catalyst, such as Amberlyst 15 with dilute acetic acid based on this study. It is evident from the TGA measurement that all adsorbed species on the Amberlyst 15 surface play important role for enhanced TON in the organic phase. This can be attributed to the replacement of adsorbed water molecules with acetic acid on the protonated sites. However, this phenomenon does not occur with regards to the single-phase or concentrated acetic acid system, where the TON of liquid acid catalyst is still more pronounced.

Acknowledgments Authors thank the National Science and Technology Development Agency (NSTDA) under the Junior Science Talent Project (JSTP # 11) and the Thailand Research Fund (TRF) under RMU50-B. Jongsomjit for the financial support.

References

1. Bianchi CL, Ragaini V, Pirola C, Carvoli G (2003) Appl Catal B Environ 40:93
2. Ragaini V, Bianchi CL, Pirola C, Carvoli G (2006) Appl Catal B Environ 64:66
3. Juan JC, Zhang J, Yarmo MA (2009) Catal Lett doi:10.1007/s10562-008-9622-2
4. Wilson K, Clark JH (2000) Pure Appl Chem 72:1313
5. Kimura M, Nakato T, Okuhara T (1997) Appl Catal A Gen 165:227
6. López DE, Suwannakarn K, Bruce DA, Goodwin JG Jr (2007) J Catal 247:43
7. Peters TA, Benes NE, Holmen A, Keurentjes JTF (2006) Appl Catal A Gen 297:182
8. Liu Y, Lotero E, Goodwin JG Jr (2006) J Mol Catal A Chem 245:132
9. Ataya F, Dubé MA, Ternan M (2006) Ind Eng Chem Res 45:5411
10. Ataya F, Dubé MA, Ternan M (2007) Energy Fuels 21:2450
11. Ataya F, Dubé MA, Ternan M (2008) Energy Fuels 22:679
12. Ataya F, Dubé MA, Ternan M (2008) Energy Fuels 22:3551
13. López DE, Goodwin JG Jr, Bruce DA, Lotero E (2005) Appl Catal A Gen 295:97
14. Kazansky VB (2001) Catal Rev Sci Eng 43:199
15. Rived F, Canals I, Bosch E, Roses M (2001) Anal Chim Acta 439:315
16. Pines E, Fleming GR (1991) J Phys Chem 95:10448
17. Nusterer E, Blochl PE, Schwarz K (1996) Chem Phys Lett 253:448
18. Liu Y, Lotero E, Goodwin JG Jr (2006) J Catal 242:278
19. Lilja J, Murzin DY, Salmi T, Aumo J, Mäki-Arvela P, Sundell M (2002) J Mol Catal A Chem 182–183:555
20. Kirumakki SR, Nagaraju N, Chary KVR (2006) Appl Catal A Gen 299:185
21. Ajaikumar S, Pandurangan A (2007) J Mol Catal A Chem 266:1
22. Teo HTR, Saha B (2004) J Catal 228:174
23. Lilja J, Aumo J, Salmi T, Murzin DY, Mäki Arvela P, Sundell M, Ekman K, Peltonen R, Vainico H (2002) Appl Catal A Gen 228:253
24. Rönnback R, Salmi T, Vuori A, Haario H, Lehtonen J, Sundqvist A, Tirronen E (1997) Chem Eng Sci 52:3369

Available online at www.sciencedirect.com
ScienceDirect
Catalysis Communications 9 (2008) 789–795
CATALYSIS COMMUNICATIONS
www.elsevier.com/locate/catcom

Impact of bimodal pore MCM-41-supported zirconocene/dMMAO catalyst on copolymerization of ethylene/1-octene

Sirinlak Bunchongturakarn, Bunjerd Jongsomjit *, Piyasan Praserthdam

Center of Excellence on Catalysis and Catalytic Reaction Engineering, Department of Chemical Engineering, Faculty of Engineering, Chulalongkorn University, Bangkok 10330, Thailand

Received 22 March 2007; received in revised form 2 September 2007; accepted 3 September 2007
Available online 7 September 2007

Abstract

The bimodal MCM-41-supported zirconocene/dMMAO catalyst exhibited higher catalytic activity for ethylene/1-octene copolymerization compared to the unimodal one. The higher activity can be attributed to lesser support interaction. The copolymer having broader MWD was obtained with the bimodal support without any significant changes in MW and polymer microstructure as seen by ^{13}C NMR.

Keywords: MCM-41; Bimodal support; Metallocene catalyst; Support interaction; Polyolefins

1. Introduction

For years, the correlation between metallocene structure and polymerization behaviors for olefin polymerization have been extensively studied and developed consistently. In general, metallocenes are single site catalysts producing polymers having narrow molecular weight distribution (MWD) and homogeneously chemical composition [1,2]. However, it is found that the homogeneous metallocene catalytic system has two major disadvantages; the lack of morphology control of polymer causing the reactor fouling and the limitation of being able to use only in the solution process whereas the existing technologies are mainly based on the gas phase and slurry processes. Therefore, binding these metallocene catalysts onto suitable inorganic supports can provide a promising way to overcome those drawbacks.

Several studies [3–9] have been concentrated on the use of supported metallocene catalyst for the olefin polymerization. Apparently, silica, alumina and magnesia supports have been the most widely used inorganic supports so far. The aim is to develop a way to attach the metallocene to the support without losing the performance of the homogeneous complex. The main immobilization techniques can be performed by direct impregnation of metallocene or cocatalyst on the support, then pretreatment of the support followed by activation of metallocene. Hence, high surface area and the presence of well-defined, stable sites for the attachment of the active component to the support are very crucial [10].

As well known, the mesoporous silica tube-like materials designated as MCM-41 was introduced in 1992 [11,12]. The MCM-41 is recognized as a well-defined as mesoporous material with narrow pore size distribution, large internal surface area, distinct adsorption properties and hexagonal arrangement of uniformly sized cylindrical pore. It has the possibility to control the internal diameter of mesopores between 15 and 100 Å by varying the chain length of the micellar surfactant template. In fact, its pore diameter can enable large metallocene molecules to be immobilized onto both the surface and inside the pore. These excellent properties of this material essentially emulate researchers to use the MCM-41 as the

* Corresponding author. Tel.: +66 2 2186869; fax: +66 2 2186877.
E-mail address: bunjerd.j@chula.ac.th (B. Jongsomjit).

1566-7367/$ - see front matter
doi:10.1016/j.catcom.2007.09.001

support for metallocene catalysts for olefin polymerization [13–19].

In general, the surface areas mainly control the dispersion of supported metal. As a matter of fact, too large surface area (small pore diameter) results in poor diffusion efficiency of reactant and products in the intra-pellet structure whereas a catalyst having too large pore diameter exhibits a small surface area leading to low metal dispersion and low catalytic activity. A support with a distinct bimodal structure has excellent advantages for solving the contradiction as mentioned before. In particular, the large pores provide rapid transportation of reactant and product molecules whereas the small pores render a large surface area. Moreover, the geometrical shape of the nano-channels of support can serve as polymerization reactors to affect the pattern and activity of monomer insertion. Thus, the arrangement of polymer chain and polymer morphology can be controlled. Many researchers are interested in obtaining bimodal polyethylene using bicomponent catalyst or support [20–22].

In this present study, the MCM-41 supports having different pore size distribution such as unimodal and bimodal pore sizes were synthesized. Then, the linear low-density polyethylene (LLDPE) was prepared by ethylene/1-octene copolymerization using various unimodal and bimodal MCM-41-supported zirconocene/dMMAO catalysts. The influences of various pore structures of MCM-41 on the catalytic activity and polymer properties were investigated. The copolymers obtained were further analyzed using GPC and ^{13}C NMR.

2. Experimental

2.1. Materials

All chemicals and polymerization were manipulated under an argon atmosphere, using a glove box and/or Schlenk techniques. Toluene was dried over dehydrated $CaCl_2$ and distilled over sodium/benzophenone before use. The *rac*-ethylenebis (indenyl) zirconium dichloride (*rac*-Et[Ind]$_2$ZrCl$_2$) was supplied from Aldrich Chemical Company, Inc. Modified methylaluminoxane (MMAO) in hexane was donated by Tosoh (Akso, Japan). Trialkylaluminum (TMA, 2 M in toluene) was supplied by Nippon Aluminum Alkyls, Ltd., Japan. Ultrahigh purity argon was further purified by passing it through columns that were packed with BASF catalyst R3-11G (molecular-sieved to 3 Å), sodium hydroxide (NaOH), and phosphorus pentaoxide (P_2O_5) to remove traces of oxygen and moisture. Ethylene gas (99.96% pure) was donated by the National Petrochemical Co., Ltd., Thailand. 1-Octene ($d = 0.715$) was purchased from Aldrich Chemical Company, Inc.

2.2. Preparation of bimodal MCM-41 support

The MCM-41 support was synthesized according to the method described by Panpranot et al. [23] using the gel composition of CTABr:0.3NH_3:4SiO_2:Na_2O:200H_2O, where CTABr denotes cetyltrimethyl ammonium bromide. Briefly, 20.03 g of colloidal silica Ludox HS 40% (Aldrich Chemical Company, Inc.) was mixed with 22.67 g of 11.78% sodium hydroxide solution. Another mixture comprised of 12.15 g of CTABr (Aldrich Chemical Company, Inc.) in 36.45 g of deionized water, and 0.4 g of an aqueous solution of 25% NH_3. Both of these mixtures were stirred by an agitator for 30 min, then heated statically at 373 K for 5 days. The obtained solid material was filtered, washed with deionized water until no base was detected and then dried at 373 K. The sample was then calcined in flowing nitrogen up to 823 K (1–2 K/min), then in air at the same temperature for 5 h. After preparation, the unimodal MCM-41 support (denoted as UMD) having the pore diameter of ca. 2 nm and surface area of 864 m^2/g was obtained. The bimodal MCM-41 having average pore diameters of ca. 5 and 6 nm (denoted as BMD1 and BMD2, respectively) was prepared by treating the UMD-MCM-41 (before calcination) with an emulsion containing *N,N*-dimethyl decylamine (0.625 g in 37.5 g of water for each gram of MCM-41) for 3 (for BMD1) and 4 days (for BMD2) at 393 K. This was washed thoroughly, dried and calcined in flowing nitrogen up to 823 K (1–2 K/min), then in air at the same temperature for 5 h.

2.3. Preparation of dried-MMAO (dMMAO)

Removal of TMA from MMAO was carried out according to the reported procedure [24]. The toluene solution of MMAO was dried under vacuum for 6 h at room temperature to evaporate the solvent, TMA, and Al(*i*Bu)$_3$ (TIBA). Then, continue to dissolve with 100 ml of heptane and the solution was evaporated under vacuum to remove the remaining TMA and TIBA. This procedure was repeated four times and the white powder of dried MMAO (dMMAO) was obtained.

2.4. Preparation of MCM-41-supported dMMAO

The MCM-41 support was reacted with the desired amount of dMMAO in 20 ml of toluene at room temperature for 30 min. The solvent was then removed from the mixture by evacuated. This procedure was done only once with toluene (20 ml × 1) and three times with hexane (20 ml × 3). Then, the solid part was dried under vacuum at room temperature. The white powder of supported cocatalyst (dMMAO/support) was then obtained.

2.5. Polymerization

The ethylene/1-octene copolymerization reaction was carried out in a 100 ml semi-batch stainless steel autoclave reactor equipped with magnetic stirrer. In the glove box, the desired amounts of *rac*-Et[Ind]$_2$ZrCl$_2$ and TMA were mixed and stirred for 5 min for aging. Then, toluene (to make a total volume of 30 ml) and 100 mg of dMMAO/sup-

port were introduced into the reactor. After that, the mixture of *rac*-Et[Ind]$_2$ZrCl$_2$ and TMA were injected into the reactor. The reactor was frozen in liquid nitrogen to stop reaction and then 0.018 mol of 1-octene was injected into the reactor. The reactor was evacuated to remove argon. Then, it was heated up to polymerization temperature (343 K) and the polymerization was started by feeding ethylene gas (total pressure 50 psi in the reactor) until the consumption of ethylene 0.018 mol (6 psi was observed from the pressure gauge) was reached. The reaction of polymerization was completely terminated by addition of acidic methanol. The time of reaction was recorded for purpose of calculating the activity. The precipitated polymer was washed with methanol and dried at room temperature.

2.6. Characterization

2.6.1. Characterization of supports and catalyst precursor

2.6.1.1. N_2 physisorption. Measurement of BET surface area, average pore diameter and pore size distribution of MCM-41 support were determined by N_2 physisorption using a Micromeritics ASAP 2000 automated system.

2.6.1.2. X-ray diffraction. XRD was performed to determine the bulk crystalline phases of samples. It was conducted using a SIEMEN D-5000 X-ray diffractometer with Cu K$_\alpha$ ($\lambda = 1.54439$ Å). The spectra were scanned at a rate of 2.4° min^{-1} in the range of $2\theta = 10$–80°.

2.6.1.3. Scanning electron microscopy and energy dispersive X-ray spectroscopy. SEM and EDX were used to determine the morphologies and elemental distribution throughout the sample granules, respectively. The SEM of JEOL mode JSM-6400 was applied. The EDX was performed using Link Isis series 300 program.

2.6.1.4. Raman spectroscopy. The Raman spectra of the samples were collected by projecting a continuous wave YAG laser of Nd (810 nm) through the samples at room temperature. A scanning range of 100–1000 cm^{-1} with a resolution of 2 cm^{-1} was applied.

2.6.1.5. X-ray photoelectron spectroscopy. XPS was used to determine the binding energies (BE) and surface concentration of samples. It was carried out using the Shimazu AMICUS with VISION 2-control software. Spectra were recorded at room temperature in high-resolution mode (0.1 eV step, 23.5 eV pass energy) for Al 2p core-level region. The samples were mounted on an adhesive carbon tape as pellets. The energy reference for Ag metal (368.0 eV for 3d$_{5/2}$) was used for this study.

2.6.1.6. Thermogravimetric analysis. TGA was performed using TA Instruments SDT Q 600 analyzer. The samples of 10–20 mg and a temperature ramping from 298 to 500 K at 2 K/min were used in the operation. The carrier gas was N_2 UHP.

2.6.2. Characterization of polymer

2.6.2.1. Gel permeation chromatography. The molecular weight (MW) and molecular weight distribution (MWD) of polymer were determined using GPC (GPC, PL-GPC-220). Samples were prepared having approximately concentration of 1–2 mg/ml in trichlorobenzene (mobile phase) by using the sample preparation unit (PL-SP 260) with filtration system at a temperature of 423 K. The dissolved and filtered samples were transferred into the GPC instrument at 423 K. The calibration was conducted using the universal calibration curve based on narrow polystyrene standards.

2.6.2.2. ^{13}C NMR spectroscopy. ^{13}C NMR spectroscopy was used to determine the triad distribution and 1-octene insertion indicating the copolymer microstructure. Chemical shift were referenced internally to the $CDCl_3$ and calculated according to the method described by Randall [34]. Sample solution was prepared by dissolving 50 mg of copolymer in 1,2,4-trichlorobenzene and $CDCl_3$. ^{13}C NMR spectra were taken at 333 K using BRUKER AVANCE II 400 operating at 100 MHz with an acquisition time of 1.5 s and a delay time of 4 s.

3. Results and discussion

3.1. Catalytic activity

The main focus of this present study was to investigate the impact of different pore structures of MCM-41 support on the catalytic activity during copolymer of ethylene/1-octene with MCM-41-supported zirconocene/dMMAO catalyst. First, the MCM-41 supports having different pore structures were prepared based on different pretreatment conditions. After preparation of supports, the unimodal MCM-41 support denoted as UMD having the average pore diameter of ca. 2 nm and surface area of 883.5 m^2/g was obtained as seen in Table 1. The pore size distribution of the MCM-41 (UMD) is shown in Fig. 1 indicating only the unimodal pore size distribution. By treating the MCM-41 (UMD) with *N,N*-dimethyldecylamine at the specified conditions, the bimodal MCM-41 supports denoted as BMD can be achieved. The BMD1 is assigned to the bimodal MCM-41 support having the average pore diameter of ca. 5 nm (surface area = 400.3 m^2/g) whereas the BMD2 refers to the bimodal MCM-41 with the average pore diameter of ca. 6 nm (surface area = 400.0 m^2/g) as also shown in Table 1 and Fig. 1. As seen in Fig. 1, it can be observed that the MCM-41 (BMD2) support exhibited larger portion of the large pore than the MCM-41 (BMD1) one. The XRD patterns (not shown) of various MCM-41 supports were similar. In fact, all MCM-41 supports gave the similar XRD patterns consisting of a broad peak of amorphous silica around 20–30°. In general, Raman spectroscopy is one of the most powerful techniques used to identify the metal compound structure. Here, it was used to identify perhaps the different structure of MCM-41

Table 1
BET surface area, average pore diameter and incremental pore volume of various MCM-41 supports

Support	BET surface area (m^2/g)	Average pore diameter (nm)		Incremental pore volume (cm^3/g)	
		Small pore	Large pore	Small pore	Large pore
MCM-41 (UMD)	863.5	2.3	–	1.78	
MCM-41 (BMD1)	400.3	3.2	24.4	1.38	0.44
MCM-41 (BMD2)	400.0	3.2	28.7	0.91	0.82

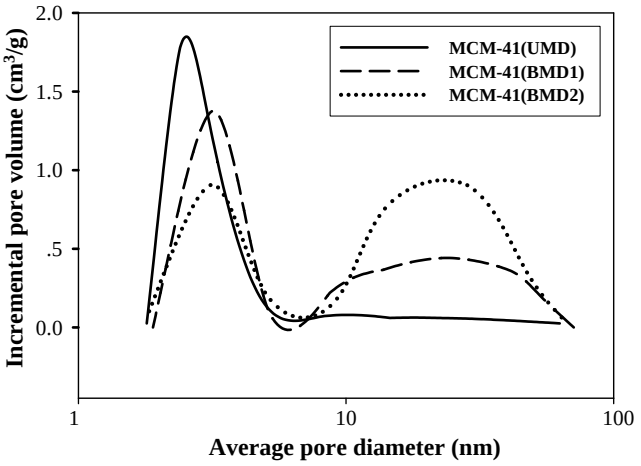

Fig. 1. Pore size distribution of various MCM-41 supports.

supports having different pore size distribution, especially for the Si–O bonds. As confirmation, no significantly different Raman bands (Fig. 2) were also observed for all MCM-41 supports within the Raman shift ranged between 200 and 1000 cm^{-1}.

After impregnation with dMMAO, the nature and surface concentrations of $[Al]_{dMMAO}$ on various MCM-41 supports were determined using the XPS measurement. The typical XPS spectra (not shown) for all MCM-41-supported dMMAO exhibited the identical binding energy (BE) of Al 2p at ca. 74.6–74.7 eV. It should be noted that the BE for Al 2p obtained here was also in accordance with

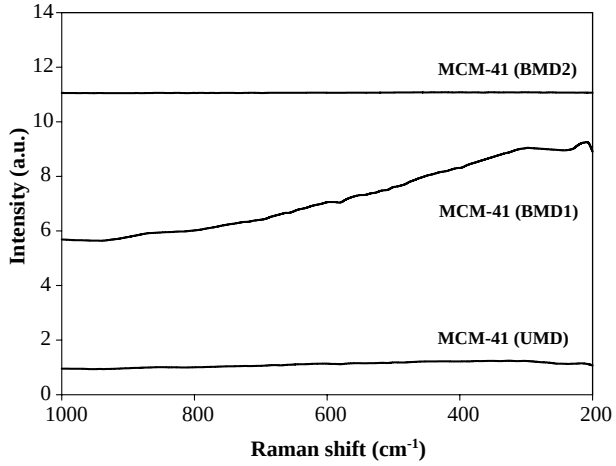

Fig. 2. Raman spectra of various MCM-41 supports.

that on silica as reported by Hagimoto et al. [24]. Thus, it indicated that no transformation of the oxidation state for the cocatalyst (dMMAO) present on various MCM-41 supports employed. The surface concentrations of $[Al]_{dMMAO}$ measured by XPS are also shown in Table 2. In fact, the surface concentration of $[Al]_{dMMAO}$ can be calculated from integration of the peak area of Al 2p (BE ~74.6–74.7 eV) obtained from the XPS measurement using VISION 2-control software. It can be observed that the surface concentrations of $[Al]_{dMMAO}$ were similar for both MCM-41 (BMD) supports having $[Al]_{dMMAO}$ at surface of 27.0 wt%. However, it appeared that the MCM-41 (UMD) support had a slightly higher amount of $[Al]_{dMMAO}$ at surface (27.3 wt%) than that of the MCM-41 (BMD) support. Based on the XPS measurement as shown in Table 2, the UMD support contains the highest amount of $[Al]_{dMMAO}$. This is probably due to higher surface area of the UMD. As the result, higher dispersion of $[Al]_{dMMAO}$ can be obtained. Besides the amounts of $[Al]_{dMMAO}$ surface concentration, one should consider the distribution of the cocatalyst on the various supports. Therefore, the elemental distribution for $[Al]_{dMMAO}$ was also performed using EDX mapping on the external surface of the catalyst precursors. The $[Al]_{dMMAO}$ distribution on various supports is shown in Fig. 3. As seen, all samples exhibited good distribution of Al without any changes in the support morphology.

The catalytic activities via various MCM-41 supports and the homogeneous system are listed in Table 3. It was obvious that the homogeneous catalytic system provided higher activity than the supported system due to the absence of supporting effect [5,8,9]. Considering the various MCM-41-supported systems, it was found that the MCM-41 (BMD) rendered higher activity than the UMD one about 1.2–1.5 times. In general, the surface areas mainly control the dispersion of supported metal (or active phase). As a matter of fact, too large surface area (small pore diameter) results in poor diffusion efficiency of reactant and products in the intra-pellet structure whereas a catalyst having too large pore diameter exhibits a small surface area leading to low metal dispersion and low catalytic activity [25]. In addition, the ratio of small pore/large pore of BMD1 was higher than that of BMD2, thus more dispersion of the $[Al]_{dMMAO}$ was obtained resulting in higher activity. This was suggested that higher portion of large pore could result in lower activity. Although the amount of $[Al]_{dMMAO}$ at surface of the MCM-41 (UMD) as measured by XPS was slightly higher, the catalytic activity

Table 2
XPS results for different supports

Support	BE for Al 2p[a] (eV)	Mass concentration (%) of Al
dMMAO/MCM-41 (UMD)	74.7	27.3
dMMAO/MCM-41 (BMD1)	74.6	27.0
dMMAO/MCM-41 (BMD2)	74.7	27.0

[a] Al 2p from dMMAO.

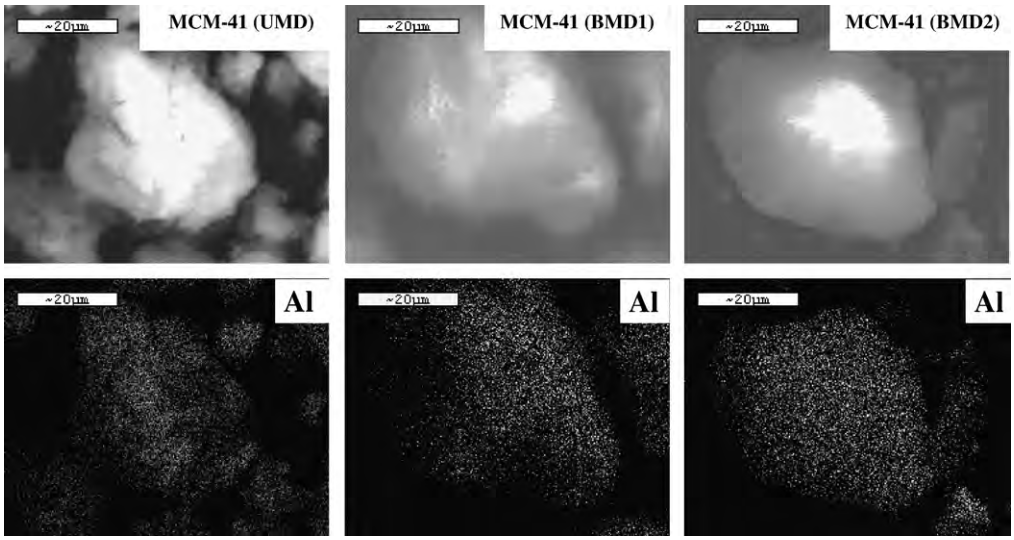

Fig. 3. SEM micrographs and $[Al]_{dMMAO}$ distribution obtained from EDX.

Table 3
Catalytic activities of various MCM-41-supported dMMAO with zirconocene catalyst during ethylene/1-octene copolymerization

System	Polymerization time (s)	Polymer yield[a] (g)	Catalytic activities[b] ($\times 10^{-4}$ kg Pol mol Zr^{-1} h^{-1})
Homogeneous	87	1.59	4.38
MCM-41 (UMD)	186	1.58	2.04
MCM-41 (BMD1)	127	1.58	2.99
MCM-41 (BMD2)	150	1.51	2.42

[a] The polymer yield was fixed [limited by ethylene fed and 1-octene used (0.018 mol equally)].
[b] Activities were measured at polymerization temperature of 343 K, [Ethylene] = 0.018 mol, $[Al]_{dMMAO}/[Zr]_{cat} = 1135$, $[Al]_{TMA}/[Zr]_{cat} = 2500$, in toluene with total volume = 30 ml and $[Zr]_{cat} = 5 \times 10^{-5}$ M.

was lower. It is known that besides the concentrations of active species, one should consider on the interaction between the active species and support. In fact, too strong interaction can result in compound formation at surface [26–30] and/or inactive species leading to low catalytic activity. A wide range of variables including nature of supports and active species, particle size, and treatment conditions can affect the degree of support interaction. Essentially, they can be superimposed on each other. However, based on this study, the active species ($[Al]_{dMMAO}$) present on different MCM-41 supports had the similar characteristics of Al 2p as measured by XPS indicating that no other compound formation on surface was formed. Thus, it was suggested that based on the similar amount of $[Al]_{dMMAO}$ added, the size of the $[Al]_{dMMAO}$ present in the small pore [MCM-41 (UMD)] was presumably smaller due to larger surface area. As a matter of fact, the smaller particle can interact more with the support resulting in stronger support interaction. In order to identify the interaction of $[Al]_{dMMAO}$ on various MCM-41 supports, the TGA measurement was performed. In order to give a better understanding, we proposed the interaction of support and dMMAO based on the review paper by Severn et al. [31]. They explained that the connection of the support and cocatalyst occurred via the $O_{support}$–$Al_{cocatalyst}$ linkage. In particular, the TGA can only provide useful information on the degree of interaction for the dMMAO bound to the support in terms of weight loss and removal temperature [32]. The TGA profiles of $[Al]_{dMMAO}$ on various MCM-41 supports are shown in Fig. 4 indicating the similar profiles for various supports. It was observed that the weight loss of $[Al]_{dMMAO}$ present on various supports were in

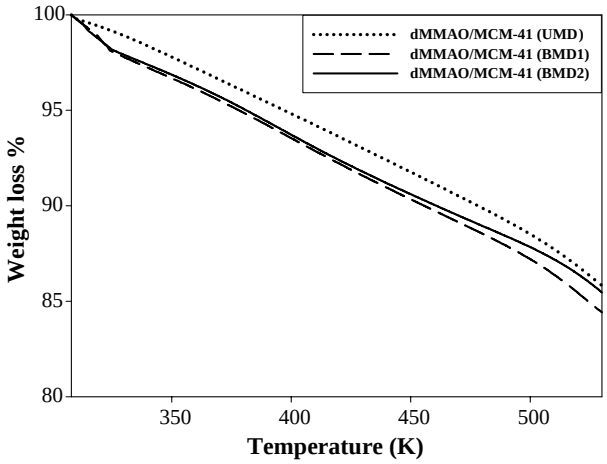

Fig. 4. TGA profiles of $[Al]_{dMMAO}$ on various MCM-41 supports.

the order of MCM-41 (BMD1) (12.8%) > MCM-41 (BMD2) (12.2%) > MCM-41 (UMD) (11.5%). Based on TGA, it indicated that the $[Al]_{dMMAO}$ present on MCM-41 (UMD) had the strongest interaction among the other supports, thus, having the lowest polymerization activity. It is worth noting that the higher activity obtained from the bimodal support can be attributed to the optimum interaction between the support and dMMAO.

3.2. Polymer characteristics

The various copolymers obtained were further characterized by means of GPC and ^{13}C NMR. The GPC was performed in order to determine the MW, M_n and MWD of polymers. The GPC results are shown in Table 4. Considering the different catalytic systems, it can be observed that the homogeneous system exhibited higher MW than the supported system did. As known from our previous works, the supported system apparently promoted the chain transfer reaction resulting in lower MW of polymers [8,33]. Based on the supported system, it revealed that the copolymer obtained from the bimodal MCM-41 supports had broader MWD than that derived from the unimodal one. It was suggested that this broad MWD copolymer can be attributed to the different natures of catalytic sites present on the bimodal supports. However, the observed MW of copolymers among all supports was slightly different. It should be mentioned that the homogeneous system usually results in the narrow MWD of polymer compared to the heterogeneous one. However, in this study, the narrower MWD of polymer obtained from the MCM-41 (UMD) was observed. This may be attributed to the more uniform catalytic sites present arising from the more well-defined structure of the unimodal MCM-41 support.

The quantitative analysis of triad distribution for all copolymers was conducted on the basis assignment of the ^{13}C NMR spectra of ethylene/1-octene (EO) copolymer [34]. The characteristics of ^{13}C NMR spectra (not shown) for all copolymers were similar indicating the copolymer of ethylene/1-octene. The triad distribution of all polymers is shown in Table 5. Ethylene incorporation in all systems gave copolymers with similar triad distribution. It was also shown a little probability to produce the dyad of OO, which is the characteristic of this zirconocene in homogeneous system [5]. No triad of OOO in the copolymers was found. Only the random copolymers can be produced in all systems. In addition, the octene incorporations in all supported systems were between 25 and 32 mol%, which was similar with that in the homogeneous system.

Table 4
Molar weight (MW) and molecular weight distribution (MWD) of polymers obtained from various MCM-41-supported dMMAO with zirconocene catalyst

System	MW[a] ($\times 10^{-4}$ g mol^{-1})	M_n[a] ($\times 10^{-4}$ g mol^{-1})	MWD[a]
Homogeneous	3.66	0.69	5.3
MCM-41 (UMD)	2.91	0.98	3.0
MCM-41 (BMD1)	2.69	0.45	6.0
MCM-41 (BMD2)	3.07	0.62	5.0

[a] Obtained from GPC and MWD was calculated from MW/M_n.

4. Conclusions

In summary, the bimodal MCM-41-supported zirconocene/dMMAO showed the enhancement of activity during copolymerization of ethylene/1-octene about 1.5 times compared with that using the unimodal one. It was proven that the higher activity could be attributed to lesser interaction between the support and cocatalyst. Besides, the bimodal MCM-41 support apparently gave broader MWD copolymer due to more different catalytic sites present. However, both unimodal and bimodal MCM-41 supports trended to produce the random copolymers with a little probability for the dyad of OO.

Table 5
^{13}C NMR analysis of ethylene/1-octene copolymer

System	Triad distribution of copolymer						Mol% of O in copolymer
	OOO	EOO	EOE	EEE	OEO	OEE	
Homogeneous	0	0.077	0.210	0.414	0.056	0.244	29
MCM-41 (UMD)	0	0.073	0.232	0.456	0.075	0.164	30
MCM-41 (BMD1)	0	0.096	0.221	0.408	0.047	0.228	32
MCM-41 (BMD2)	0	0.057	0.196	0.456	0.057	0.234	25

E refers to ethylene monomer and O refers to 1-octene comonomer.

Acknowledgements

We thank the Thailand Research Fund (TRF) for RMU50-B. Jongsomjit, the National Research Council of Thailand (NRCT) and the graduate school at Chulalongkorn University (90th Anniversary of CU) for financial support of this project. Guidance of the MCM-41 preparation by Dr. Panpranot is greatly appreciated.

References

[1] J.D. Kim, J. B.P. Soares, G.L. Rempel, J. Polym. Sci. Part A: Polym. Chem. 37 (1999) 331.
[2] J.D. Kim, J.B.P. Soares, Macromol. Rapid Commun. 20 (1999) 347.
[3] H. Rahiala, I. Beurroies, T. Eklund, K. Hakala, R. Gougeon, P. Trens, J.B. Rosenholm, J. Catal. 188 (1999) 14.
[4] K.-S. Lee, C.-G. Oh, J.-H. Yim, S.-K. Ihm, J. Mol. Catal. A: Chem. 159 (2000) 301.
[5] B. Jongsomjit, P. Kaewkrajang, S.E. Wanke, P. Praserthdam, Catal. Lett. 94 (2004) 205.
[6] B. Jongsomjit, P. Praserthdam, P. Kaewkrajang, Mater. Chem. Phys. 86 (2004) 243.
[7] B. Jongsomjit, P. Kaewkrajang, T. Shiono, P. Praserthdam, Ind. Eng. Chem. Res. 43 (2004) 7959.
[8] B. Jongsomjit, S. Ngamposri, P. Praserthdam, Catal. Lett. 100 (2005) 139.
[9] B. Jongsomjit, S. Ngamposri, P. Praserthdam, Molecules 10 (2005) 603.
[10] F. Ciardilli, A. Altomare, M. Michelotti, Catal. Today 41 (1998) 149.
[11] J.S. Beck, J.C. Vartuli, W.J. Roth, M.E. Leonowicz, C.T. Kresge, K.D. Schmitt, C.T.-W. Chu, D.H. Olson, E.W. Sheppard, S.B. McCullen, J.B. Higgins, J.L. Schlenker, J. Am. Chem. Soc. 114 (1992) 10834.
[12] C.T. Kresge, M.E. Leonowicz, W.J. Roth, J.C. Vartuli, J.S. Beck, Nature 359 (1992) 710.
[13] Y.S. Ko, S.I. Woo, Macromol. Chem. Phys. 202 (2001) 739.
[14] Z. Ye, S. Zhu, W.J. Wang, H. Alsyouri, Y.S. Lin, J. Polym. Sci. Part B: Polym. Phys. 41 (2003) 2433.
[15] D.E.B. Lopes, M.V. Marques, M.L. Dias, M.R. Ribeiro, J.P. Lourenco, Eur. Polym. J. 40 (2004) 2555.
[16] X.C. Dong, L. Wang, W.Q. Wang, H.J. Yu, J.F. Wang, T. Chen, Z.R. Zhao, Eur. Polym. J. 41 (2005) 797.
[17] S.T. Chen, C.Y. Guo, L. Liu, H. Xu, J.X. Dong, Y.L. Hu, Polymer 46 (2005) 11093.
[18] X.C. Dong, L. Wang, G.H. Jiang, Z.R. Zhao, T.X. Sun, H.J. Yu, W.Q. Wang, J. Mol. Catal. A: Chem. 240 (2005) 239.
[19] X.C. Dong, L. Wang, J.J. Wang, J.F. Zhou, T.X. Sun, J. Phys. Chem. B. 110 (2006) 9100.
[20] A. Reb, H.G. Alt, J. Mol. Catal. A: Chem. 174 (2001) 35.
[21] J.D. Kim, J.B.P. Soares, J. Polym. Sci. Part A: Polym. Chem. 38 (2000) 1427.
[22] Q. Wang, H.X. Yang, Z.Q. Fan, Macromol. Rapid Commun. 23 (2002) 639.
[23] J. Panpranot, K. Pattamakomsan, J.G. Goodwin Jr., P. Praserthdam, Catal. Commun. 5 (2004) 583.
[24] H. Hagimoto, T. Shiono, T. Ikeda, Macromol. Chem. Phys. 205 (2004) 19.
[25] Y. Zhang, M. Koike, N. Tsubaki, Catal. Lett. 91 (2005) 193.
[26] B. Jongsomjit, J. Panpranot, J.G. Goodwin Jr., J. Catal. 204 (2001) 98.
[27] B. Jongsomjit, J.G. Goodwin Jr., Catal. Today 77 (2002) 191.
[28] B. Jongsomjit, J. Panpranot, J.G. Goodwin Jr., J. Catal. 215 (2003) 66.
[29] B. Jongsomjit, C. Sakdamnuson, P. Praserthdam, Catal. Lett. 94 (2004) 209.
[30] T. Wongsalee, B. Jongsomjit, P. Praserthdam, Catal. Lett. 108 (2006) 55.
[31] J.R. Severn, J.C. Chadwick, R. Duchateau, N. Friederichs, Chem. Rev. 105 (2005) 4073.
[32] C. Ketloy, B. Jongsomjit, P. Praserthdam, Appl. Catal. A: Gen. 327 (2007) 270.
[33] B. Jongsomjit, S. Ngamposri, P. Praserthdam, Ind. Eng. Chem. Res. 44 (2005) 9059.
[34] J.C. Randall, J. Macromol. Sci. Rev. Macromol. Chem. Phys. C 29 (1989) 201.